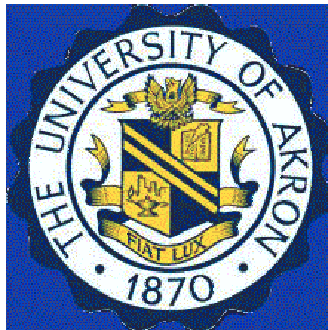


# **DRILLED SHAFT FOUNDATIONS FOR NOISE BARRIER WALLS AND SLOPE STABILIZATION**

**BY**  
**Robert Y. Liang**  
**Department of Civil Engineering**  
**The University of Akron**  
**Akron, Ohio 44325-3905**

Prepared in Cooperation with the Ohio Department of  
Transportation and the U.S. Department of Transportation,  
Federal Highway Administration



**December 2002**

1. Report No. FHWA/OH-2002/038	2. Government Accession No.	3. Recipient's Catalog No.	
4. Title and subtitle. Drilled Shaft Foundations for Noise Barrier Walls and Slope Stabilization		5. Report Date December 2002	
		6. Performing Organization Code	
7. Author(s) Dr. Robert Liang		8. Performing Organization Report No.	
		10. Work Unit No. (TRAIS)	
9. Performing Organization Name and Address Department of Civil Engineering The University of Akron Akron, Ohio 44325-3905		11. Contract or Grant No. State Job No. 14705(0)	
		13. Type of Report and Period Covered Final Report	
12. Sponsoring Agency Name and Address Ohio Department of Transportation 1980 W Broad Street Columbus, OH 43223		14. Sponsoring Agency Code	
		15. Supplementary Notes	
16. Abstract <p>This primary objective of this research is twofold: (i) development of a methodology for using the Standard Penetrating Testing (SPT) blow count to design the laterally loaded drilled shafts, and (ii) development of a methodology for design of drilled shafts to stabilize unstable slopes or embankments.</p> <p>The research has resulted in a development of a large database containing a total of 58 lateral load test results of drilled shafts, together with SPT information of the soils at the test site. The drilled shaft sizes range from 10 ft to 90 ft in length, and 16 inch to 72 inch in diameter. Both cohesionless and cohesive soils are included in the test database.</p> <p>Correlations between the SPT blow count and the soil parameters needed for establishing the p-y curves for COM624 computer analysis have been developed. The established correlations for p-y curve construction would allow the COM624 computer to predict accurately the drilled shaft deflections and bending moments when subjected to lateral loads and overturning moments.</p> <p>Both finite element analysis and centrifuge model testing techniques have been used in the research to gain quantitative understanding of the soil arching effect between the drilled shafts in stabilizing the unstable slopes. It was observed that S/D ratio (where S = clear spacing of the drilled shaft, and D = diameter of the shaft) plays a major role in controlling the development of soil arching in between the drilled shafts. A slope stability analysis procedure that incorporates the soil arching effect has been developed on the basis of the method of slices for any compound failure surfaces. The method can be applied to assess the global factor of safety of the drilled shafts reinforced slopes as well as the structural forces and moments applied to the drilled shafts.</p>			
17. Key Words Drilled shafts, lateral load, SPT, slope stability.		18. Distribution Statement No Restrictions. This document is available to the public through the National Technical Information Service, Springfield, Virginia 22161	
19. Security Classif. (of this report) Unclassified	20. Security Classif. (of this page) Unclassified	21. No. of Pages	22. Price

# **DRILLED SHAFT FOUNDATIONS FOR NOISE BARRIER WALLS AND SLOPE STABILIZATION**

**BY**  
**Robert Y. Liang**  
**Department of Civil Engineering**  
**The University of Akron**  
**Akron, Ohio 44325-3905**



*“The contents of this report reflect the views of the authors who are responsible for the facts and the accuracy of the data presented herein. The contents do not necessarily reflect the official views or policies of the Ohio Department of Transportation or the Federal Highway Administration. This report does not constitute a standard, specification or regulation.”*

*December 2002*

**Drilled Shaft Foundations for Noise Barrier Walls and Slope Stabilization**  
**FHWA/OH-2002/038**  
**Dr. Robert Liang**  
**University of Akron**  
**State Job No. 14705(0)**  
**December 2002**

**FOR COPIES OF THIS REPORT, CONTACT:**  
**Ohio Department of Transportation**  
**Office of Research and Development**  
**(614) 644-8173**  
[research@dot.state.oh.us](mailto:research@dot.state.oh.us)

**EXECUTIVE SUMMARY**

This research project is focused on two primary objectives. The first objective relates to the development of a methodology for using the SPT (Standard Penetration Test) results to design the laterally loaded drilled shafts. The second objective aims to develop a methodology for design of drilled shafts to stabilize unstable slopes or embankments. The research has resulted in suggestions of two implementation items.

In the course of the research work, a large database has been established to contain a total of 58 lateral load test results and the pertinent soil information at each test site. Among these test data, 32 load tests are from ODOT projects performed by the principal investigator. The drilled shaft sizes range from 10 ft to 90 ft in length, and 16 inch to 72 inch in diameter. Both cohesionless and cohesive soils are present in the test sites.

Correlations between the SPT N values and the pertinent soil parameters needed for p-y curve construction in the COM624 analysis have been developed from the database and statistical comparisons. The predictions of drilled shaft deflections at the load point under different load levels are compared fairly well with the measured data, when these empirical correlations are used.

To aid in the development of a design method for drilled shafts to stabilize an unstable slope, both centrifugal model study and finite element simulation techniques have been used in this research. The measured strains of the model shafts in the centrifuge tests allow for the determination of the deflections of the shafts and the net soil forces applied to the shafts. Soil arching between the adjacent drilled shafts in stabilizing the slope has been quantified from these centrifugal experiments. Specifically, in the sandy slopes, when S/D (S = clear spacing of shafts, and D = Diameter of shafts) is equal to 2, soil arching effect is most pronounced. Similarly, S/D = 1.5 appears to promote most the development of soil arching in cohesive soil slopes.

Finite element analysis of soil arching also confirms that S/D ratio plays the most important role in controlling the development of soil arching in between the drilled shafts. Based on a series of finite element simulation results, the soil arching effect on the net earth forces applied to the drilled shafts has been quantified and summarized in a design table. Also, a slope stability analysis procedure that incorporates the soil arching effect has been developed on the basis of method of slices for any composite shape of failure surface. The method has been validated against other slope stability programs and been used successfully to assist ODOT to design slope stabilization schemes for several slope rehabilitation projects.

## TABLE OF CONTENTS

	<b>PAGE</b>
<b>LIST OF FIGURES</b> .....	iv
<b>LIST OF TABLES</b> .....	xi
<b>CHAPTER</b>	<b>PAGE</b>
<b>I. INTRODUCTION</b> .....	1-1
1.1 Statement of the Problem.....	1-1
1.2 Objectives of the Study.....	1-4
1.3 Outline of the report.....	1-5
<b>CHAPTER</b>	<b>PAGE</b>
<b>II. BACKGROUND AND LITERATURE REVIEW</b> .....	2-1
2.1 Design and analysis of laterally drilled shafts.....	2-1
2.2 SPT and correlations.....	2-2
2.3 Correlations for sands.....	2-4
2.4 Correlations for clay.....	2-17
2.5 Drilled shafts for stabilizing a slope.....	2-22
2.6 Centrifuge testing.....	2-23
<b>CHAPTER</b>	<b>PAGE</b>
<b>III. SPT TO PREDICT DEFLECTION OF LATERALLY LOADED DRILLED SHAFTS</b> .....	3-1

3.1	p-y curve parameters in COM624 program.....	3-1
3.2	General information of database.....	3-2
3.3	Correlation studies.....	3-3
3.4	Evaluations of the recommended correlations.....	3-4

<b>CHAPTER</b>	<b>PAGE</b>	
<b>IV</b>	<b>CENTRIFUGE TESTING OF SOIL SLOPES STABILIZED WITH DRILLED SHAFTS.....</b>	<b>4-1</b>

4.1	Overview of centrifuge testing.....	4-1
4.2	Centrifuge facility.....	4-4
4.3	Centrifuge models.....	4-5
4.4	Soil used and slope preparation.....	4-6
4.5	Centrifuge test program.....	4-7
4.6	Tests results.....	4-8

<b>CHAPTER</b>	<b>PAGE</b>	
<b>V</b>	<b>NUMERICAL STUDY OF SOIL ARCHING MECHANISM IN DRILLED SHAFTS FOR SLOPE STABILIZATION.....</b>	<b>5-1</b>

5.1	Introduction.....	5-1
5.2	Finite-element modeling.....	5-4
5.3	Validation of finite element simulation.....	5-8
5.4	Influence of parameter variations on soil arching .....	5-12
5.5	Conclusions.....	5-18

## TABLE OF CONTENTS (Continued)

CHAPTER	PAGE
<b>VI STABILITY ANALYSIS OF DRILLED SHAFTS REINFORCED SLOPE</b> .....	6-1
6.1 Introduction.....	6-1
6.2 General statements.....	6-5
6.3 Mathematical formulation.....	6-7
6.4 Soil arching mechanism and the reduction factor R.....	6-8
6.5 Example studies.....	6-15
6.6 Case study.....	6-16
6.7 Conclusions.....	6-22
CHAPTER	PAGE
<b>VII SUMMARY AND CONCLUSIONS</b> .....	7-1
7.1 Major research results.....	7-1
7.2 Recommendations for implementation.....	7-4
7.3 Recommendation for future research.....	7-5
CHAPTER	PAGE
<b>VIII REFERENCES</b> .....	8-1

## LIST OF FIGURES

Figure		Page
2.1	Winkler nonlinear elastic spring representation of lateral soil-shaft interaction.....	2-33
2.2	Efficiency factors $e_1$ and $e_2$ .....	2-34
2.3	Laboratory tests .....	2-35
2.4	Effect of particle size, aging and overconsolidation.....	2-36
2.5	Effect of relative density.....	2-37
2.6	Effect of overburden pressure.....	2-38
2.7	Influence of aging on standard penetration resistance of NC sands.....	2-39
2.8	Revised Terzaghi-Peck classification (1948) for NC sands.....	2-40
2.9	Effect of overburden stress and $D_r$ on SPT N value .....	2-41
2.10	Relative density-N-stress relationship.....	2-42
2.11	Relative density-N-stress relationships for several sands .....	2-43
2.12	Empirical correlation between $N_{60}$ and $\phi$ for uncemented sands .....	2-44
2.13	Approximate correlation between $\phi'$ and quartz sands .....	2-45
2.14	N versus $\phi'_{tc}$ .....	2-46
2.15	N versus overburden stress .....	2-47
2.16	Young's modulus E as a function of N .....	2-48
2.17	Young's modulus E as a function of N .....	2-49
2.18	Selected relationship between N and $s_u$ .....	2-14

## LIST OF FIGURES (Continued)

Figure		Page
2.19	Relation between $s_u$ and SPT N value.....	2-51
2.20	Field unconfined strength versus SPT N .....	2-52
2.21	Laboratory unconfined strength versus SPT N .....	2-53
2.22	Strength and penetration resistance versus depth for glacial lake deposits....	2-54
2.23	Test data for glacial deposits till soils ( $S_r \geq 0.9$ ).....	2-55
2.24	Test data for glacial deposits till soils ( $S_r \geq 0.9$ ).....	2-56
2.25	Strength and penetration resistance versus depth for glacial deposits.....	2-57
2.26	Comparison of published current data.....	2-58
2.27	Modulus of elasticity versus SPT N value .....	2-59
2.28	Laboratory modulus of elasticity versus SPT N value .....	2-60
2.29	Field modulus of elasticity versus field unconfined strength .....	2-61
2.30	Arching effect .....	2-62
2.31	P-reduction factor versus $S/b$ .....	2-63
2.32	Efficiency of pile groups.....	2-64
2.33	Construction of design envelopes using the empirical design charts .....	2-65
3.1	SPT database statistics for cohesive soil .....	3-12
3.2	SPT database statistics for cohesionless soil .....	3-13
3.3	SPT database statistics (0-25% lateral load) for cohesive soil .....	3-14

## LIST OF FIGURES (Continued)

<b>Figure</b>		<b>Page</b>
3.4	SPT database statistics (25-50% lateral load) for cohesive soil.....	3-15
3.5	SPT database statistics (50-75% lateral load) for cohesive soil .....	3-16
3.6	SPT database statistics (75-100% lateral load) for cohesive clay .....	3-17
3.7	SPT database statistics (0-25% lateral load) for cohesionless soil .....	3-18
3.8	SPT database statistics (25-50% lateral load) for cohesionless soil .....	3-19
3.9	SPT database statistics (50-75% lateral load) for cohesionless soil.....	3-20
3.10	SPT database statistics (75-100% lateral load) for cohesionless soil .....	3-21
4.1	Schematics of centrifuge slope models with stabilizing piles.....	4-15
4.2	Strain gage locations .....	4-16
4.3	Top view of instrumented centrifuge model.....	4-17
4.4(a)	Moment distribution in dense sandy slope with $S/D = 1.5$ .....	4-18
4.4(b)	Moment distribution in loose sandy slope with $S/D = 1.5$ .....	4-19
4.5(a)	Moment distribution in dense sandy slope with $S/D = 2$ .....	4-20
4.5(b)	Moment distribution in loose sandy slope with $S/D = 2$	4-21
4.6(a)	Moment distribution in dense sandy slope with $S/D = 2.5$ .....	4-22
4.6(b)	Moment distribution in loose sandy slope with $S/D = 2.5$ .....	4-23
4.7(a)	Normalized maximum bending moment vs. $S/D$ ratio ( $N = 16$ ).....	4-24
4.7(b)	Normalized maximum bending moment vs. $S/D$ ratio ( $N = 24$ ).....	4-25

## LIST OF FIGURES (Continued)

Figure		Page
4.7(c)	Normalized maximum bending moment vs. S/D ratio (N = 32).....	4-26
4.7(d)	Normalized maximum bending moment vs. S/D ratio (N = 48).....	4-27
4.8(a)	Net force distribution with depth in dense sand slopes (S/D = 1.5).....	4-28
4.8(b)	Net force distribution with depth in loose sand slopes (S/D = 1.5).....	4-29
4.9(a)	Net force distribution with depth in dense sand slopes (S/D = 2).....	4-30
4.9(b)	Net force distribution with depth in loose sand slopes (S/D = 2).....	4-31
4.10(a)	Net force distribution with depth in dense sand slopes (S/D = 2.5).....	4-32
4.10(b)	Net force distribution with depth in loose sand slopes (S/D = 1.5).....	4-33
4.11	Net force vs. S/D in sand slope (N = 16).....	4-34
4.12	Net force vs. S/D in sand slope (N = 24).....	4-35
4.13	Net force vs. S/D in sand slope (N = 32).....	4-36
4.14	Net force vs. S/D in sand slope (N = 48).....	4-37
4.15	Moment distribution of test C1.....	4-38
4.16	Moment distribution of test C2.....	4-39
4.17	Moment distribution of test C3.....	4-40
4.18	Moment distribution of test C4.....	4-41
4.19	Moment distribution of test C5.....	4-42
4.20	Moment distribution of test C6.....	4-43

## LIST OF FIGURES (Continued)

Figure		Page
4.21	Moment distribution of test C7.....	4-44
4.22	Moment distribution of test C8.....	4-45
4.23	Moment distribution of test C9.....	4-46
4.24	Normalized maximum moment for pile in clay with slope angle = $34^{\circ}$ .....	4-47
4.25)	Normalized maximum moment for pile in clay with slope angle = $45^{\circ}$ .....	4-48
4.26	Normalized maximum moment for pile in clay with slope angle = $57^{\circ}$ .....	4-49
4.27	Force distribution of test C1.....	4-50
4.28	Force distribution of test C2.....	4-51
4.29	Force distribution of test C3.....	4-52
4.30	Force distribution of test C4.....	4-53
4.31	Force distribution of test C5.....	4-54
4.32	Force distribution of test C6.....	4-55
4.33	Force distribution of test C7.....	4-56
4.34	Force distribution of test C8.....	4-57
4.35	Force distribution of test C9.....	4-58
4.36	Normalized net force for pile in clay with slope angle = $34^{\circ}$ .....	4-59
4.37	Normalized net force for pile in clay with slope angle = $45^{\circ}$ .....	4-60
4.38	Normalized net force for pile in clay with slope angle = $57^{\circ}$ .....	4-61

## LIST OF FIGURES (Continued)

<b>Figure</b>		<b>Page</b>
5.1	Drilled shafts in a row for stabilizing a deforming ground .....	5-20
5.2	FEM modeling .....	5-21
5.3	Schematics of arching effect .....	5-22
5.4	Displacement contour ( $s = 2d$ with $d = 5$ cm).....	5-23
5.5	Principal stress direction ( $s = 2d$ with $d = 5$ cm).....	5-24
5.6	Load acting on the pile versus soil movement ( $d = 3$ cm).....	5-25
5.7	Load acting on the pile versus soil movement: $s = 2d$ .....	5-26
5.8	Load acting on the pile versus soil movement: $s = 4d$ .....	5-27
5.9	Load acting on the pile versus soil movement: $s = 8d$ .....	5-28
5.10	Percent of residual load acting on soil between piles versus spacing ratio ...	5-29
5.11	Effect of variation in pile spacing: cohesionless soil with $\phi = 40^\circ$ .....	5-30
5.12	Effect of variation in pile shape.....	5-31
5.13	Effect of variation in internal friction angle: cohesionless soil ( $d = 91.44$ cm )	5-32
5.14	Effect of variation in cohesion: $s=2d$ with $d = 91.44$ cm .....	5-33
5.15	Effect of variation in cohesion: $s=4d$ with $d = 91.44$ cm .....	5-34
6.1	Drilled shafts in a row for stabilizing a slope.....	6-23
6.2	Forces acting on a typical slice .....	6-24
6.3	Schematic of arching effect .....	6-25

## LIST OF FIGURES (Continued)

Figure		Page
6.4	Effect of variation in pile spacing ratio: cohesionless soil with $\phi=40^\circ$ .....	6-26
6.5	Effect of variation in internal friction angle: cohesionless soil .....	6-27
6.6	Effect of variation in cohesion: $s = 4d$ with $d = 91.44$ cm .....	6-28
6.7	Example problem.....	6-29
6.8	Example problem two.....	6-30
6.9	Distribution of the ratio of drilled shaft lateral force $F$ over the maximum $F_{\max}$ .....	6-31
6.10	Distribution of the global factor of safety.....	6-32
6.11	Global factor of safety versus the ratio of spacing to diameter .....	6-33
6.12	Cross-section C-C of Pomeroy landslide .....	6-34

## LIST OF TABLES

<b>Table</b>		<b>Page</b>
2.1	Efficiency coefficient $e_3$ .....	2-4
2.2	Laboratory tests.....	2-6
2.3	Relation between SPT N and $\phi'_{tc}$ .....	2-11
2.4	Equations for modulus from SPT results.....	2-15
2.5	Values of $s_1$ and $s_2$ for equation 2.9.....	2-16
2.6	Approximate $s_u$ versus N relationship.....	2-19
2.7	Typical values of static elastic modulus for clays.....	2-22
2.8	Summary of findings concerning pile spacing effects on pile group behavior.	2-24
3.1	Summary of input parameters.....	3-1
3.2	Laterally loaded drilled shaft and pile parameters for SPT database...	3-3
3.3	Modified correlations of cohesionless soil for predicting lateral deflection.	3-8
3.4	Modified correlations of cohesive soil for predicting lateral deflection...	3-8
3.5	Statistical analysis of correlations.....	3-10
3.6	Statistical analysis.....	3-10
4.1	Summary of test program for sandy slope.....	4-10
4.2	Summary of clayey slopes in centrifuge tests.....	4-11
4.3	Prototype properties at different centrifugal accelerations.....	4-11

## LIST OF TABLES (Continued)

Table		Page
5.1	Parameters used in the analysis .....	5-9
5.2	Parameters used in the analysis.....	5-10
5.3(a)	Percent of residual load acting on soil mass between piles (d = 30.48 cm).....	5-14
5.3(b)	Percent of residual load acting on soil mass between piles (d = 60.96 cm).....	5-15
5.3(c)	Percent of residual load acting on soil mass between piles (d = 91.44 cm).....	5-16
6.1	Percent of pressure acting on soil mass between piles (d = 91.44 cm).....	6-12
6.2	Comparison of factors of safety for example problem (circular slip surface)....	6-16
6.3	Comparison of factors of safety for example problem (composite slip surface)	6-17
6.4	Comparison of results (plain slope).....	6-18
6.5	Influence of shaft location on shaft force and global factor of safety .....	6-19
6.6	Influence of shaft layout on global factor of safety.....	6-20
6.7	Comparison of factors of safety.....	6-21

# CHAPTER I

## INTRODUCTION

### 1.1 STATEMENT OF THE PROBLEM

Drilled shafts foundations have been used for a variety of applications in highway constructions. For example, bridges, highway overhead signs, noise walls, and earth retaining structures are usually supported by drilled shafts. In most instances, the drilled shafts are subjected to both horizontal and vertical loads. However, in applications such as noise wall foundations and earth slope retention and stabilization, the primary force exert on the drilled shafts are lateral forces. For the drilled shafts subjected to lateral loads, two major categories can be made: active drilled shafts in which the lateral loads are transferred from the super-structures, and the passive drilled shafts in which the earth pressure acting on the drilled shafts is depends on the soil movement surrounding the shafts.

Analysis of the laterally loaded drilled shafts has been handled by the theory of beam on elastic foundation, with the subgrade reactions being modeled as nonlinear springs characterized by the p-y curves (p is the net soil reaction force per unit length of the drilled shaft, and y is the deflection of the drilled shaft). The current p-y criteria are based on semi-empirical curve fitting techniques on the strain measurements from the lateral load tests of piles and drilled shafts. Correlations with soil properties, shaft diameter, and depth were used to give generality to the methods. The fact that any one set of p-y construction method is only related to just one or two lateral load tests data should be

considered in using these curves for design. Furthermore, the determination of soil properties is based on UU (unconsolidated untrained) tests, which is problematic as documented in numerous studies.

The recommendations for constructing the p-y curves involve the use of several parameters, which are related to soil properties. In most cases, when subsurface soil investigations are performed, there are uncertainties about the correct values of soil parameters. As a result, there have been significant efforts devoted to the development of in-situ testing techniques to derive p-y curves. The pressuremeter test is one of such in-situ tests. However, the standard penetration test (SPT) is still the most widely practiced site investigation test in the U.S; therefore, it seems highly desirable to develop a methodology which would allow for the use of the SPT to deduce the site specific p-y curves for analysis of laterally loaded drilled shafts.

The SPT-based design methodology is a logical approach due to the following specific advantages. First, the SPT is conducted in-situ, which provides almost continuous information about soil resistance and consistency. Secondly, the SPT can be performed in almost all soil and rocks, except when large-size boulders exist. Thirdly, SPT allows for retrieving soil samples for visual classification of the soil types at the site. Finally, and perhaps most importantly, SPT is the most widely used in-situ testing technique in the United States. The development of the SPT-based design methodology for laterally loaded drilled shafts would certainly bridge the gap existing between the SPT data and soil properties needed for analyzing laterally loaded drilled shafts.

In recent years, ODOT had seen an increasing number of projects in which the drilled shafts have been used to stabilize the unstable slopes and highway embankments. However, the stabilization mechanisms due to the drilled shafts are poorly understood and the methodology for calculating the factor of safety of the slope reinforced with drilled shafts is lacking. Furthermore, the earth pressures acting on the drilled shafts installed on the slope cannot be estimated accurately at the present time. Consequently, the structure design of the drilled shaft is highly conservative, resulting in excessive size of the shaft and reinforcement quantities. Ohio Department of Transportation continues to spend 10 to 20 million dollars of construction money for noise barriers walls. Nearly half of this cost is related to drilled shaft foundations. Therefore, an accurate design method based on SPT soil data would be highly desirable to enable ODOT to design drilled shaft foundation with adequate safety while reducing construction cost.

At the present time, there is no universally accepted method for an analysis of the passive drilled shafts in stabilizing an unstable slope. Currently, ODOT engineers design such a stabilization system based on an empirical approach coupled with a great deal of conservatism. Furthermore, the calculation and design are often carried out by hand calculations, requiring an extended period of time before a design recommendation can become available. As a result, the size and reinforcement of the drilled shafts are often over-designed. It is therefore essential that a concerted effort be devoted to gain a better understanding of the stabilization mechanisms due to the installed drilled shafts and at the same time to develop an improved and computer-based analysis/design method for economic and safe design of the drilled shafts in stabilizing the unstable slopes.

## **1.2 OBJECTIVES OF THE STUDY.**

The main objectives of this research are twofold:

(1) Develop a methodology that would allow the use of the SPT results for analysis and design of the laterally loaded drilled shafts, and

(2) Develop a methodology for design the drilled shafts to stabilize the unstable slopes and embankments. Specifically, the following tasks are to be accomplished:

- Development of a relevant database containing both lateral load tests data and SPT data of the test sites.
- Utilize the established database to develop correlations between the p-y curves parameters used in COM624 computer program and the SPT N values for both cohesive and cohesionless soils.
- Investigate the arching mechanisms by means of a finite elements analysis program, PLAXIS and from which develop practical solution charts for use in the limit equilibrium based slope stability analysis.
- Develop an analysis algorithm for determining the global factor of safety of a slope reinforced with a row of drilled shafts, taking into consideration of both arching and reinforcing effects.
- Perform a series of centrifuge modal tests on both clayey and sandy slopes reinforced with drilled shafts to determine the forces and displacement of the model shafts under different shaft dimensions and spacings for different slope geometries and soil densities.
- Develop a PC based slope stability analysis program, incorporating the findings from both numerical and centrifugal studies, to enable ODOT

engineers to design a drilled shaft based slope stabilization scheme more efficiently.

### **1.3 OUTLINE OF THE REOPRT**

Chapter I provides a statement of the problem to be addressed in this research, along with the objectives and specific tasks to be accomplished. In addition, the outline of the report is described.

Chapter II presents a comprehensive literature review for the research project. Specifically, the current design/analysis methods for drilled shafts subjected to lateral loads, the existing correlations between SPT N values and various soil parameters for both clay and sand, and the design methods for analyzing the drilled shafts stabilized slopes, are reviewed in details in this chapter.

Chapter III summarizes a large database of lateral load tests results of drilled shafts. The database consists of actual load tests performed by the researchers for ODOT over the past several years as well as reported case studies in the open literature. SPT blow counts versus depth, along with soil profiles, are also collected for each test site. A computer program COM624, along with appropriate p-y curves, are used to establish correlations between SPT N values and p-y curves parameters. A statistical analysis of the accuracy of the correlations is shown to lend support of the developed correlations.

Chapter IV provides the details of the centrifugal modeling techniques developed in this research for the study of the drilled shaft behavior in stabilization of the slopes.

Centrifugal soil slope models, together with modeling laws and data acquisition techniques, used in this study are described in detail. Centrifugal test results of a series of model tests are analyzed to provide insights on the arching reinforcement mechanisms. The centrifugal test results are used to develop the methodology for design of drilled shafts to stabilize a slope.

Chapter V presents a finite element analysis technique for quantitatively studying the soil arching mechanisms associated with the drilled shafts stabilized soil slope. The modeling techniques and the constitutive relationships of the soils are described in detail. By performing a series of numerical studies, the load transfer characteristics due to soil arching are quantified for both cohesive and cohesionless soils. Among the parameters investigated, the ratio of shaft spacing,  $s$ , to the shaft diameter,  $d$ , was found to exert the greatest influences on the development and intensity of soil arching. Practical design tables have been developed to relate the arching-induced stress transfer to the  $s/d$  ratio, shaft diameter, and soil strength parameters. It was found that the smaller the  $s/d$  ratio and the higher friction angle of cohesionless soils, the more soil stresses are being transfer to the drilled shafts due to soil arching. The cohesive soils have greater tendency for soil arching as shown by a small cohesion value needed for fully developing the soil arching. The propensity of cohesive soils to creep may negate the arching to some extent.

Chapter VI presents a limit equilibrium based slope stability analysis technique that would allow for the determination of the safety factor of the reinforced slope and the forces acting on the drilled shafts. Specifically, the finite element analysis generated load

transfer characteristic curves were incorporated into the traditional method of slice approach to account for the soil arching effects. Mathematical formulation of the proposed analysis method is given in detail, followed by validation of the approach with other analysis methods. Examples of the slopes with or without the drilled shafts are given to illustrate the reasonableness of the solution provided by the proposed approach. The efficiency of using drilled shafts to stabilize a slope is discussed by examining the influence of the shaft location, shaft size and spacing on the calculated safety factor. Finally, a practical case involving the use of the proposed approach is presented.

Finally, Chapter VII provides a summary of the major research results from this study, along with recommendations of two items for implementations. Recommendations for future research are included at the end of the chapter.

## **CHAPTER II**

### **BACKGROUND AND LITREATURE REVIEW**

#### **2.1 DESIGN AND ANALYSIS OF LATERALLY DRILLED SHAFTS**

In highway construction, drilled shafts have been designed to withstand significant lateral loads in addition to axial loads. In the past, the research led by Professor Reese and his associates has culminated in publication of handbook and the computer program COM624 by the Federal Highway Administration (Reese, 1984) to analyze the laterally loaded drilled shafts.

The soil structure interaction of laterally loaded drilled shafts can be described mathematically by the beam-column on inelastic foundation theory (Hetenyi, 1946). A Winkler nonlinear elastic spring shown in Figure 2.1 is used to represent the load-deflection characteristics of the soil surrounding the drilled shafts. Vesic (1963) showed that solutions of the beam-on-elastic foundation problem using Winkler's assumption do not differ appreciably from solutions assuming the soil to be an isotropic, elastic continuum.

As a representation of the force-displacement relationship of the Winkler spring, a p-y curve concept was introduced, where p stands for a net soil reaction force per unit length of the shaft, and y represents the corresponding shaft deflection. The present methods of constructing p-y curves were derived largely from the measured bending

strain in the lateral load tests on piles and drilled shafts. Correlations with soil properties, shaft diameter, and depth were used to give generality to the methods.

The research reported herein advocates the development of an SPT-based in-situ testing technique for determining the p-y curves. The main motivation is derived from the fact that most geotechnical consulting firms in the U.S. adopt SPT in their site investigation. Developing an SPT-based design methodology is, therefore, fulfilling the needs of the practitioners. A detailed review of the existing correlations between the SPT N values and various soil properties is presented below. This literature review serves as the foundation and the starting point for further development of the correlations sought in the present research.

## **2.2 SPT AND CORRELATIONS**

In the USA, Canada, UK, Australia, and other countries, the SPT (Standard Penetration Test) is a widely used in situ test for geotechnical site exploration. In addition to providing a measure of soil resistance, SPT provides a unique capability to supply soil samples for soil classification purposes. It offers the advantages of low cost, applicability to a wide range of soil types, and extensive existing correlations with soil properties and foundation performance. Major limitations of SPT, however, include poor reproducibility, sensitivity to details of apparatus and procedures, and empiricism in data interpretation.

The most critical criticism against SPT has been a lack of standard in practice. However, due to concerted efforts in the industry in the last fifteen years, it is now possible to measure, or at least to evaluate the energy delivered to the drilling rod during SPT. In addition, since the mechanisms of SPT have been investigated extensively by Schmertmann (1979), among others, it is believed that SPT will gain even wider acceptance in geotechnical practice here in the U.S.

The history and early developments of the SPT have been summarized in numerous excellent publications such as the state of art report by De Mello (1971) and Nixon (1982) and the SPT International Reference Test Procedure by Decourt, et al. (1988).

Some Important factors influencing the SPT results are enumerated as follows:

1. Kinetic energy: The most important factor that would affect the kinetic energy is the way the hammer is lifted and released. The actual energy ( $E_v$ ) of the hammer when it hits the anvil is given by  $E_v = e_1 E^*$ , where  $E^*$  is the theoretical free fall energy given by  $W \cdot H = 63.5 \text{ Kg} \cdot 0.76 \text{ m} = 48.26 \text{ Kg.m}$  or 474 J; and  $e_1$  is an efficiency factor. Figure 2.2 shows  $e_1$  as a function of how the hammer is lifted and released.

2. Enthu energy: another loss of energy occurs when the hammer strikes against the anvil, where the anvil weight affects the energy transmission. Schmertmann and Palacios (1976) referred to the energy that reaches the rod as the Enthru energy,  $E_i = e_1 e_2 E^*$ , where  $e_2$  is an efficiency factor shown in Figure 2.2, in which  $e_2$  is a function of the anvil weight.
3. Critical length: studies by Palacios (1977) and Schmertmann and Palacios (1979) have demonstrated that  $E_i$  only fully reaches the rod when the rod length is equal to or greater than the critical length  $l_c$ , defined as the rod length weighing the same as the hammer. For rod lengths smaller than  $l_c$ , another correction factor  $e_3$  should be introduced. Table 2.1 gives  $e_3$  as a function of  $m$ , where  $m = M_r/M_h$ ,  $M_r$ =weight of rod and  $M_h$ = weight of hammer.

**Table 2.1 Efficiency coefficient  $e_3$**

<b>m</b>	0.1	0.2	0.3	0.4	0.5	0.6	0.7	0.8	0.9	1.0
<b><math>e_3</math></b>	0.33	0.55	0.70	0.80	0.85	0.90	0.93	0.96	0.99	1.0

## **2.3 CORRELATIONS FOR SANDS**

### **2.3.1 RELATIVE DENSITY $D_r$**

Since the late forties (Terzaghi and Peck, 1948), tentative suggestions have been made to correlate quantitatively the SPT resistance,  $N$ , with the in-situ state of densification of the cohesionless deposits. Furthermore, quantitative empirical correlations of the type  $D_r = f(N, \sigma'_{vo})$  have been developed by Gibbs and Holtz (1957),

Bazaraa (1969), and Marcuson and Bieganousky (19977, 1977a). Skempton (1986) studied the effect of overburden pressure, relative density, particle size, aging, and overconsolidation on sandy soils.

For consistency it is essential to correct the observed blow count  $N$  to the value which would have been measured using a specified rod energy. A recommended value, which should be recognized internationally, is 60% of the free fall energy of the standard hammer weight and drop. The corrected blow count is then designated as  $N_{60}$  and the normalized value  $(N_1)_{60}$  at unit effective pressure (1 Kg/cm<sup>2</sup> or 100 Kpa) may be regarded as basic characteristic of the sand. An examination of selected field and laboratory data (Skempton, 1986) shows that the relation between blow count, effective overburden pressure  $\sigma'_v$  and relative density is given to a close approximation by an equation of the form proposed by Meyerhof:  $N_{60} = (a + b\sigma'_{v0}) D_r^2$  or  $(N_1)_{60} = (a + b) D_r^2$ , where  $a$ ,  $b$  are constants for a particular sand within the range  $0.35 < D_r < 0.85$  and  $0.5 \text{Kg/cm}^2 < \sigma'_v < 2.5 \text{Kg/cm}^2$ . The parameters  $a$  and  $b$ , values for which are given for all cases studied, tend to increase with increasing grain size, with increasing age of the deposit, and with increasing overconsolidation ratio.

The long standing apparent discrepancy between field and laboratory tests is resolved when the effects of differing rod energy ratios and the 'aging' are taken into account. Also, the Terzaghi-Peck limits of blow count for various grades of relative density, as enumerated by Gibbs and Holtz, are shown to be good average values for normally

consolidated natural sand deposits, provided the blow counts are corrected to  $(N_1)_{60}$  values.

At a constant overburden pressure,  $N$  increases roughly as  $D_r^2$ . Thus a first approximation, as pointed out by Meyerhof (1957)

$$\frac{N}{D_r^2} = a + b\sigma'_v \quad (2.1)$$

But when the whole set of tests is considered, it is seen that at a given relative density and overburden pressure,  $N$  is higher for sands with larger mean grain size ( $D_{50}$ ). Average values of the parameters  $a$  and  $b$ , within the limited range of  $\sigma'_v$  and  $D_r$  mentioned, are given in Table 2.2

**Table 2.2. Laboratory tests (Skempton, 1986)**

Sand	Tested	$D_{50}$ : mm	UC*	Fines: %	$D_r$ :	$N_1$	$\frac{N_1}{D_r^2}$	$\frac{N}{D_r^2}$	$\frac{ER_r}{60}$	$(N_1)_{60}$	$\frac{(N_1)_{60}}{D_r^2}$	$\frac{N_{60}}{D_r^2}$
PR	Wet	2.0	5.3	0	0.4	7.5	47	$30+22\sigma'_v$	1.1 <sup>†</sup>	8	52	$33+24\sigma'_v$
					0.6	19	53			21	58	
					0.8	30	58			41	64	
GHC	Dry and Moist	1.5	5.5	0	0.4	6.5	40	$18+22\sigma'_v$				
					0.6	14.5	40					
					0.8	25	39					
SCS	Wet	0.51	2.5	4	0.4	7	44	$21+24\sigma'_v$	1.1 <sup>†</sup>	7.5	48	$23+26\sigma'_v$
					0.6	16	44			18	48	
					0.8	29	45			32	49	
RB M	Wet	0.23	1.8	2	0.4	5.5	34	$16+17\sigma'_v$	1.1 <sup>†</sup>	6	37	$17+19\sigma'_v$
					0.6	12	33			13	36	
					0.8	21	33			23	36	
GHF	Dry	0.3	7	14	0.4	4.5	28	$15+18\sigma'_v$				
					0.6	12	33					
					0.8	23	36					

\*Uniformity coefficient

<sup>†</sup> Includes a correction for no fines

To make use of equation 2.1, the parameter  $\frac{N_1}{D_r^2}$  is used;  $D_r$  is expressed as a ratio, not a percentage. In the tests  $N_1$  is found simply by interpolation as shown in Figure

2.3. The normalized values  $(N_1)_{60}$  and  $\frac{(N_1)_{60}}{D_r^2}$  are given in Table 2.2 together with the corresponding corrected parameters a and b.

It was stated that insufficient information is available to allow an estimate to be made of the rod energy ratio applicable to the USBR tests. However, the results of these tests are broadly compatible with those at the WES. Average values of  $\frac{(N_1)_{60}}{D_r^2}$  for the three WES sands are plotted against  $D_{50}$  in Figure 2.4. The tendency to increase with increasing grain size is clearly seen, it is probably related to a similar trend in  $\phi$  (at a given relative density). Figure 2.5 shows the relationship between  $\frac{N_{60}}{D_r^2}$  with N for sands tested at WES compared to Terzaghi and Peck (1948). Figure 2.6 shows the effect of overburden pressure on N values. The curves in the two figures can be taken as typifying laboratory tests on fine and medium-coarse normally consolidated sands.

Regarding these correlations the following comments apply (Jamiolkowski, et al. 1988):

- a) The Gibbs and Holtz (1957) correlation (GH), still widely applied in practice, may be approximated by the following formula (Meyerhof, 1957):

$$D_r = \left[ \frac{N_{SPT}}{23\sigma'_w + 16} \right]^{0.5} \quad (2.2)$$

where:

$N_{SPT}$  = SPT resistance in blows/30 cm ,and

$\sigma'_w$  = Effective overburden stress acting at the depth of the SPT test, expressed in bars

( 1 bar=98.1 Kpa).

The GH correlation has been obtained for clean predominantly silica sands. By analogy with what had been ascertained for the CPT performed in sands (Shmertmann, 1976; Baldi et al., 1985; 1986; Jamiolkowski et al., 1985), and because this correlation is referred to  $\sigma'_{vo}$ , its application should be restricted to normally consolidated (NC) sands. The use of this correlation in overconsolidated (OC) sands leads to an overestimate of the in-situ  $D_r$ , unless a correction similar to the one suggested by Skempton (1986) is adopted. Since the rod energy achieved during the Gibbs and Holtz (1957) Calibration Chamber tests are unknown, it is impossible to account for the influence of the specific driving procedure used during the SPT (Seed et al., 1984; Seed and De Alba, 1986; Skempton, 1986). This represents an additional uncertainty when evaluating  $D_r$ .

b) The peck and Bazaraa (1969) correlation corresponds to the upper limit of  $D_r = f(N_{SPT}, \sigma'_{vo})$  for dense quaternary sands deposits. Otherwise, all other comments already mentioned in the case of GH correlation apply.

c) Marcuson and Bieganousky's (1977,1977a) correlation (MB) obtained in fine and coarse sand is the only one that attempts to take into account the influence of OCR. In this case the level of the rod energy is known, leading to an energy ratio  $ER \approx 83\%$  ( $ER$  actual rod energy/theoretical energy).

d) The GH and MB correlations have been established on the basis of calibration chamber on samples reconstituted in the laboratory. Recent re-analysis by Skempton(1986) of the available SPT's performed in NC natural and man-made sand deposits, where  $ER$ ,  $D_r$  and age of the deposits are known, suggests that the empirical relations as the one given by equation (2.2) may be influenced by aging. This is

reflected in the increase of the ratio:  $\frac{(N_1)_{60}}{D_r^2} = a + b$  with increasing the age of the NC

deposit, see Figure 2.7. On the basis of these findings, one can argue that the use of the existing  $D_r$  vs  $N_{SPT}$  established on the basis of calibration tests can lead to an overestimate of in-situ  $D_r$  in all sand deposits, except recently man-made fills.

e) All the available  $D_r$  vs  $N_{SPT}$  correlations have been established for predominantly silica sands. Their use in more crushable and compressible sands., like calcareous sands or even silica sands containing a non-negligible amount of fines, may lead to underestimate of  $D_r$  ( Tatsuoka et al., 1978).

f) In Figure 2.8 Terzaghi and Peck's (1948) classification for NC silica sands are revised by Skempton (1986) so that one refers to the normalized SPT blow/count,  $(N_1)_{60}$ . Kulhawy and Maine (1990) present the laboratory research on the influence of overburden stress on the SPT N values. Figure 2.9 adopted from Gibbs and Holtz (1957) shows these results, which were based on calibration chamber tests. For practical use in estimating  $D_r$  from N and  $\sigma'_{vo}$ , these results were representative in alternative forms as that shown in Figure 2.10.

Additional research showed that these relationships are even more complex and dependent upon other factors, including vertical stress, stress history, and sand type (primarily compressibility), as a minimum. Figure 2.11 illustrates some of these complexities. The studies by Macruson and Bieganousky (1977) presented in Figure 2.11 led to a correlation for estimating  $D_r$  from SPT N values that includes the effect of

overburden stress  $\sigma'_{vo}$ , particle size distribution ( $C_u$ ), and stress history ( $OCR = \frac{\sigma_p}{\sigma'_{vo}}$ ), as

given below

$$D_r(\%) = 12.2 + 0.75 \left[ 222N + 2311 - 711OCR - 799 \left( \frac{\sigma'_{vo}}{p_a} \right) - 50C_u^2 \right]^{0.5} \quad (2.3)$$

Regression analysis of the data gave  $r^2=0.77$ . The data were unaged with OCR equal to 1 to 3.

It is almost a universal practice to correlate penetration resistance against relative density ( $D_r$ ); but as mentioned by Parkin (1988), this tradition should not be accepted without question. De Mello, since 1967, raised very sharp criticism against such correlations, arguing that  $N_{SPT}$  values should be correlated with  $\phi'$  and not with  $D_r$ . Any correlation of  $N$  against  $D_r$  should necessarily be made through  $\phi'$ .

Even for the classification purposes, it seems to be more logical and comprehensive to compare different sands stating their  $(N_1)_{60}$  values, then by qualitative designation of their compactness (loose, dense, etc.). But notwithstanding all this reasoning, if one wants to know  $D_r$  from  $N_{SPT}$  values, the correct way of doing it is first to estimate  $\phi'$  from  $(N_1)_{60}$  using the empirical correlation for uncemented sand suggested by De Mello (1971) shown in Figure 2.12, and then to use  $\phi'$  vs  $D_r$  correlations. For instance the one presented in Figure 2.13 by Schmertmann (1975).

### 2.3.2 FRICTION ANGLE $\phi'$

Correlations of the effective stress friction angle have been made with the standard penetration test, cone penetration test, pressuremeter test, and dilatometer test. The CPT correlations are perhaps the best developed, followed by the SPT. In all cases, it is presumed that the triaxial compression friction angle  $\phi'_{ic}$  corresponding to the appropriate stress and/or relative density conditions.

Correlations of effective stress friction angle with the SPT N-value have been made for many years. Early work by Meyerhof (1956) and Peck, et al. (1974) on this subject attempted to relate N to  $\phi'_{ic}$  directly as shown in Table 2.3 The Peck, et al. (1974) approach appears to be more common, perhaps it is more conservative. The values are also shown in Figure 2.14.

**Table 2.3. Relation between SPT N and  $\phi'_{ic}$**

N Value	Relative Density	Approximate $\phi'_{ic}$ (degrees)	
		Peck, et al. (1974)	Meyerhof (1956)
0 to 4	very loose	<28	<30
4 to 10	loose	28 to 30	30 to 50
10 to 30	medium	30 to 36	35 to 40
30 to 50	dense	36 to 41	40 to 45
>50	very dense	>41	>45

De Mello (1967-1971), using Gibbs and Holtz's data from USBR, established correlations of N against  $\phi'$  or  $\sigma'_w$  assuming the current analogy with a point bearing resistance condition. This correlation is presented in Figure 2.12.

To make De Mello's correlations useful for practical applications, at least two correction factors must be applied. One is to take into account the effect of aging on the penetration resistance, and the other is to normalize the measured penetration resistance to that corresponding to the standard  $E_i$  of 60%, and the vertical effective stress of 98.1 Kpa. There is evidence that the resistance of sand to deformation is greater for a longer period of consolidation. This aging effect is reflected in higher blow count (Skempton, 1986). Aging could be evaluated by considering the ratio of the Japanese Tombi ( $E_i \cong 85\%$ ) to the energy of the G and H's equipment assumed to be ( $E_i \cong 45\%$ ). The other correction is to change the measured N values to take into account the standard 60% energy.

Field measured 'N' values should be multiplied by the inverse of the aging factor (AF), which, for the considered fine sand is about 5.3(45/85). But the G & H's test performed with an equipment which had an energy  $E_i$  of about 45%. So to change from  $N_{60}$  to  $N_{G\&H}$ , N values should be multiplied by 60/45, the overall correction then being

$$N_{G\&H} = \frac{45}{80} \times \frac{60}{45} N_{60} = 0.705 N_{60} \quad (2.4)$$

It is very important to note that this correction factor is adequate for the assumed energy for the G & H's tests.

Rearranging the equation proposed by De Mello for sands and taking into account the above correction while considering the overburden pressure constant equal to 98.1 Kpa, we have,

$$(N_1)_{60} = -5.66 + 0.03 \left\{ \frac{6.8}{\tan \phi'} \left[ \tan^2 \left( 45 + \frac{\phi'}{2} \right) e^{\pi \tan \phi'} - 1 \right] + 10 \tan^2 \left( 45 + \frac{\phi'}{2} \right) e^{\pi \tan \phi'} \right\} \quad (2.5)$$

Figure 2.12 represents the variation of angle of internal friction  $\phi'$  as a function of  $(N_1)_{60}$ .

To assess  $\phi'$  from a field measurement of 'N' value, one should proceed as follows:

- 1) Correct N to  $N_{60}$  using

$$N_{60} = 0.0167 N E_i \quad (2.6)$$

$E_i$ , in percent, being the measured energy or the estimated using equation (2.1).

- 2) Assume a value of  $\phi'$  and compute the value of OCR and the  $K_o$ .

- 3) Change  $N_{60}$  to  $(N_1)_{60}$  using the equation

$$(N_1)_{60} = \left[ \frac{(\sigma'_{oct})_1}{(\sigma'_{oct})} \right]^{0.5} N \quad (2.7)$$

- 4) Enter in Fig. 12 with  $(N_1)_{60}$  and find  $\phi'$

- 5) Compare the assumed  $\phi'$  with the calculated value. If they are different, start every thing again considering now for OCR and  $K_o$  determinations.

It is very difficult to check the validity of this correlation against field data since it is very difficult to have undisturbed sand samples for the laboratory determination of the friction angle  $\phi'$

The N value actually depends upon stress level. Figure 2.15 is representative of the correlations between N and  $\phi'_{tc}$  as a function of stress level. This correlation can be approximated as follows:

$$\phi'_{tc} = \tan^{-1} \left[ N / \left( 12.2 + 20.3 \frac{\sigma'_{vo}}{p_a} \right) \right]^{0.34} \quad (2.8)$$

These results tend to be somewhat conservative and should not be used at very shallow depths, say less than 1 to 2 m (3.3 to 6.6 ft).

### 2.3.3 MODULUS OF ELASTICITY E FOR SANDS

Nowadays, it is well known, Vesic (1965), that the bearing capacity of deep foundation is not a sole function of  $\phi'$ , since it also depends on the stiffness of sand mass, where stiffness is a function of many other things among which are particle roughness and the composition of the grains. A number of authors have tried to correlate the modulus of granular soils with the standard penetration resistance. Callanan and Kulhawy (1985) collected some of these correlations for the standard penetration N values versus E as presented in Table 2.4. It should be remembered that these simplified relationships are intended primarily for settlement analysis on direct bearing, rather than side shear, and are meant to be used within a specified analysis procedure.

Many correlations have been proposed to relate SPT N values to the modulus of elasticity E, or the constrained modulus, M, of sand. Unfortunately, the various methods

**Table 2.4. Equations for modulus from SPT results (Callanan & Kulhawy, 1985)**

Author and soil Type	Modulus (tsf) for N in blows/ft
D'Appolonia, D'Appolonia and Brisette (1997) Normally consolidated sand Preloaded sand	$E_s=196+7.9 N$ $E_s=416+10.9 N$
Schmertmann (1970) Submerged SP and SW sands Submerged SP and clayey sands	$E_s=5(N+15)$ $E_s=3.3(N+5)$
NAVAC DM 7-1 (1982) Silts, sands silts, slightly cohesive silt-sand mixtures Clean, fine to medium sands and slightly silty sands Coarse sands and sands with little gravel Sandy gravel and gravel	$E_s=4 N$ $E_s=7 N$ $E_s=10 N$ $E_s=12 N$

produce dramatically different results (Mitchell and Gardner, 1975), so it is difficult to determine which, if any, are correct.

Different correlations between the number of blows N and Young's modulus E are in use today.

The most commonly used correlations are linear relationship as

$$E=s_1N+s_2 \quad (2.9)$$

where  $s_1$  and  $s_2$  are constants. Denver (1982) developed empirical correlations between SPT N values and the modulus of elasticity of sand, mainly fine sand. He compared his work with those published in the literature, as shown in Table 2.5 and Figure 2.16. The study suggested a relation between N and E in the form

$$E = (7\sqrt{N}) \quad Mpa \quad (2.10)$$

**Table 2.5. Values of  $s_1$  and  $s_2$  for equation 2.9**

Number of curve on Fig.18	$s_1$ (MPa)	$s_2$ (MPa)	Remark	Reference
1	0.756	18.75	Normally loaded sand and gravel	D'Appolonia et al., 1970
2	1.043	36.79	Preloaded sand	D'Appolonia et al., 1970
3	0.517	7.46		Schultz & Menzenbach, 1961
4	0.478	7.17	Sand-saturated	Webb, 1970
5	0.316	1.58	Clay & sand	Webb, 1970

Anagnostopoulos et al. (1982), based on the results from the tests on the undisturbed and semi-disturbed samples and for pressure equal to the effective overburden, suggested a linear correlation between  $E_s$  and  $N$  expressed by the formula  $E_s = C_1 + C_2 N$ . Figure 2.17 shows these correlations.

A comprehensive plot of drained modulus correlations for sand with the SPT are shown in Figure 2.16 (Callanan and Kulhawy, 1985). Kulhawy and Maine (1990) suggested the following approximate relationships:

For sand with fines  $E = 5 \sigma_r N_{60}$

For clean, normally consolidated sands  $E = 10 \sigma_r N_{60}$

For clean, overconsolidated sands  $E = 15 \sigma_r N_{60}$

In USSR (Trofimenkov, 1974), an equivalent modulus of elasticity  $E_s = (35 \text{ to } 50) \log N_{30}$  is used to estimate the settlement of footings on sand based on the results from SPT. Parry (1971) proposed the relationship  $E_s = 5 N_{30}$ , while Webb (1969) suggested the expression  $E_s = 0.537(N_{30} + 15)$  (MPa) for saturated medium sand and  $E_s = 0.358(N_{30} + 5)$  (MPa) for a saturated clayey fine sand.

## 2.4 CORRELATIONS FOR CLAY

The values of undrained shear strength of clay  $s_u$ , from the SPT currently are obtained from analytical models, empirical correlations, or calibration with known reference strength. Each in-situ test provides a different  $s_u$  particular to the boundary conditions imposed, rate of loading, direction of loading, etc.

De Mello in his article about standard penetration test, compares penetration resistance to cohesion values as determined from the unconfined compressive test on a 2-inch Shelby samples. From the data, he suggested the following correlation equation

$$N=9.0 + 6.76c \quad (2.11)$$

To illustrate the influence of depth  $z$  below ground surface on the correlation between  $N$  and  $c$ , two extensive sets of data from the U.S.B.R. (1960) report were analyzed. The following were found from the analysis, for high degree of reliability

$$N=1.7+0.848c - 0.0473z \quad (2.12)$$

where  $c$  is in psi and  $z$  in ft, and for high and medium reliability

$$N=0.36+0.644c-0.5517z \quad (2.13)$$

For highly plastic normally consolidated Santos (Brazil) clay, a concomitant regression with respect to in-situ vane shear strengths proves somewhat better based on 92 pairs of values as shown in equation 2.14.

$$N=0.87+1.464c \quad (2.14)$$

The following two equations 2.15 and 2.16 suggested by De Mello show that there is a high degree of significance of the dependence on  $z$  for the case of vane  $c$ .

$$N=-16.93+5.96q_u+1.155z \quad (2.15)$$

$$N=0.51+1.066c+0.046z \quad (2.16)$$

Note that sensitivity of clay should have a significant influence on the correlation of SPT ( $F(q_u)$ ), so that it is absolutely unacceptable to employ a single indication of tabulated SPT values as a basis for classification of clays via soft, medium, stiff, very stiff, and hard.

Stroud (1974) shows that simple correlations appear to exist in many clays and weak rocks between N values and mass in-situ shear strength. The correlation is of the form,

$$c = f_1 N \quad (2.17)$$

Down to a depth of about 50m below ground level,  $f_1$  appears to be essentially independent of depth and of discontinuity spacing in the clay up to at least 200mm. The value of  $f_1$  is found to increase with decreasing plasticity index and varies from about 4.0  $\text{KN/m}^2$  in materials of medium plasticity. For many of the harder and more brittle clays, the results are more variable, but this may be largely due to the increased difficulty of sampling and triaxial testing in these materials. The lowest value of  $f_1$  obtained was 3.1  $\text{KN/m}^2$ .

The relationships between the undrained shear strength  $s_u$  and N are primarily empirical correlations, even though it is known that these correlations are weak. It is important to define clearly which test was used to determine the shear strength. The most common of these correlations shown in Table 2.6 are reviewed by Terzaghi and Peck (1948), based on unconfined compression tests. From the results of this table,  $s_u$  can be approximated in equation 2.18

$$\frac{S_u}{P_a} \cong 0.06N \quad (2.18)$$

**Table 2.6. Approximate  $s_u$  versus N relationship**

N Value (blows/ft or 305 mm)	Consistency	Approximate $s_u/p_a$
0 to 2	very soft	$< 1/8$
2 to 4	soft	$1/8$ to $1/4$
4 to 8	medium	$1/4$ to $1/2$
8 to 15	stiff	$1/2$ to 1
15 to 30	very stiff	1 to 2
$> 30$	hard	$> 2$

Many other relations have been proposed as well, and several of these are shown in Figure 2.18. Using data in Figure 2.18, it appears that a universal relationship between  $s_u$  and N is unlikely. This is because these relationships represent a wide variety of interpretations of soil types and testing conditions. There are several problems exist with Figure 2.18:

- a) The SPT N values have not all been standardized to the same energy level.
- b) There is no indication of the reference strength used to determine  $s_u$ . The mixing of different undrained strength data is inconsistent, and it increases the scatter in the reported trends.
- c) The sensitivity of the clay can affect the N-value greatly.

Hara (1985) studied the correlation of SPT N values with the undrained shear strength on clayey soils with the same geology. The shear strength was obtained from the results of triaxial compression test on undisturbed soil samples. A correlation in the form of  $s_u = aN^b$  was found as

$$\frac{S_u}{P_a} = 0.29N^{0.72} \quad (2.19)$$

This equation is derived by Hara et al. (1985) from 25 clay silt in Japan, with PI=10-95, OCR=1-3, number of samples=180, and  $r^2 = 0.865$ .

Figure 2.19 indicates this behavior over a wide range of N values where the same drilling equipment, SPT procedure, and consistent reference strength (UU triaxial) were employed.

Beha poor and Ghahramani(1989) studied the correlation of the SPT to the strength of cohesive soils. About 60 projects corresponding to clayey and silty clay soils (CL and CL-ML) have been selected and used to study the correlation of standard penetration tests to the strength of soils. It was found that for clayey and silty clay soils, the correlation with the SPT number are good. Test results correlate better for  $N_{30} < 25$ . Figure 2.20 shows the variation of field unconfined strength with SPT N number; equations 2.20 and 2.21 show this relation. Figure 2.21 shows the variation of laboratory unconfined strength with SPT N number. Equation 2.22 shows this relation. Accordingly, the authors concluded that standard penetration tests yield valuable results for predicting strength and elastic modulus and the pessimistic view of applicability of SPT to cohesive soils is not warranted.

$$q_{uf}(Kpa) = 15 \times N_{30} \quad (N_{30} < 25) \quad (2.20)$$

$$q_{uf}(Kpa) = 15 \times N_{30} \quad (N_{30} < 25) \quad (2.21)$$

$$N = 3.7 \ln(6.9 q_u) \quad (2.22)$$

Hegedus and Peterson (1988) discussed the use of penetration testing as in-situ test method to predict the undrained shear strength of cohesive soils (silty clays encountered primarily along the southern shores of lake Erie in the northern part of

Ohio). They included nearly 470 standard penetration, unconfined compression and other soil properties tests. Empirical correlations were developed to forecast shear strength from penetration resistance based on statistical analysis results. The following correlations were suggested for both soil types, i.e. for Glacial Deposits

where  $q_u$  is in Ksf. For Glacial Till.

$$S_r > 0.9 \quad N = 6.7 \ln(3.3 q_u) \quad (2.23)$$

$$S_r < 0.9 \quad N = 5.1 \ln(6.9 q_u) \quad (2.24)$$

$$S_r < 1.0 \quad n = 6.2 \ln(3.1 q_u) \quad (2.25)$$

The data for equations 2.23, 2.24, 2.25 are presented in Figure 2.22, 2.23 and 2.24, respectively. Figure 2.25 shows the variation of the data for glacial lake deposits. The comparison of the finding of their study with the literature is presented in Figure 2.26.

#### **2.4.1 CORRELATION WITH MODULUS OF ELASTICITY OF COHESIVE SOILS**

Terzaghi and Peck (1948) suggested the following variations for static modulus of elasticity of clayey soils, as shown in Table 2.7. Beha-poor and Ghahramani (1989) studied the correlation of the elastic modulus of cohesive soils with the SPT N values. They suggested the following correlation for E and N:

$$E(\text{MPa}) = 0.17 * N_{30} \quad (N_{30} < 25) \quad (2.26)$$

The results from their study are presented in Figure 2.27 for field correlation and Figure 2.28 for laboratory correlation. Figure 2.29 shows their results correlating field modulus of elasticity versus unconfined strength.

**Table 2.7. Typical values of static elastic modulus for clays**

N Value (blows/ft )	Consistency	Elastic Modulus, $E_s$ (tsf)
2-4	soft	50-150
4-15	medium to stiff	150-500
15->30	very stiff to hard	500-1000

## **2.5 DRILLED SHAFTS FOR STABILIZING A SLOPE**

During the past two decades, the use of drilled shafts has been shown to be an effective deterrent to extensive soil movement (Merriam, 1960; Andrews and Klasell, 1964; Bulley, Adachi et al., 1989; Nethero, 1982). There are two major issues involved in the design of drilled shafts to correct and stabilize slopes. The first is to determine the load distribution along the length of the drilled shaft in order to assess the shear forces and bending moments the shaft has to sustain. The second is to evaluate the overall stability of the corrected slope.

### **2.5.1 ARCHING MECHANISM**

Arching effect in the sandy soil was first proposed by Terzaghi (1934), where arching was defined as the transfer of stresses from a yielding mass of soil onto the adjoining stationary part of soil. By placing sand above a platform that contains a narrow strip of trap door, Terzaghi (1936) showed that when the trap door was lowered slightly, the vertical earth pressure on the adjoining parts of the platform increased. This phenomenon was attributed to the shearing stresses developed between the moving (yielding) mass and the adjoining stationary sand mass.

Adachi, et al (1990) conducted a series of two dimensional laboratory model tests to investigate the stabilizing mechanism of piles in a slope. The arching mechanism of a pile group can be demonstrated in Figure 2.30, where it can be seen that an arch was formed between two adjacent piles.

One important consideration in the design of drilled shafts in stabilizing the slope is the maximum allowable spacing between the drilled shafts so that soil arching can still be developed. One solution to this may be obtained from the study of the group effects of drilled shafts. Experimental studies conducted by Parakash (1962), Wang and Reese (1986), Leing (1988) have included lateral loading tests on a group of piles in a side-by-side configuration. Assuming that  $P$  represents the force acting on a single pile due to soil pile interaction, when these piles arranged in a group, the lateral load applied to each pile is reduced. The factor for reducing the applied  $P$  is defined as the ratio of average capacity of individual pile in a group to the pile capacity of a single pile.

The load-reduction factor versus pile spacing is shown in Figure 2.31 (Reese et al., 1992). It can be seen that when the ratio of pile spacing to pile diameter,  $s/b$ , is three or larger, the group effect (or load-reduction factor) is almost negligible. When  $s/b$  is larger or equal to four, the load-reduction factor is close to one, indicating that there is no group effect.

Cox et al (1983) conducted laboratory model tests to investigate the efficiencies of pile group under lateral loading. The loading was slow and monotonic. Test results indicated that, when the pile spacing was equal to or larger than three times the pile

diameter, then the pile in a group behaved as if they were single piles, as shown in Figure 2.32.

Shibata, et al (1989) conducted model tests to study the response of the laterally loaded free-headed pile groups. The piles were embedded in sand. Several test parameters, such as pile spacing and pile number in a row, were varied in the test program. According to their experimental results, it seemed that when the ratio of pile spacing to diameter,  $s/d$ , was larger than or equal to five, then there was no group effect.

McVay, et al (1995), studied the response of laterally loaded pile groups using the centrifuge model testing techniques. Their findings, together with other observations discussed above, regarding the effect of pile spacing on the pile group behavior, are summarized in Table 2.8

**Table 2.8. Summary of findings concerning pile spacing effects on pile group behavior**

Reference	Source of data	Threshold ratio ( $s/d$ )
Parakash (1962), Wang and Reese (1986), and Lieng (1988)	Empirical curve derived from experimental studies, cited by Reese, et al (1992)	3.5-4.0
Cox, et al (1983)	Laboratory model test	3.0
McVay, Casper, and Shang (1995)	Experience and centrifuge model	5.0
Shibata, et al (1989)	Laboratory model test	5.0

## 2.5.2 REINFORCEMENT MECHANISM

Drilled shafts designed to prevent excessive movement of a slope are installed beyond the depth of a potentially sliding surface and often times into a hard soil layer

underneath. Since the displacement of soil mass above a potentially sliding surface is expected to be more than that beneath the sliding surface, a shear force will develop in the drilled shaft at the location close to the potential sliding surface. Furthermore, the earth pressure on the drilled shaft needs to be transferred to the soil beneath. Therefore, excessive soil movement in the potential sliding soil mass can be prevented, through the reinforcement mechanism.

A literature review indicates that there have been numerous efforts devoted in the past to develop a simple, yet rationale, method for analysis and design of drilled shafts to stabilize a slope. These methods may be categorized into four groups: (1) empirical method, (2) earth pressure method, (3) displacement-based method and (4) finite element analysis method. A brief review of each method is given below.

### **2.5.3 EMPIRICAL METHODS**

Several empirical relationships have been proposed on the basis of field laboratory test results for estimating maximum bending moment in the drilled shafts installed in a slope. For example, Stewart et al (1994) collected data from different sites and laboratory tests and developed two kinds of charts: (1) maximum bending moment versus relative stiffness, and (2) drilled shaft head deflection versus relative stiffness. However, because the data showed a great deal of scatter, a design envelope for maximum bending moments and deflection was suggested as shown in Figure 2.33. The advantage of this method is that it can provide a means for a quick and rough estimate of the likely behavior of a group of drilled shafts. On the other hand, the design chart cannot

be used if the specific site condition is different from the site condition from which the data was obtained. Furthermore, the empirical method cannot take into account the effects such as drilled shaft spacing, the drilled shaft size, and slope angle.

#### **2.5.4 EARTH PRESSURE BASED METHOD**

In essence, this method relies on the semi-analytically derived pressure distribution, or the resultant force, acting on the drilled shaft to determine the factor of safety of the drilled shafts stabilized slope. There are two steps involved in the determination of earth pressures acting on the drilled shafts constructed on a slope. The first step is to determine the earth pressure in the section of a slope where the drilled shafts will be installed; the second step is to determine the distribution of the calculated earth pressures onto each drilled shaft. Recent development in this approach is represented by the method proposed by Ito et al, (1975; 1979) and the method proposed by Reese et al. (1992).

In Ito, et al. (1975, 1979) method, the theoretical equations to calculate the lateral force acting on the drilled shaft were derived based on a consideration of plastic deformation of the soil between the adjacent shafts. A total of four main assumptions were invoked in deriving the analytical equations, including (i) soil becomes plastic only in the area just around the drilled shafts; (ii) two vertical sliding surfaces will occur along the lines making an angle of  $(\pi/4 + \phi/2)$  with soil movement direction; (iii) friction force acting on the sliding surfaces is neglected; and (iv) the active pressure is assumed to act on the plane along pile row direction. Once the lateral force has been calculated, then the stability of the shafts and the stability of the slope can be analyzed separately.

Regarding the pile stability, they proposed that an analytical method of pile subjected to horizontal loads such as the subgrade modulus reaction method be applied. As for the slope stability calculation, the analysis can be carried out by making a comparison between the resisting and driving moments,  $M_r$  and  $M_d$ , acting on the potential sliding soil mass. The resisting moment may be obtained as the sum of both the resisting moments,  $M_{rs}$ ,  $M_{rp}$ , due to the shearing resistance along the potential sliding surface and the reaction force of the shafts in a row, respectively.

In the Reese et al's method, two cases were cited where the lateral thrust from the moving soil and the response of a pile can be readily computed: (1) when the piles are side-by-side with no spacing in between (a wall), and (2) when the piles are so widely spaced that no interaction occurs. In the former case, the earth pressure theories for computing passive earth pressure on retaining walls can be used. In the latter case, the concept of the failure soil wedge presented by Reese et al (1974) was used to compute the lateral thrust on each drilled shaft. For a general case where pile spacing falls within these two limiting cases, an empirical curve for the load reduction factor was suggested.

### **2.5.5 DISPLACEMENT-BASED METHOD**

In this method, the magnitude and pattern of the lateral soil displacement is used to determine the resulting deflection and bending moment of the drilled shaft. One of such method was recently developed by Stewart et al (1944). The particular situation considered was an embankment on soft clay foundation as an approach to a piled bridge abutment. They suggested two types of displacement-based design methods. One was the

method proposed by Springman (1989, in which a simple soil deformation mechanism was used in deriving the relationship between the lateral earth pressure acting on a pile and the relative soil-pile displacement. A simple triangular displacement pattern was assumed such that the displacement  $y_s$  at any depth is expressed as:

$$y_s = \frac{t_{mob}(h_s - z)}{2G_m} \quad (2.27)$$

where  $z$  is depth below surface,  $G_m$  is mean shear modulus of the soil layer,  $h_s$  is thickness of the soil layer.

The other displacement-based method was developed by Poulos (1994), in which the free field soil movement was used as input on a simplified boundary element method to compute the axial and lateral response of piles subjected to these prescribed soil movements. The influencing factors such as pile position, shear strength of the soil, soil layer thickness, condition of fixity and restraint at the pile head, and the installation sequence of piles can be considered. Generally speaking, the displacement-based method is superior to the earth pressure based method, because it reflects the true mechanism of soil-shaft interaction. However, it should be pointed out that the accurate description of free field soil movements is a prior to the accuracy of the calculated loads applied to the drilled shaft.

## **2.5.6 FINITE ELEMENT ANALYSS METHOD**

There have been numerous types of finite element representations for piles subjected to lateral soil movements. For example, some were axisymmetric analysis with

non-symmetric loading (Carter 1982), some were plane strain analysis (Sirawardane et al, 1984 and Stewart et al. 1993), and some were three-dimensional analysis (Oakland et al, 1984 and Springman, 1989). Each of these representations has its own merits, but obviously plane strain is probably the most convenient way to approximate the three-dimensional nature of the problem. The soil stratigraphy and embankment loading of a typical problem of this nature can often be depicted adequately by a cross-section parallel to the direction of the soil movement. Representation of this cross-section with a finite element mesh is then relatively straightforward, and the piles could be modeled with elements similar to those used for the soil (Siawardane et al. 1984). Alternatively, beam elements could be incorporated into the mesh (Stewart et al. 1993).

The effect of a row of drilled shaft can be considered by an equivalent sheet-pile wall and with equivalent properties assigned. It is obvious that, in plane strain representation where the pile is explicitly represented in the finite element mesh, the soil cannot deform and flow around the pile. Thus, the FEM analysis results may be significantly in error. To remedy this problem, Oakland et al (1984) modeled the pile with eight node elements, in which the beam nodes are defined separately from those describing the soils. In this way, the relative soil movement around the pile was allowed, thus modeling more accurately the soil flow around the pile. It should be pointed out that this relative movement may be of minor importance for very flexible piles, but it can become very significant as the pile stiffness increases. Calculation results of the finite element method not only depend on the proper element representation of the soil and the

pile, but also on the proper representation of boundary conditions, the soil-pile interface, and the soil model.

## 2.6 CENTRIFUGE TESTING

The purpose of centrifuge testing is to reproduce the field (prototype) response in a scaled model. Since soil behavior is pressure sensitive, the gravity stresses, which are significant in deep foundation, must be reproduced in the model. This is accomplished by subjecting the model to an elevated gravitational level (g-level),  $N$ , when  $N$  is the ratio of the gravitational acceleration produced during the centrifuge testing to the earth's gravitational acceleration. The linear model dimensions (length, width, etc.) are transformed by a scaling factor  $1/N$ . For instance, a  $1/45$  scaled model would require that a prototype drilled shaft 15 m (49.2 ft) long by 0.6 m (2.0 ft) in diameter be modeled by a 0.33 m-long (13 in) by 13.5 mm-diameter (0.53 in) drilled shaft. In terms of stress, if the prototype was expected to carry an axial load of 890 kN (100 tons), the stress on the cross-section would compute to be 442 psi. This would require a model load of  $0.44 N$  (99 lb) (prototype load/ $N^2$ ) to give the same stress in the model as the prototype. The significance of modeling the soil's gravity stress has been shown recently in studies by Feld et al. (1994) and Yet et al. (1994), in which the axial capacities of model piles were reduced by 50 to 70% when driven at 1 g (while the centrifuge is stationary) and subsequently loaded at the scaled ( $N$ ) g-levels, compared to driving and loading in continuous flight.

Scott (1981) was the first to laterally load piles in a centrifuge. One pile was installed by driving at 1 g, and another was installed by raining sand around it at 1 g. The

pile were then accelerated and loaded. Scott stated that neither method of installation represented the prototype conditions.

Barton (1984) was the first to test a pile group (two rows, installed at 1 g). It was verified that the first row (lead row) carried 60% of the lateral load, and the second row (trail row) carried 40% of the lateral load at a pile spacing of two pile diameter (2D).

Oldham (1985) was the first to instrument a single pile with strain gages, drive the pile in flight via a pneumatic jack, and laterally load it. Terashi et al. (1990) obtained results and validated the scaling relationships. Bloomquist et al. (1991) and McVay et al. (1994) were recent investigators who achieved in-flight driving of a group of piles and derived useful design guidelines for lateral response of pile groups.

A review of existing literature reveals that there are numerous reports of research on the use of centrifuge to investigate the single pile and pile group behavior when subjected to lateral loads ( e.g, Bouafia and Garnier, 1991; Cyran et al., 1991; Finn et al., 1984; Garnier et al., 1989; King, 1994; Kitazume and Miyajima, 1994; Kotthaus and Jessberger, 1994; Lyndon and Pearson, 1988; Mezazigh et al, 1994, Nunez et al., 1998; Scott, 1981). Nevertheless, it appears that only one or two centrifuge studies have been carried out in the past to study the mechanisms of drilled shafts (or piles) reinforced slope. Notable reports on this subject were found in Wei and Tu (1991); Springman et al. (1991); and Terashi et al. (1991). The centrifuge model study to be carried out in this research project will undoubtedly be among the few that exist and will contribute to the

basic understanding of the subject matter and provide insight for the development of the analysis/design methodology.

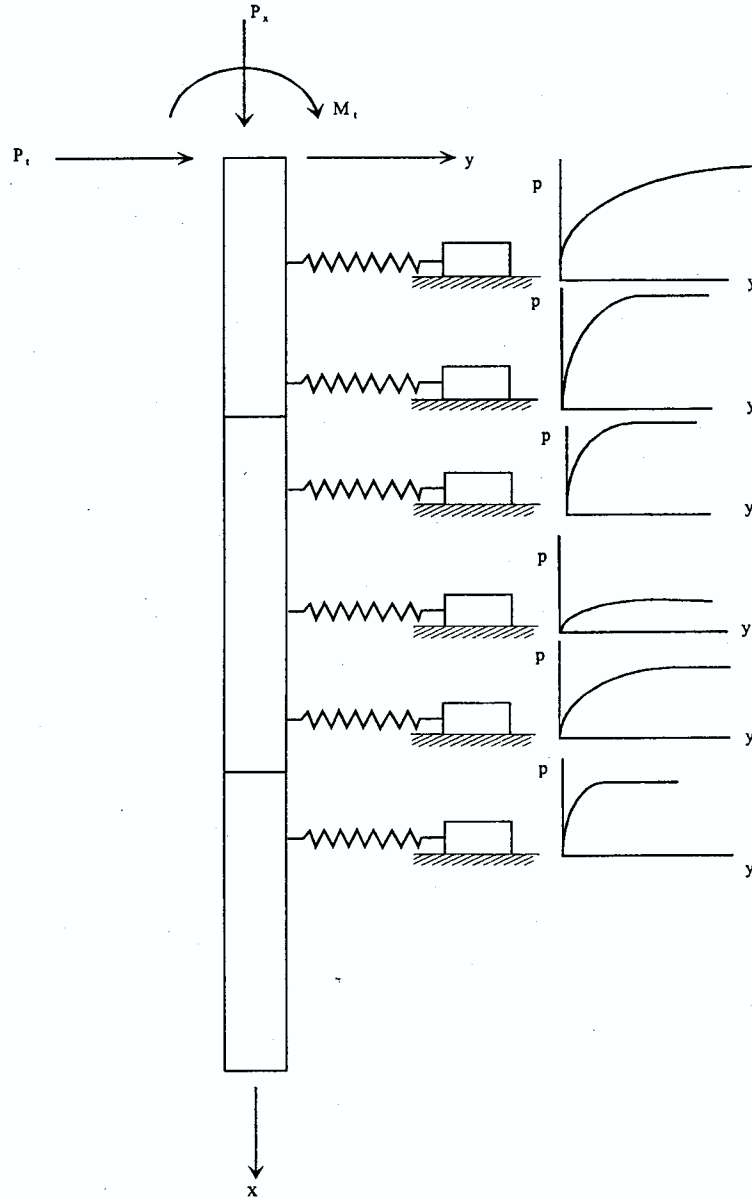


**Figure 2.1 Winkler Nonlinear Elastic Spring Representation of Lateral Soil-Shaft Interaction.**

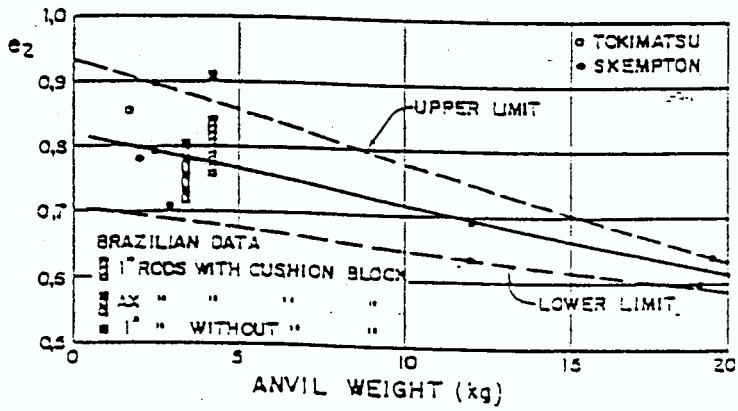
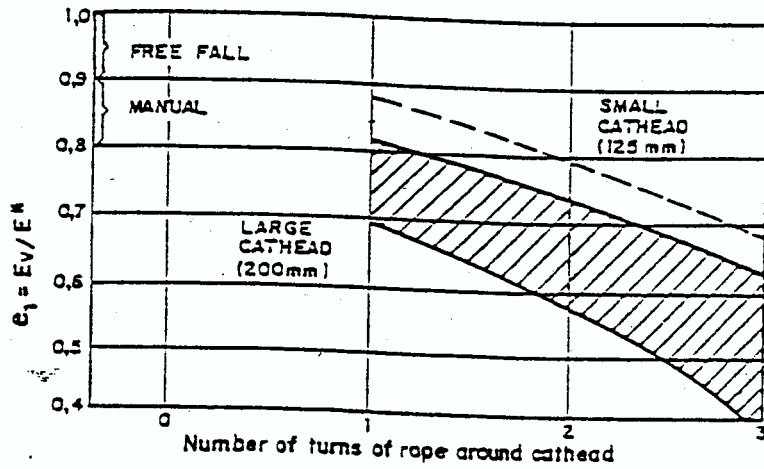


Fig. 2.2 Efficiency Factors  $e_1$  and  $e_2$

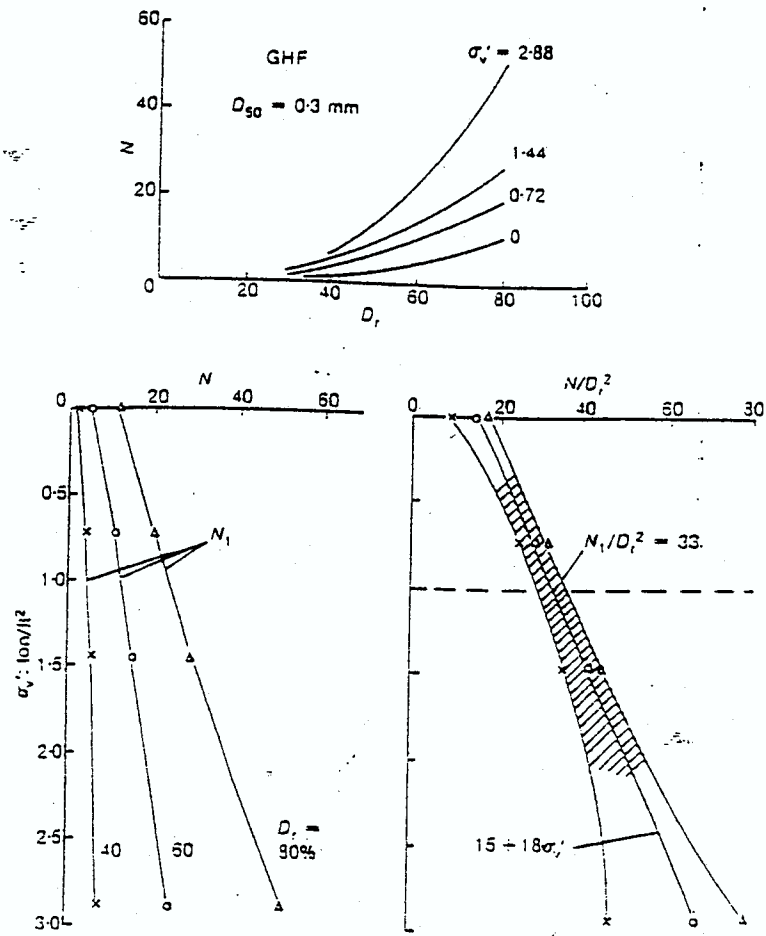


Figure 2.3 Laboratory Tests (Skempton, 1986)

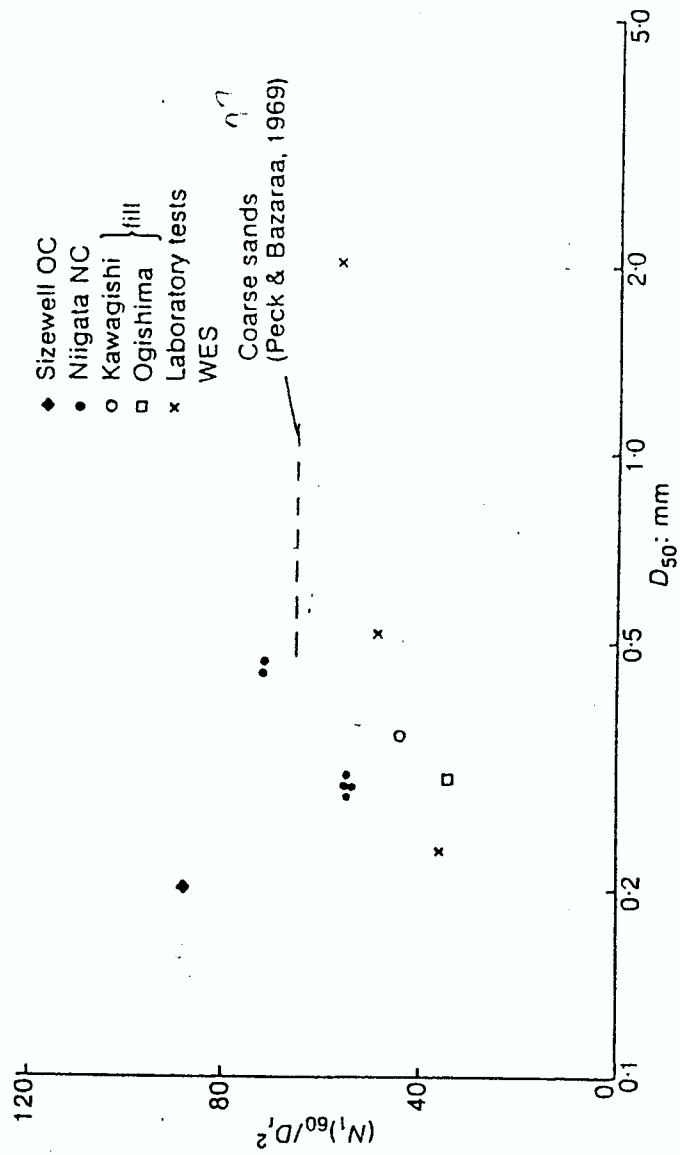


Figure 2.4 Effect of Particle Size, Aging and Overconsolidation (Skempton, 1986)

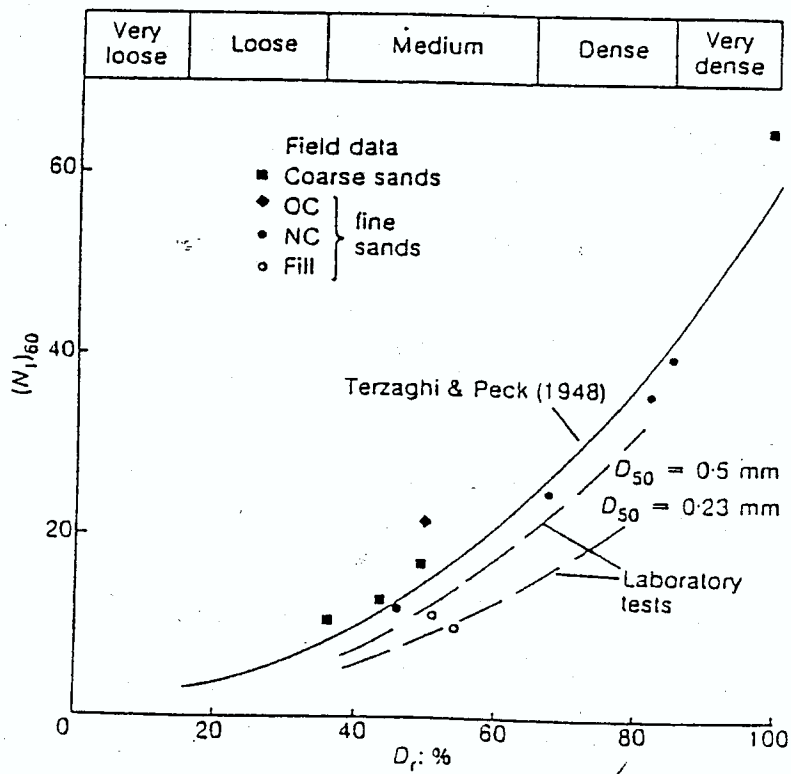


Figure 2.5. Effect of Relative Density (Skempton, 1986)

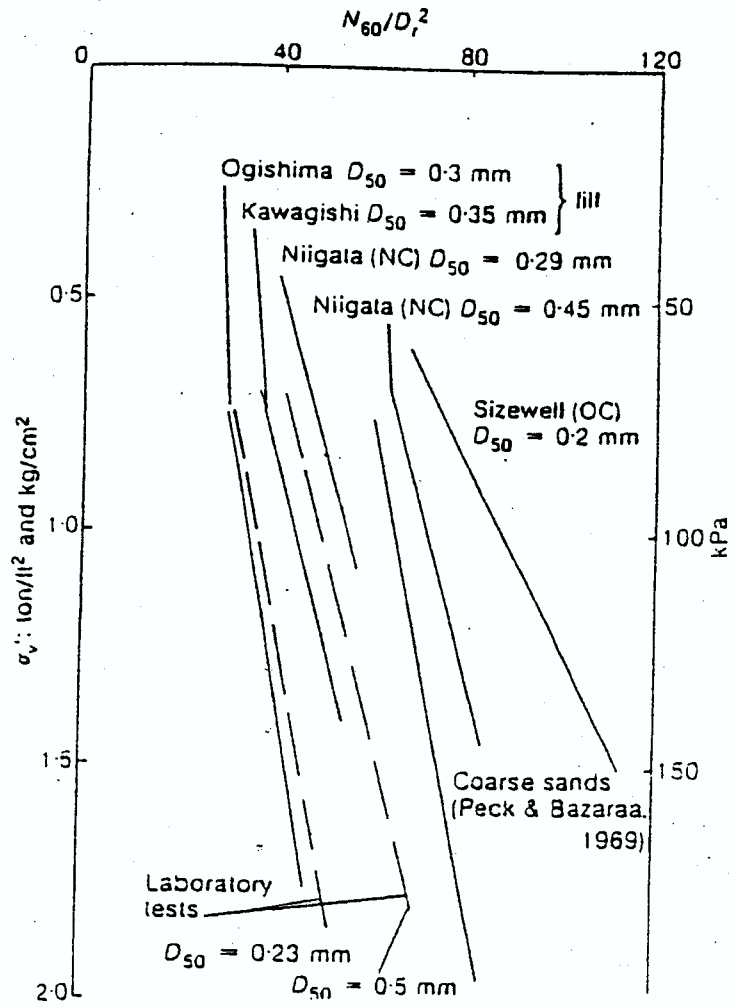


Figure 2.6. Effect of Overburden Pressure (Skempton, 1986)

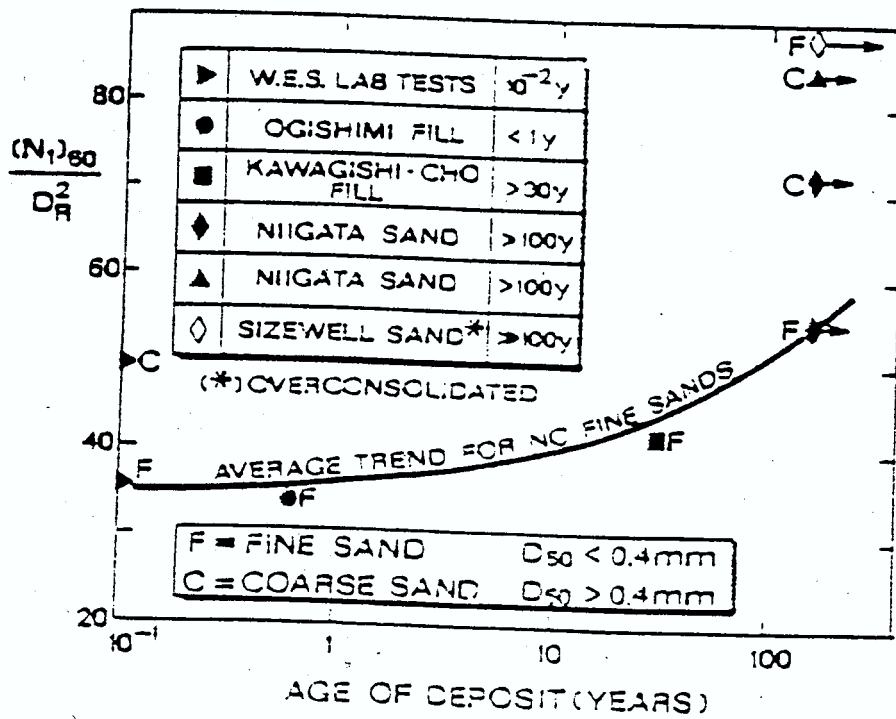
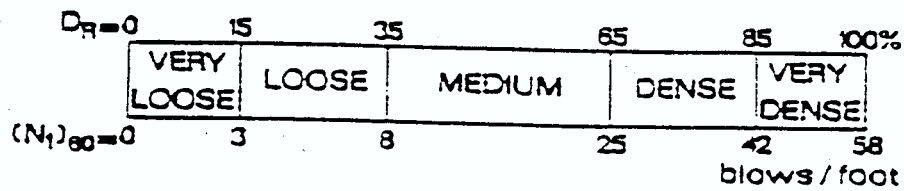


Figure 2.7 Influence of Aging on Standard Penetration Resistance of NC Sands (Adapted Skempton, 1986)



- FOR  $D_r \geq 35\% \rightarrow \frac{(N_1)_{60}}{D_r^2} \approx 60$

- FOR COARSE SANDS  $N_{SPT}$  SHOULD BE REDUCED IN THE RATIO  $\frac{55}{60}$

- FOR FINE SANDS  $N_{SPT}$  SHOULD BE INCREASED IN THE RATIO  $\frac{65}{60}$

Figure 2.8 Revised Terzaghi-Peck Classification (1948) for NC Sands (Adapted Skempton, 1986)

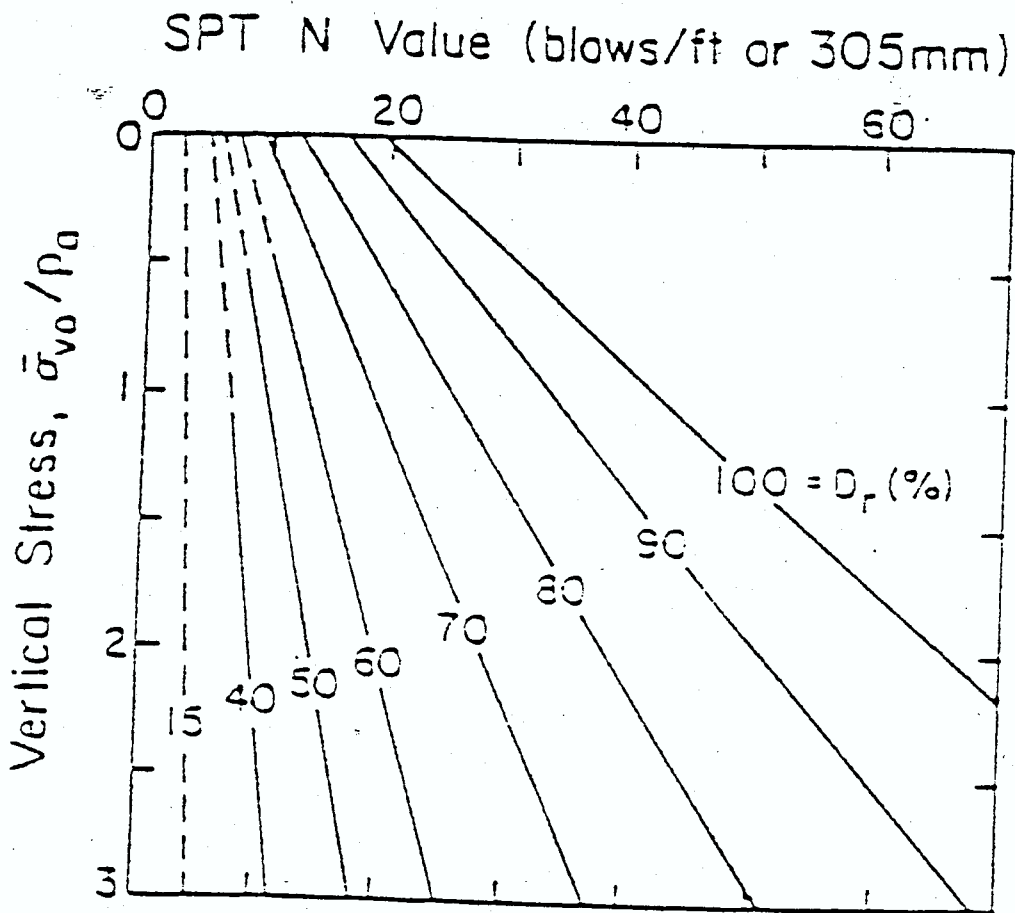


Figure 2.9. Effect of Overburden Stress and  $D_r$  on SPT N Value (Gibbs and Holtz, 1957)

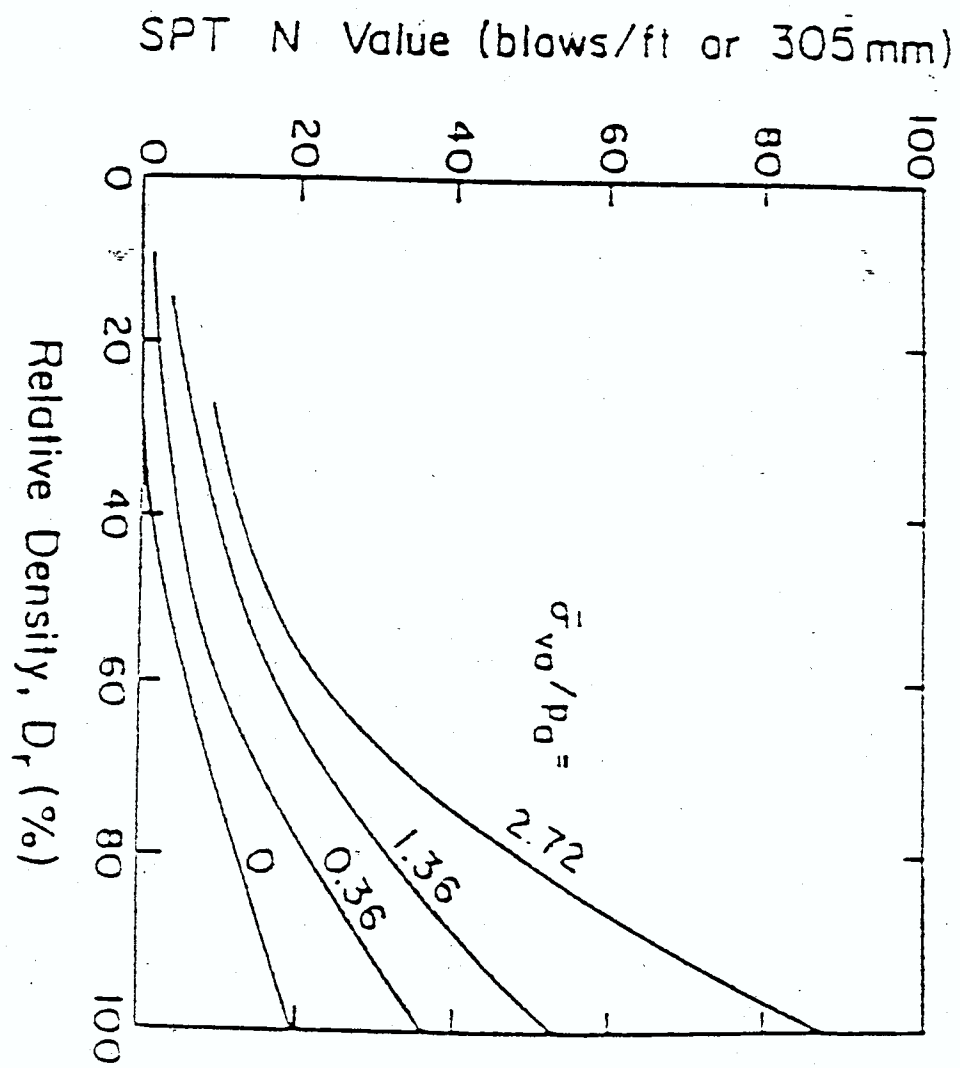


Figure 2.10 Relative Density–N-Stress Relationship  
(Gibbs and Holtz, 1957)

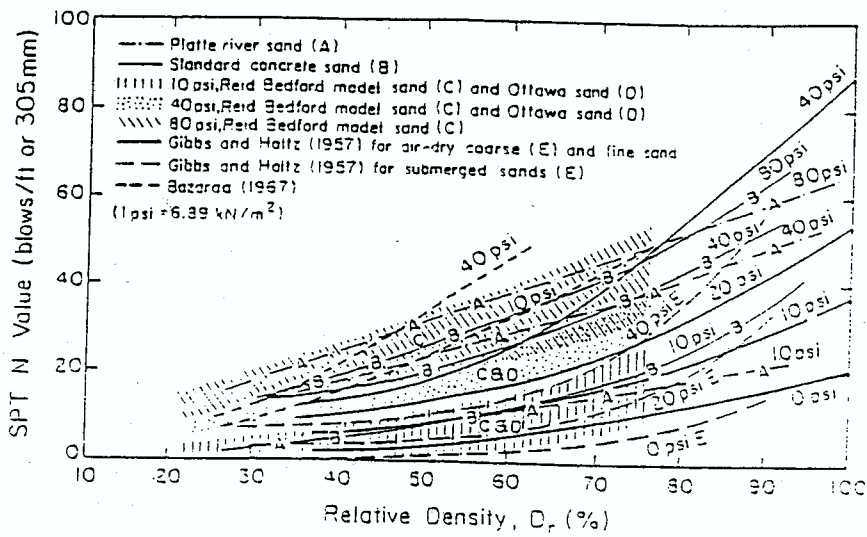


Figure 2.11 Relative Density -N-Stress Relationships for Several Sands (Marcuson and Bieganousky, 1977)

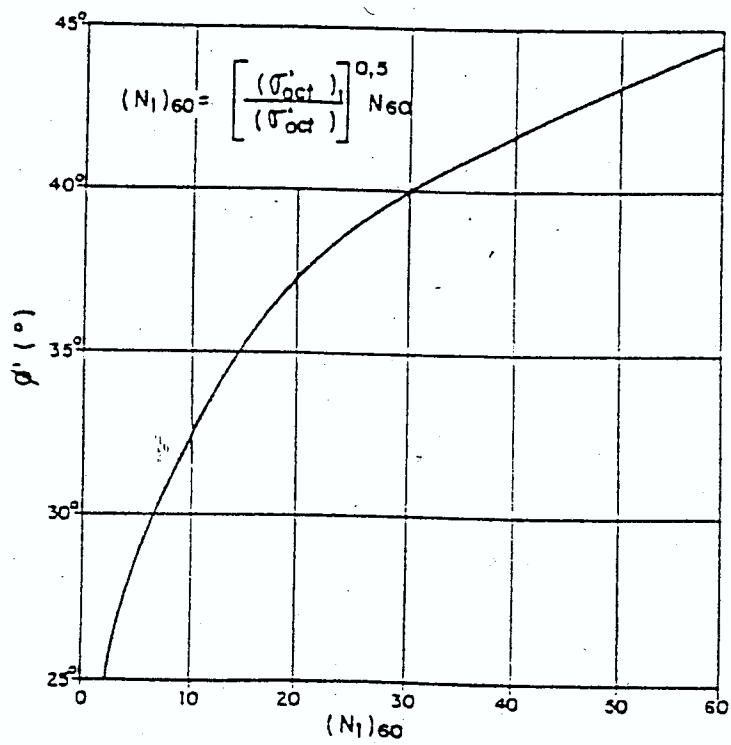
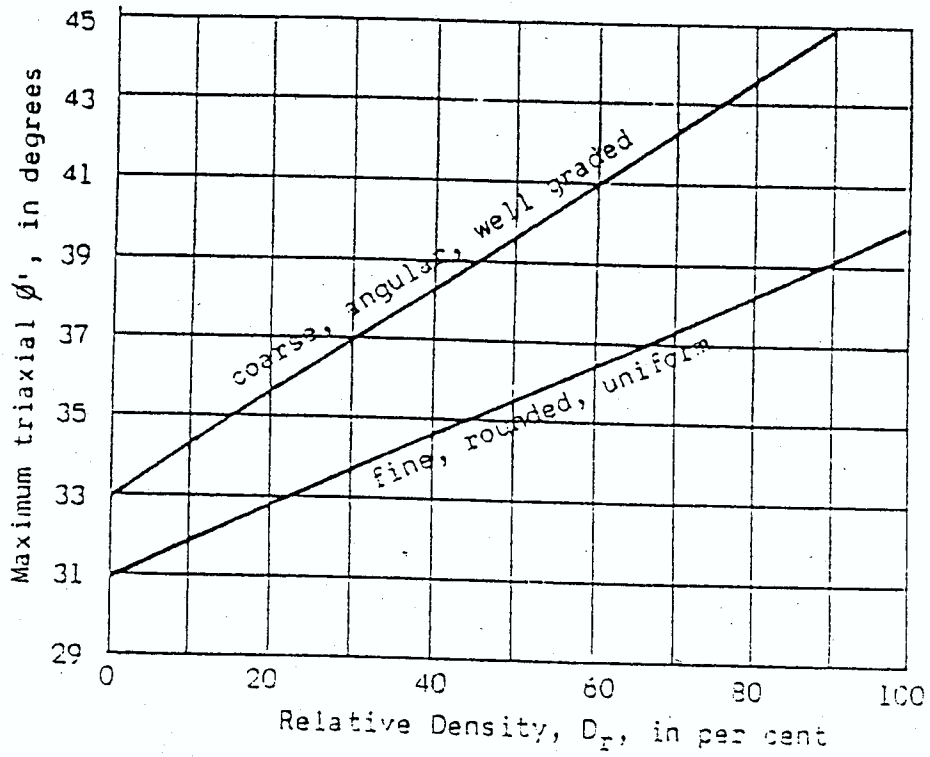


Figure 2.12 Empirical Correlation Between  $N_{60}$  and  $\phi$  for Uncemented Sands  
(Adopted from DeMello, 1971)



**Figure 2.13 Approximate Correlation Between  $\phi'$  and quartz Sands  
(Adopted from Shmertman, 1975)**

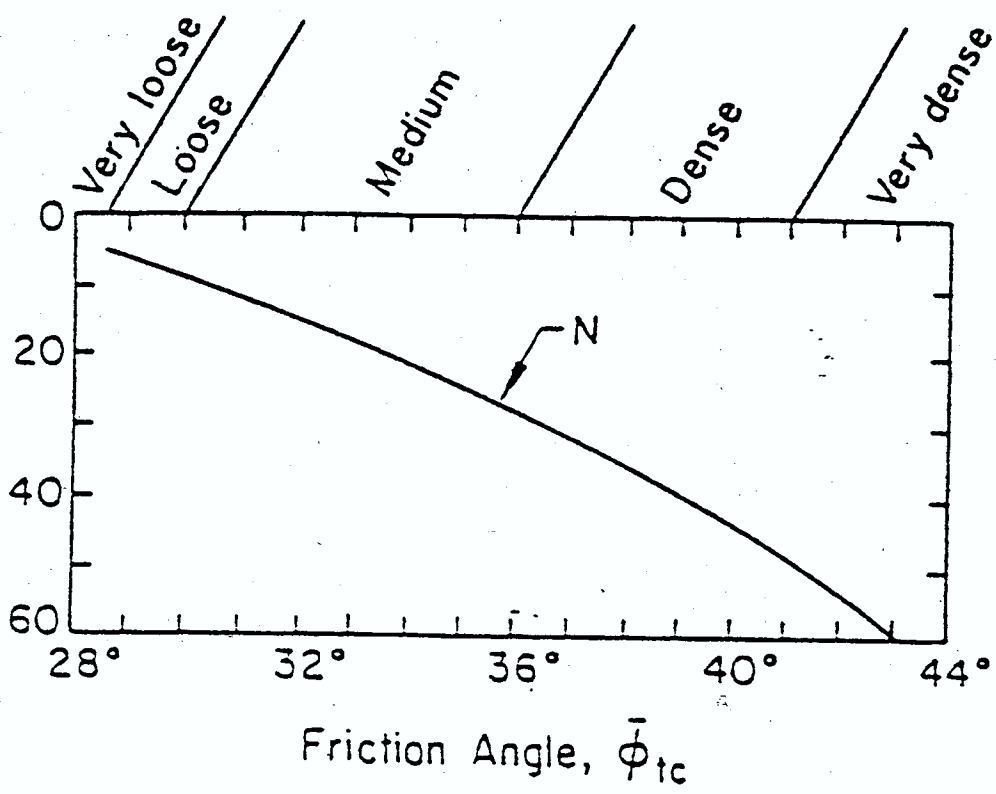


Figure 2.14 N versus  $\bar{\phi}'_{tc}$

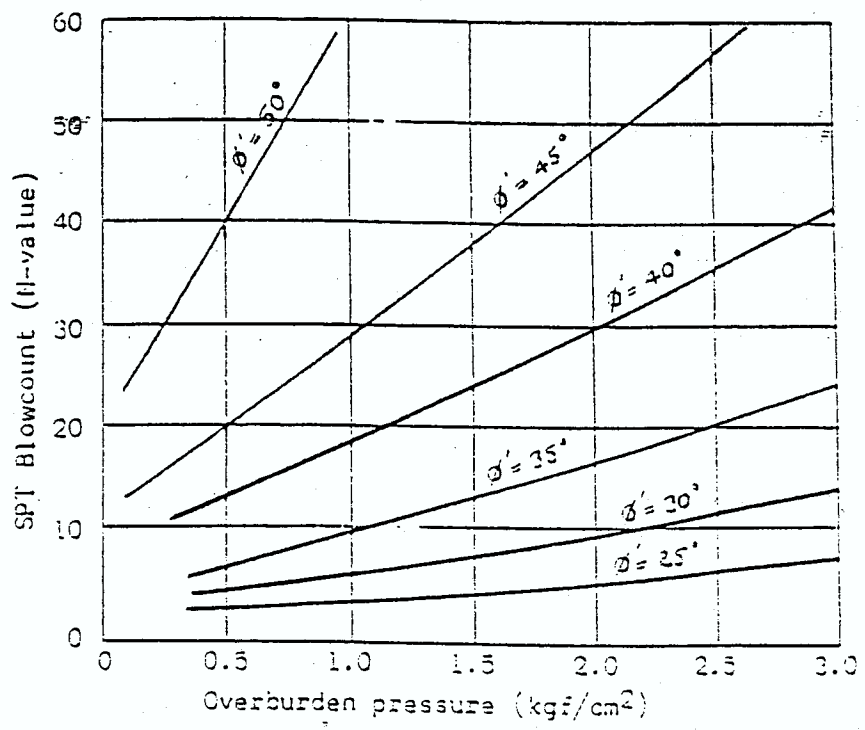


Figure 2.15. N versus Overburden Stress (Schmertmann, 1975)

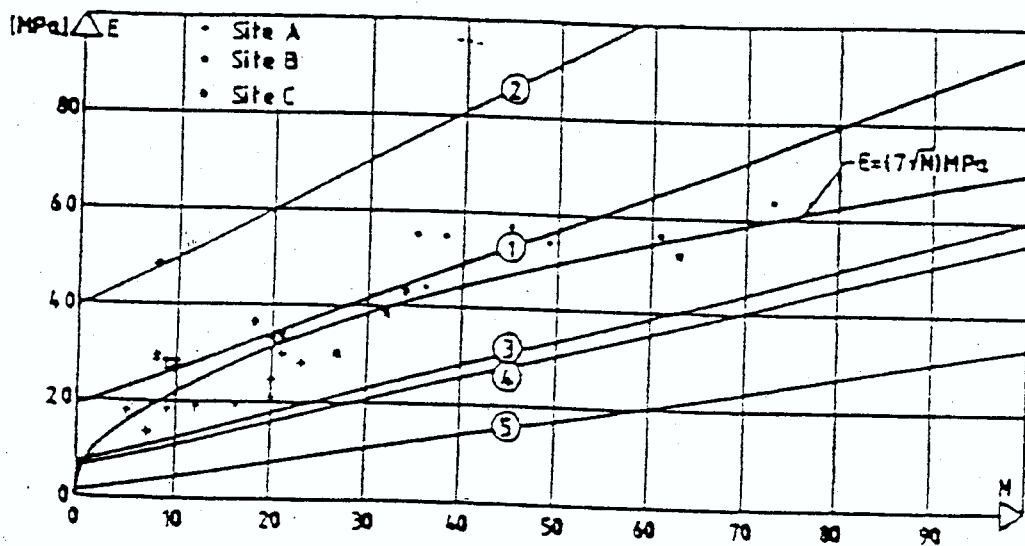


Figure 2.16 Young's Modulus E as A Function of N

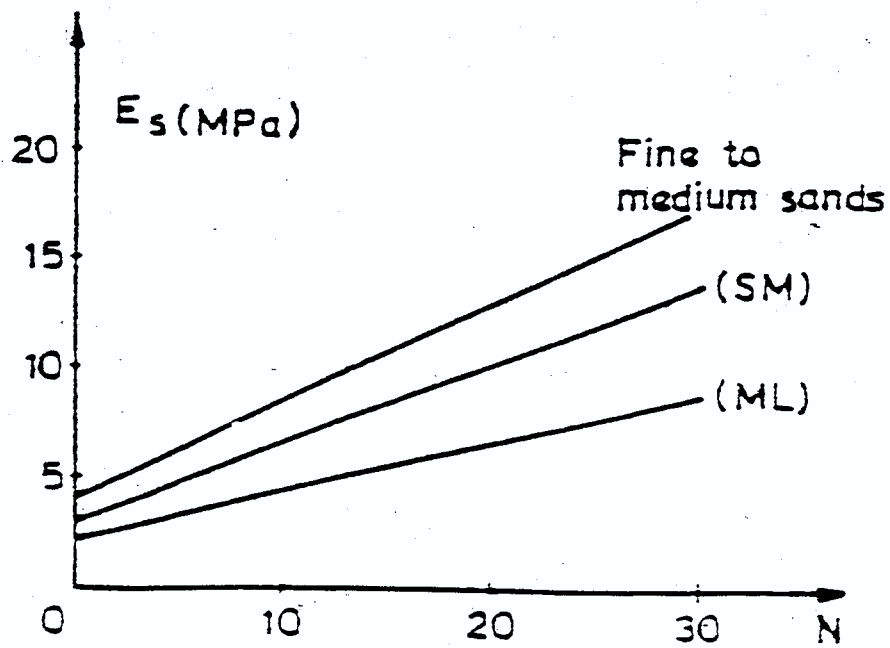


Figure 2.17. Young's Modulus  $E$  as A Function of  $N$  (Anagnostopoulos, 1982)

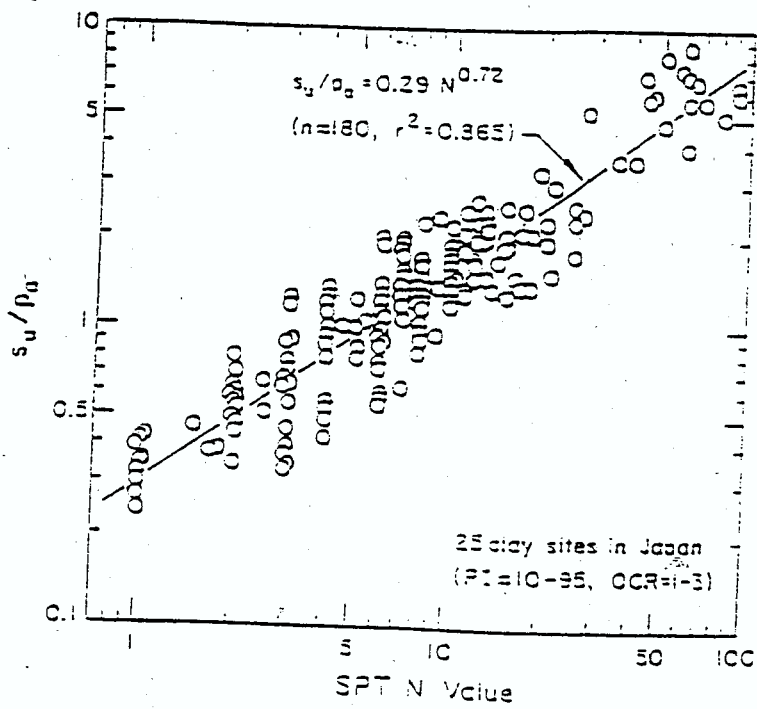


Figure 2.18 Selected Relationships Between N and  $s_u$

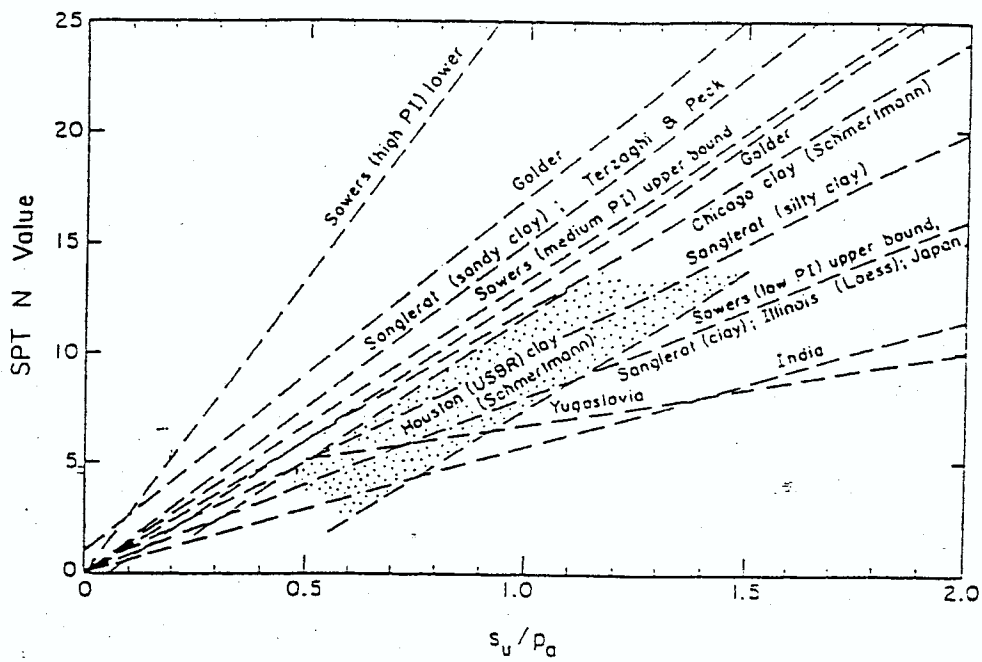


Figure 2.19 Relation Between  $s_u$  and SPT N Value (Hara, 1985)

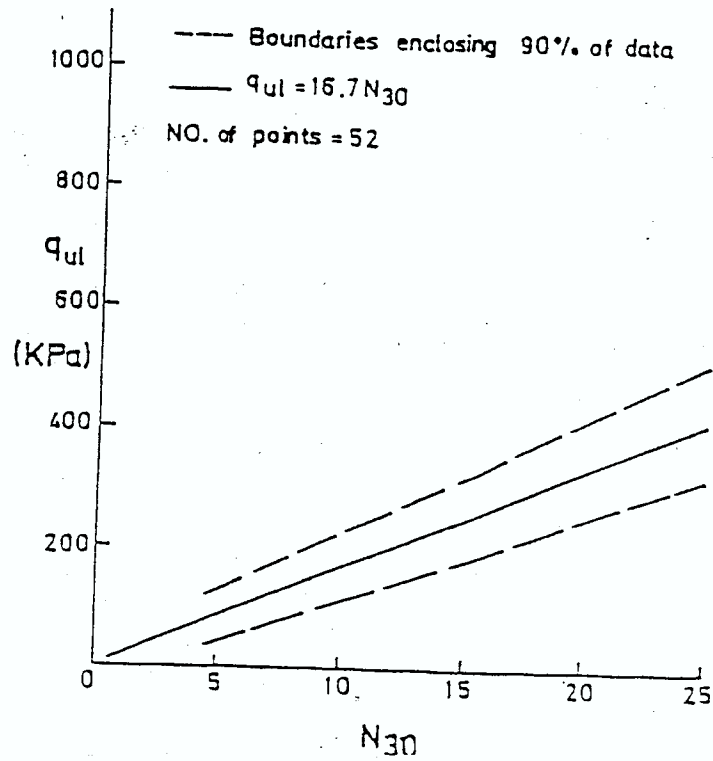


Figure 2.20 Field Unconfined Strength versus SPT N.  
(Behpoor and Ghaharamani, 1989)

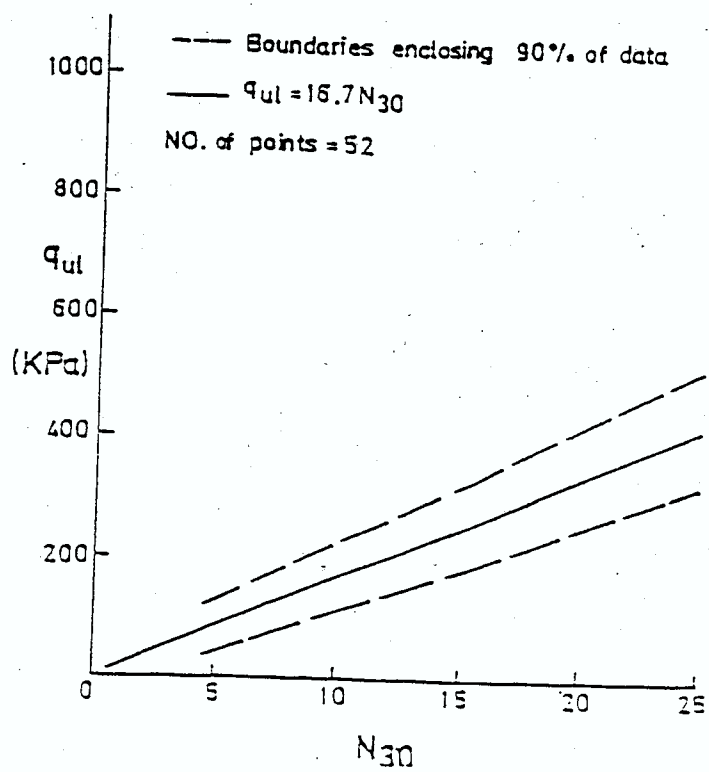


Figure 2.21. Laboratory Unconfined Strength versus SPT N (Behpoor and Ghaharamani, 1989)

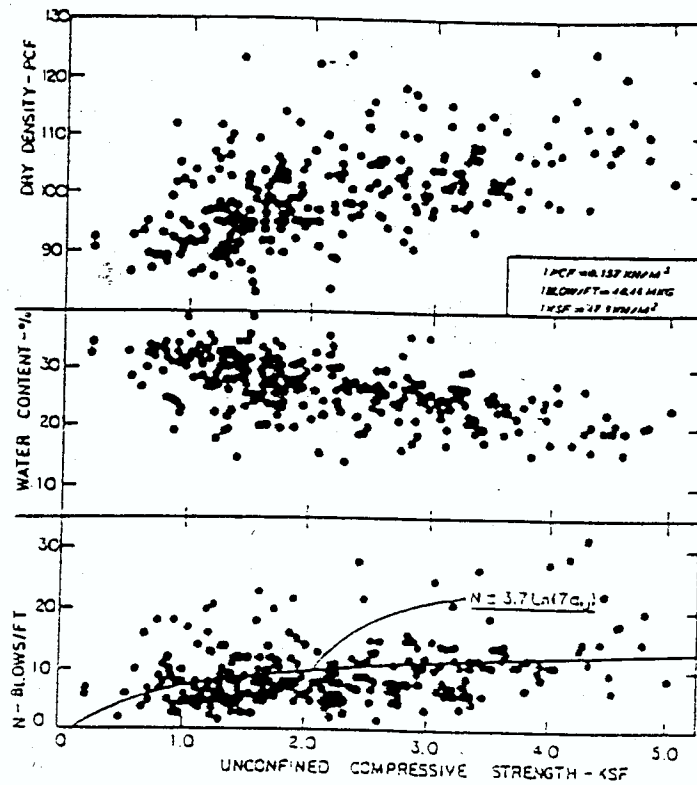


Figure 2.22 Strength and Penetration Resistance versus Depth for Glacial Lake Deposits. (Hegedus and Peterson, 1988)

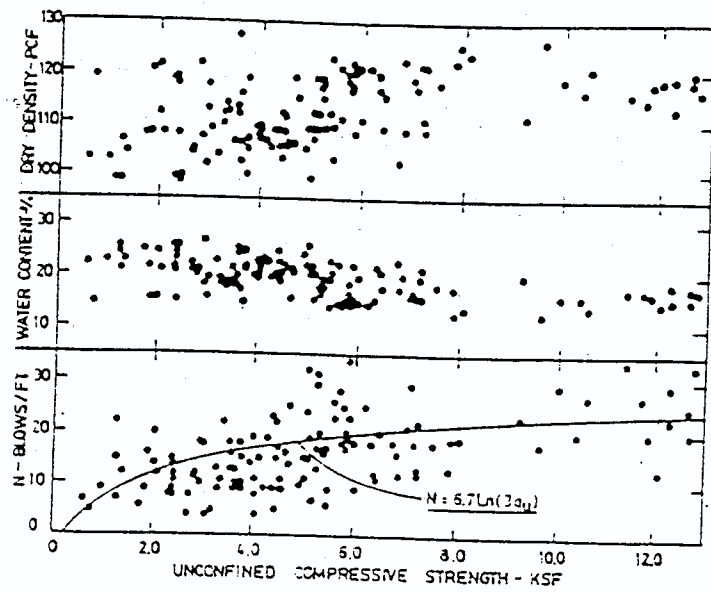


Figure 2.23. Test Data for Glacial Deposits Till Soils ( $S_r \geq 0.9$ ) (Hegedus and Peterson, 1988)

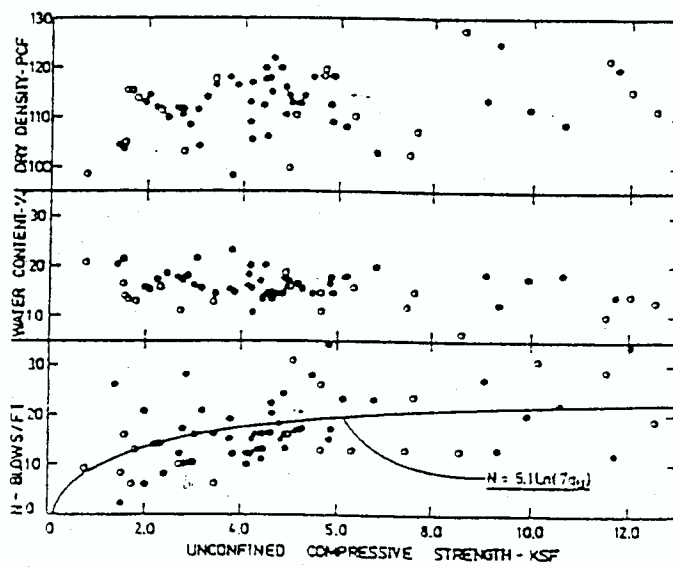


Figure 2.24 Test Data for Glacial Till Soils ( $S_r \geq 0.9$ )  
(Hegedus and Peterson, 1988)

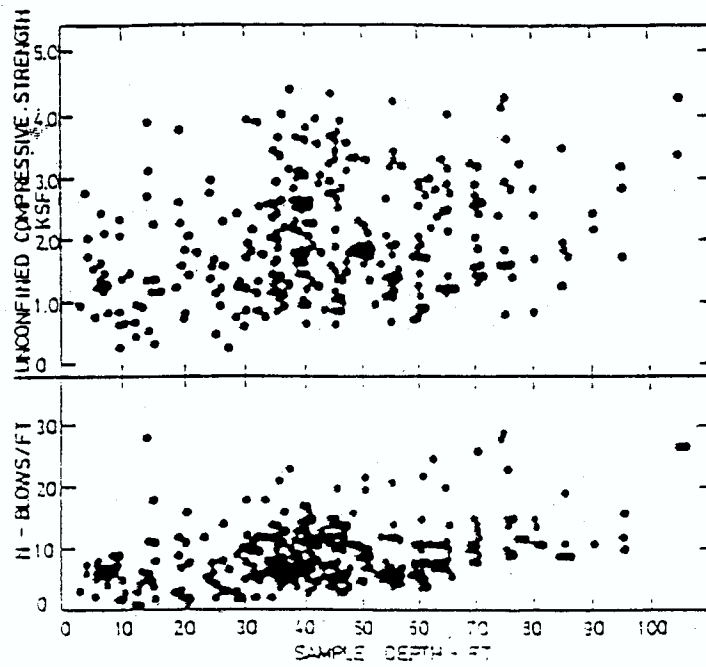


Figure 2.25 Strength and Penetration Resistance versus Depth for Glacial Deposits (Hegedus and Peterson, 1988)

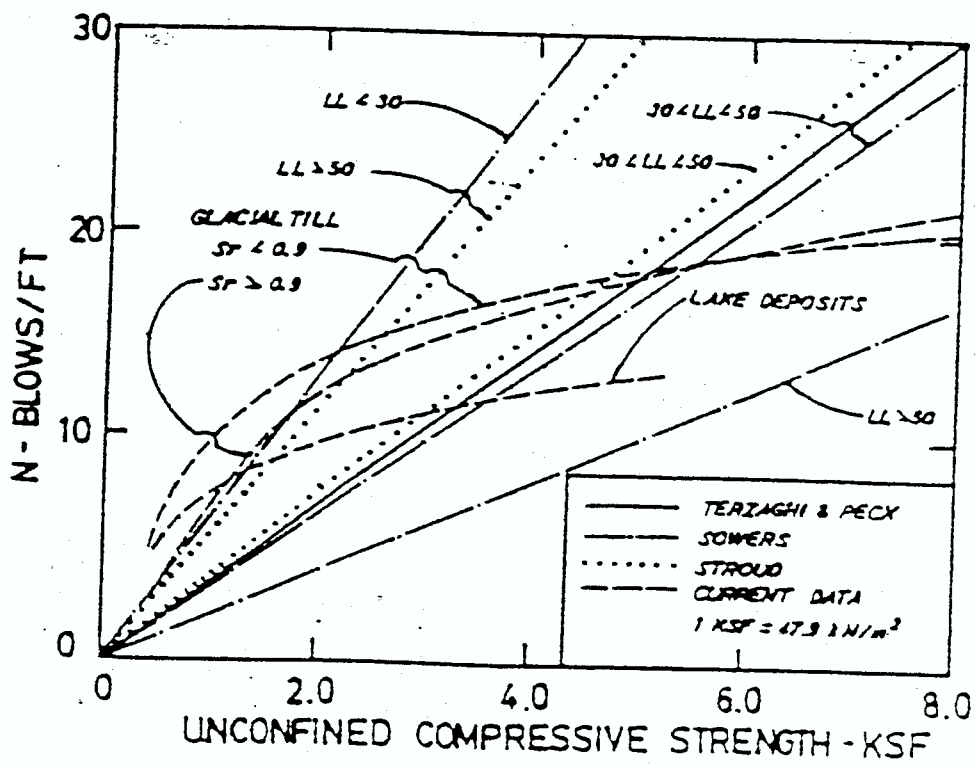


Figure 2.26 Comparison of Published Current Data  
(Hegedus and Peterson, 1988)

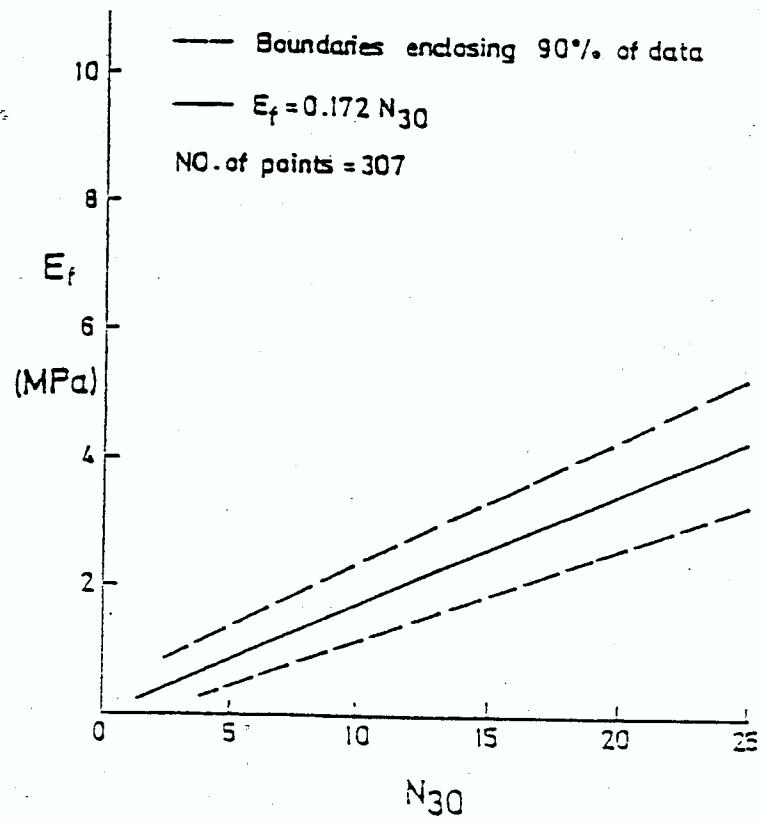


Figure 2.27. Modulus of Elasticity versus SPT N Value (Behpoor and Ghaharamani, 1989)

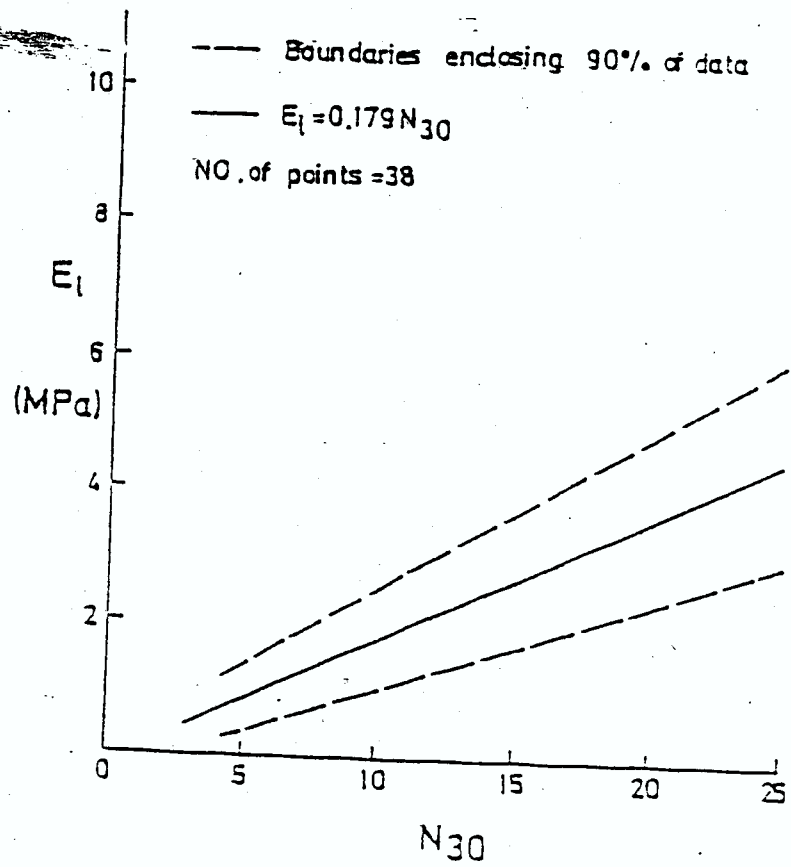
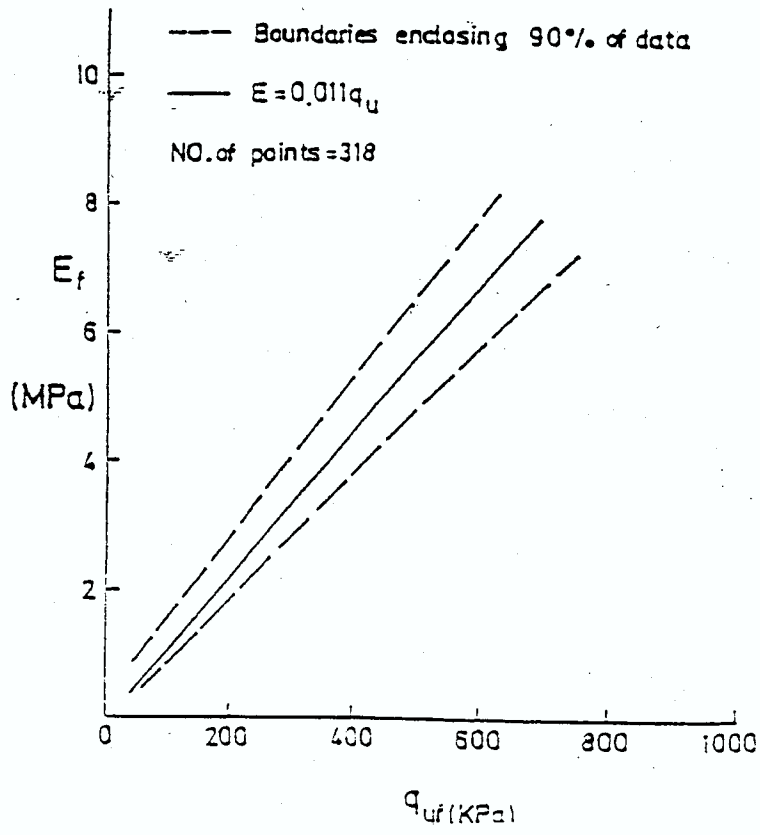


Figure 2.28. Laboratory Modulus of Elasticity versus SPT N Value (Behpoor and Ghaharamani, 1989)



**Figure 2.29. Field Modulus of Elasticity versus Field Unconfined Strength**  
 (Behpoor and Ghaharamani, 1989)

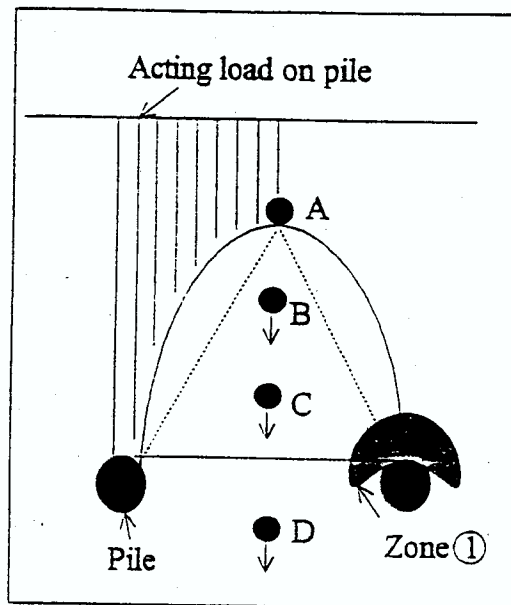


Figure 2.30. Arching Effect (By Adachi, 1990)

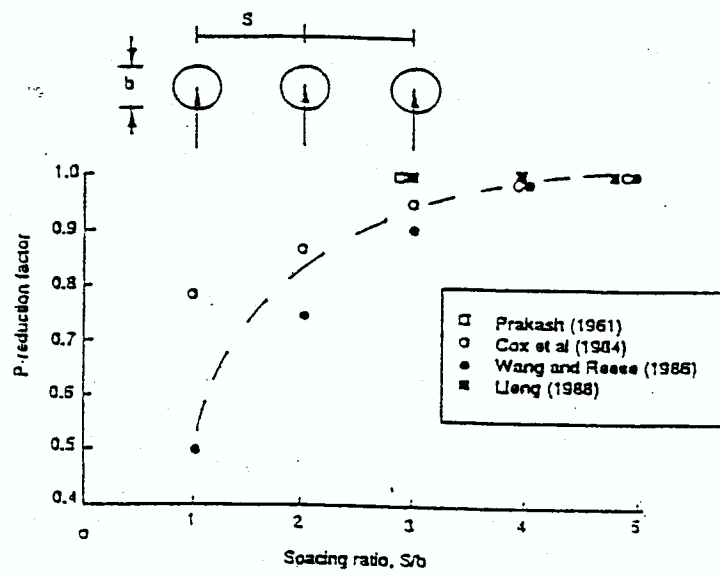


Figure 2.31. P-reduction Factor versus S/b (Reese et al., 1992)

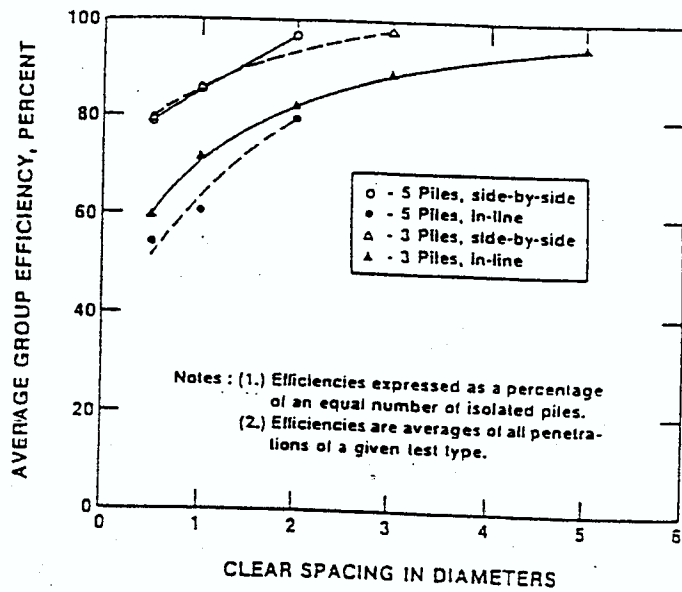


Figure 2.32 Efficiency of Pile Groups (Cox et al., 1984)

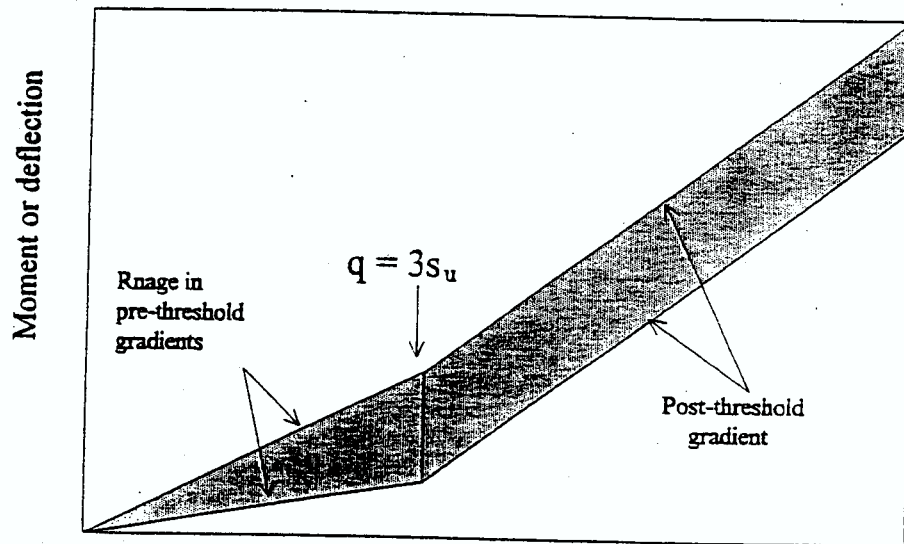


Figure 2.33. Construction of Design Envelopes Using The Empirical Design Charts

**CHAPTER III**

**SPT TO PREDICT DEFLECTION OF Laterally LOADED  
DRILLED SHAFTS**

**3.1 *p-y* CURVES PARAMETERS IN COM624 PROGRAM**

The COM624 computer program is based on an extension of Winkler’s foundation by representing the soil-shaft interaction as a set of nonlinear springs. The load-deflection curves of these nonlinear springs are characterized by the so-called *p-y* curves. The *p-y* curves represent the net soil resistance per unit length at a particular depth versus shaft deflection.

Currently, the *p-y* curves are available for five different soil conditions. These soil conditions are summarized in Table 3.1, along with the references. As can be seen, for the cohesionless soils, the soil parameters needed for constructing the *p-y* curves include the friction angle, the subgrade reaction modulus, and unit weight of the soil. For the cohesive soils, the soil parameters needed for constructing the *p-y* curves are the undrained shear strength determined by the unconfined compression tests, the strain corresponding to 50% of ultimate strength, the subgrade reaction modulus, and the unit weight.

**Table 3.1 Summary of input parameters**

Soil type	Soil stiffness	Soil location	Parameters	Model
Sand	Loose to dense	Above and below GWT	$\phi', k, \gamma$	Reese et al., 1974
Clay	Soft	Above and below GWT	$s_u, \epsilon_{50}, \gamma, k$	Matlock, 1970
	Stiff	Above GWT	$s_u, \epsilon_{50}, \gamma, k$	Reese & Welch, 1974
		Below GWT	$s_u, \epsilon_{50}, \gamma, k$	Reese et al., 1975

Soil information is typically provided in the form of SPT blow count along with a description of soil types. Furthermore, there have been numerous research efforts in developing the correlations between the soil parameters and SPT blow counts. Unfortunately, none of these correlations have been validated for the accuracy in constructing p-y curves and the subsequent prediction of drilled shaft deflections under lateral loads. A recent publication by Anderson and Townsend (2001) appears to be the only attempt in this regard. The database used in Anderson and Townsend study, however, does not include any Ohio test data. This chapter will present a statistically based study in establishing the correlations between the SPT N values and the pertinent p-y curves soil parameters.

### **3.2 GENERAL INFORMATION OF DATABASE**

A database has been developed to contain the lateral load test results as well as information related to the drilled shafts and site soil conditions, including soil types and SPT profiles. The database is consisted of a total of 56 load tests, among which 32 tests were conducted for the Ohio Department of Transportation over the past 5 years. The remaining 26 load test data are collected from the literature. Table 3.2 provides a summary of the load tests, including the dimension of the drilled shafts and soil types at each test site.

**Table 3.2 Laterally loaded drilled shaft and pile parameters for SPT database**

No.	Project Name	Depth of shaft D, ft	Diameter of shaft D, in	Predominant Soil Type	Rock Socket Length, ft	Rock Socket Diameter, in
1	LUC-280, Maumee River	93	102	Clay	1	102
2	I-70 (Columbus, OH), Shaft 1	9.5	30	Clay		
3	I-70 (Columbus, OH), Shaft 2	9.5	30	Clay		
4	I-90 Sound Barriers, Shaft 1	13	30	Clay		
5	I-90 Sound Barriers, Shaft 2	12	30	Clay		
6	I-90 Sound Barriers, Shaft 3	8'-8"	30	Clay		
7	I-90 Sound Barriers, Shaft 4	8'-5"	30	Clay		
8	Lake-91(South Abutment) Shaft 5	17	48/36	Clay/Shale	8	36
9	Lake-91(South Abutment) Shaft 8	17	48/36	Clay/Shale	8	36
10	Lake-91 (North Abutment) Shaft 67	20	48/36	Clay/Shale	11	36
11	Lake-91 (North Abutment) Shaft 70	20	48/36	Clay/Shale	11	36
12	Lorain-6, Shaft 19	36	48/36	Clay/Shale	6.2	36

**Table 3.2 Laterally loaded drilled shaft and pile parameters for SPT database**

No.	Project Name	Depth of shaft D, ft	Diameter of shaft d, in	Predominant Soil Type	Rock Socket Length, ft	Rock Socket Diameter, in
13	Lorain-6, Shaft 20	39	48/36	Clay/Shale	7.2	36
14	Lorain, Shaft 22	24	48	Clay		
15	Lorain-6, Shaft 22	24	48	Clay		
16	Lorain-6, Shaft 23	38.6	48/36	Clay/Shale	6.5	36
17	Lorain-6, Shaft 88	13	48	Clay		
18	Lorain-6, Shaft 89	39	48/36	Clay/Shale	6.3	36
19	Lorain-6, Shaft 91	39	48/36	Clay/Shale	6.1	36
20	Lorain-6, Shaft 92	37	48/36	Clay/Shale	4.0	36
21	WAS-PUT St. Bridge, Shaft 1	46	48	Clay		
22	WAS-PUT St. Bridge, Shaft 2	46	48	Clay		
23	WAS-PUT St. Bridge, Shaft 1	29.5	48	Clay		
24	WAS-PUT St. Bridge, Shaft 1	29.5	48	Clay		
25	HAM/CLE-50, Shaft T25	18	42	Clay/Shale	7	42

**Table 3.2 Laterally loaded drilled shaft and pile parameters for SPT database** **Con'd**

No.	Project Name	Depth of shaft D, ft	Diameter of shaft d, in	Predominant Soil Type	Rock Socket Length, ft	Rock Socket Diameter, in
26	HAM/CLE-50, Shaft T27	18	42	Clay/Shale	7	42
27	HAM/CLE-50, Shaft T21	26	48	Clay		
28	HAM/CLE-50, Shaft T23	26	48	Clay		
29	CUY-90-15.24, Shaft 1	141	72	Clay		
30	CUY-90-15.24, Shaft 3	141	72	Clay		
31	I-90 Noise Wall, Shaft 1 (P101)	12	30	Clay		
32	I-90 Noise Wall, Shaft 2 (P100)	10	36	Clay		
33	10.75" Dia. Steel Pipe Pile <sup>1)</sup>	38.7	10.75	Clay		
34	48" Dia Steel Pipe Pile <sup>1)</sup>	37.5	48	Clay		
35	72" Dia. Drilled Shaft <sup>1)</sup>	36.2	72	Clay		
36	Roosevelt Bridge <sup>2)</sup>	46	30	Sand		
37	Caisson Pile, Case 3 <sup>3)</sup>	26	48	Sand		

**Table 3.2 Laterally loaded drilled shaft and pile parameters for SPT database** **Con'd**

No.	Project Name	Depth of shaft D, ft	Diameter of shaft d, in	Predominant Soil Type	Rock Socket Length, ft	Rock Socket Diameter, in
38	Caisson Pile, Case 4 <sup>3)</sup>	26	30	Sand		
39	Caisson Pile, Case 5 <sup>3)</sup>	26	30	Sand		
40	Caisson Pile, Case 6 <sup>3)</sup>	26	30	Sand		
41	Caisson Pile, Case 7 <sup>3)</sup>	26	20	Sand		
42	Caisson Pile, Case 8 <sup>3)</sup>	26	20	Sand		
43	Precast Concrete Pile, Pile 26 <sup>3)</sup>	41	20	Sand		
44	Precast Concrete Pile, Pile 27 <sup>3)</sup>	41	20	Sand		
45	Pored Pile, Case 10, Pile 1 <sup>3)</sup>	78	48	Sand		
46	Pored Pile, Case 10, Pile 2 <sup>3)</sup>	78	48	Sand		
47	Franki Pile, Case 11 <sup>3)</sup>	37	16	Sand		
48	Franki Pile, Case 12 <sup>3)</sup>	37	16	Sand		
49	Franki Pile, Case 13 <sup>3)</sup>	37	20.5	Sand		
50	Franki Pile, Case 14 <sup>3)</sup>	37	20.5	Sand		

**Table 3.2 Laterally loaded drilled shaft and pile parameters for SPT database**

No.	Project Name	Depth of shaft D, ft	Diameter of shaft d, in	Predominant Soil Type	Rock Socket Length, ft	Rock Socket Diameter, in
51	Franki Pile, Case 15 <sup>3)</sup>	37	21	Sand		
52	Bored Pile, Case 16 <sup>3)</sup>	37	28	Sand		
53	Precast Concrete, SB-2 <sup>4)</sup>	60	16	Sand		
54	Concrete Filled Steel Pile, P-3 <sup>4)</sup>	65	16	Sand		
55	Precast Concrete Square Pile, C-6 <sup>4)</sup>	60	16	Sand		
56	Cast-in-Place Concrete Pile R-5A <sup>4)</sup>	60	16.375	Sand		
57	Bored Concrete Pile, Shaft 1 <sup>5)</sup>	95	16	Clay	3 m	0.4 m
58	Bored Concrete Pile, Shaft 2 <sup>5)</sup>	20	27	Clay	2 m	0.68 m

Note: <sup>1)</sup> Todd W. Dunnavant, Dissertation, “Experimental Investigation of the Behavior of Single Piles in Overconsolidation Clay

Subjected to Cyclic Lateral Loads”, University of Houston.

<sup>2)</sup> Townsend et al., “Prediction and Evaluation of a Laterally Loaded Pile Group at Roosevelt Bridge”, FDOT

<sup>3)</sup> L. Decourt, “Load-Deflection Prediction for Laterally Loaded Pile Based on N-SPT Values”

<sup>4)</sup> S. Kumar, “Lateral Load-Deflection Response of Single Piles in Sand”, EJGE

<sup>5)</sup> C. F. Leung & Y. K. Chow, “Performance of Laterally Loaded Socketed Pile”, National University of Singapore.

### 3.3 CORRELATION STUDIES

A significant amount of work has been carried out by the researcher to investigate the sensitivity of various correlations reviewed in Chapter II. Particularly, for sand, the correlations between SPT N values and friction angle and subgrade modulus, suggested by Peck, et al. (1974), Terzaghi (1955), Gibbs and Holtz (1957), and Teng (1962) were investigated. After carefully evaluating the predictions made by these correlations, a suggested correlation for cohesionless soils is given in Table 3.3.

**Table 3.3 Modified correlation of cohesionless soil for predicting lateral deflection**

SPT-N		2 to 4	4 to 10	10 to 20	20 to 30	30 to 50	50 to 60
$\phi$		25 to 35	20 to 38	33 to 41	35 to 43	37 to 45	39 to 48
$k_s$ lb/in <sup>3</sup>	A.W.T.	< 25	25	90	90	225	250
	B.W.T.	< 20	20	60	60	125	140
$\gamma_{moist}$ pcf	Min.	104 to 108	108 to 112	115 to 120	120 to 125	124 to 128	128 to 130
	Max.	114 to 118	120 to 124	122 to 130	128 to 132	130 to 145	140 to 145

Similarly, for cohesive soils, various correlations reviewed in Chapter II were investigated. Based on extensive sensitivity study results of these correlations, a suggested correlation for cohesive soils is presented in Table 3.4.

**Table 3.4 Modified correlations of cohesive soil for predicting lateral deflection**

$N_{1,60}$	0 to 2	2 to 4	4 to 8	8 to 16	16 to 32	32 to 64
$S_u$ (psi)	0 to 1.88	1.88 to 3.75	3.75 to 7.53	7.53 to 15.00	15.00 to 30.00	30.00 to 55.6
$\epsilon_{50}$	> 0.02	0.02-0.001	0.01 to 0.007	0.007 to 0.005	0.005 to 0.004	0.004 to 0.002
$k_s$ (lb/in <sup>3</sup> )	< 30	30	100	500	1000	2000
$\gamma_{sat}$ (pcf)	100 to 120	110 to 130	110 to 130	120 to 135	130 to 145	140 to 145

### 3.4 EVALUATIONS OF THE RECOMMENDED CORRELATIONS

The correlations recommended in previous section are used to generate the pertinent soil parameters as an input into the computer program COM624 for analyzing each load test. The calculated drilled shaft deflections at the point of load application are compared with the measured and presented in Fig. 3.1 and Fig. 3.2 for cohesive soil and cohesionless soil sites, respectively. In general, each load test would provide about eight comparison points corresponding to different load levels.

In order to gain a better understanding of the accuracy of the calculations based on the recommended correlations, a numerical index,  $r$ , is introduced as given in Eq. (3.1)

$$r = \frac{\sum \frac{D_m}{D_p}}{n} \quad (3.1)$$

$$RSD = \sqrt{\frac{\sum ((D_p - D_m)/D_p)^2}{n - 1}}$$

Where  $n$  = number of samples,  $D_p$  = predicted deflection,  $D_m$  = measured deflection, RSD = relative standard deviation. To further differentiate the quality of predictions, the comparisons are made for four different ranges of load levels, i.e. 0-25%, 25-50%, 50-75%, and 75-100% of the maximum applied load for each load test. These plots are shown in Figs.3.3 to 3.6 for clay sites, and Figs. 3.7 to 3.10 for sand sites, respectively. Also shown in the figures are the best-fit equations and the  $R^2$  of the regression analysis. Table 3.5 provides a summary of the quantitative comparison index  $r$  and the corresponding standard deviations, while Table 3.6 gives a summary of the curve fitting equation and the corresponding  $R^2$ .

**Table 3.5 Statistical analysis of correlations**

Soil Type	Load Range	0-25%	25-50%	50-75%	75-100%	Total
Clay	r	1.1016	1.0260	0.8301	0.9240	0.9581
	RSD	43%	53%	36%	30%	38%
Sand	r	0.9120	0.7742	0.7800	0.8820	0.8324
	RSD	54%	32%	28%	22%	37%

**Table 3.7 Statistical analysis**

Soil Type	Load	0-25%	25-50%	50-75%	75-100%	0-100%
Clay	Equation	$y=1.035x$	$y=0.837x$	$y=0.914x$	$y=0.964x$	$y=0.932x$
	R <sup>2</sup>	0.626	0.529	0.721	0.784	0.899
Sand	Equation	$y=0.721x$	$y=0.745x$	$y=0.747x$	$y=0.930x$	$y=0.889x$
	R <sup>2</sup>	0.848	0.737	0.740	0.828	0.769

Note:  $R^2 = \frac{(\sum (D_p - \bar{D}_p)(D_m - \bar{D}_m))^2}{\sum (D_p - \bar{D}_p)^2 \sum (D_m - \bar{D}_m)^2}$ ;  $D_p$  = Predicted deflection,  $D_m$  = Measured deflection

Based on the above correlation studies, the best-fit regression lines can be seen often lie below the 45 degree line, indicating that the predictions are generally larger than the measured deflections at various load levels. This is acceptable because the predictions tend to be on safe side. However, in the lower load level, say 0-25% of the ultimate applied load, the predicted deflections tend to be slightly less than the measured. However, since most of the working load will be in the 30 to 50% of the maximum applied load, underprediction of the shaft deflection in the small load level may not be critical.

In attempting to develop the correlations between the SPT N values and pertinent soil parameters needed for constructing p-y curves, one needs to keep in mind that actual

drilled shaft behavior under load is a complex phenomenon. Factors other than soil properties, such as construction method, drilled shaft properties and dimensions, and load testing details, could also exert significant influences on the measured drilled shafts deflections. In addition, further study on the effect of nonlinear EI of the drilled shafts on the prediction accuracy is warranted. Nevertheless, given the fact that SPT data will be available for all ODOT project sites, the development of such correlations between the soil parameters and SPT N values is highly useful and practical.

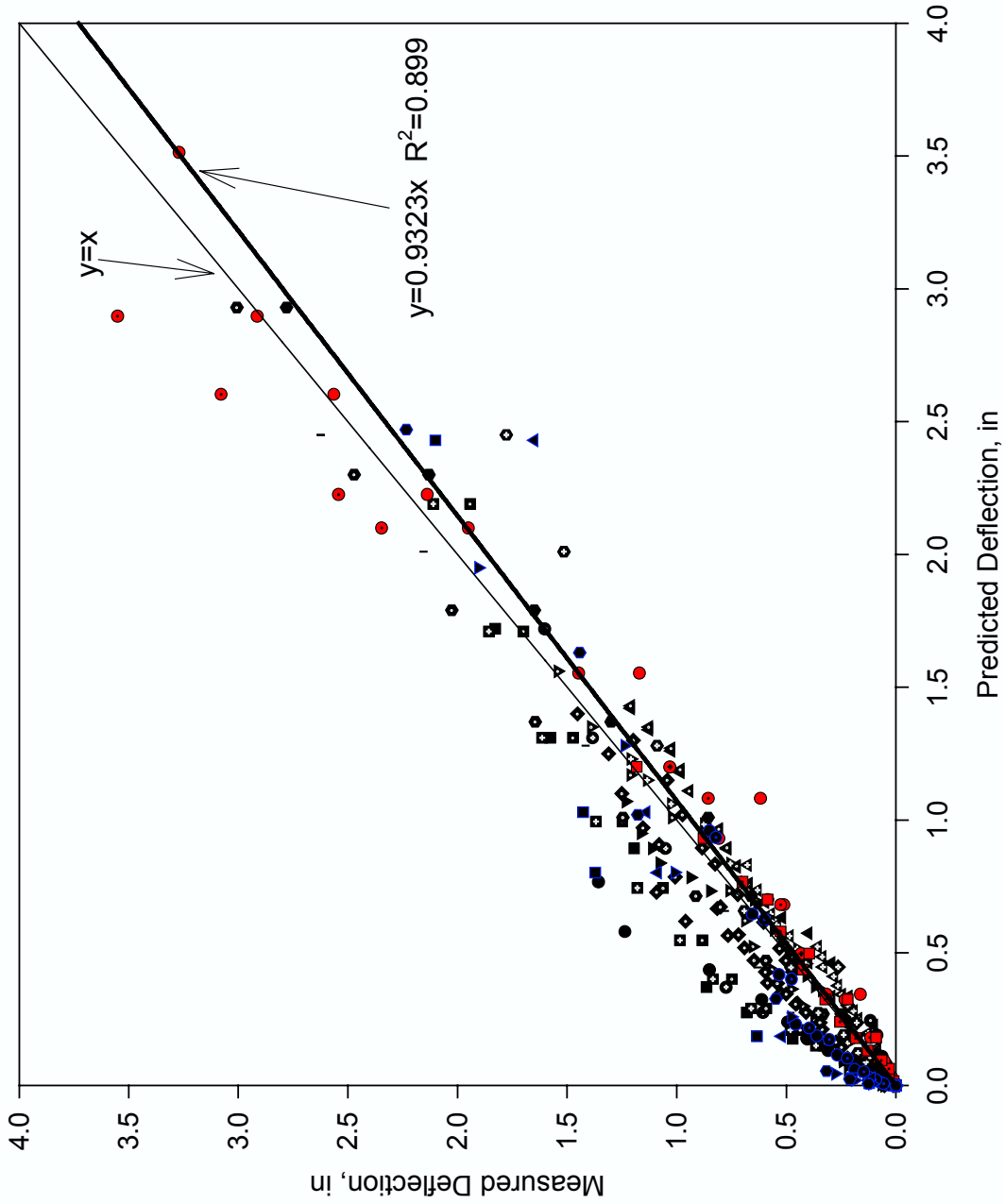


Fig. 3.1 SPT Database Statistics for Cohesive Soil

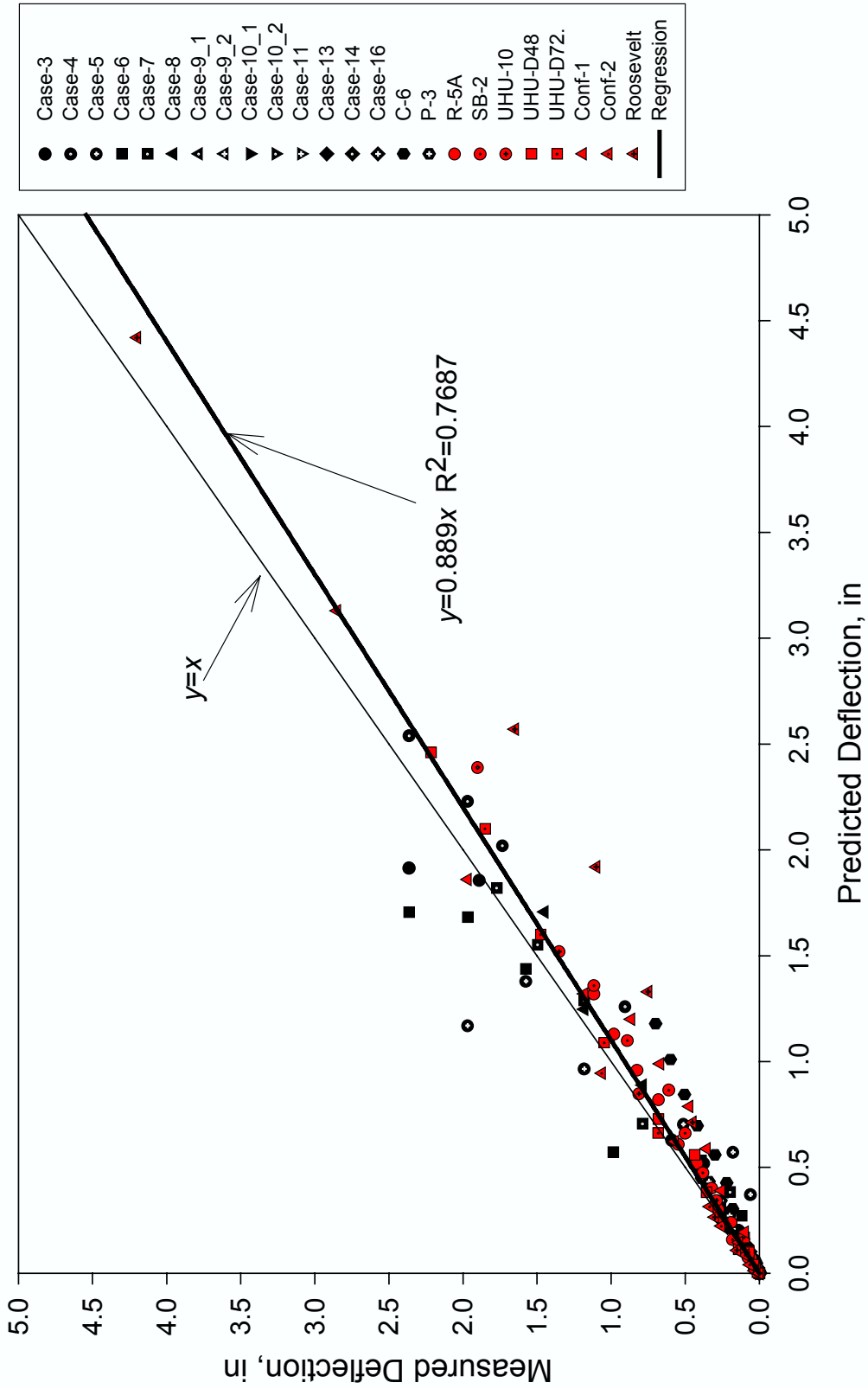


Fig. 3.2 SPT Database Statistics for Cohesionless Soil

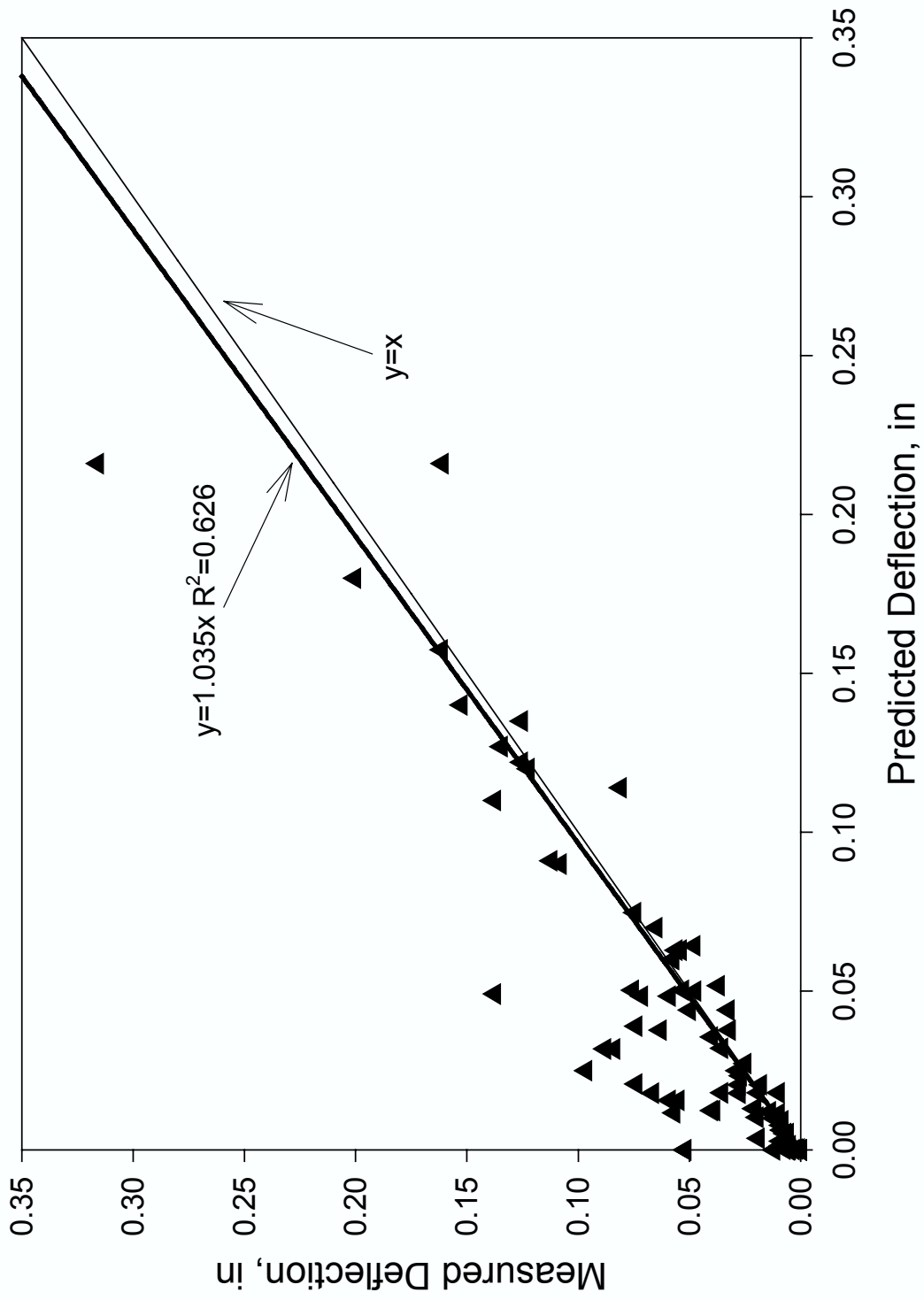


Fig. 3.3 SPT Database Statistics (0~25% Lateral Load) for Cohesive Soil

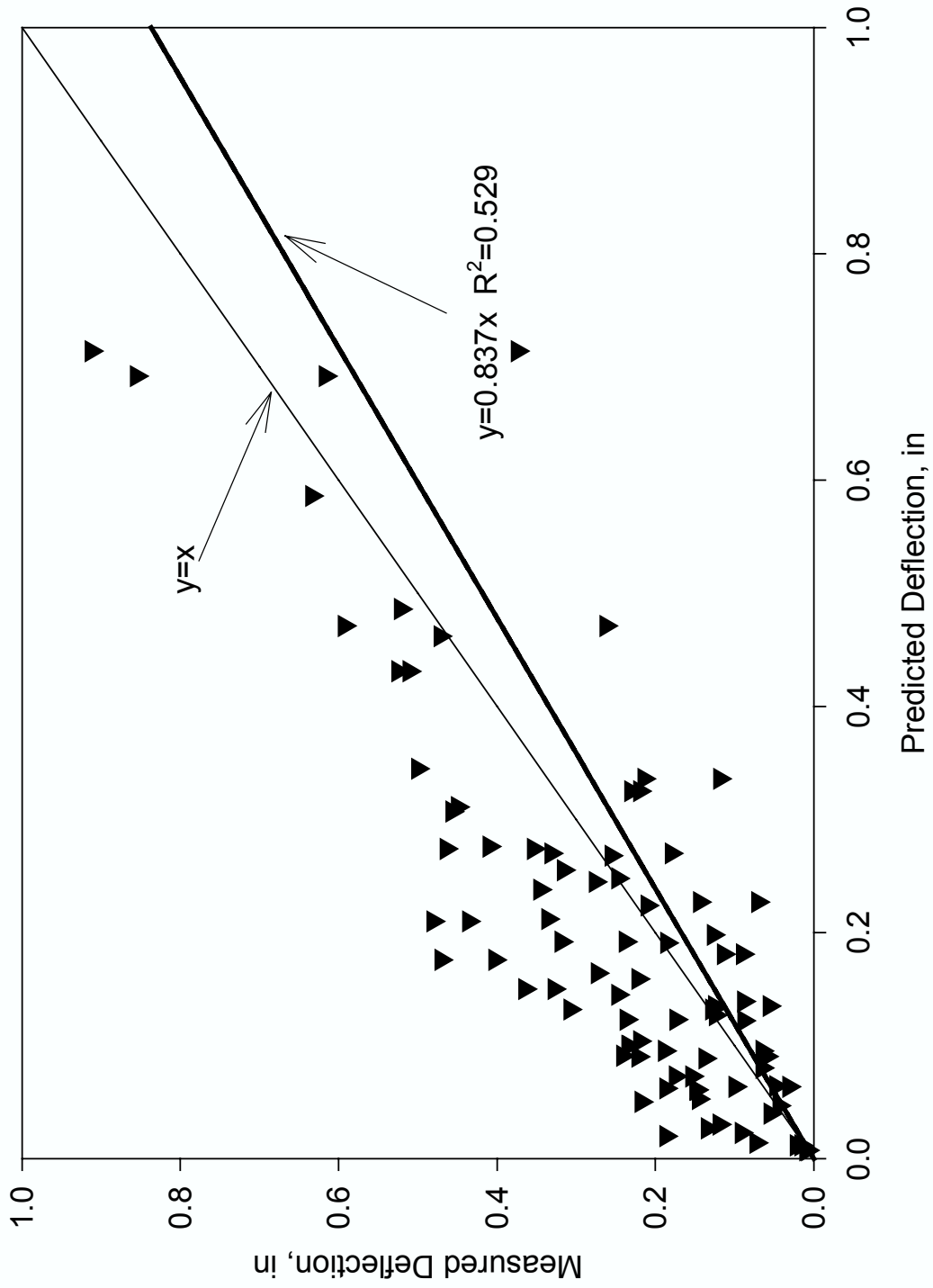


Fig. 3.4 SPT Database Statistics (25%-50% Lateral Load) for Cohesive Soil

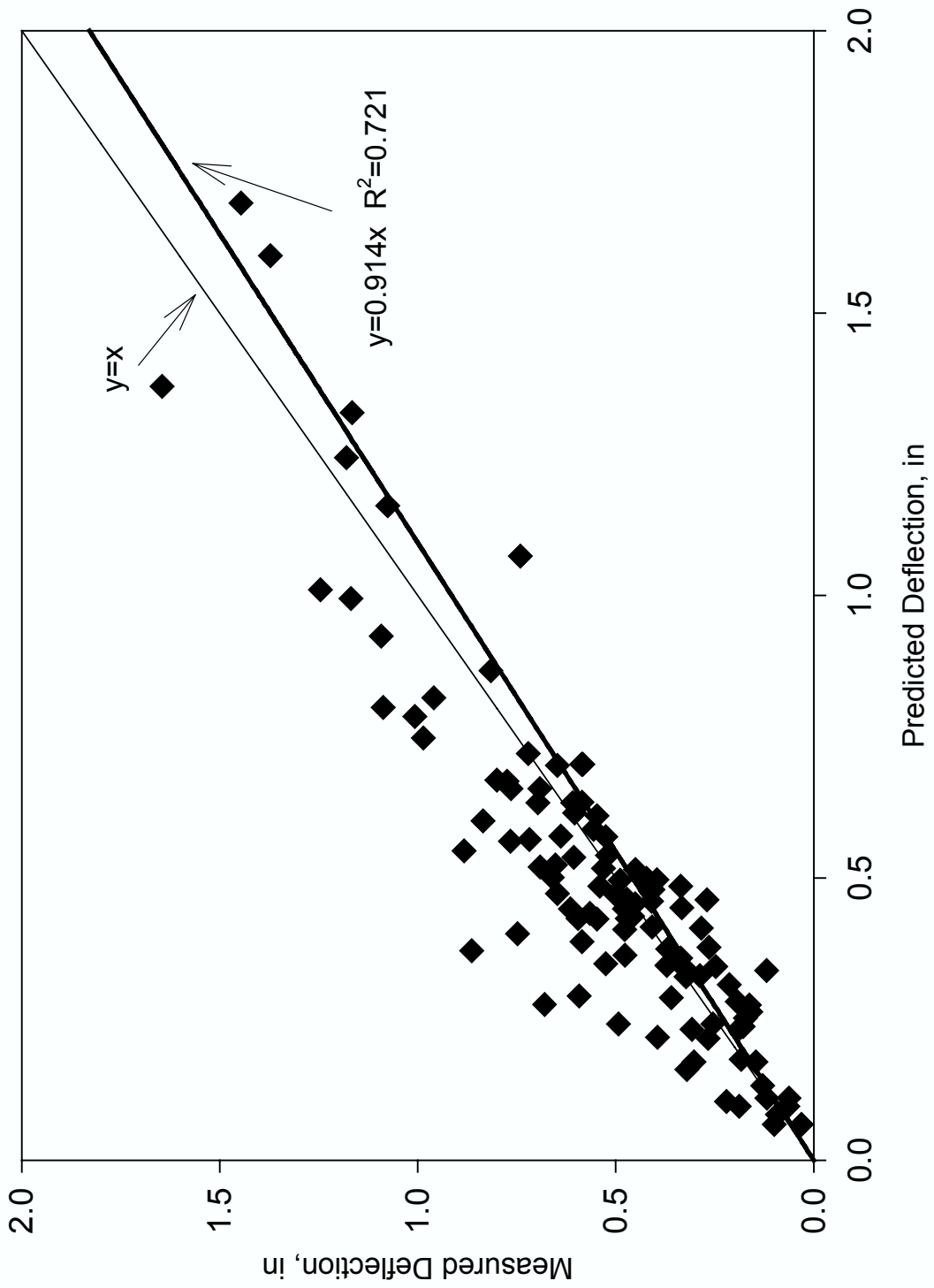


Fig. 3.5 SPT Database Statistics (50%~75% Lateral Load) for Cohesive Soil

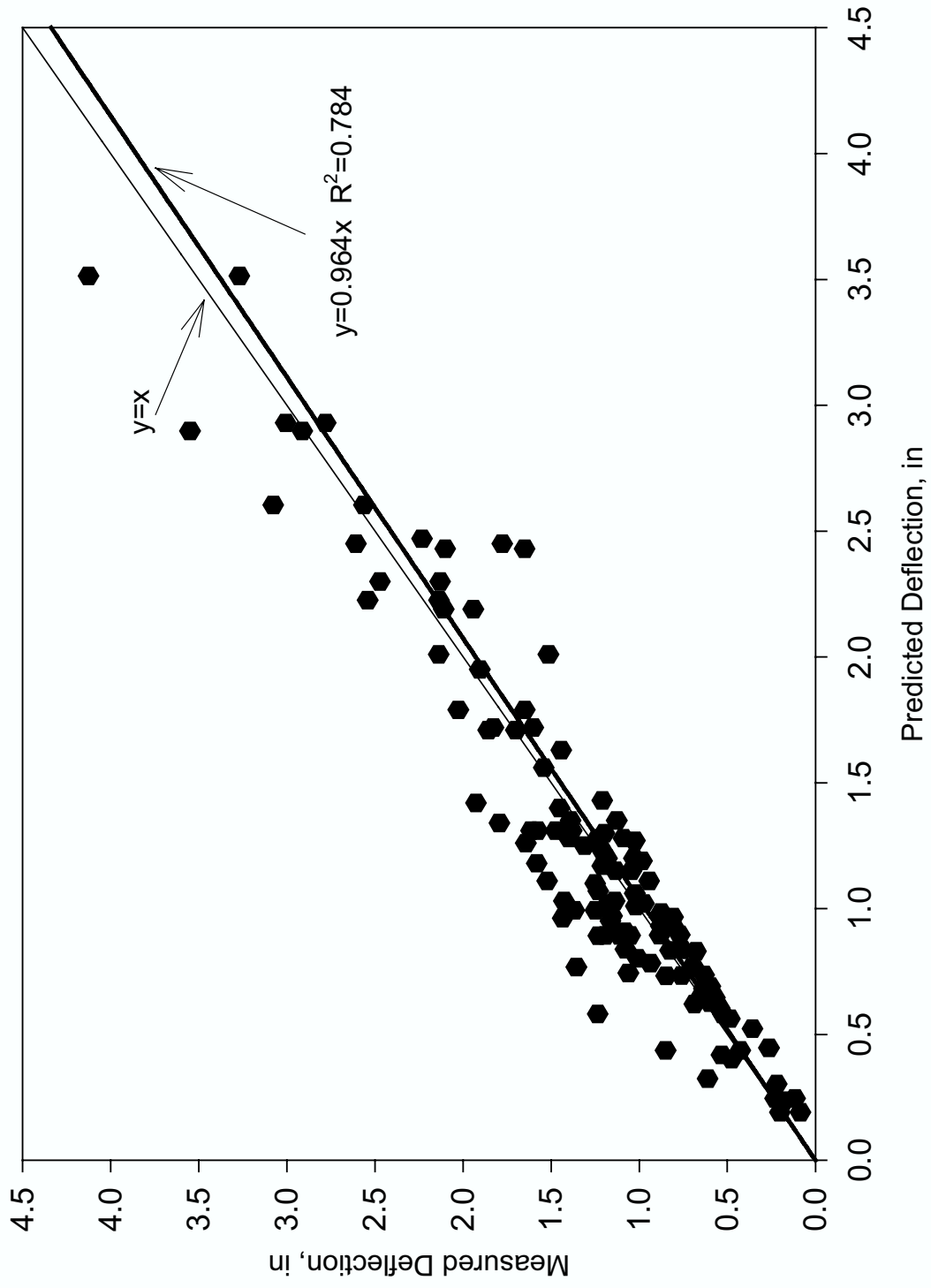


Fig. 3.6 SPT Database Statistics (75%~100% Lateral Load) for Cohesive Clay

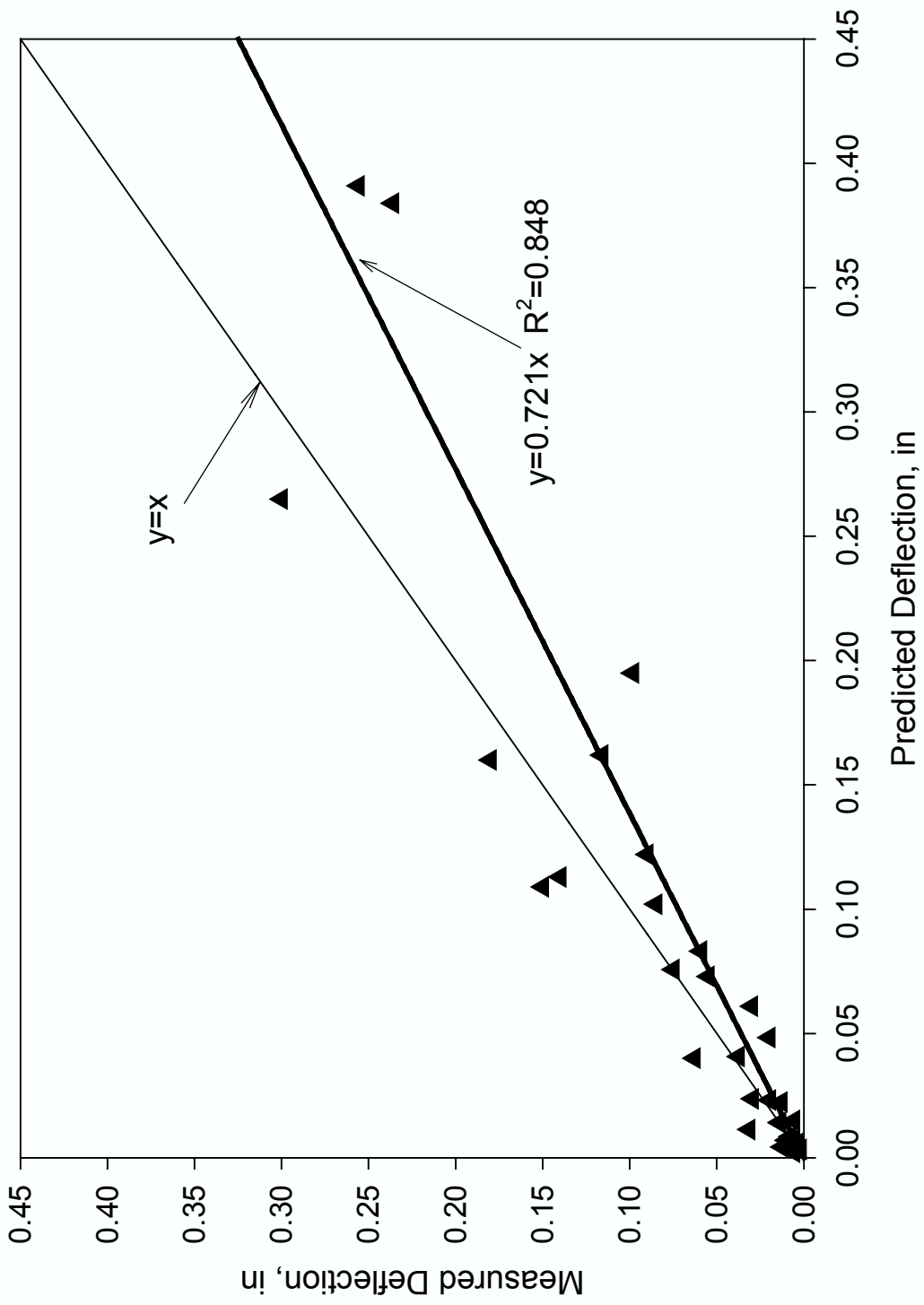


Fig. 3.7 SPT Database Statistics (0~25%Load) for Cohesionless Soil

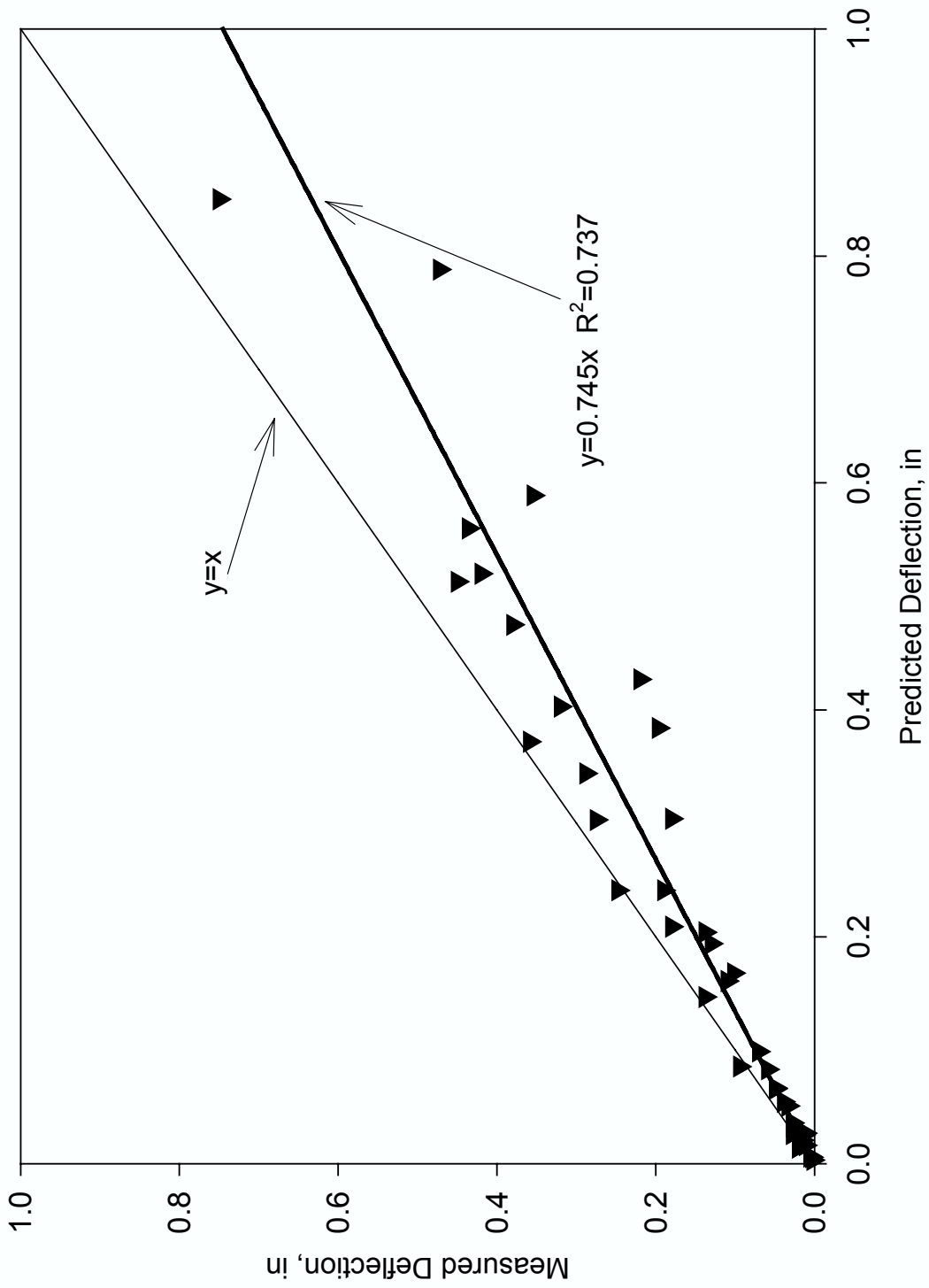


Fig. 3.8 SPT Database Statistics (25~50%Load) for Cohesionless Soil

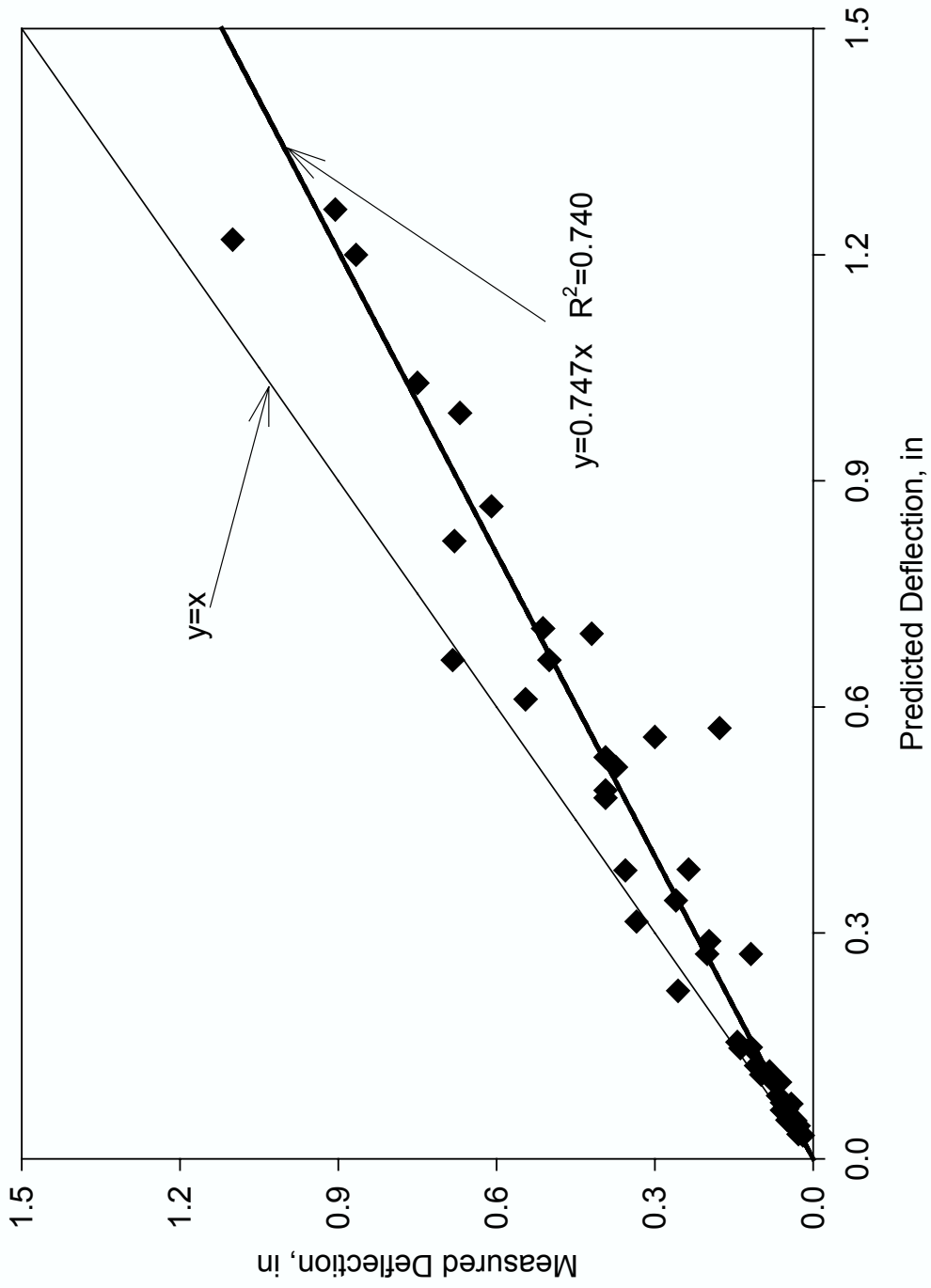


Fig. 3.9 SPT Database Statistics (50~75% Load) for Cohesionless Soil

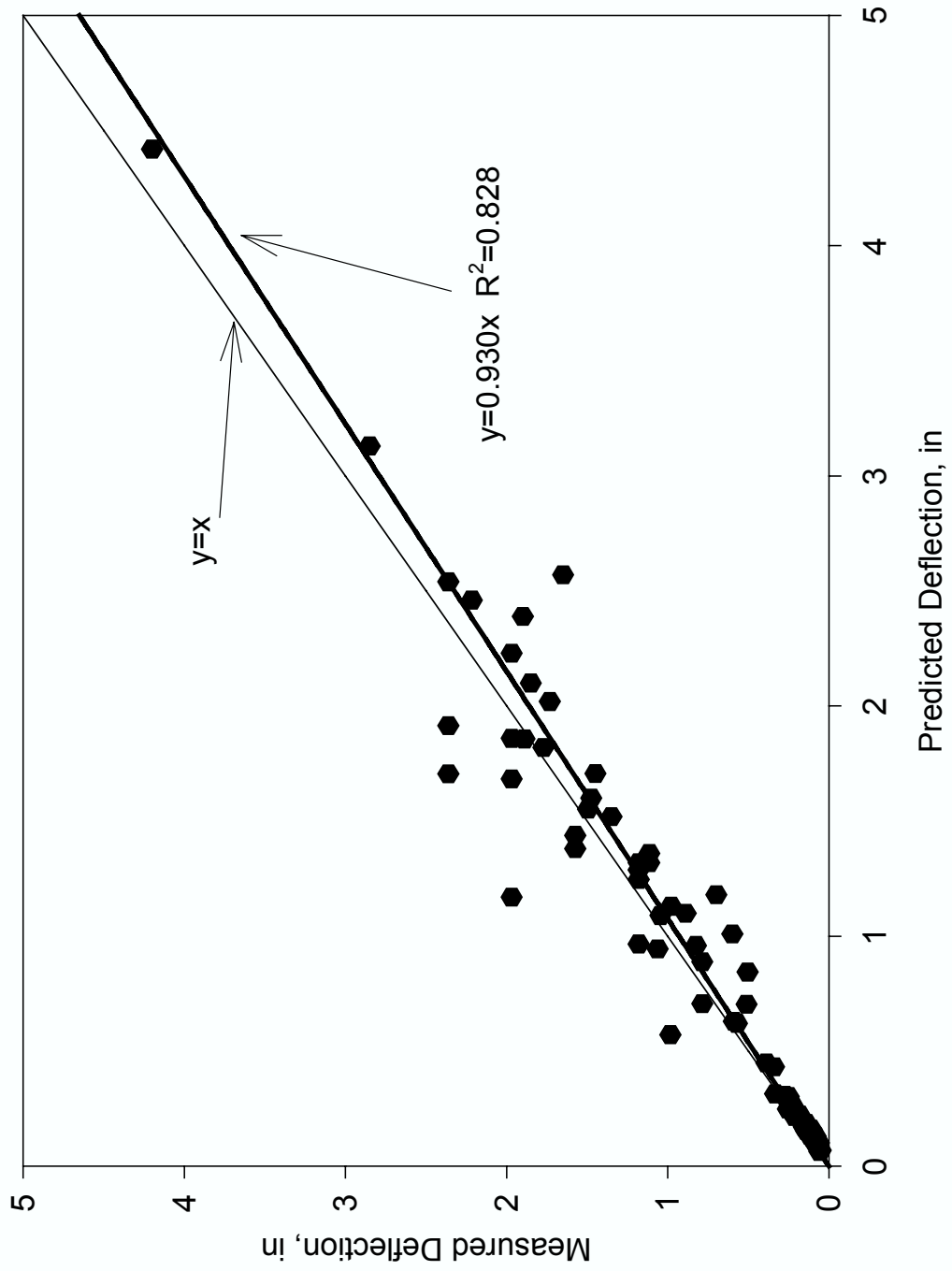


Fig. 3.10 SPT Database Statistics(75~100%Load) for Cohesionless Soil

## **CHAPTER IV**

### **CENTRIFUGE TESTING OF SOIL SLOPES STABILIZED WITH DRILLED SHAFTS**

#### **4.1 OVERVIEW OF CENTRIFUGE TESTING**

Modeling of earth structures is not an easy task due to the fact that scaled models cannot reproduce gravity induced stress field in the prototype. To reproduce actual stress field, full-scale prototype test is most desirable. However cost and variability of in-situ soil conditions often prohibit its extensive uses for investigating geotechnical problems. As an alternative, centrifuge modeling can be used as a useful tool to scale-up stress field and provide a control of the test conditions. Advantages from using centrifuge modeling can be enumerated as follows:

1. Cheap: since full scale testing of a prototype structure is expensive.
2. Most of full-scale testings are time consuming, while centrifuge tests can be done within relatively short period of time for most cases.
3. The ability to control the testing conditions and soil parameters easily.
4. The ability to extrapolate centrifuge results to prototypes.
5. Due to the high degree of accuracy, when centrifuge tests were done properly, it can be used as a tool to verify analytical methods.
6. It can be used to model prototypes of large structures when it is difficult to conduct full-scale testing.

The idea of using centrifuge was born by Edouard Philips in 1869 as a method to test models of metal bridge for spanning the British channel (Craig et al, 1988). In 1930 Philip Bucky in the United States proposed using centrifuge to produce gravitational acceleration that can replicate the effects of body forces in scaled models of earth structures. At the same time, Pokrovskii and Fiodorov were working independently in the USSR on the same idea. The first two papers written by Pokrovskii and Fiodorov in the early 1930's were on the deformation of rock beams in underground chambers and the stability of slopes in riverbanks. They also utilized centrifuge to solve problems in hydraulic engineering, particularly in analyzing the stability of slopes of rivers. As a result of their work, the first centrifuge was built in the USSR to simulate various processes in rocks and soils (Yakovleva, 1988). All the other centrifuge machines that were designed and built during 1940's and 1960's in the USSR were under the guidance of Fiodorov.

In the United States, early applications of centrifuge were restricted to mining because of the wide interests in mining operation at that time. In Japan, Mikasa initiated centrifuge testing in 1965. The first study was primarily on the consolidation problems of very soft clay deposits. Some of the subsequent studies were on the deformation and stability of soil slopes, stability of rock fill dams, the bearing capacity of saturated clay, and sheet piling.

In the United Kingdom, Schofield was the first to initiate the use of centrifuge in the early 1960's. The centrifuge was used as a tool for better understanding of the fundamental behavior of idealized soils. During 1970's, several other researchers

participated in centrifuge study, such as Craig, Fuglsang, Rowe, and others.

In 1980's the earthquake simulation shaker was developed to be placed on centrifuge flight to allow for study of liquefaction and stability of slope during earthquakes. During the 1990's the number of centrifuge machines increased rapidly. More than 100 centrifuge machines are in operation all over the world, with more than 40 in Japan and 20 in the USA.

Some of the centrifuge applications include soil consolidation, stability of clay slopes and rock fill dams, retaining structures, buried structures, tunneling, deep excavations, shallow and deep foundations, earthquake modeling, dynamic behavior of embankments and foundations, gravity walls, blast models, environmental aeromechanics, and cold region's engineering studies.

The accuracy and the reliability of the centrifuge results may be affected by many factors. Two important factors are discussed below.

#### **Grain Size Effect.**

As the centrifuge acceleration increases, the size of the soil particles increases proportionally. This has raised concerns about "Grain Size Effect", due to the inability to scale down the soil particles in a centrifuge model. However, for the case of laterally loaded piles, no significant particle size effect has been reported. As a general rule it is recommended to maximize the model pile size (diameter) while conforming

to other experimental constraints such as container size, centrifuge capacity, and method of installation (Kusakabe, 1995). Nunez (1988) suggested that the ratio of the pile circumference to the soil particle size to be 150-600 for piles in tension. Ovesen (1979) showed that the ratio of the pile circumference to the soil particle size should be 20-40 for foundations in quartz sand.

### **Pile Installation Effect**

For the study of laterally loaded piles, Craig (1984) found that the overall behavior between the piles installed in-flight and those installed at stationary position (at 1g) was about the same. Stress conditions in the soils were shown to be insensitive to the method of pile construction in clay model. In-flight and stationary construction methods showed similar stress conditions at the end of construction (Beasley, 1973). Moreover, Bouafia and Garnier (1991) reported the same results for piles installed with different methods, such as jacking, hammering, placement in boreholes or pluviation of sand around the pile at 1g.

## **4.2 CENTRIFUGE FACILITY**

The geotechnical centrifuge facility at the Case Western Reserve University (CWRU) was used for this study. A full description of the facility was given by Figueroa et al (1998). The 20 g-ton centrifuge has dual platforms with a radius of 1.37m. A maximum payload of 182 kg can be placed in a platform measuring 61x45x61 cm. The support structure of the centrifuge consists of the main shaft, rotational bearings, bearing housings, a triangular shaped support skirt, and three 15

cm by 25 cm tie down footings. The maximum imbalance force that can be accommodated by the main shaft is equivalent to 22 KN. The maximum operating speed is 360 RPM. The centrifuge can go up to a maximum acceleration of 200g for static tests and 100g for dynamic tests.

Centrifuge tests can be monitored through a 400-line video camera linked to image capturing and video computer boards, as well as a video recorder. The data acquisition system has the ability to accommodate up to 16 independent transducers.

### **4.3 CENTRIFUGE MODELS**

The schematics of the centrifuge model is depicted in Fig 4.1, where a uniform soil slope is underlain by a firm rock and reinforced by a row of model piles. The dimension of the model container is 40.6 cm long x 30.5 cm wide x 35.6 cm high. The model pile is 19.6 cm long with a circular cross section. The outside diameter of the model pile is 3.8 cm and wall thickness is 1.6 mm. The modulus of elasticity of aluminum model pile is  $6.895 \times 10^6$  kN/m<sup>2</sup>. The simulated firm rock layer was prepared by mixing fine sand with cement and water.

Each model pile was instrumented with 5 stations of full-bridge strain gages (Micro Measurement Group Model 250 UW-120). The location of strain gage stations is shown in Fig 4.2. Notice that one gage station is located in the firm rock layer. Calibration of strain gages was done in 1g by using a 4-point load bending test procedure.

The linear variable differential transformers (LVDT) were used in the centrifuge model to measure the deflection of the model piles during centrifuge flight. **Fig 4.3** shows the top view of the instrumented centrifuge model, with LVDTs in position and strain gage cables running to the data acquisition system.

#### **4.4 SOIL USED AND SLOPE PREPARATION**

##### **4.4.1 SANDY SLOPE**

A uniform silica sand was used for building the sandy slope. Direct shear tests were performed to obtain friction angles of 30° and 42° for the dry sand density of 13.7 kN/m<sup>3</sup> and 17.1 kN/m<sup>3</sup>, respectively. The sandy slope in the centrifuge model was built with a pluviation technique and the desired density of the sandy slope was achieved by tamping with a rubber hammer on the sidewall of the container. Two sand densities achieved for the sandy slope were: dense sand of 16.7 kN/m<sup>3</sup>, and loose sand of 14 kN/m<sup>3</sup>, respectively.

##### **4.4.2 CLAYEY SLOPE**

Creamy white kaolin clay powder known as Florida Edgar Kaolin, was used to construct the clayey slopes. It has liquid limit of 54%, plastic limit of 32% and specific gravity of 2.65. A water content between 46.3% to 49% was chosen for mixing water and clay. The clayey slope was built by hand layer-by-layer, similar to embankment construction. To account for evaporation of water during slope construction and centrifuge run, a small amount of additional water was added to the

mix.

The correlations developed by Mesri et al. (1996) were used to estimate the undrained shear strength of the clays. For normally consolidated clay, the undrained shear strength can be estimated as:

$$S_u = \frac{1}{3} \left[ \frac{S_u(TC)}{\sigma'_p} + \frac{S_u(DSS)}{\sigma'_p} + \frac{S_u(TE)}{\sigma'_p} \right] \sigma'_p \quad (4.1)$$

where

$S_u(TC)$  = undrained shear strength under triaxial compression test.

$S_u(DSS)$  = undrained shear strength under direct simple shear test.

$S_u(TE)$  = undrained shear strength under triaxial extension test.

A simplified relationship is shown below:

$$S_u = 0.22\sigma'_p \quad (4.2)$$

The above average is mostly studied for circular arc stability analysis.

#### **4.5 CENTRIFUGE TEST PROGRAM**

A centrifuge test program was designed to systematically study the effect of pile diameter, pile spacing, slope geometry (height and slope angle) on the forces applied to the piles.

To model different simulated prototype, centrifuge models were subjected to an increase of centrifugal accelerations in an incremental manner. After each acceleration increment, the centrifugal acceleration was held constant for a sustained period of time until the strain reading and the LVDT reading showed constant values.

For testing of the sandy slope models, centrifugal acceleration was increased from 8g to 80g in increment of 4g. For testing of clay slopes, centrifugal acceleration was increased from 8g to 56g in increment of 4g as well. A much longer hold time was used in each stage of centrifugal acceleration in testing clay slope models to allow for reaching pore pressure equilibrium condition.

The pile spacing was varied as follows: 1.5D, 2.0D, and 2.5D, where D = pile diameter. The slope angle in sandy slopes was varied as follows: 32°, 35°, and 40°. The slope angle in clay slope was varied as follows: 34°, 45°, and 57°. Table 4.1 and Table 4.2 provide a detailed summary of centrifuge models for sandy and clay slopes, respectively. As a reference, Table 4.3 provides information on equivalent prototype structure properties at different centrifugal accelerations.

## **4.6 TEST RESULTS**

### **4.6.1 DATA DEDUCTIONS**

The moments along the pile were deduced using the strains that were recorded by the strain gages during the test. A polynomial curve fitting technique along with prescribed boundary conditions were used to determine the moment distribution with pile depth. The net forces applied to the pile per unit length of pile were calculated using the method of double differentiation of the moments. The reduced moment distribution curves are shown. The deflections of the piles were calculated based on the double integration of the moments as given in the following equation

$$y = \iint \frac{M}{EI} dx \quad (4.3)$$

#### 4.6.2 BEHAVIOR OF PILES IN SANDY SLOPES

The moment distribution of the piles in sandy slopes are plotted in Fig.4.4 to Fig.4.6 for  $S/D = 1.5, 2, \text{ and } 2.5$ , respectively. In each figure, part (a) exhibits the moment distribution in dense sand, while part (b) presents the moment distribution in loose sand. The centrifuge acceleration levels at  $N = 8, 16, 24, 32$  and  $48$  are selected for plotting the results. In general, the maximum bending moments occur at location above the elevation of rocks in dense sand. However, as the sand becomes loose, then the maximum bending moments occur near the interface between the sand and rock. For a given condition (i.e, centrifugal acceleration level, slope geometry, and pile spacing), the higher the density the larger the bending moments developed in the piles. The increase in slope angle tends to also increase the maximum bending moments in the piles. To investigate the influence of pile spacing on the development of maximum bending moments, a series of plots were presented in Fig 4.7 (a) to 4.7(d) for  $N=16, 24, 32, \text{ and } 48$ , respectively. In each Figure, the maximum bending moment for each model condition is normalized by  $EI/L$  of the pile and then plotted against  $S/D$ . In general,  $S/D=2$  seems to produce the maximum bending moment, perhaps indicating that arching effect is prominent in this particular pile spacing.

**Table 4.1 Summary of test program for sandy slopes**

Test Designation	Spacing	Slope angle (Deg)	Unit Weight (KN/m <sup>3</sup> )	Soil Friction Angle (Deg)	Relative Density Dr (%)	Case
S1	1.5D	32.6	15.8	37	67	Dense
S2	1.5D	36	16.8	41	93	Dense
S3	1.5D	40.1	16.7	40.8	92	Dense
S4	1.5D	31.5	14.0	32	10	Loose
S5	1.5D	35.4	14.1	33	12	Loose
S6	1.5D	39	15.0	35	44	Loose
S7	2D	32.6	15.8	37	67	Dense
S8	2D	36	16.8	41	93	Dense
S9	2D	40.1	16.7	40.8	92	Dense
S10	2D	31.5	14.0	32	10	Loose
S11	2D	35.4	14.1	33	12	Loose
S12	2D	39	15.0	35	44	Loose
S13	2.5D	32.6	15.8	37	67	Dense
S14	2.5D	36	16.8	41	93	Dense
S15	2.5D	40.1	16.7	40.8	92	Dense
S16	2.5D	31.5	14.0	32	10	Loose
S17	2.5D	35.4	14.1	33	12	Loose
S18	2.5D	39	15.0	35	44	Loose

**Table 4.2 Summary of clayey slopes in centrifuge tests**

Test Designation	Spacing	Slope angle (Deg)	Unit Weight (KN/m <sup>3</sup> )	Water Content (%)
C1	1.5D	34	14.7	46.5
C2	1.5D	45	14.8	47.6
C3	1.5D	57	15.4	49.6
C4	2D	34	14.7	46.1
C5	2D	45	14.8	47.2
C6	2D	57	15.4	49
C7	2.5D	34	14.7	46.3
C8	2.5D	45	14.8	47.4
C9	2.5D	57	15.4	48.9

**Table 4.3 Prototype properties at different centrifugal accelerations.**

N (g)	Pile diameter (m)	Pile length (m)	EI (KN.m <sup>2</sup> )
8	0.31	1.56	8586
12	0.46	2.35	43467
16	0.61	3.13	137377
20	0.76	3.91	335394
24	0.91	4.70	695473
28	1.10	5.48	1288449
32	1.22	6.26	2198034
40	1.52	7.82	5366303
48	1.83	9.40	11127565
50	1.91	9.78	13101325
60	2.30	11.74	27166907
70	2.70	13.70	50330049
80	3.10	15.65	85860841

The net forces applied to the piles are normalized with  $L^2/EI$  and plotted in Fig.4.8 (a) and Fig.4.8 (b) for dense sand and loose sand, respectively. Similarly, for  $S/D= 2$  and  $S/D = 2.5$ , the normalized net forces along the length of the piles

are shown in Fig. 4.9 and Fig. 4.10, respectively. Part (a) of each figure is for dense sand, while part (b) is for loose sand. Based on these test results, one can see that the location of the maximum net force on the pile is near the rock-sand interface. As the slope angle increase, the net forces on the pile also increase. Also, as expected, the net forces on the pile increase with increasing pile diameter (i.e., at higher centrifugal acceleration level).

The net forces are plotted against S/D in Figs 4.11-4.14 for N = 16, 24, 32, and 48, respectively. In most cases, at S/D=2.0, the net force reaches the maximum value when compared to the cases of S/D=1.5 and S/D=2.5. It appears that arching becomes most pronounced at S/D =2.0 in sandy slope.

### **4.6.3 BEHAVIOR OF PILES IN CLAYEY SLOPES**

The bending moment distributions along the length of the piles are shown in Figs. 4.15-4.23 for Tests C1 to C9, respectively. For acceleration up to 32 g (i.e., prototype pile diameter = 1.22m), the maximum bending moment occurs at the location below the rock and clay interface. For acceleration above 32 g, however, the maximum bending moment occurs at the location above the interface. In fact, as the pile spacing increases, the maximum bending moment occurs at the location further above the rock-clay interface. In general, the moments on piles increase as clayey slope angle increases.

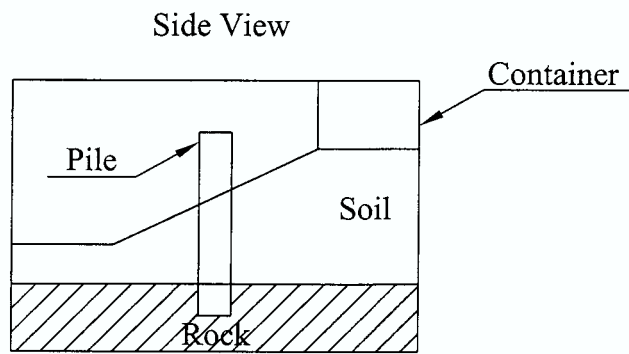
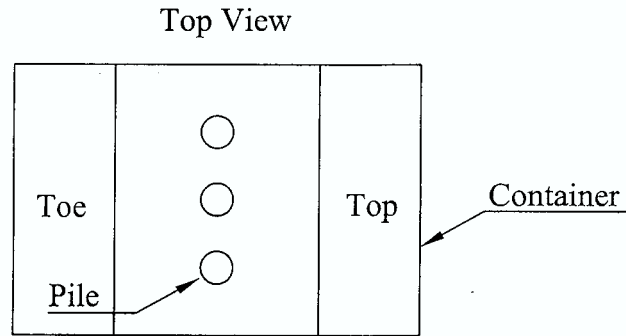
To further investigate the effect of S/D on the maximum moments on piles,

Fig.4.24-Fig.4.26 are prepared for slope angles=34°, 45°, 57°, respectively. It seems that at S/D=1.5, the maximum moments applied on the piles are much larger than those at S/D=2 and S/d=2.5. This phenomenon indicates that arching effect is most pronounced at S/D=1.5 in clayey slopes.

The distributions of net forces on the piles are plotted for different acceleration levels for Tests C1 to C9 in Figs. 4.27-4.35. Also plotted are the normalized maximum net forces for three pile spacing (S/D) ratios at different acceleration levels. These plots are presented in Figs. 4.36 to 4.38 for slope angle=34°, 45° and 57°, respectively. Again, at S/D=1.5, arching effect is most pronounced as maximum net force is largest at this pile spacing.

Centrifuge model tests on slopes stabilized with piles were successfully carried out in this research project. The behavior of the piles under working stress conditions was measured during the centrifuge runs. Both sandy and clayey slopes underlain by a rigid layer were studied. The strain readings of the model piles at different centrifuge accelerations were used to deduce the bending moments and the net forces on the piles. Various parameters affecting the behavior of the piles in the slopes were systematically studied in the centrifuge model study. Specifically, the effects of slope angle, sand density, pile length and diameter, and pile spacing were investigated. The behavior of piles can be summarized as follows:

1. In sandy slopes, the maximum bending moment usually occurs either at or slightly below the soil-rock interface. On the other hand, in clayey slopes, the maximum bending moment usually occurred at the location above the rock-clay interface. For large size piles (larger than 1.22 m), the maximum bending moment, however, occurs below the clay-rock interface.
2. For both clayey and sandy slopes, the maximum net force acting on the pile occurs at the interface of the soil and rock.
3. The arching effect on the force applied to the piles has been clearly documented in the centrifugal tests results. In sandy slopes,  $S/D=2$  appears to give most pronounced arching effect. In clayey slope,  $S/D =1.5$  gives the strongest arching effect.
4. In general, as the slope angle increases, the forces and moment developed in the piles decrease.



**Figure 4.1 Schematics of centrifuge slope models with stabilizing piles**

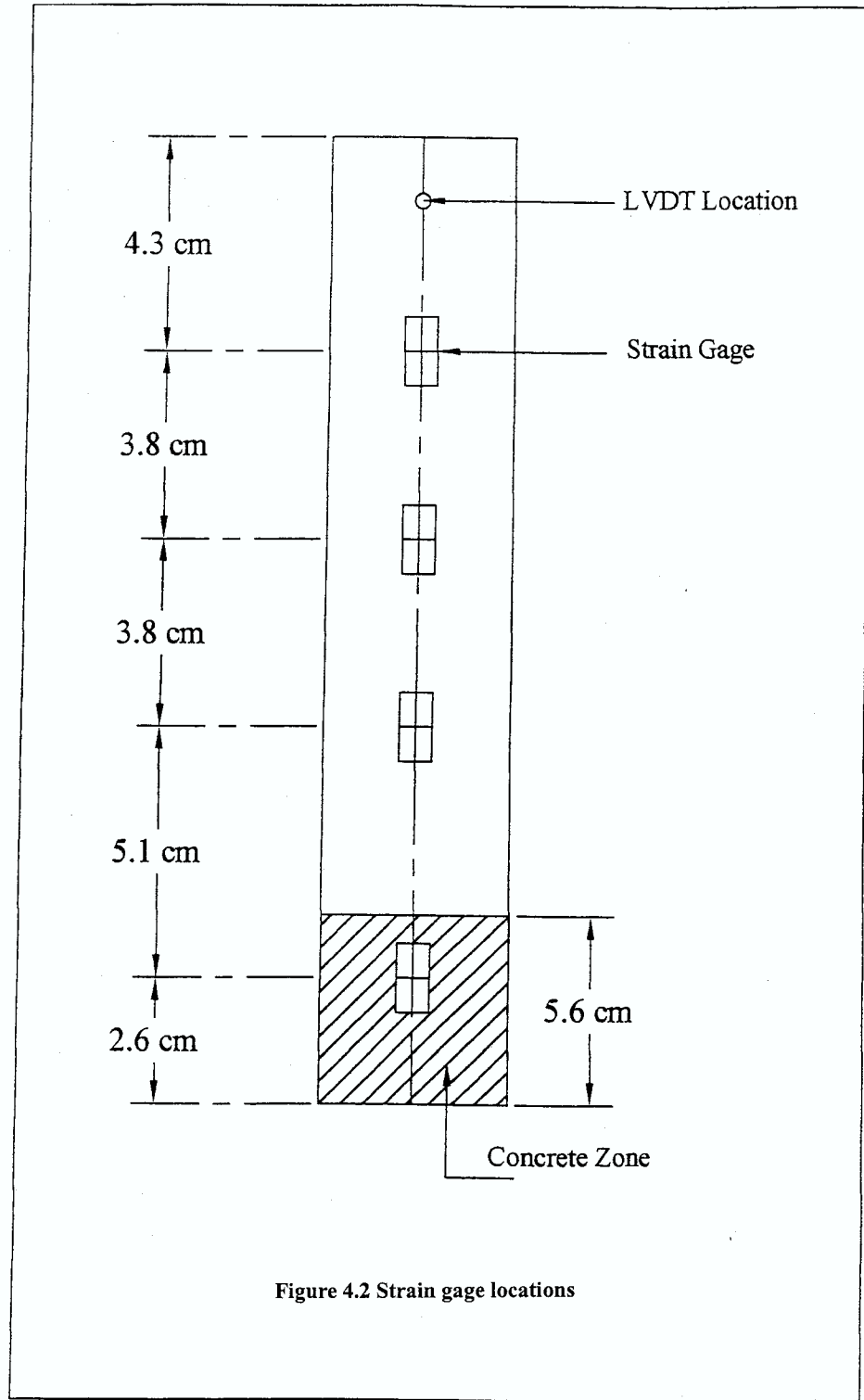
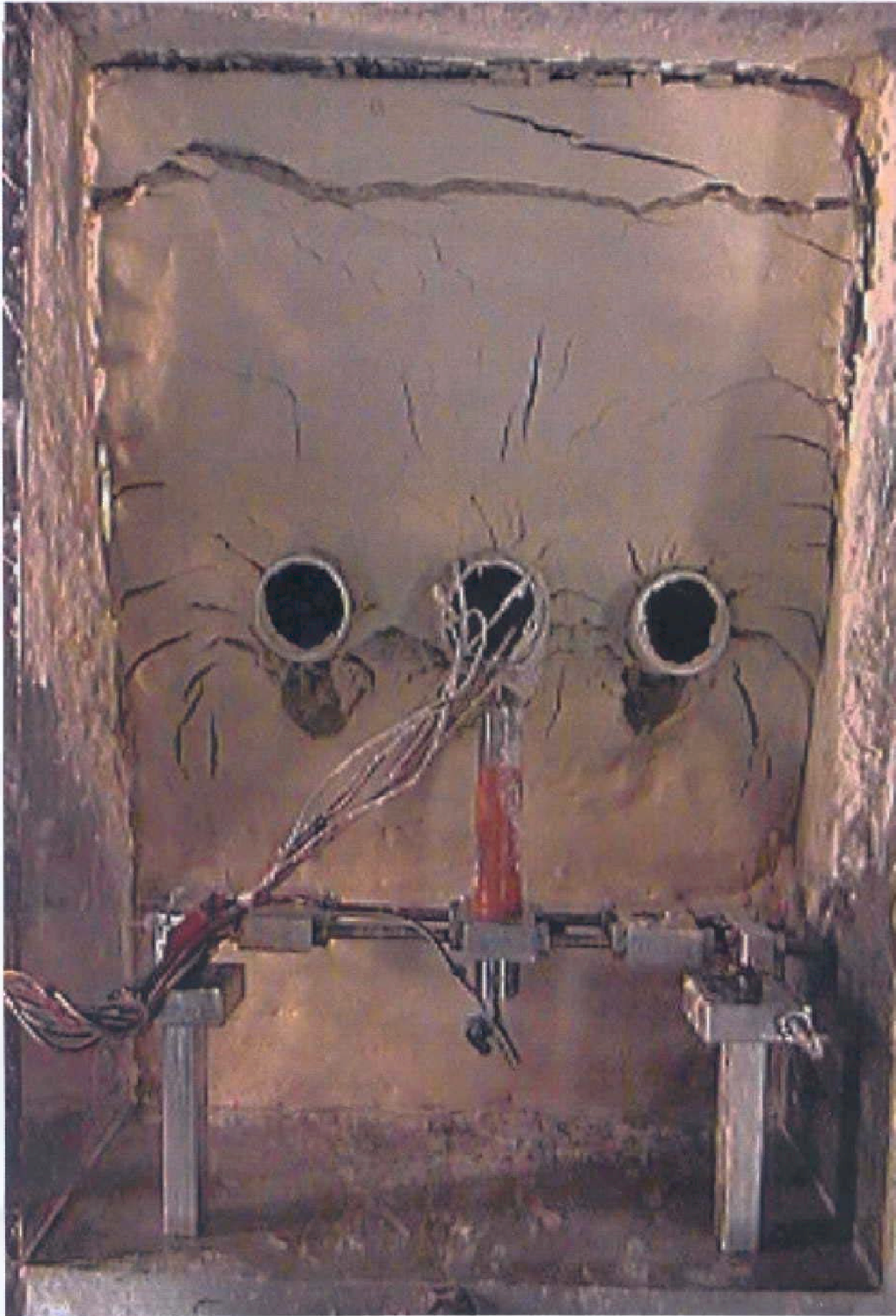


Figure 4.2 Strain gage locations



**Figure 4.3 Top view of instrumented centrifuge model**

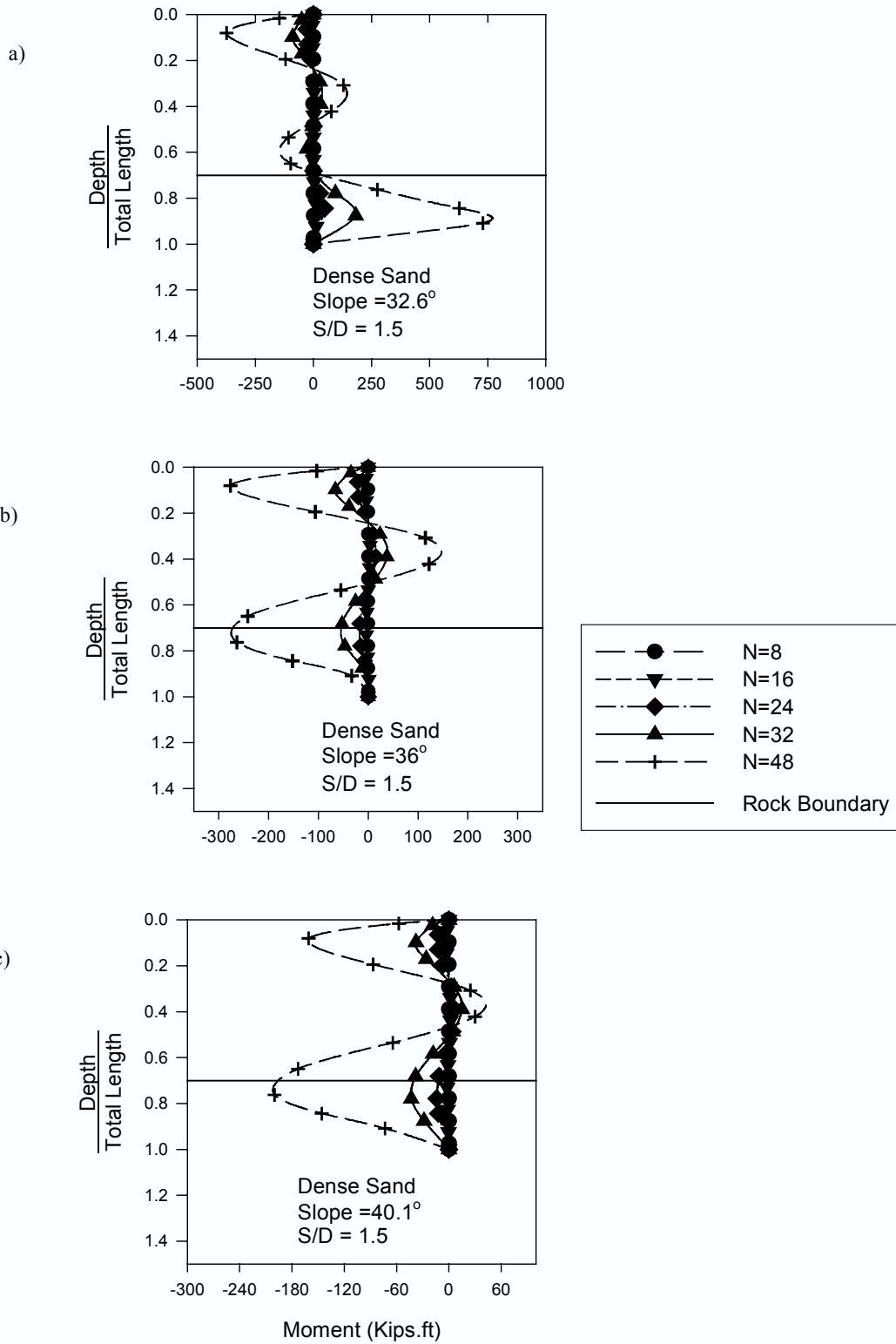
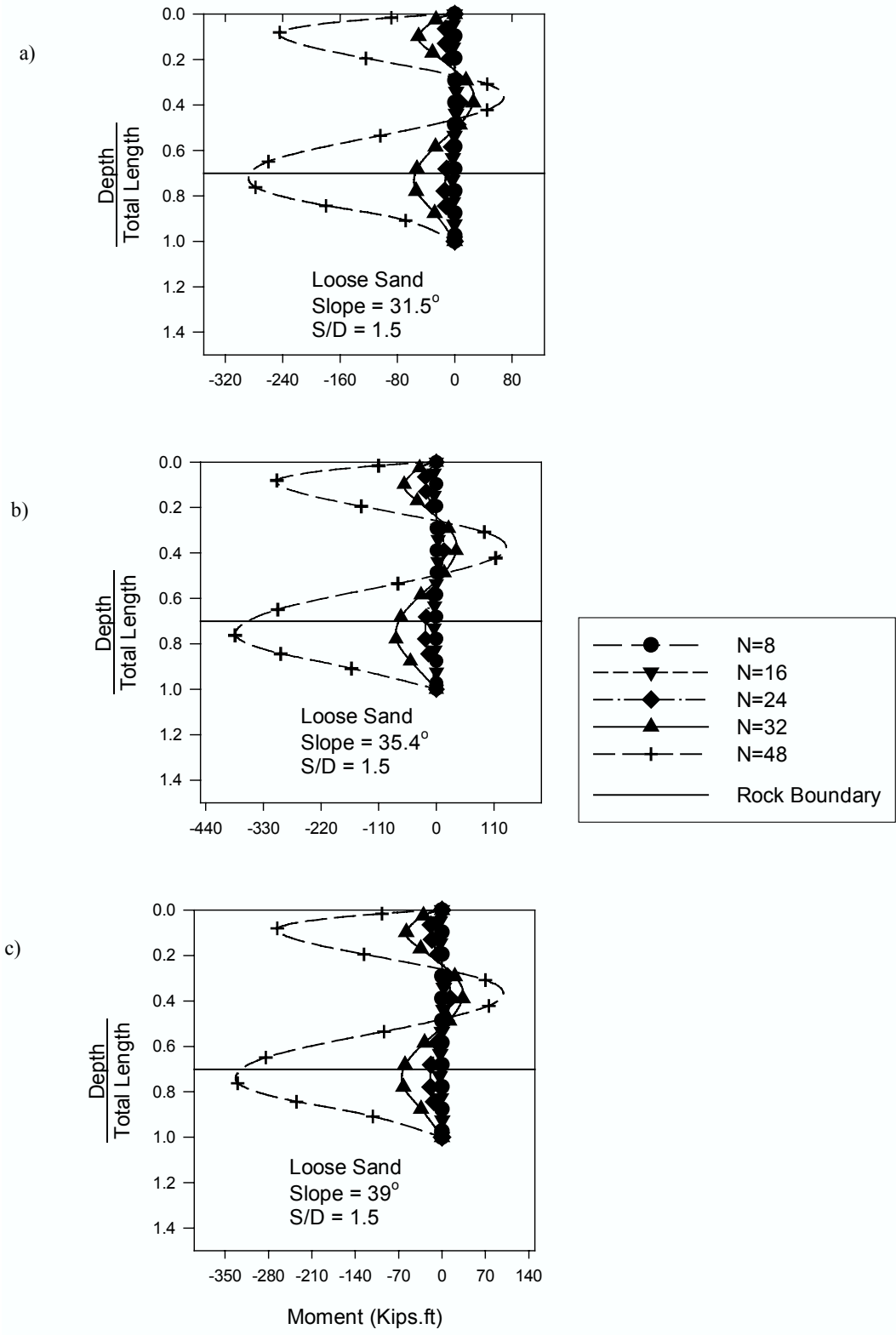
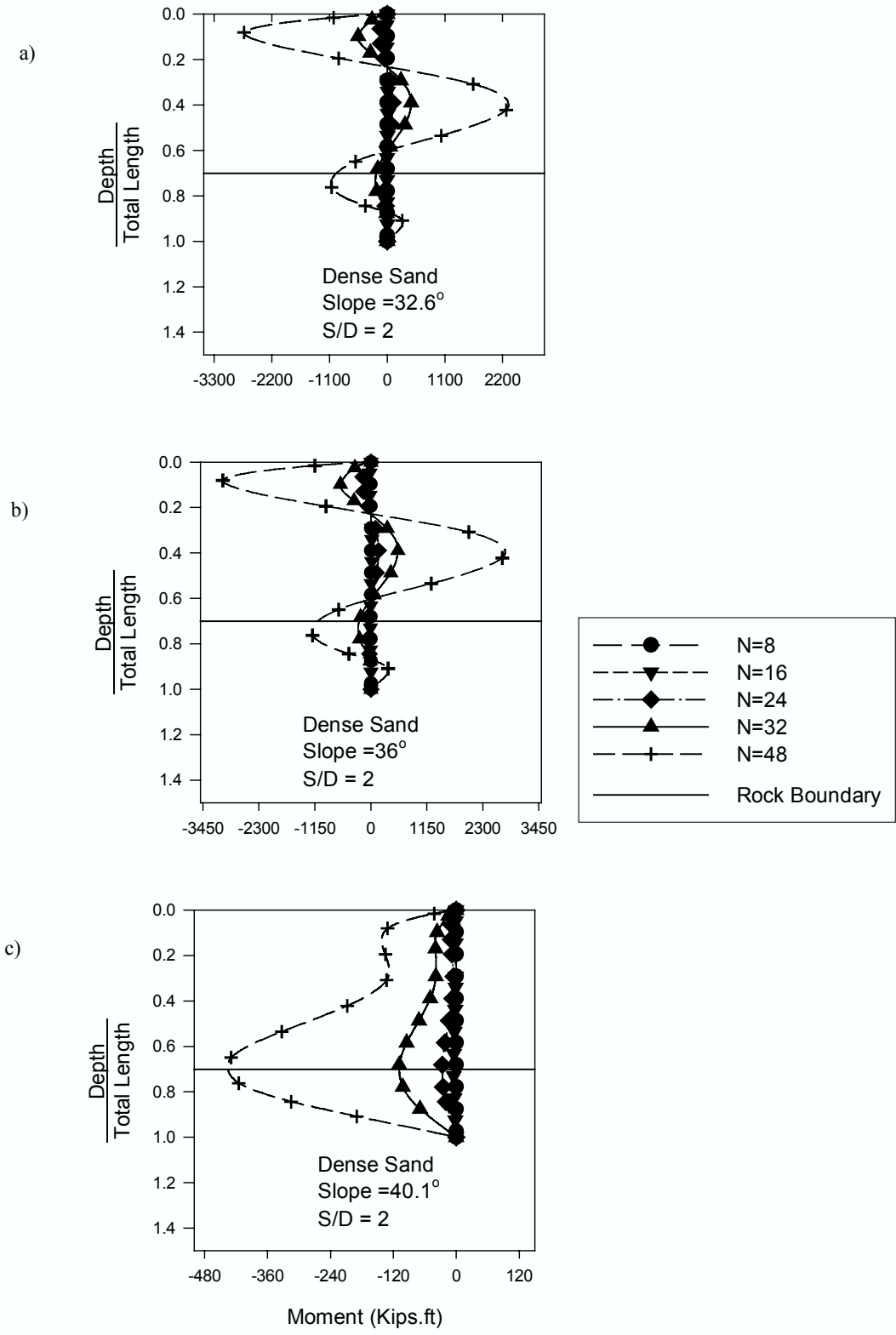


Figure 4.4(a) Moment distribution in dense sandy slope with S/D = 1.5



**Figure 4.4(b) Moment distribution in loose sandy slope with S/D = 1.5**



**Figure 4.5(a) Moment distribution in dense sandy slope with S/D = 2**

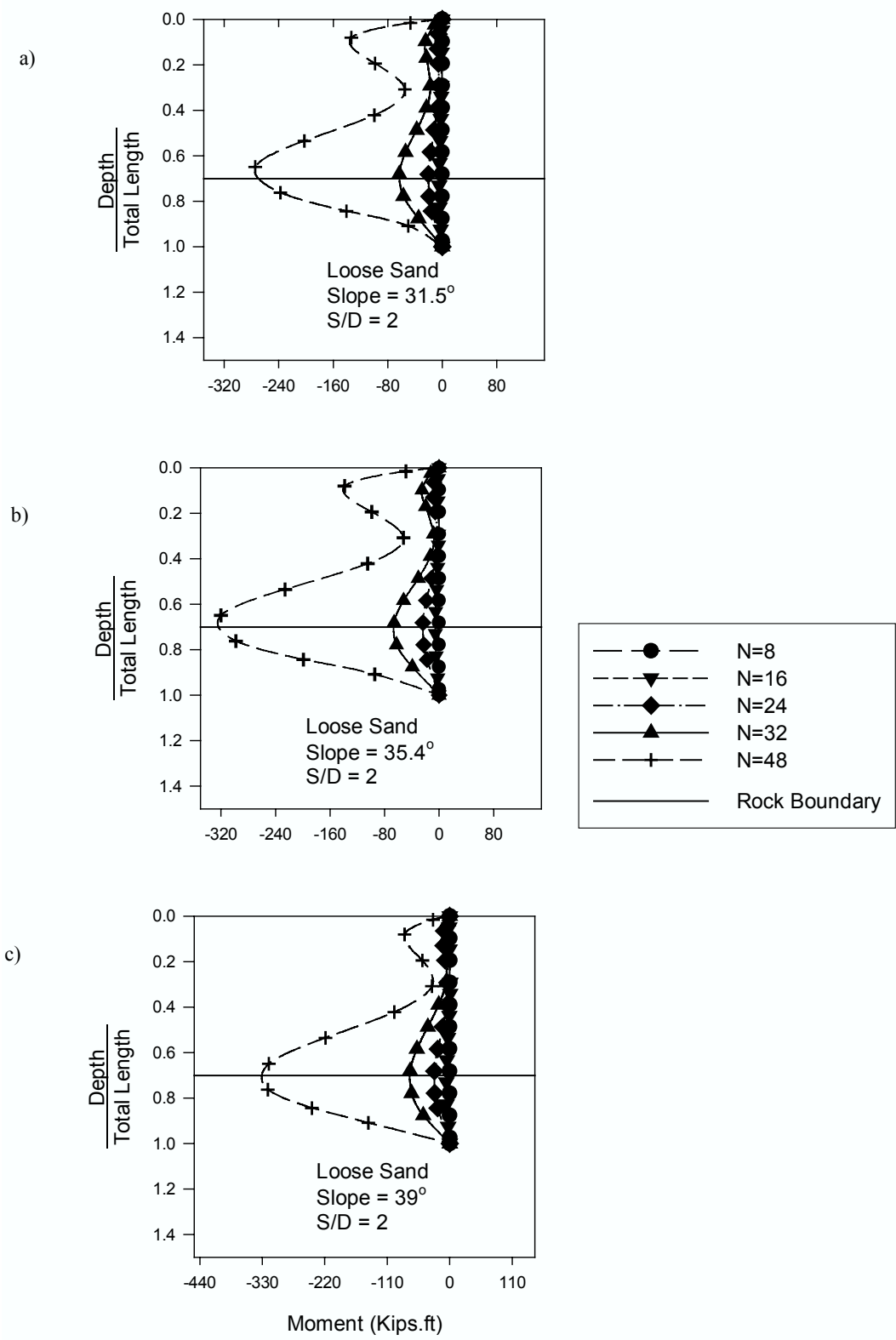


**Figure 4.5(b) Moment distribution in loose sandy slope with S/D = 2**

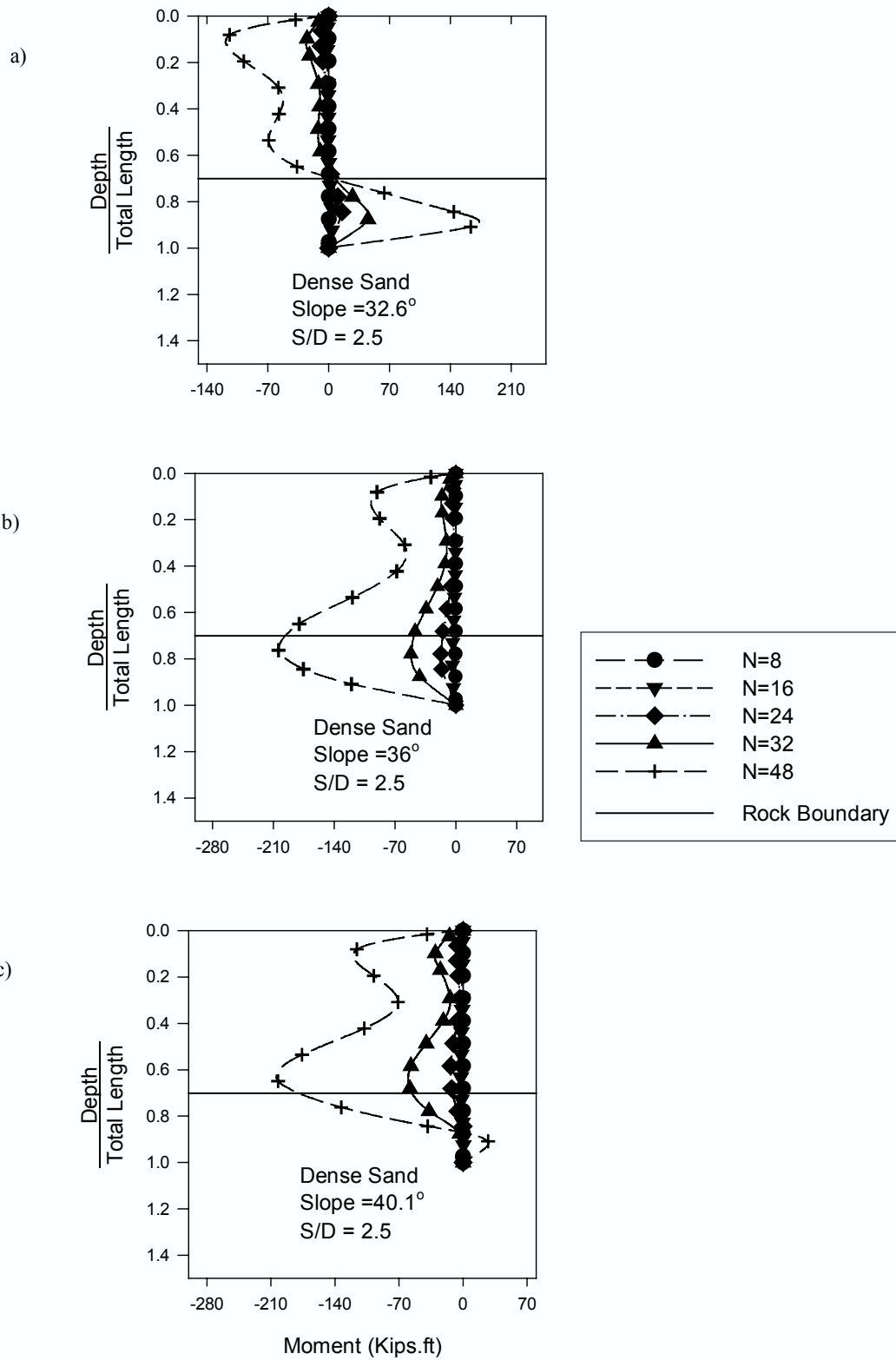


**Figure 4.6(a) Moment distribution in dense sandy slope with S/D = 2.5**

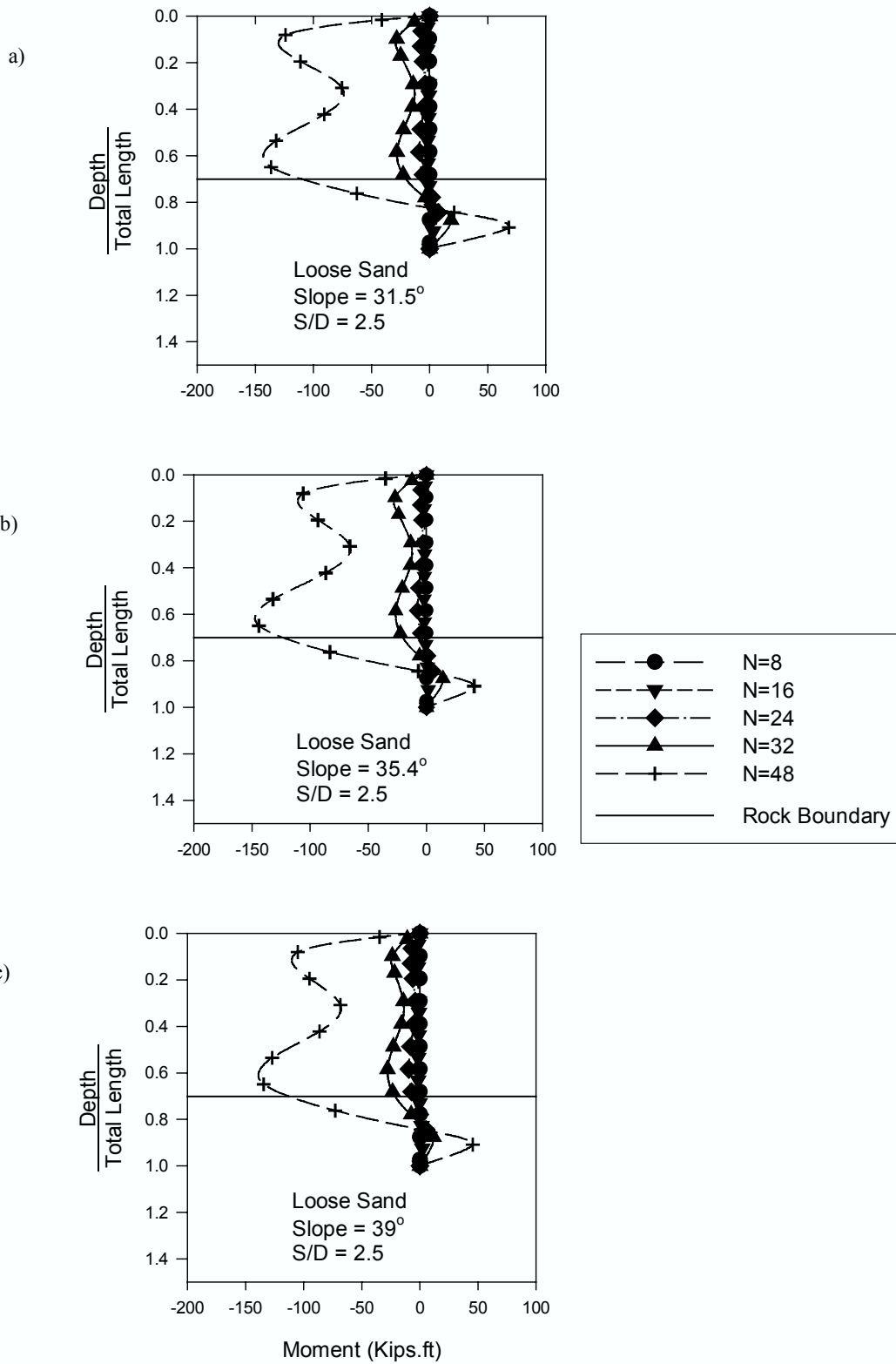


**Figure 4.6(b) Moment distribution in loose sandy slope with S/D = 2.5**

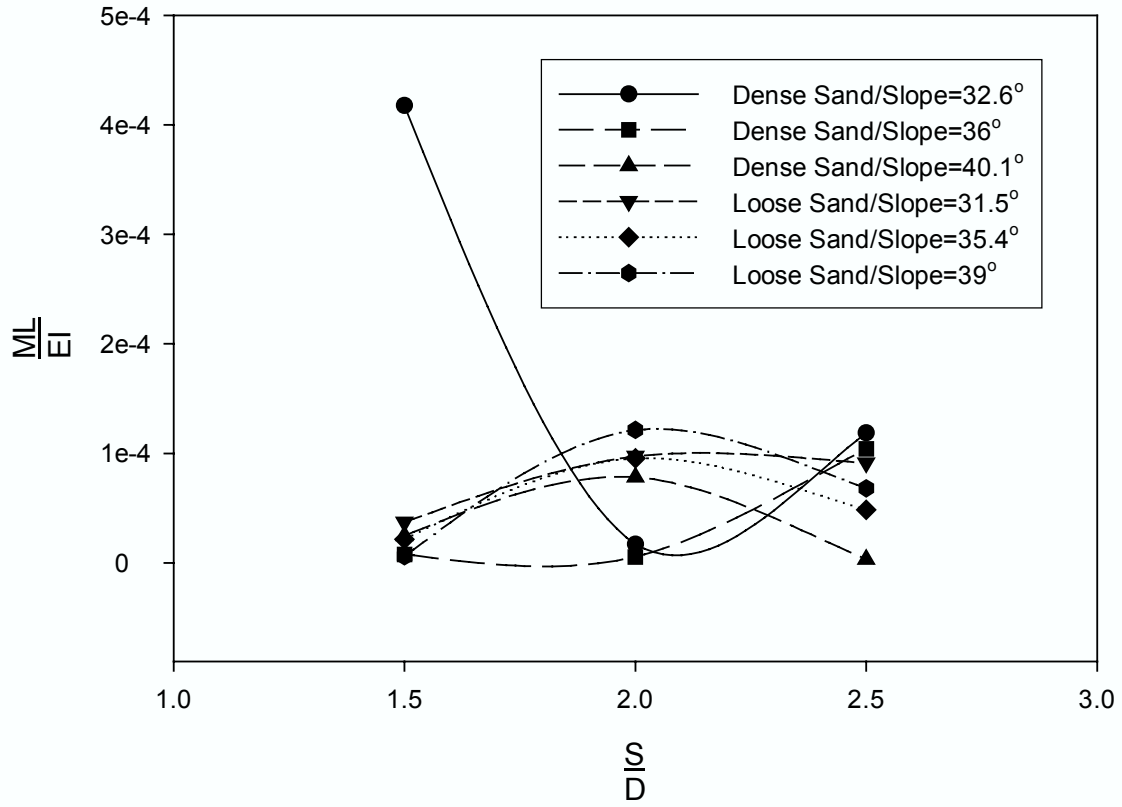


Figure 4.7(a) Normalized maximum bending moment vs. S/D ratio (N = 16)  
 Fig. 7.(N=16)

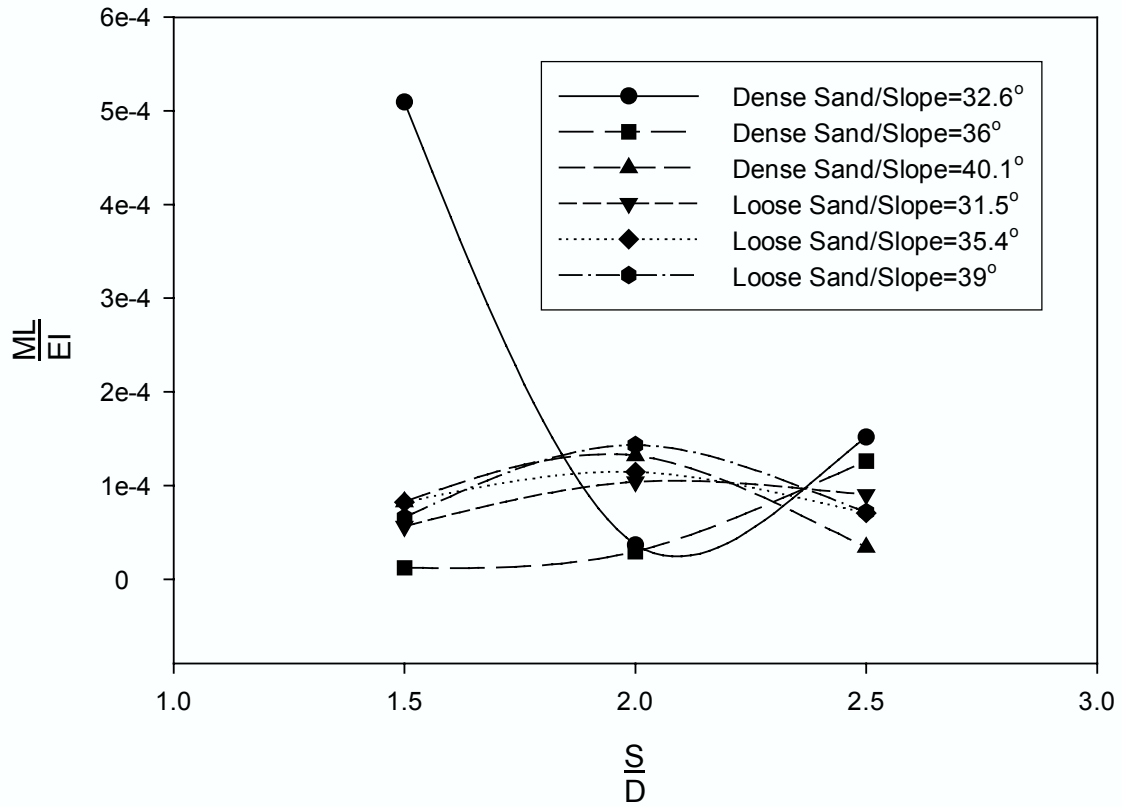


Figure 4.7(b) Normalized maximum bending moment vs. S/D ratio (N = 24)

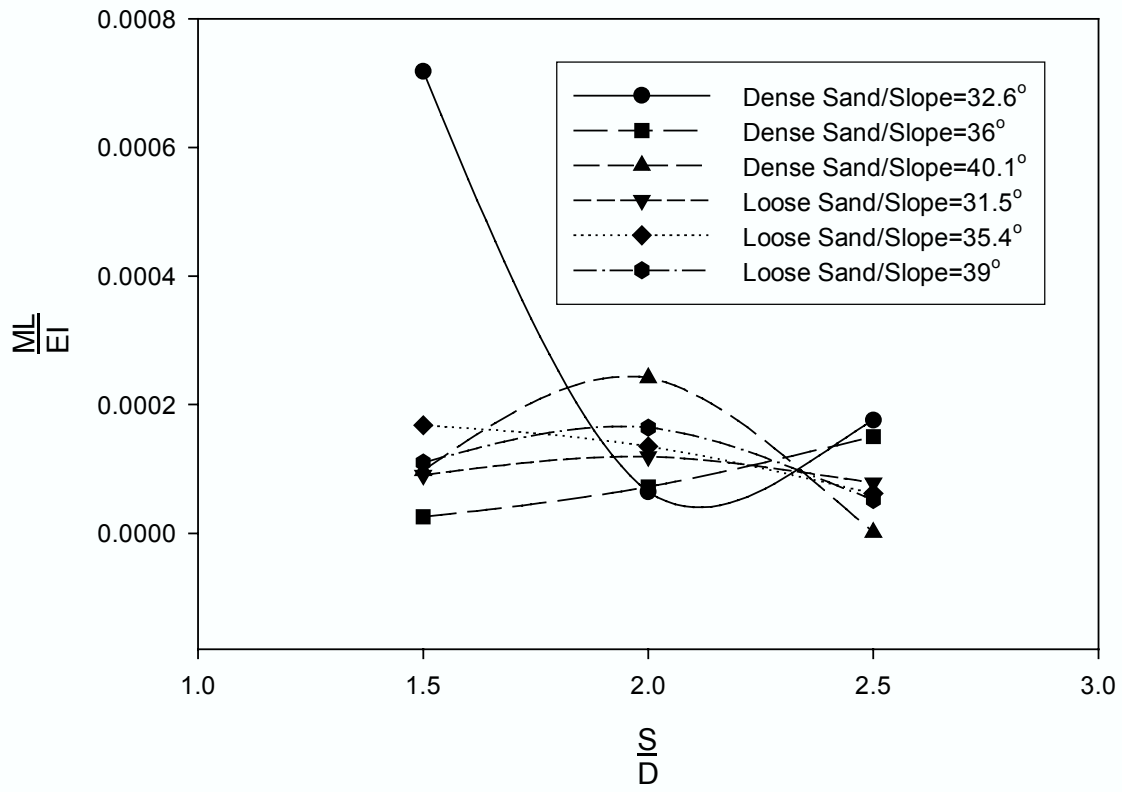


Figure 4.7(c) Normalized maximum bending moment vs. S/D ratio (N = 32)

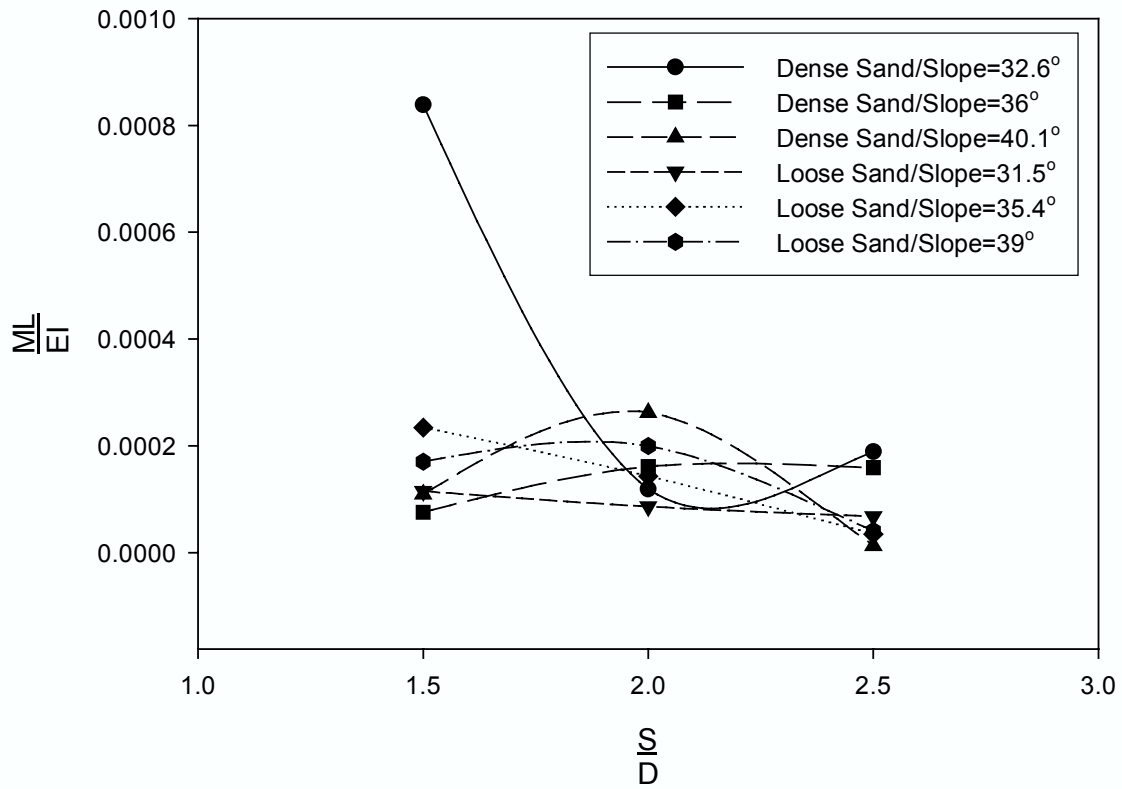
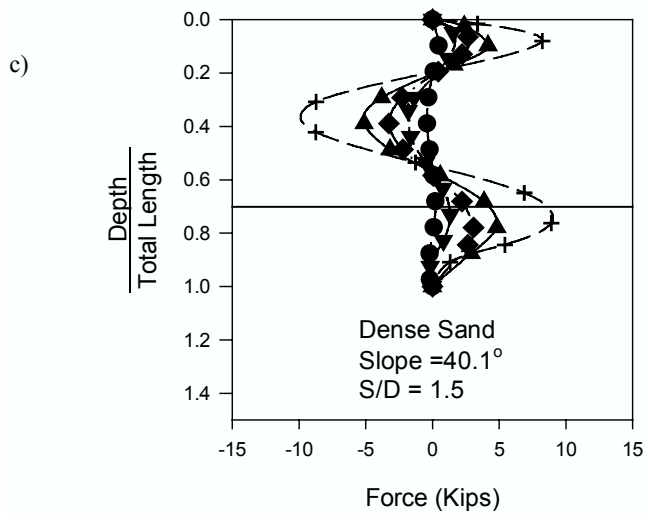
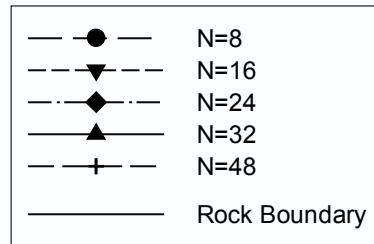
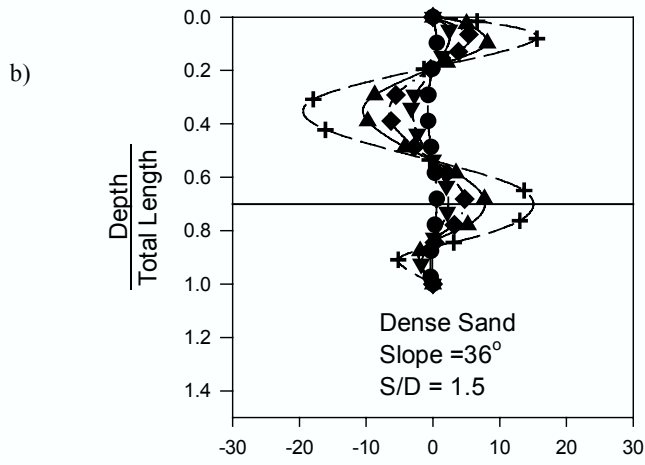
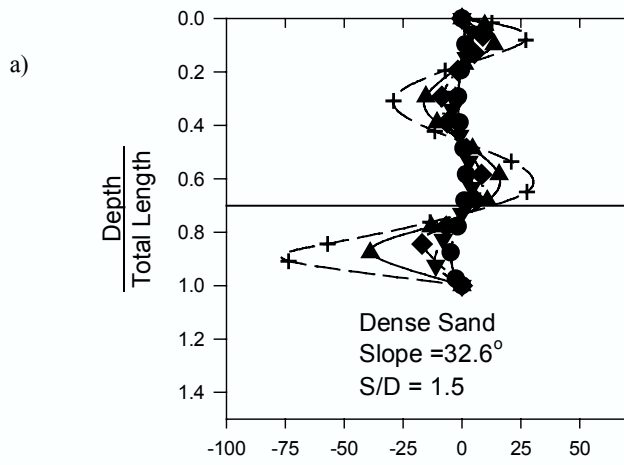
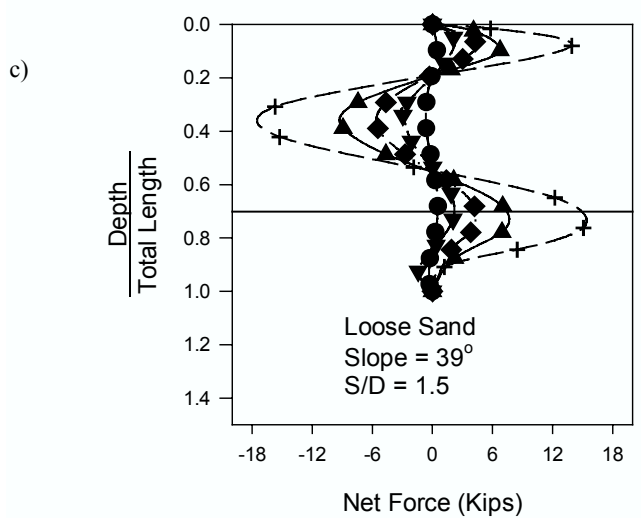
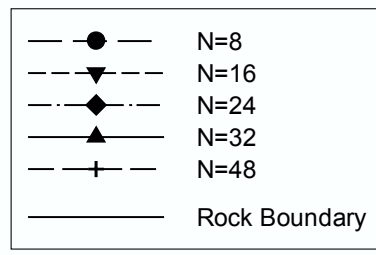
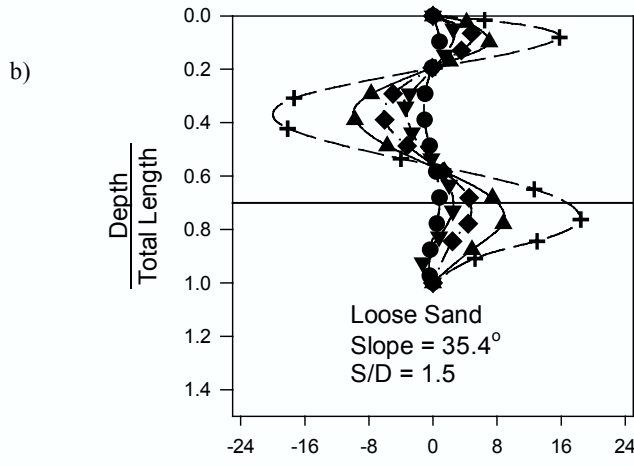
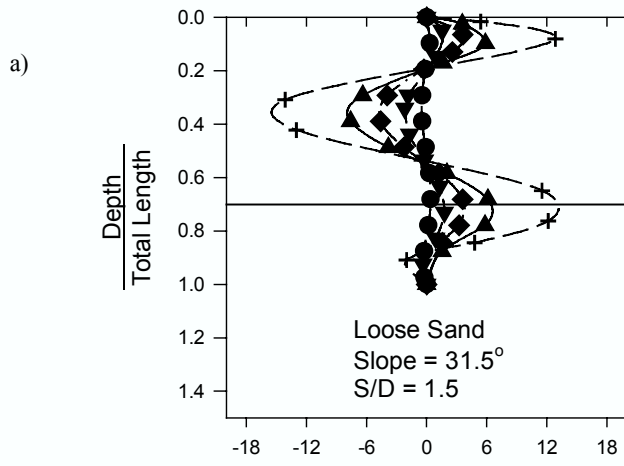
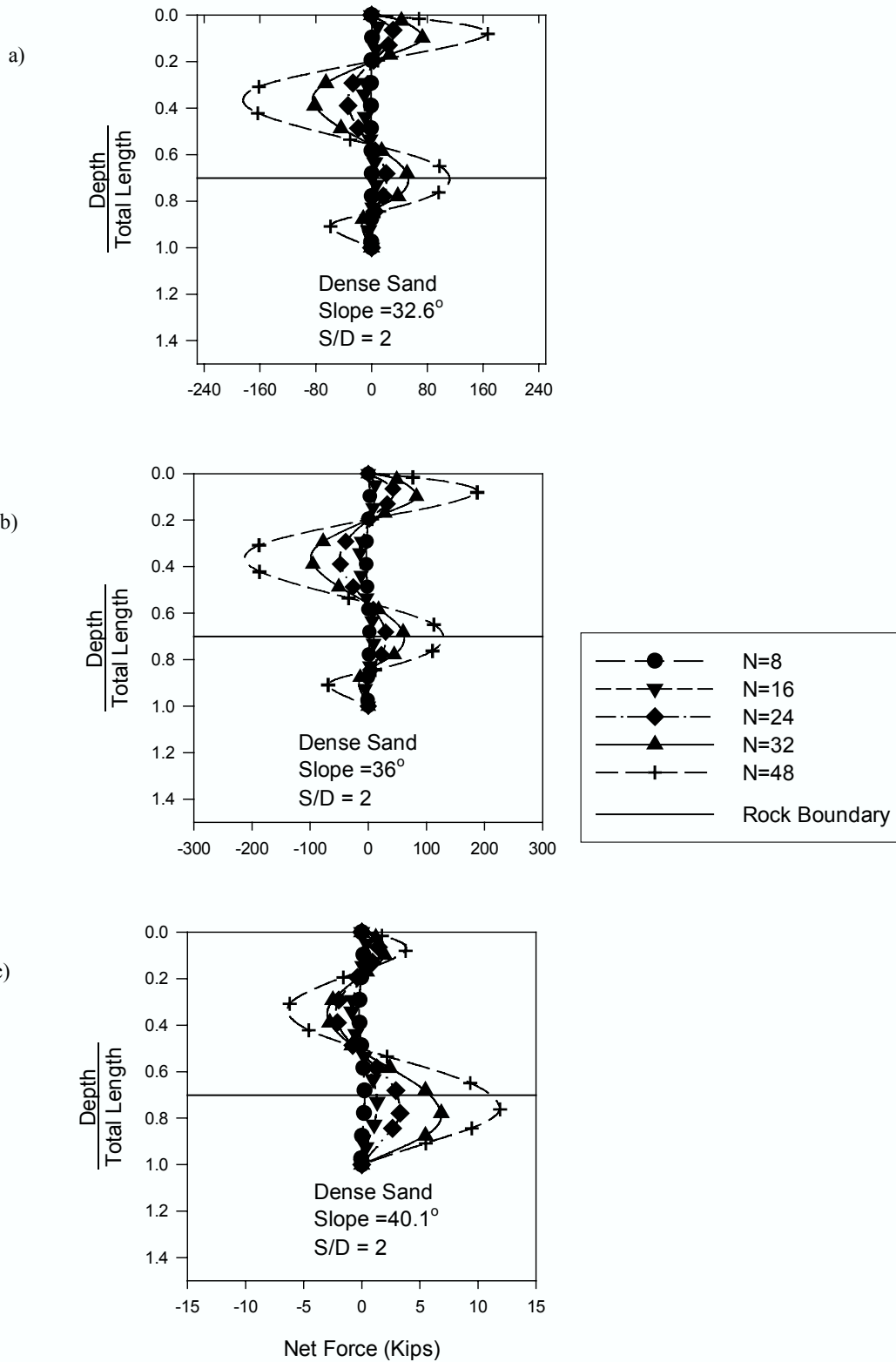


Figure 4.7(d) Normalized maximum bending moment vs. S/D ratio (N = 48)  
 Fig. 10.(N=48)







**Figure 4.9(a) Net force distribution with depth in dense sand slopes (S/D=2)**

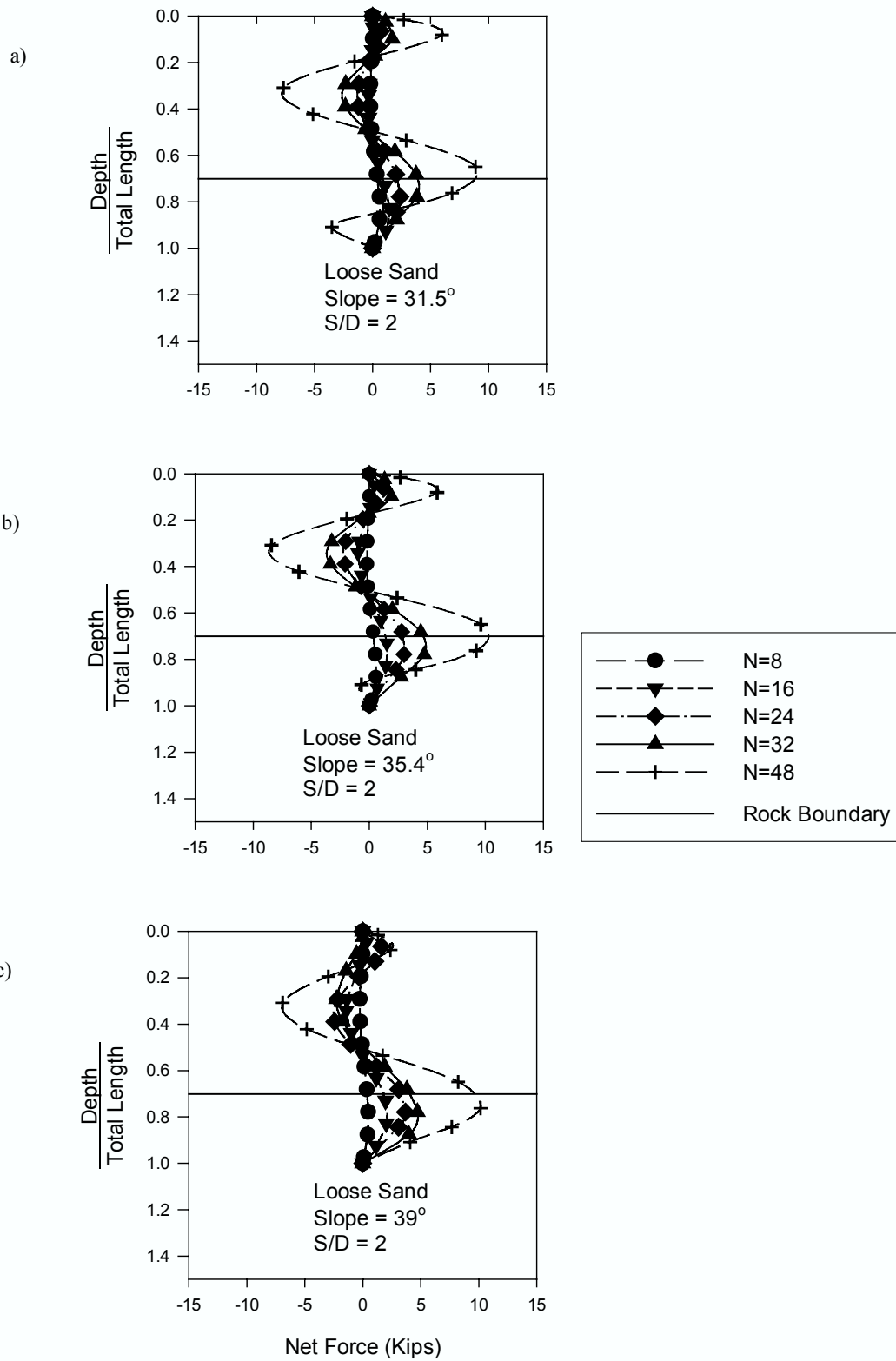


Figure 4.9(b) Net force distribution with depth in loose slopes (S/D=2)

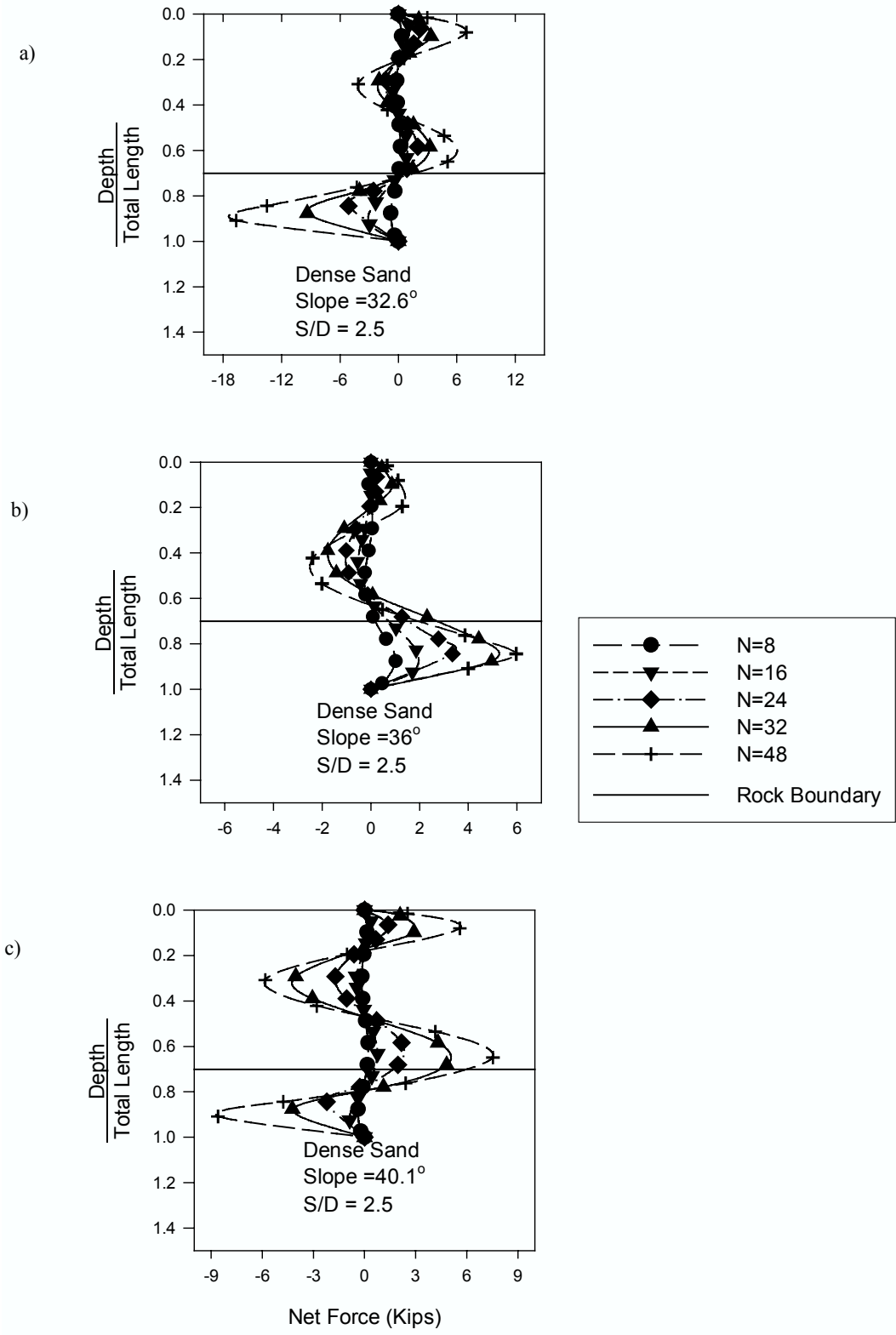


Figure 4.10(a) Net force distribution with depth in dense sand slopes (S/D=2.5)

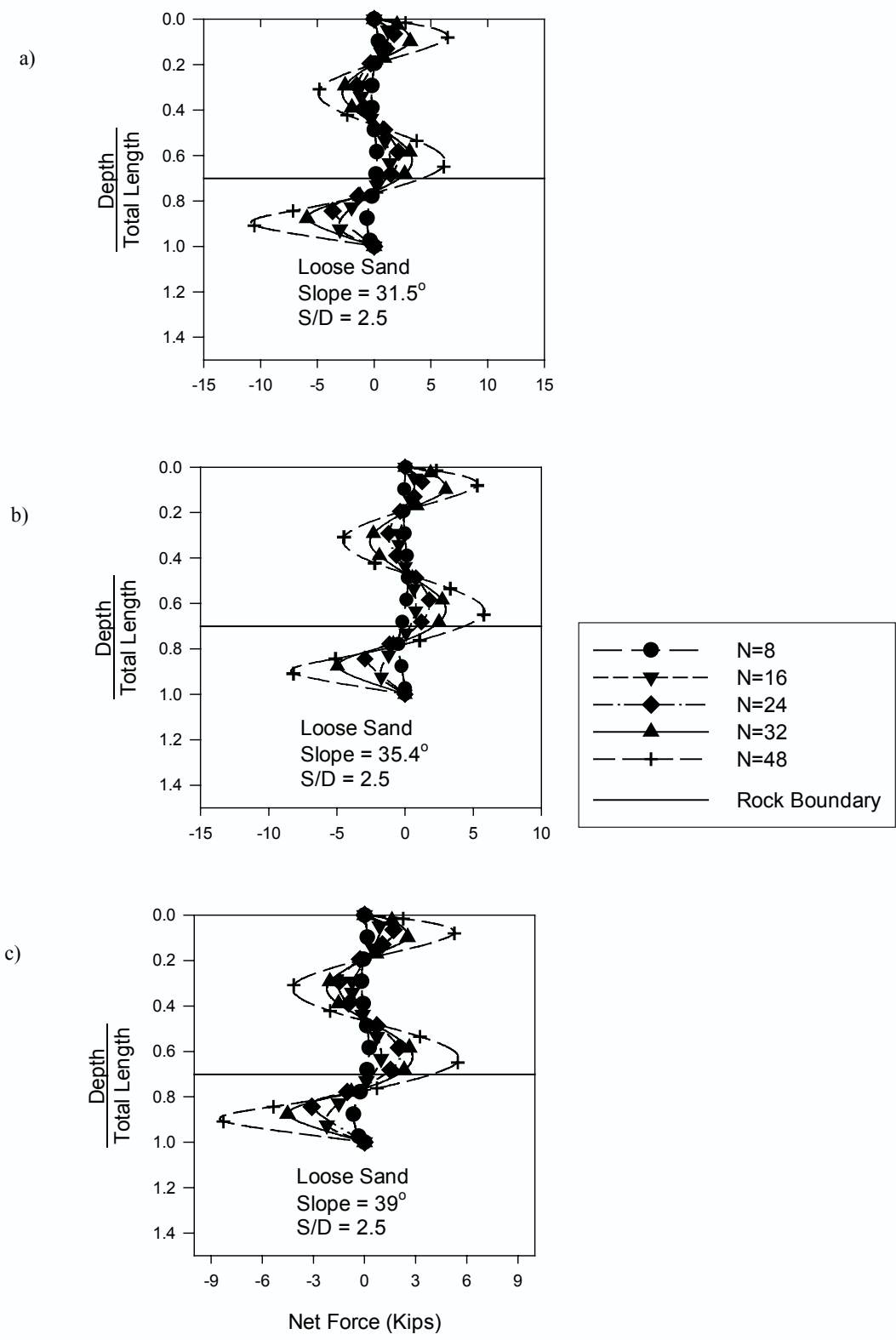
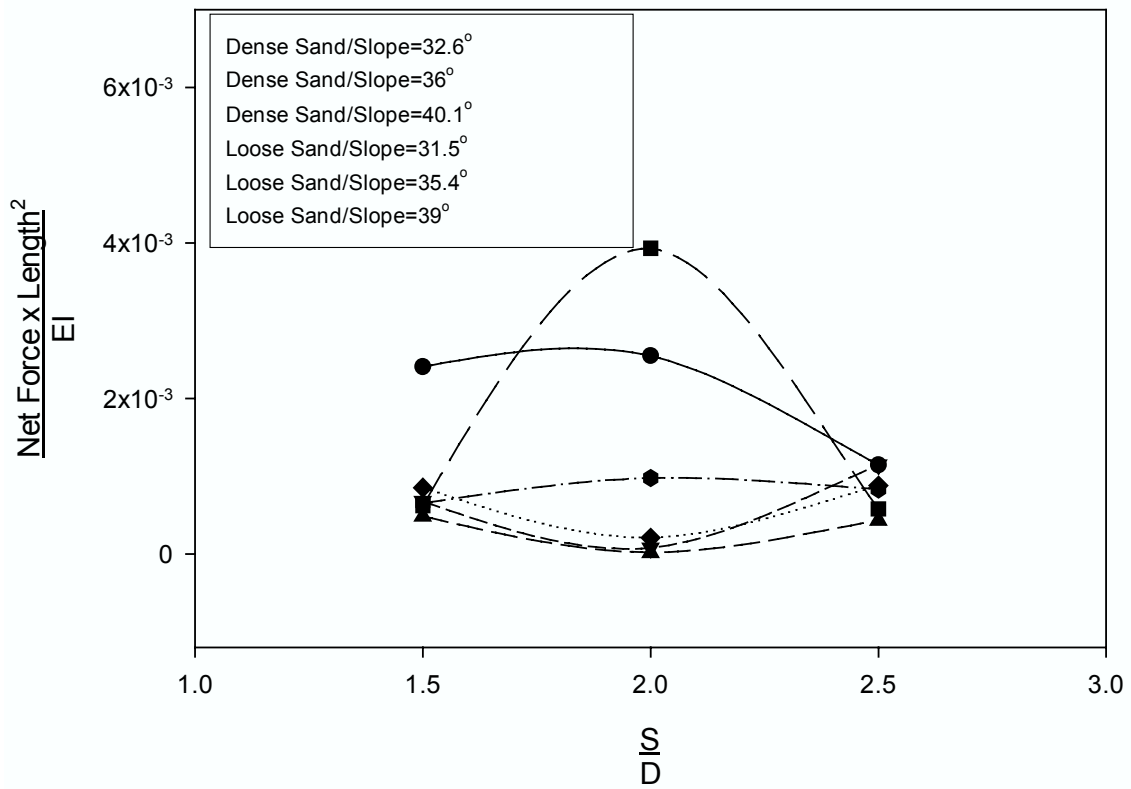


Figure 4.10(b) Net force distribution with depth in loose sand slopes (S/D=2.5)



**Figure 4.11 Net force vs. S/D in sand slope (N=16)**

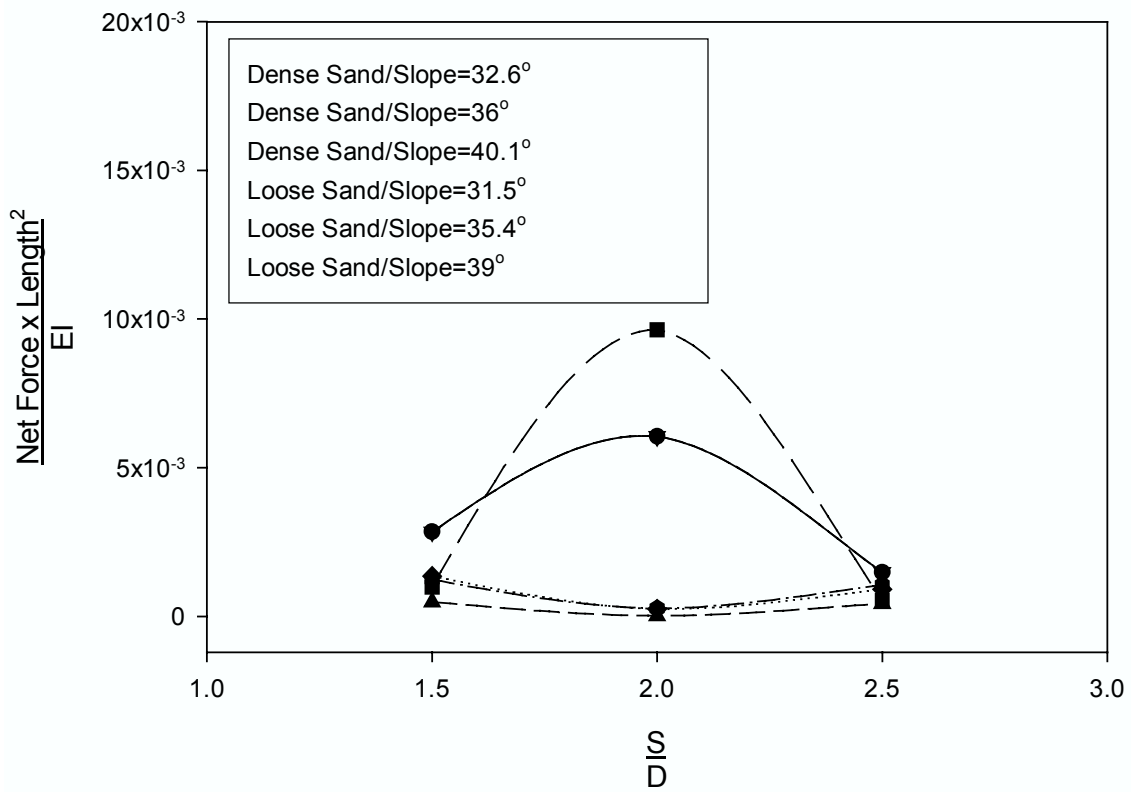
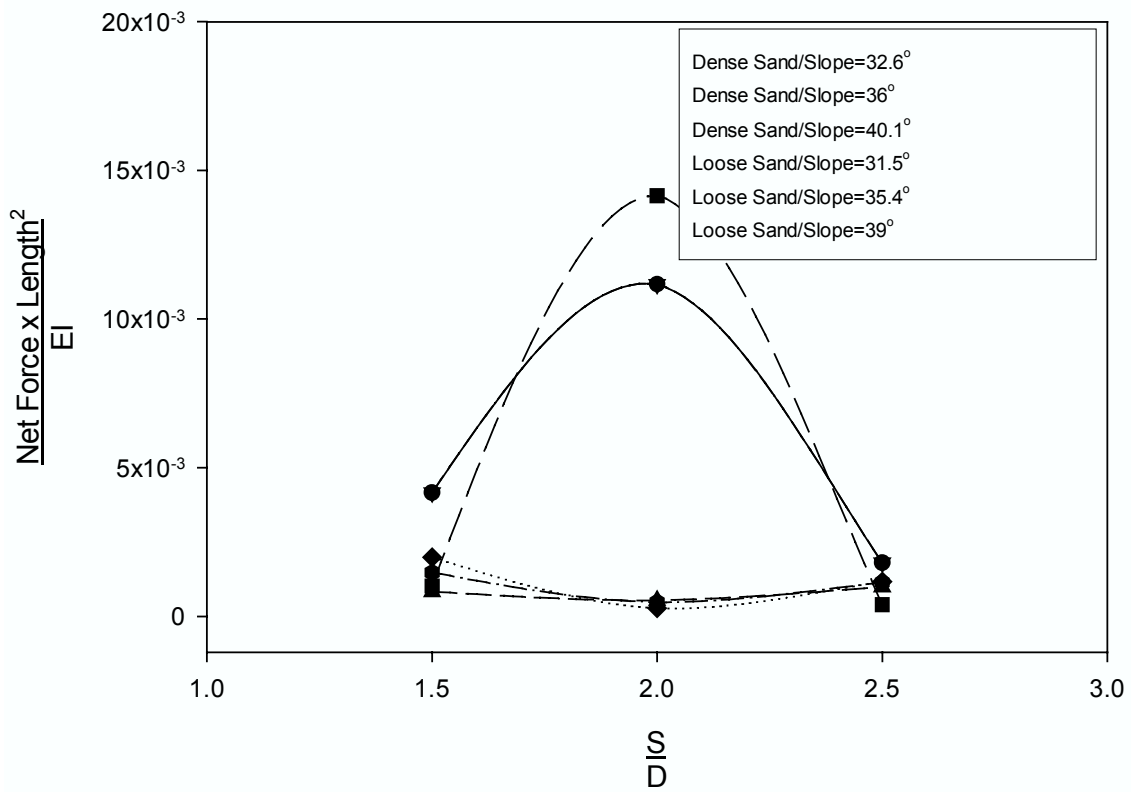
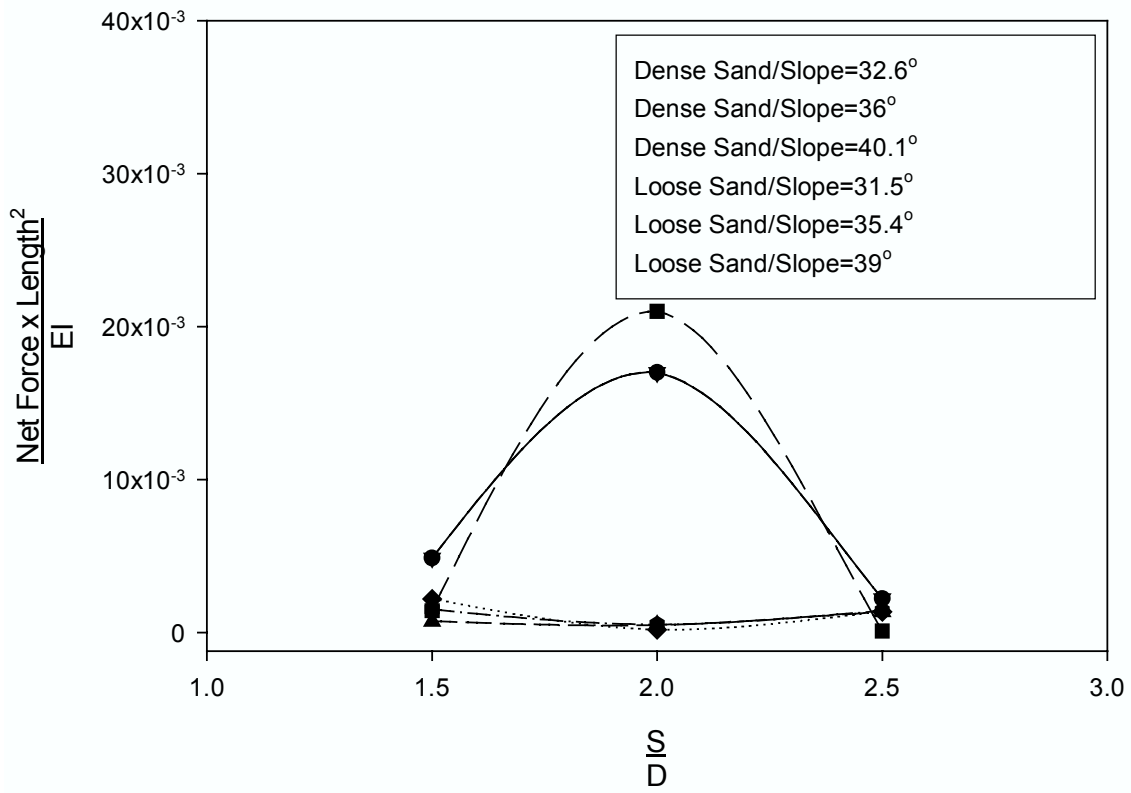


Figure 4.12 Net force vs. S/D in sand slope (N=24)



**Figure 4.13 Net force vs. S/D in sand slope (N=32)**



**Figure 4.14 Net force vs. S/D in sand slope (N=48)**

Fig. 20.(N=48)

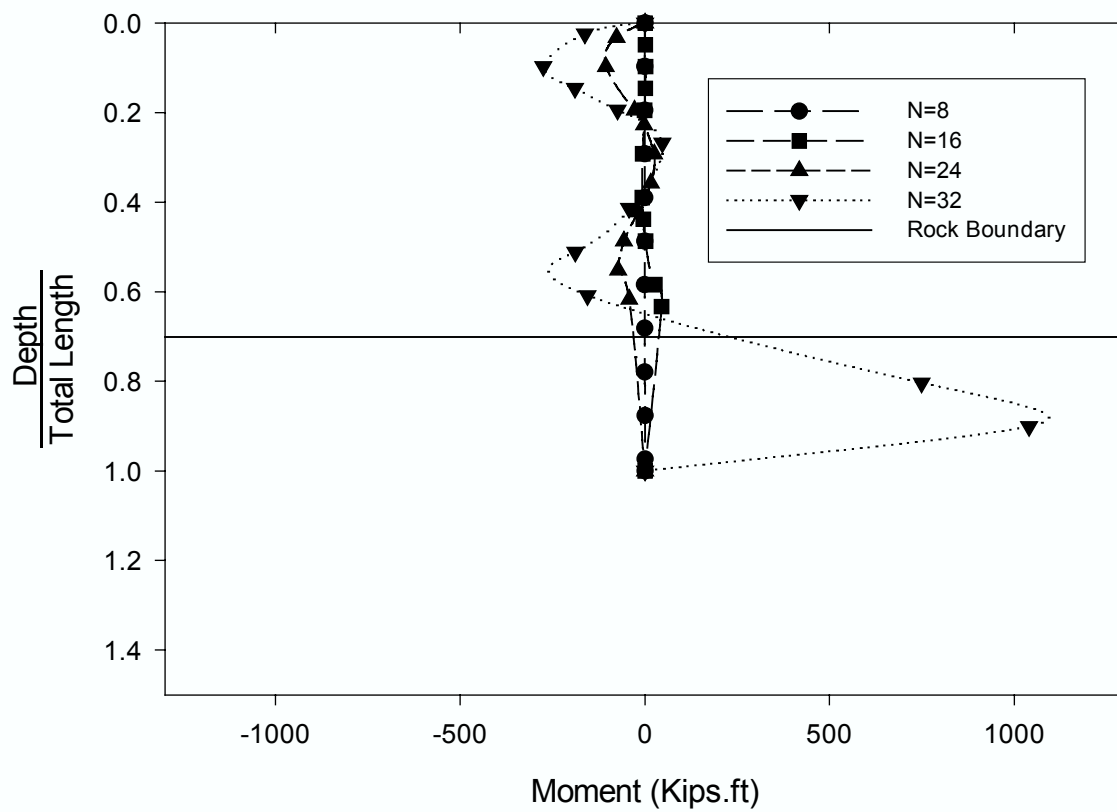


**Figure 4.15 Moment distribution of test C1**

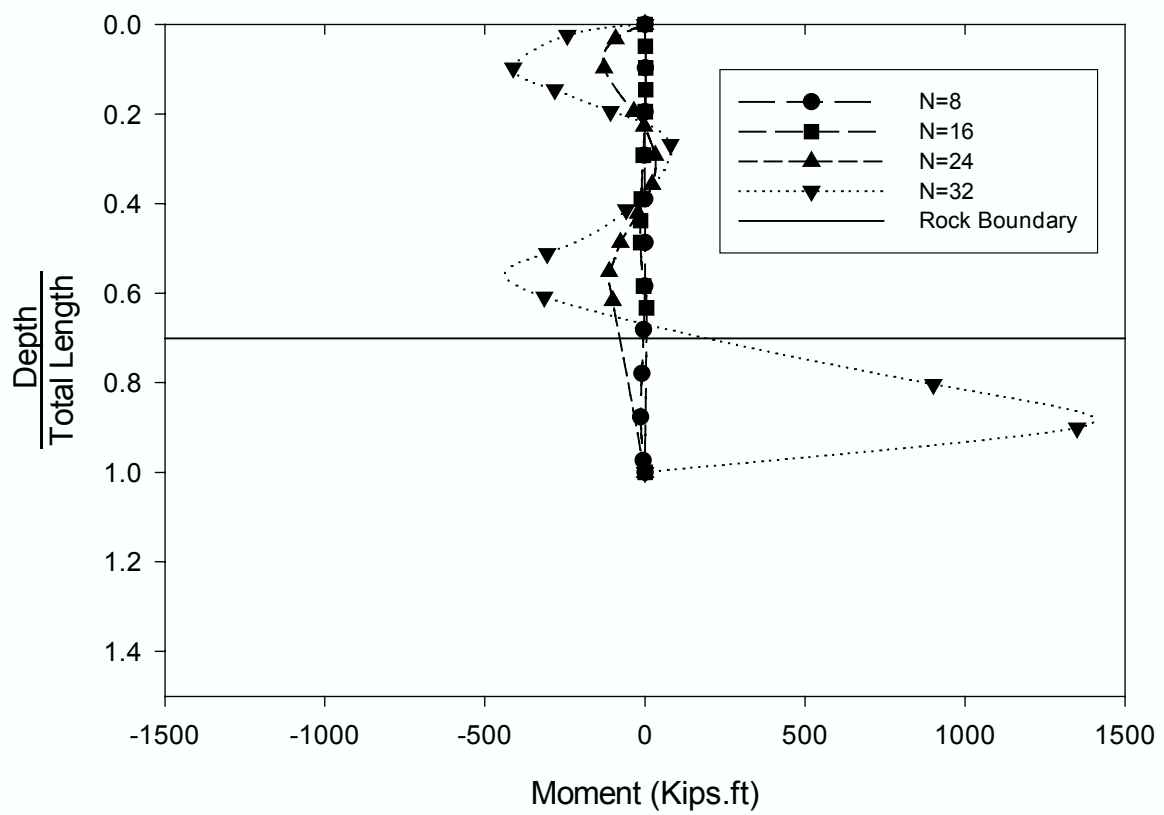


**Figure 4.16 Moment distribution of test C2**

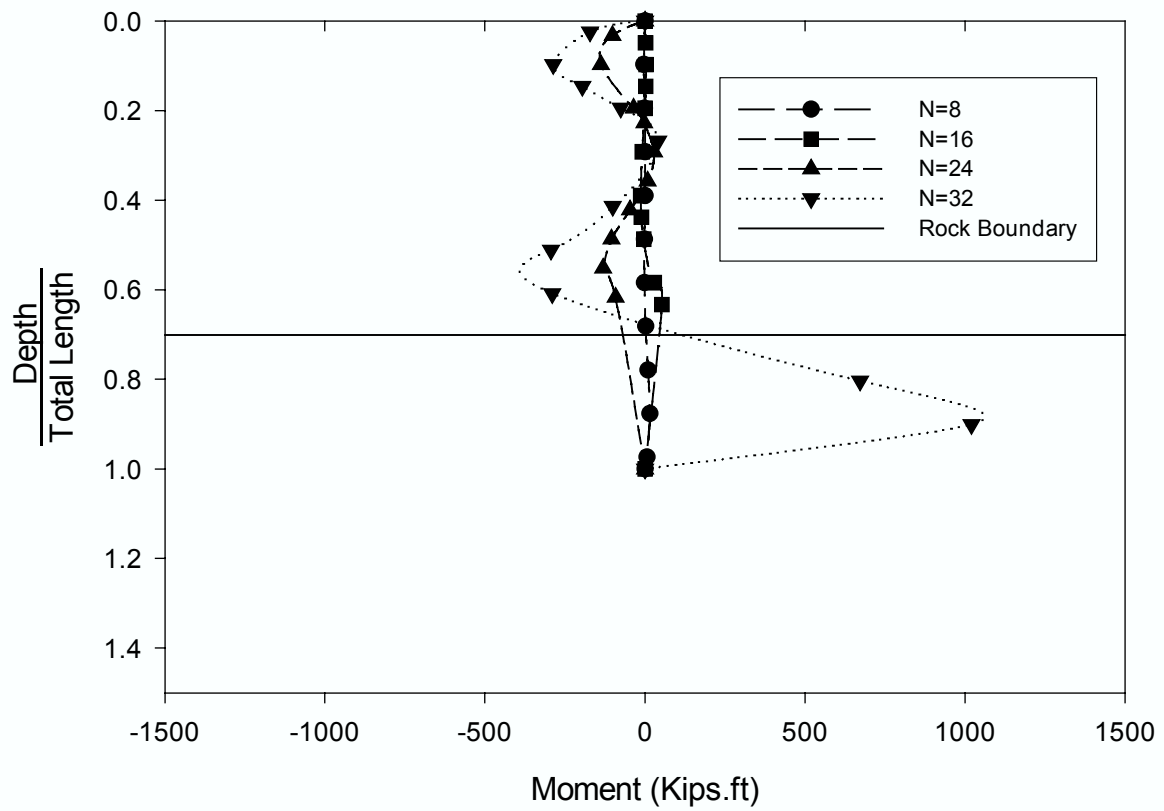


**Figure 4.17 Moment Distribution of test C3**

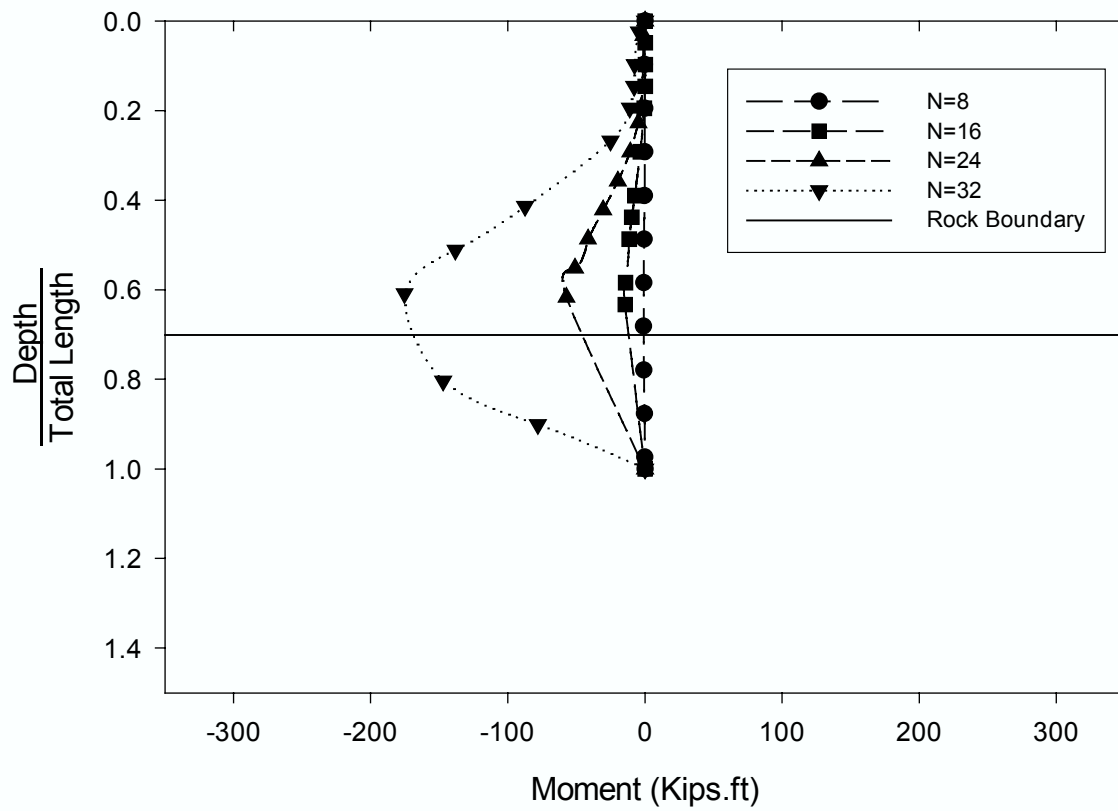


**Figure 4.18 Moment distribution of test C4**

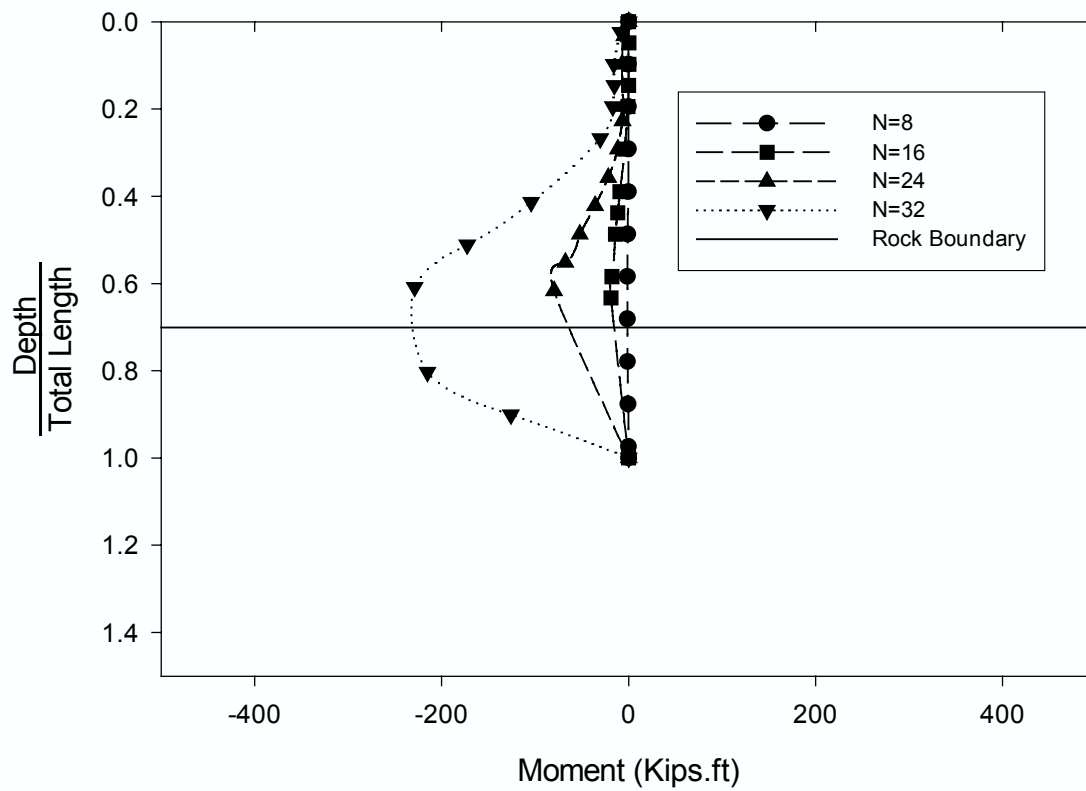


**Figure 4.19 Moment distribution of test C5**

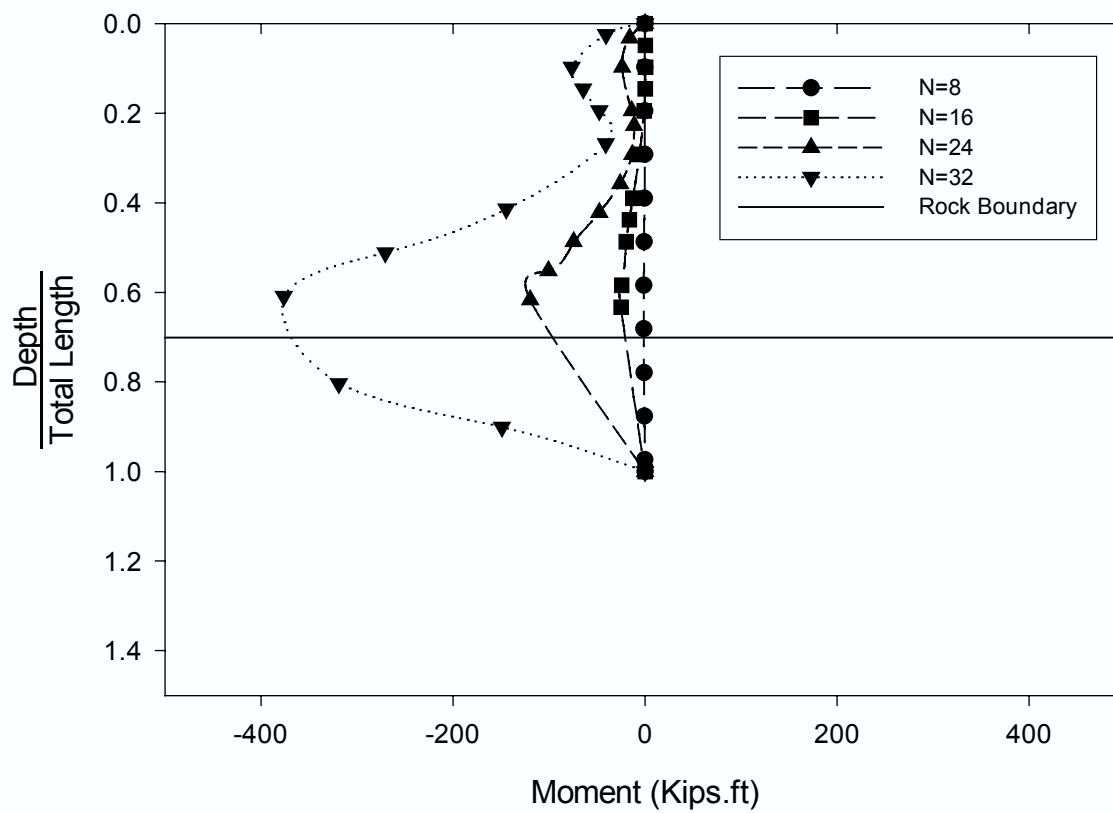


**Figure 4.20 Moment distribution of test C6**

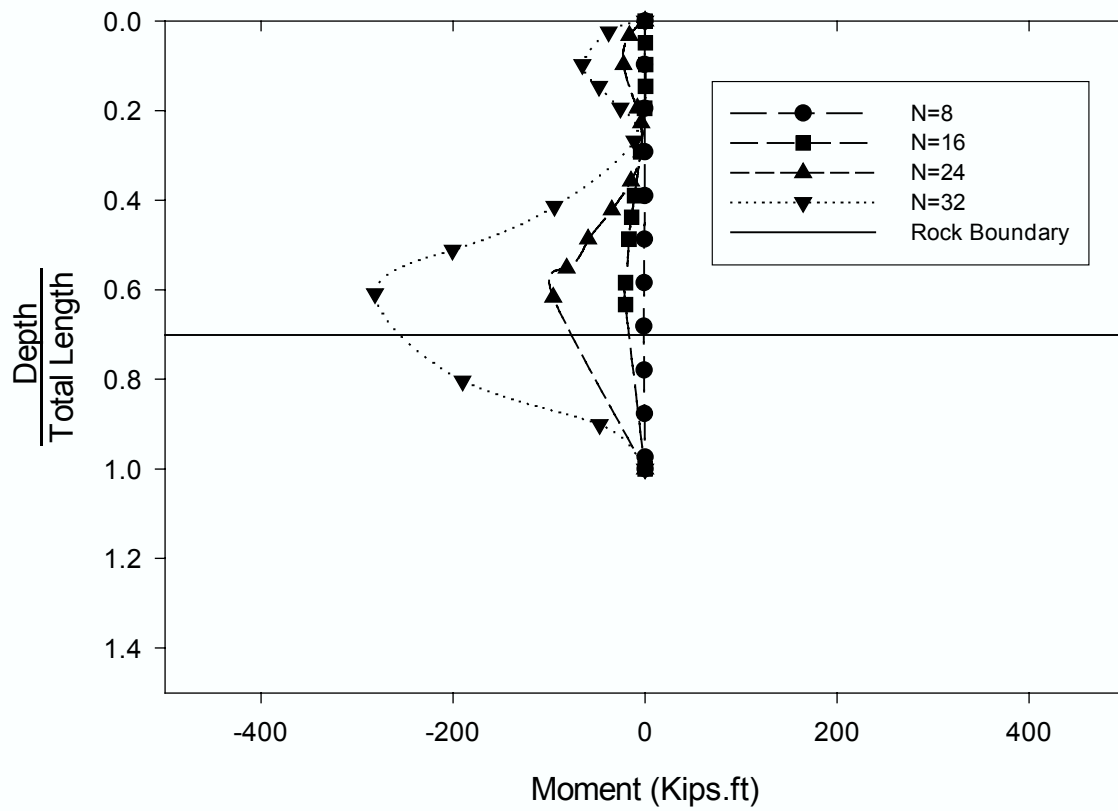


**Figure 4.21 Moment Distribution of test C7**

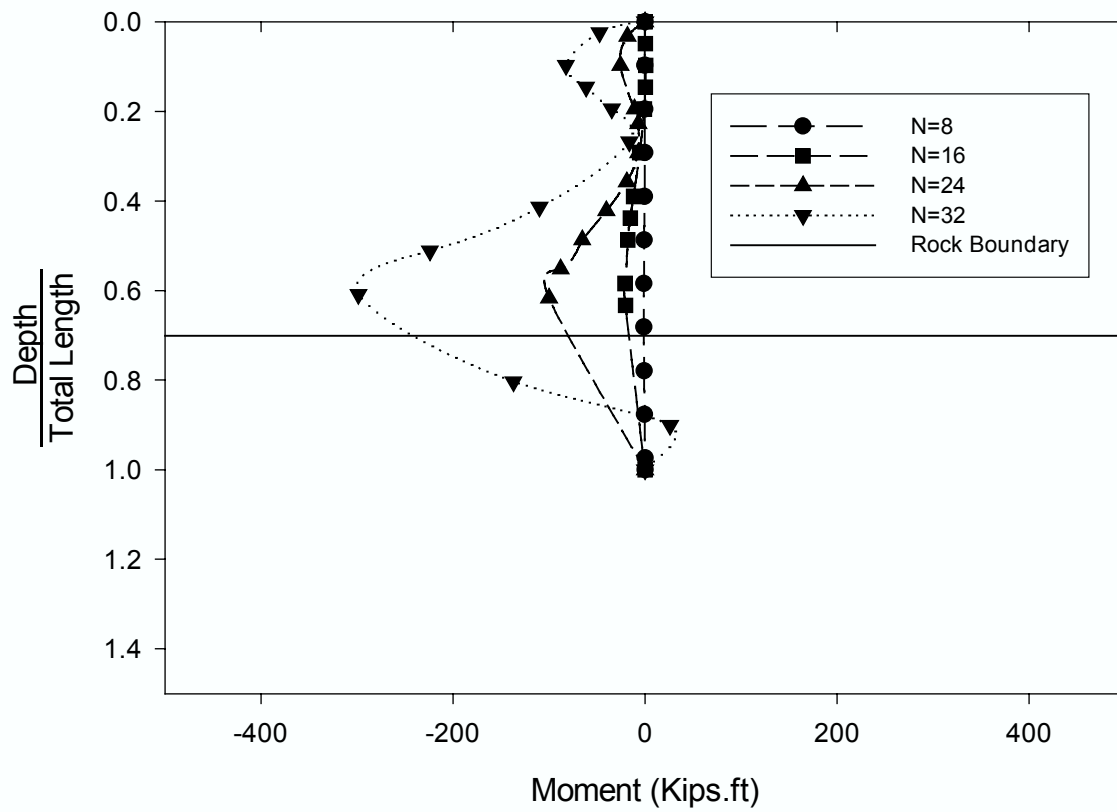
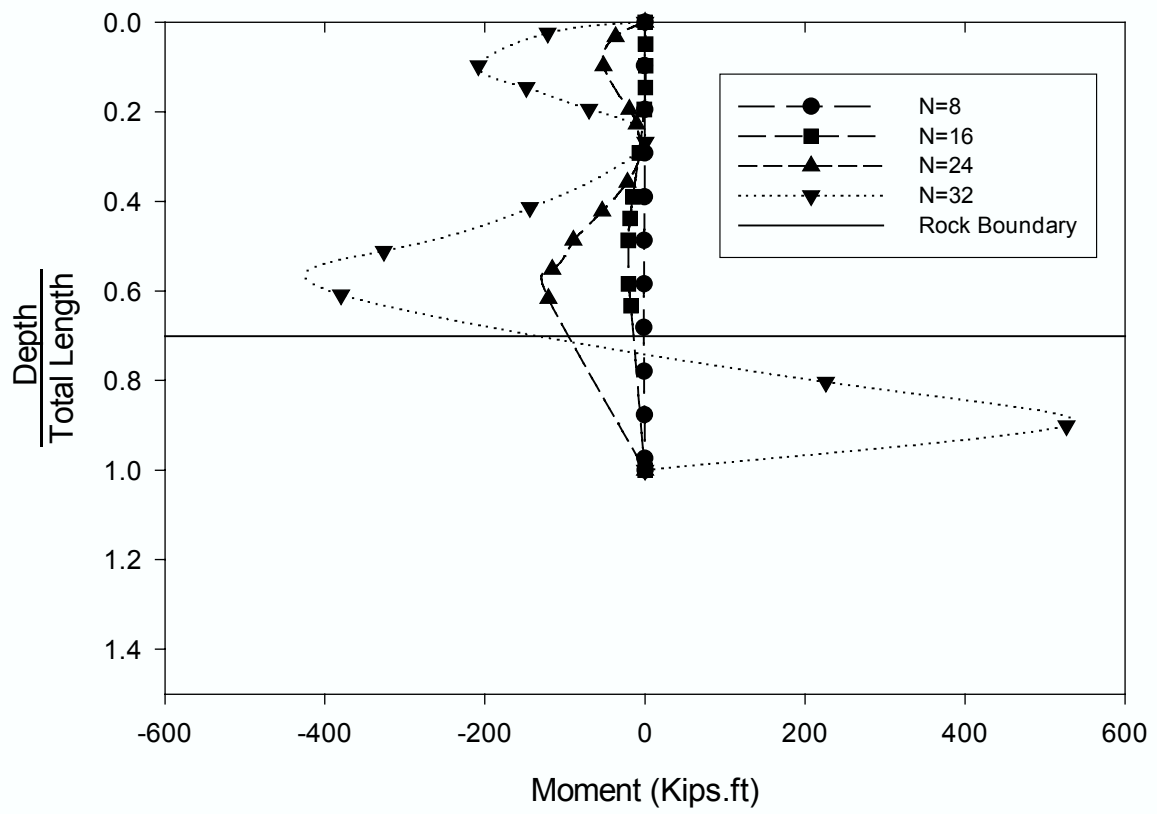
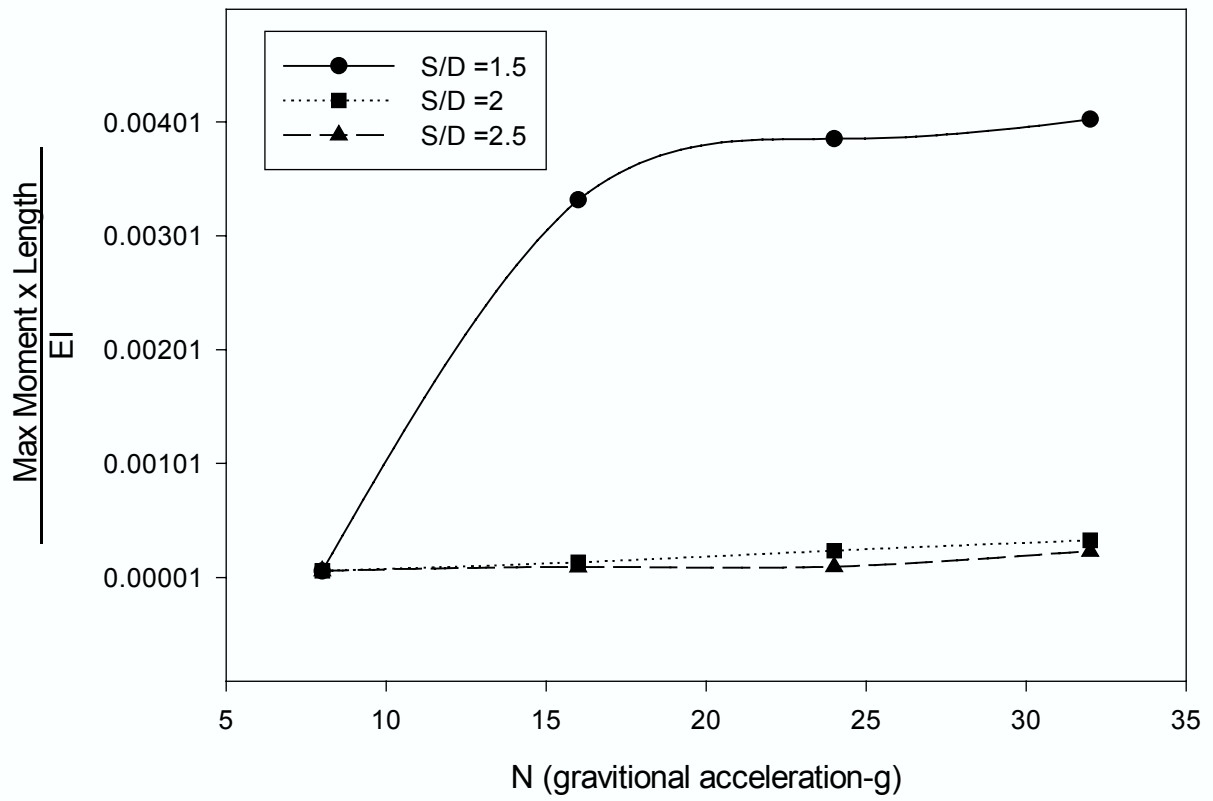


Figure 4.22 Moment distribution of test C8



**Figure 4.23 Moment distribution of test C9**



**Figure 4.24 Normalized maximum moment for pile in clay with slope angle =34°**

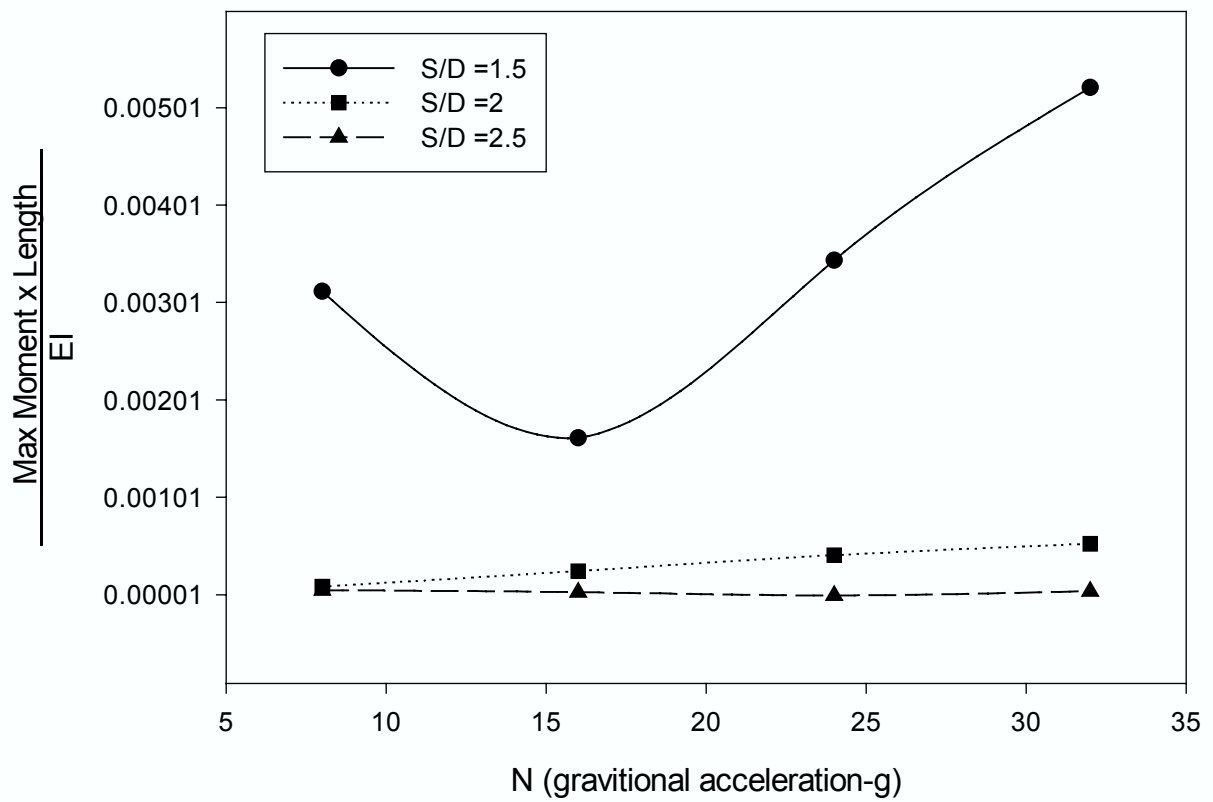


**Figure 4.25 Normalized maximum moment for pile in clay with slope angle =45°**

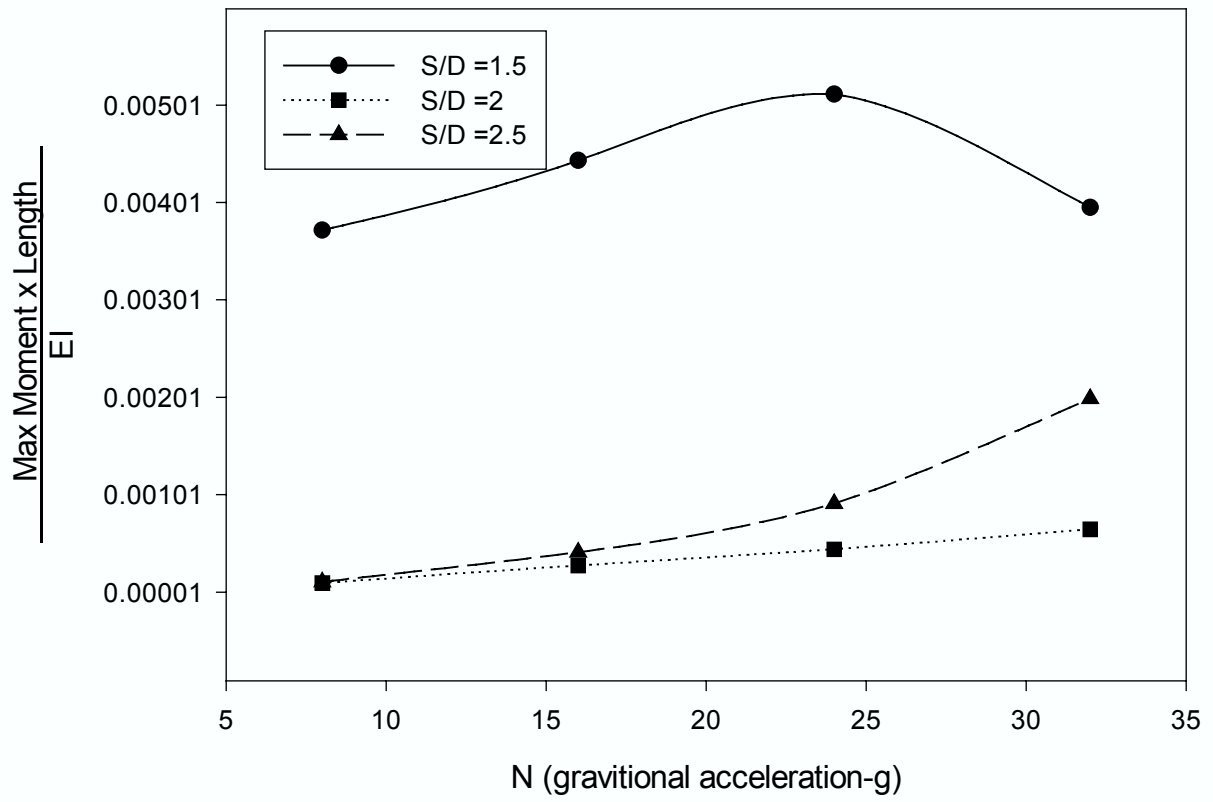
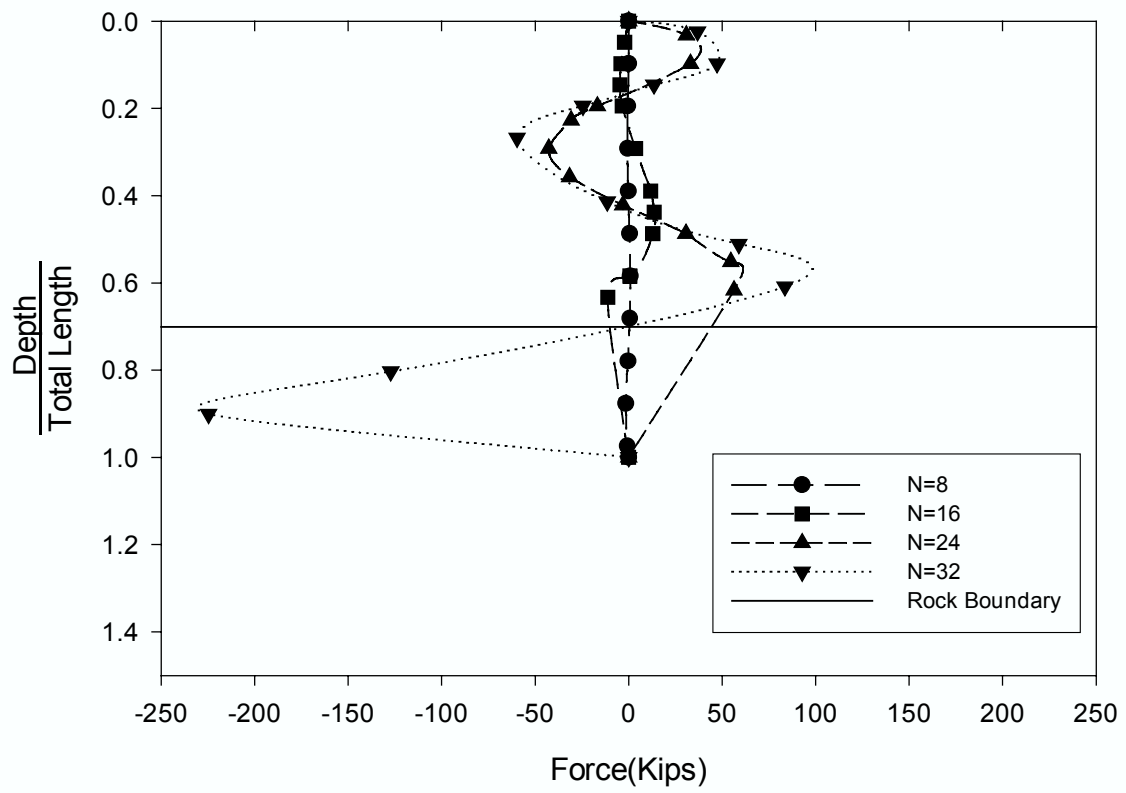
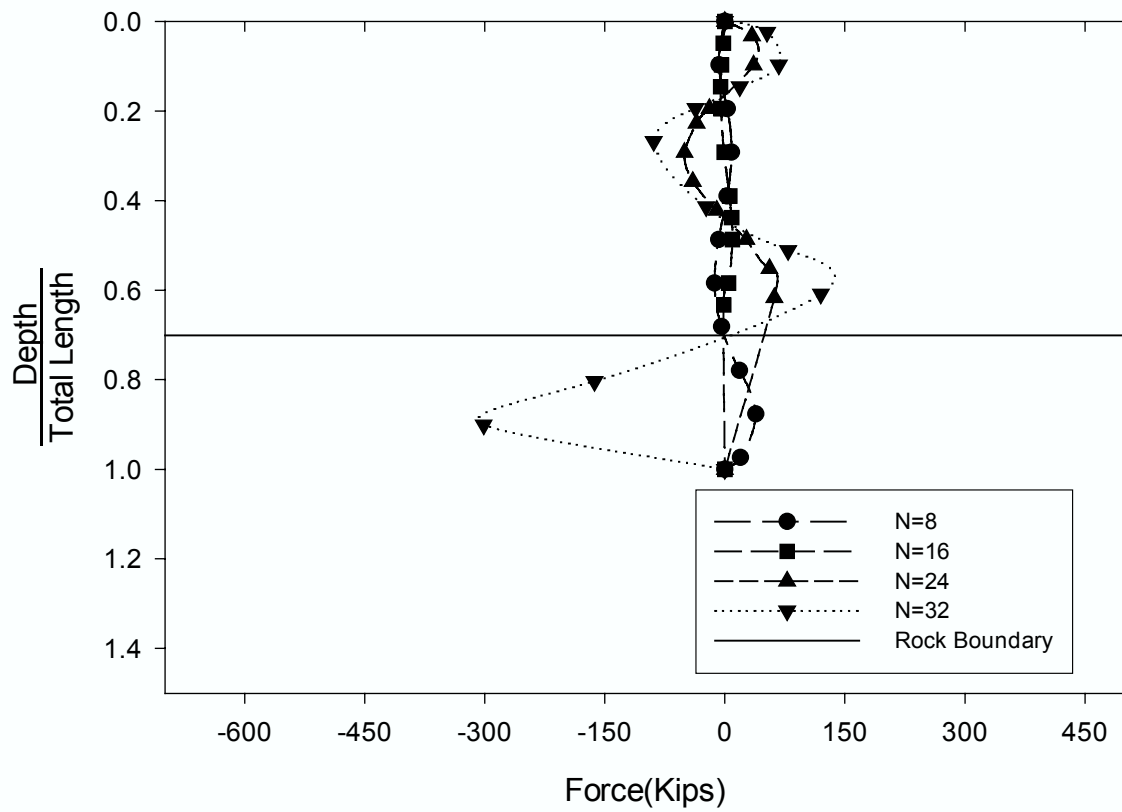


Figure 4.26 Normalized maximum moment for pile in clay with slope angle =57°



**Figure 4.27 Force distribution of test C1**



**Figure 4.28 Force distribution of test C2**

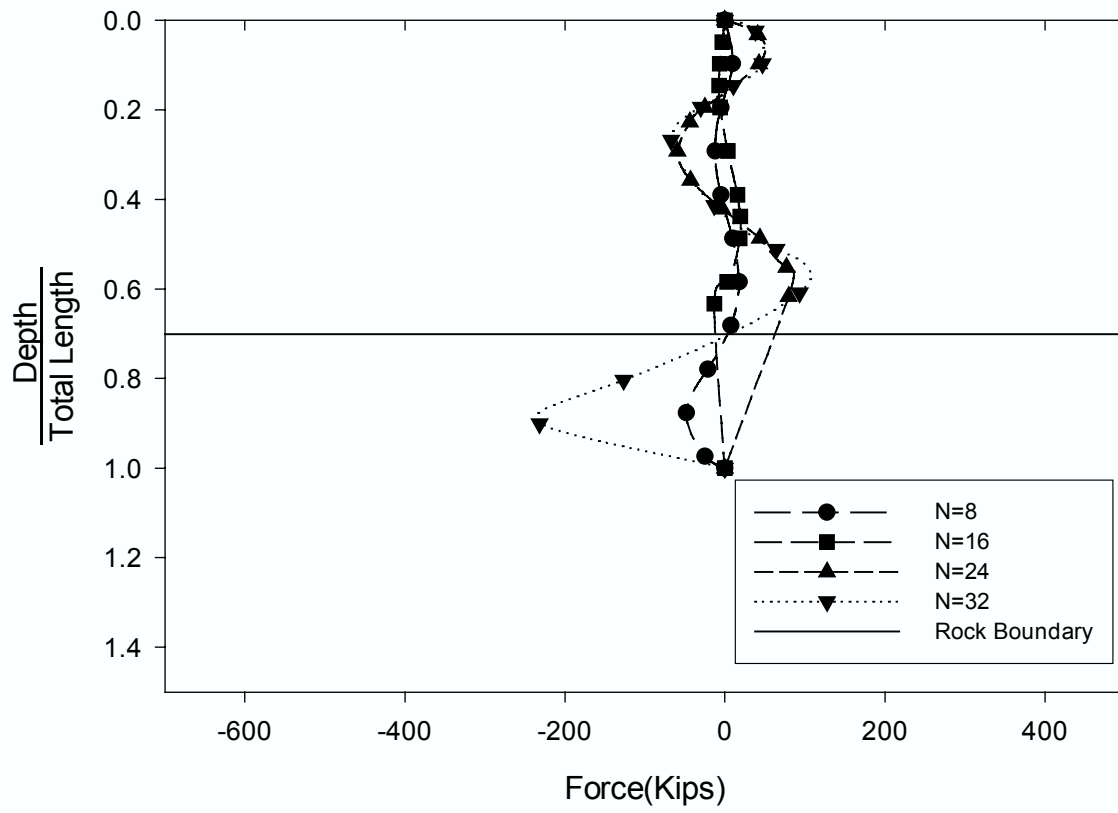


**Figure 4.29 Force distribution of test C3**

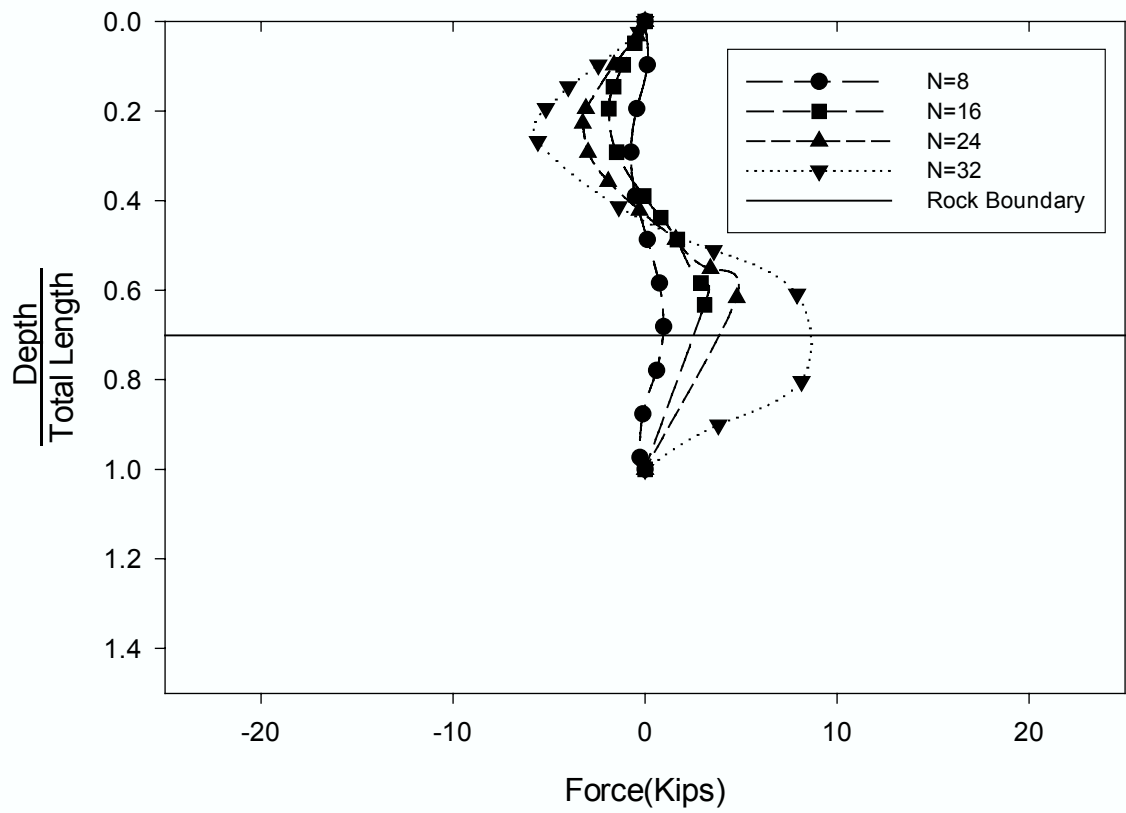


**Figure 4.30 Force distribution of test C4**

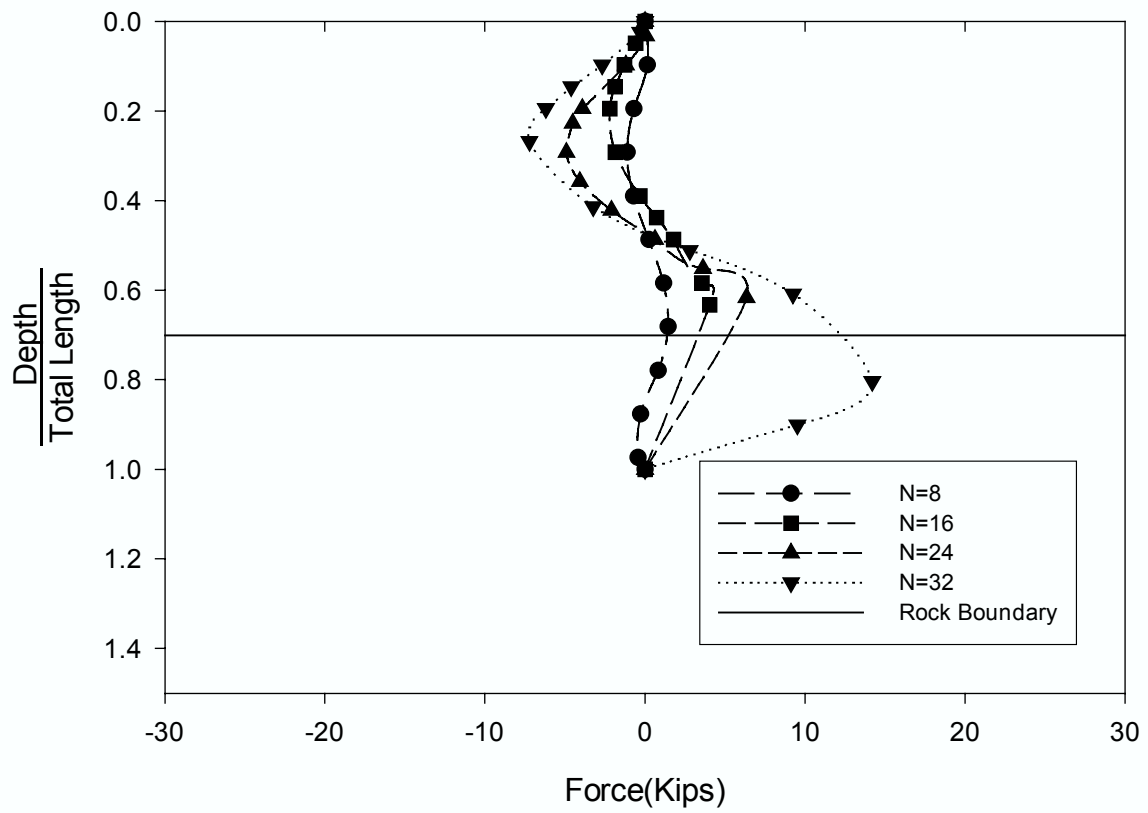


**Figure 4.31 Force distribution of test C5**

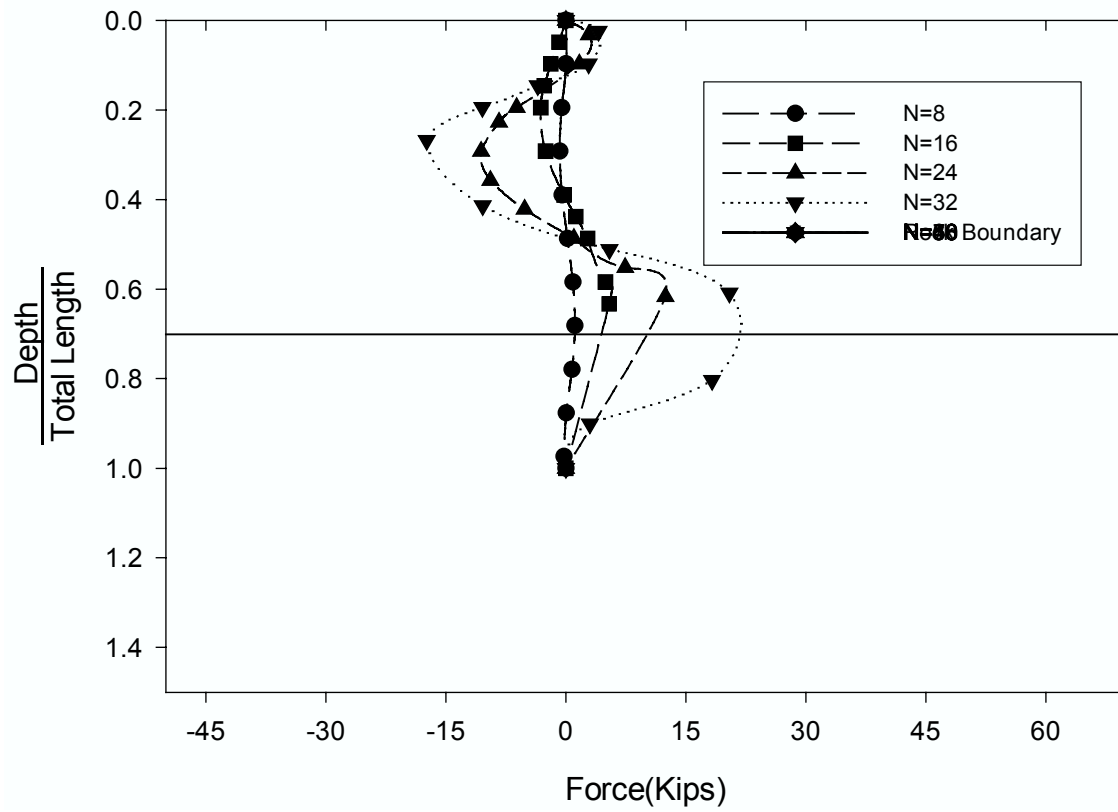
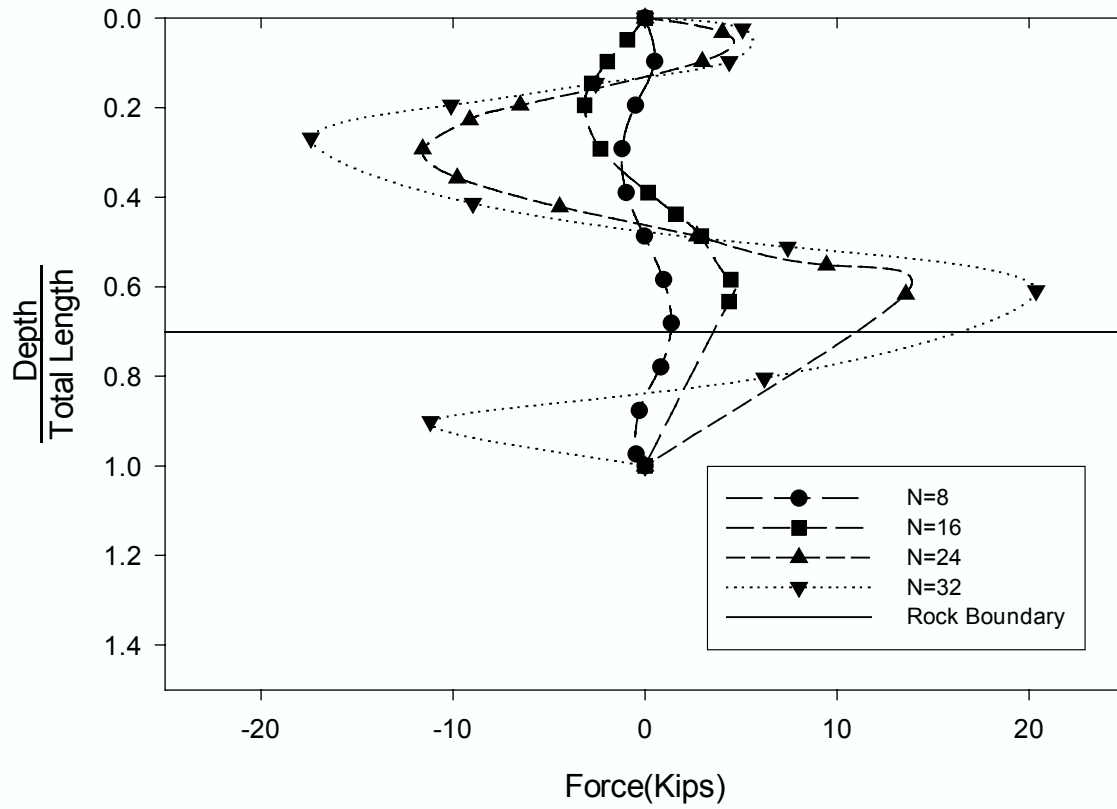
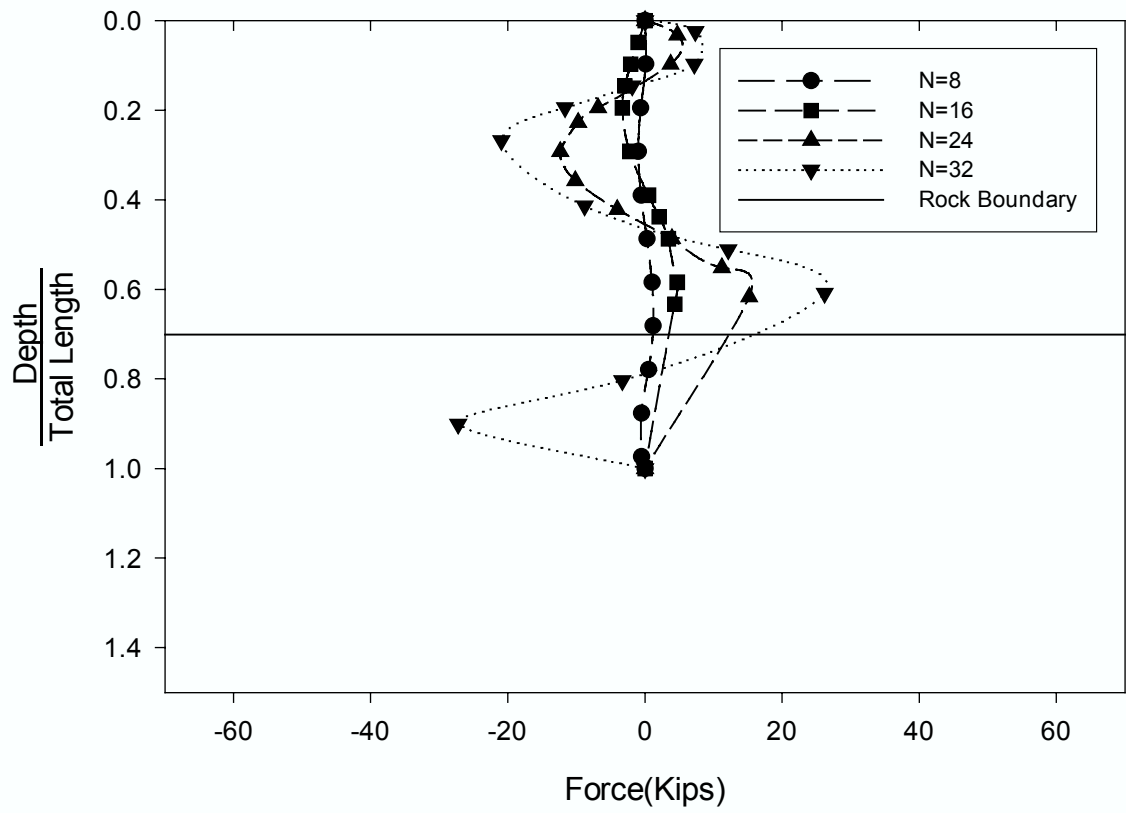


Figure 4.32 Force distribution of test C6



**Figure 4.33 Force distribution of test C7**



**Figure 4.34 Force distribution of test C8**

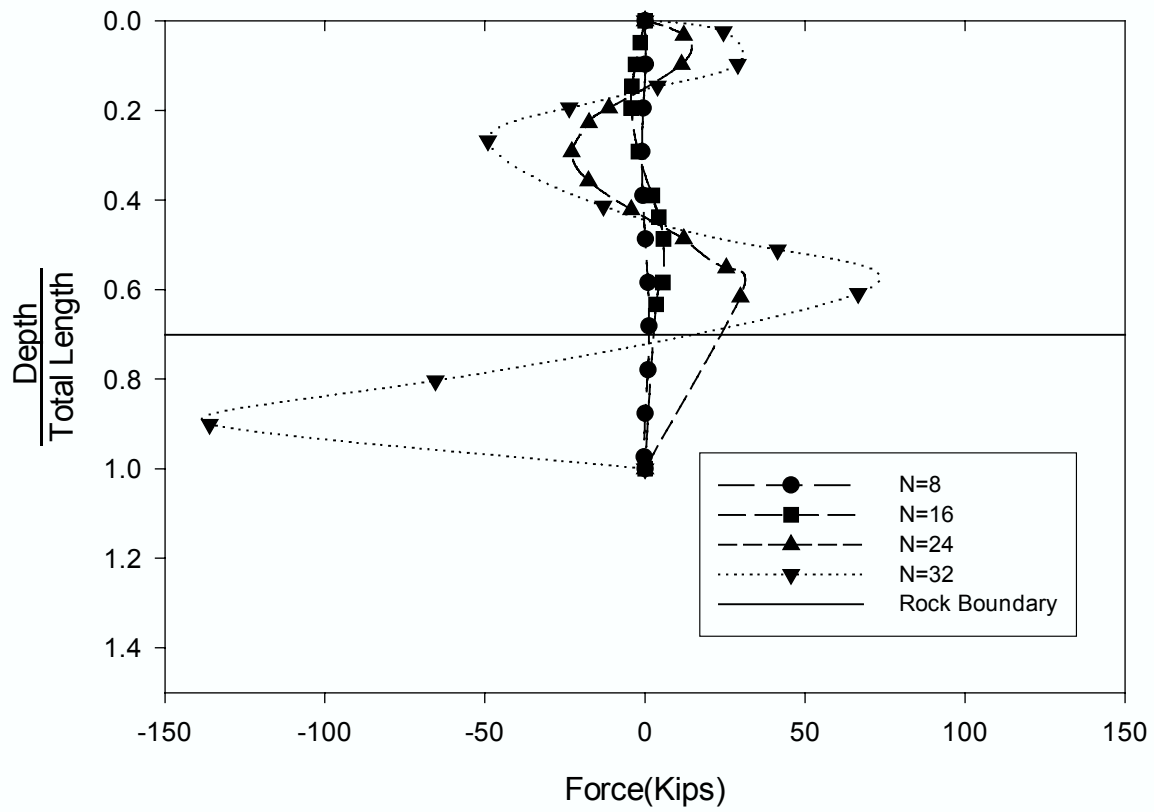


**Figure 4.35 Force distribution of test C9**

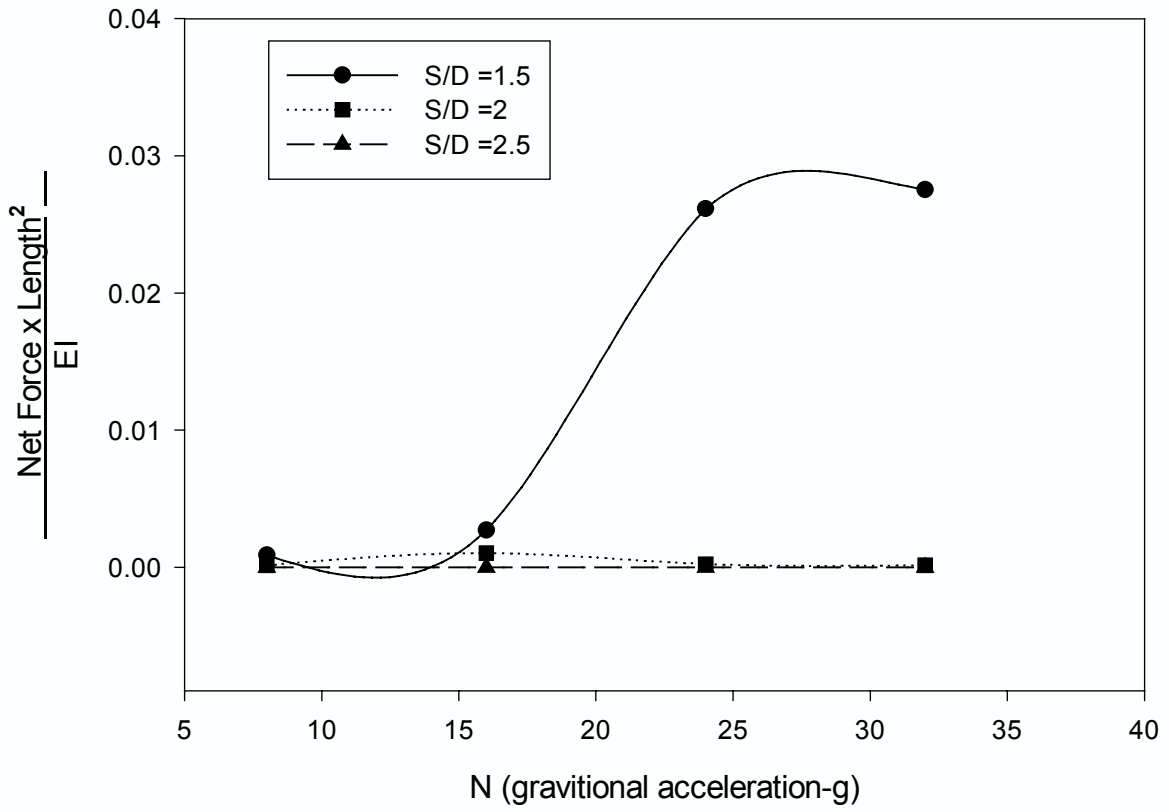


**Figure 4.36 Normalized net force for pile in clay with slope angle =34°**

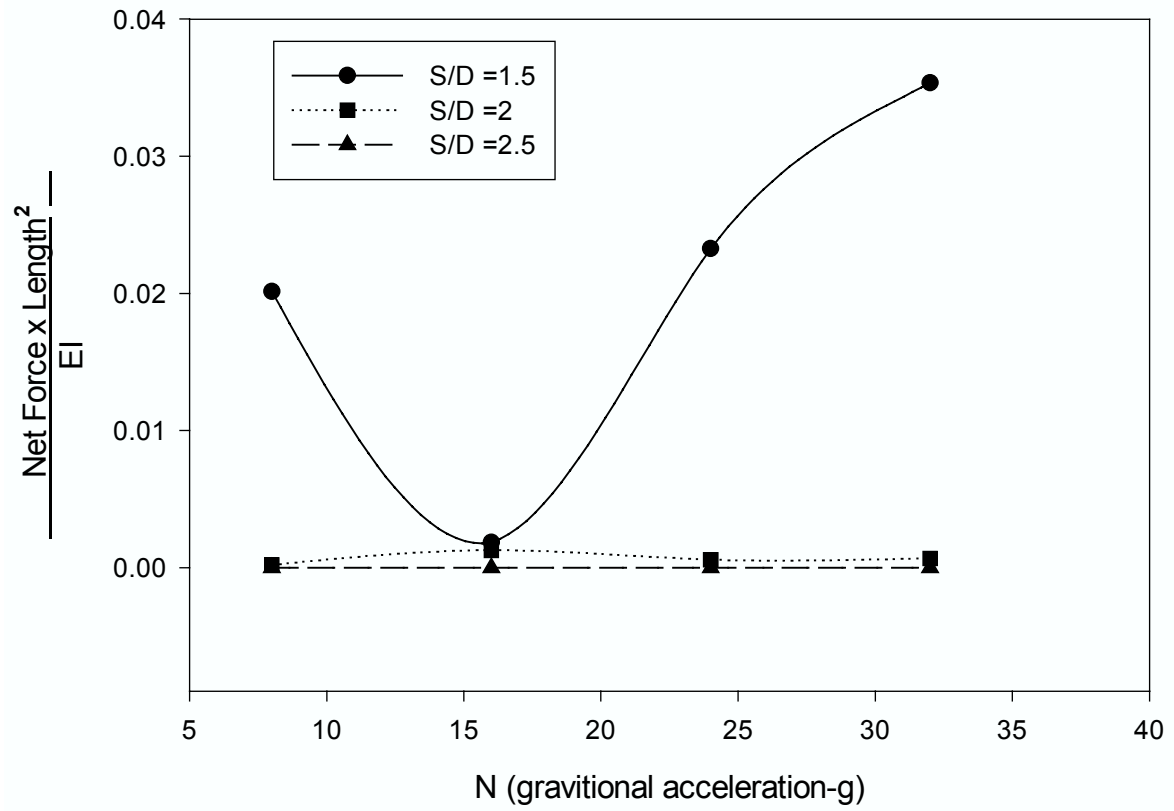


**Figure 4.37 Normalized net force for pile in clay with slope angle =45°**

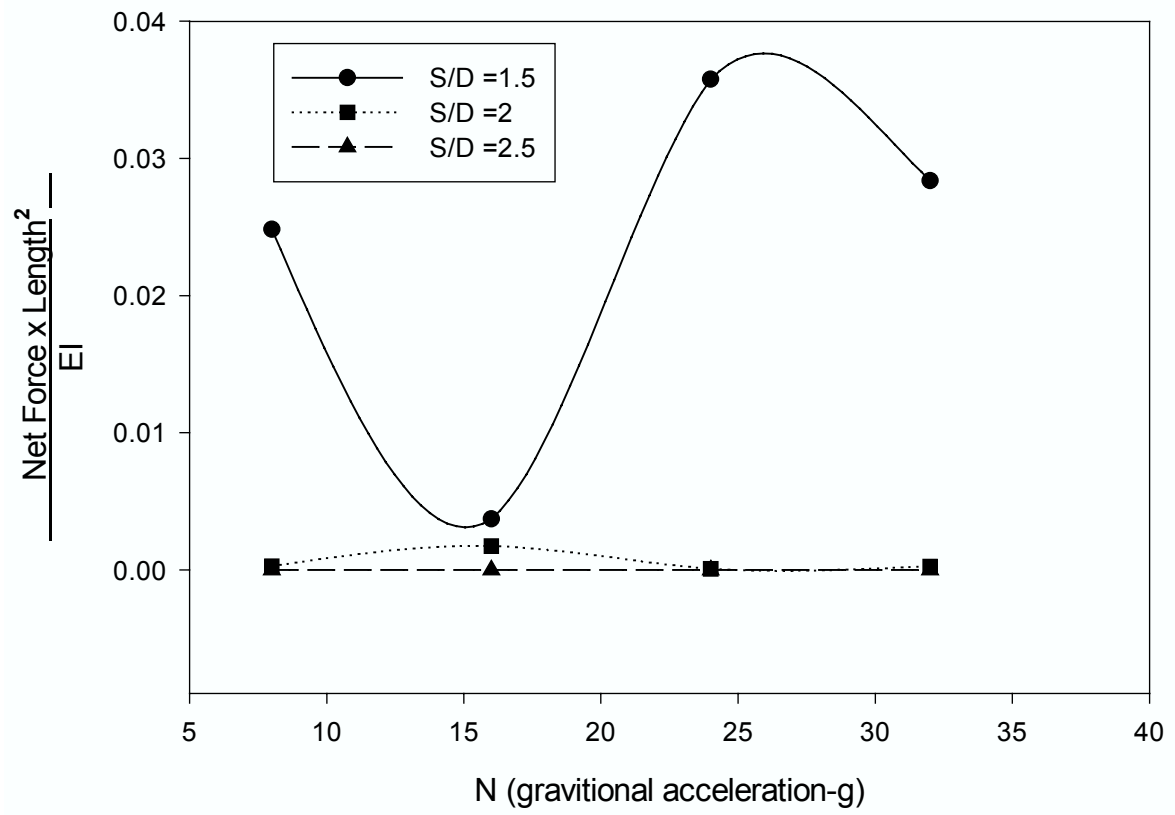


**Figure 4.38 Normalized net force for pile in clay with slope angle =57°**

## **CHAPTER V**

### **NUMERICAL STUDY OF SOIL ARCHING MECHANISM IN DRILLED SHAFTS FOR SLOPE STABILIZATION**

#### **5.1 INTRODUCTION**

During the past decades, the installation of drilled shafts for slope stabilization purpose has come into comparatively widespread use and proven to be an effective means against excessive slope movement. The methods used for the design and analysis of drilled shaft stabilization, however, vary widely due to the lack of sufficient information on the stabilization mechanisms.

It is a general practice that drilled shafts designed to prevent excessive movement of a slope are normally installed beyond the depth of a potentially sliding surface and most often into a firm, non-yielding soil strata underneath. Since the displacement of the soil mass above the potentially sliding surface is expected to be more significant than that beneath the sliding surface, significant shear force and bending moment will develop in the drilled shaft at the location close to the potential sliding surface. This mechanism works in a way similar to a cantilever beam with the earth pressure on the drilled shaft as load and the part of the drilled shaft socked in rock as the fixed end. It is in this way the earth pressure developed due to a potential sliding soil mass is transferred to the soil beneath the potential sliding surface. Therefore, excessive soil movement can be

prevented, and a slope is thus stabilized through the reinforcement mechanism.

On the other hand, since the drilled shafts installed in a row with certain spacing between them are discrete structures rather than a continuous retaining wall the soil mass between the drilled shafts can move under certain circumstances where localized soil failure may occur. The subsequent movement may cause the slope soil mass to go around the drilled shafts and experience considerable extra movement. Consequently, the effectiveness of using drilled shafts to stabilize a slope is highly dependent on the drilled shafts (size, spacing, and location) and the soil conditions.

Engineering practices and laboratory experiments have shown that discrete piles such as drilled shafts embedded into a firm, non-yielding base in a slope can provide significant additional stability to a slope if conditions for soil arching are met (Bosscher et al., 1986). Soil arching is also referred to as a localized mechanism by which the stresses in the yielding soil are redistributed unto the unyielding portion of the soil and eventually unto the supporting piles. As a result, the driving force exerting on the soil mass between the piles is reduced, leading to a higher factor of safety of the slope.

Soil arching, the transfer of soil stresses from a yielding mass of soil onto adjacent stationary parts, is a phenomenon commonly encountered in geotechnical engineering. The arching effect in sandy soil was first investigated and defined by Terzaghi (1936, 1943). By placing sand above a platform that contained a narrow strip of a trap door, Terzaghi (1936) showed that when the trap door was lowered slightly, the vertical earth pressure exerted on the door decreased greatly whereas the pressure on the adjoining parts of the platform increased. This was attributed to the shearing stresses developed between

the moving (yielding) mass and the adjoining stationary sand mass, which resisted the descent of the mass of sand located above the yielding trap door. More recently, Atkinson and Potts (1977) and Bolton (1979) studied soil arching in connection with the stability of tunnels. Soil arching in piled walls was found to occur as the soil attempted to move through the fixed piles which were firmly embedded in a non-yielding base (Bosscher and Gray, 1986).

One important consideration in the design of drilled shafts in stabilizing a slope is the maximum allowable spacing between the drilled shafts so that soil arching still maintains. One practical solution may be obtained from the laboratory study. Chen et al. (1997) conducted a series of laboratory tests on the group effects of drilled shafts subjected to soil movement, where the effects of free head and capped head were studied respectively. Test results indicated that, when the pile spacing was equal to or larger than eight times of pile diameter, the pile in a group behaved as if they were single piles. Similar results regarding the critical ratio of clear spacing to pile diameter was also found in the arching model test conducted by Adachi et al. (1989).

The other important consideration about drilled shaft design is how much percentage of force, which was originally transmitted to the soils between the piles, would be transferred to the supporting piles under various conditions. Ito and Matsui (1975) developed an analytical procedure to derive closed-form equations for determination of earth pressure acting on the soil between the piles. These analytical results were helpful for a better understanding of the arching effects. Similarly, the work by Wang and Yen (1974), Bransby and Smith (1975), and Wang and Liang (1979) have

provided various forms of analytical models for studying the piles subjected to soil movements.

Bosscher et al. (1986) conducted a laboratory test to experimentally model soil arching for the sandy slope, where the fixed gates and swing gates were used to simulate embedded vertical piles and the soil mass between piles, respectively. By adjusting the width of swing gates, in conjunction with other variations in soil properties, the influence of variation of various controlling parameters was recorded. It was found that the gate width was the key controlling factor, and the proportion of the load on the swing gate increased as the swing gate increased in width. In other words, adopting the analogy between the swing gate width and the spacing between piles, the closer of the pile spacing, the stronger arching effect. Consequently, more loads would have transferred to the fix piles. Typical experimental results showed that when the clear spacing was three times of the pile diameter, the percent of load transfer was around 30% for the case investigated.

In other experimental studies (Adachi et al., 1989; Low et al., 1994; 1996; Chen et al., 1997), results also indicated that the arching effect existed and it would significantly increase the slope stability, depending on the soil and pile conditions. Incorporating the arching mechanism into slope stability analysis and thereafter the stabilization design, however, requires a comprehensive investigation of the conditions for soil arching to develop. At present, the lack of an adequate information leads to a design engineer to err on the conservative side, and to place the piles closer together than they need be.

The objective of this study is to provide quantitative information base and data

pool of soil arching in drilled shafts stabilized slopes. In order to obtain enough data to cover a wide spectrum of drilled shafts and soil conditions encountered in geotechnical practices, all potential factors that may exert influences on the development of soil arching are investigated by a series of numerical simulations with aid of the finite element method (FEM). In addition, quantitative examinations are made by varying combinations of some key factors. The FEM analysis results form a base for the development of a methodology to determine the force acting on the drilled shafts in slopes, considering the soil arching mechanism. As a part of verification of the accuracy of numerical analysis, comparisons are then carried out between the experimental measurements available in the literature and the numerical predictions.

## **5.2 FINITE-ELEMENT MODELING**

As shown in Fig.5.1, drilled shafts of diameter  $d$  with spacing  $s$  are installed in a row through a moving soil mass into a firm, non-yielding base underneath. Once the excessive movement occurs within the slope above the slip surface, a soil-shaft interaction induced lateral force is expected to provide an additional resistance to slope movement. This lateral force would be much higher if soil arching develops. The effect of soil arching can thus be characterized as the phenomenon of stress or load transfer. In this study, the load transfer curves will be examined based on relative movement between the soil mass and the drilled shafts. Taking a slice of soil with unit thickness as shown in Fig. 5.1(a) and assuming that soil movement is confined to in-plane movement, then a two-dimensional modeling is considered to be sufficient to capture the local soil movement

around the drilled shafts. Due to symmetry, only a region between the drilled shafts needs to be analyzed, as shown by the shadowed portion in Fig.5.1(b). A typical model with the boundary conditions and the FEM mesh is showed in Fig.5. 2.

The soil movement is simulated by the prescribed displacements imposed on the boundary BC. The 6-node triangular elements with the second order interpolation for displacement are used to represent both the soil mass and the shaft domain. In addition, the interface elements, provided by program PLAXIS with the ability to model discontinuity of displacement, are embedded between the piles and the soil to account for potential slippage.

The constitutive behavior of soil is simulated by an elastic perfectly-plastic model with Mohr-Coulomb yield criterion. According to the classical theory of plasticity, plastic strain rates are proportional to the derivative of the yield function with respect to the stresses. This is referred to as associated plasticity. However, for the dense cohesionless soil or sand which tends to experience plastic volumetric strain increments (or dilatancy) during shearing, the theory of associated flow rule leads to an erroneous prediction of soil deformation. Therefore, in addition to the yield function, a plastic potential function incorporating the dilation characteristics is introduced for the determination of plastic strain rates. This form of modified theory is denoted as non-associated plasticity and herein employed in the finite element program PLAXIS runs.

The Mohr-Coulomb yield condition is an extension of Coulomb's friction law to general states of stress. In Fact, this condition ensures that Coulomb's friction law is obeyed in any plane within a material element. The full Mohr-Coulomb yield condition

can be defined by three yield functions when formulated in terms of principal stresses (Smith and Griffith, 1982):

$$f_1 = \frac{1}{2}|\sigma'_2 - \sigma'_3| + \frac{1}{2}(\sigma'_2 + \sigma'_3) \sin \phi - c \cos \phi \leq 0 \quad (5.1a)$$

$$f_2 = \frac{1}{2}|\sigma'_3 - \sigma'_1| + \frac{1}{2}(\sigma'_3 + \sigma'_1) \sin \phi - c \cos \phi \leq 0 \quad (5.1b)$$

$$f_3 = \frac{1}{2}|\sigma'_1 - \sigma'_2| + \frac{1}{2}(\sigma'_1 + \sigma'_2) \sin \phi - c \cos \phi \leq 0 \quad (5.1c)$$

where the model parameters  $c$  and  $\phi$  are the cohesion and friction angle, respectively. In addition to the yield functions, three plastic potential functions used to determine the strain rates for elastoplasticity are defined for the Mohr-Coulomb model (Bolton, 1986):

$$g_1 = \frac{1}{2}|\sigma'_2 - \sigma'_3| + \frac{1}{2}(\sigma'_2 + \sigma'_3) \sin \psi \quad (5.2a)$$

$$g_2 = \frac{1}{2}|\sigma'_3 - \sigma'_1| + \frac{1}{2}(\sigma'_3 + \sigma'_1) \sin \psi \quad (5.2b)$$

$$g_3 = \frac{1}{2}|\sigma'_1 - \sigma'_2| + \frac{1}{2}(\sigma'_1 + \sigma'_2) \sin \psi \quad (5.2c)$$

Here, the third model parameter  $\psi$  is the dilatancy angle. Normally, this parameter is required to model positive plastic volumetric strain increments as actually observed for dense sands. For extremely loose sands, however, small negative value for  $\psi$  may be expected. Detailed information about specifying  $\psi$  can be found in PLAXIS (1998) reference manual. Suggestions regarding the link between the friction angle and dilatancy in sand can be found in Bolton (1986).

### 5.3 VALIDATION OF FINITE ELEMENT SIMULATION

The drilled shafts used for stabilization of slopes have been referred to as passive piles, due to the fact that the force acting on the shafts depends on the movement of the sliding soil mass. The problems involved in the simulation of passive drilled shafts are associated with the evolving mechanism of the lateral force acting on the shafts during the course of soil arching.

Two sets of existing experimental model tests results (Adachi, et al., 1989; Bosscher and Gray, 1986) on soil arching are re-examined herein by the finite element simulation technique, to serve as a validation of the numerical method presented herein. Once the validation is done, then a systematic parametric study on soil arching effects will be performed. The first set of model tests was conducted by Adachi, et al.(1989) using a trap door capable of uniformly moving the bottom plate downward. With the downward movement of the trap door's bottom plate, soil arching took place. With the displacement tracing targets buried in the model soil and the strain gages affixed to the piles, the soil deformation and the load acting on the pile due to soil arching were recorded and the load transfer-curve was established.

In Adachi, et al (1989) test, soil arching phenomenon was observed by examining the deformation pattern of soil particles, as depicted in Fig.5. 3, and characterized by the load transfer-curves. A typical test model with parameters as shown in Table 5.1 was simulated and the FEM numerical predictions using the PLAXIS program were compared with the experimental results. The parameters used in FEM analysis were taken directly from Adachi et al. (1989) for consistency. The soil-pile interface parameters were

selected to be 2/3 of the soil parameters according to the suggestions in the PLAXIS computer program reference manual. This is to reflect the strength reduction due to slippage of the soil around the pile. The dilatancy angle required as input in the analysis was selected as a small number,  $\psi = 2^\circ$ , due to the consideration that aluminum rods in the experiment would not exhibit significant dilatancy. Figs.5.4 and 5.5 show the displacement contour and the principal stresses direction, respectively, where the soil arching is present for the case of spacing  $s = 2d$ .

**Table 5.1. Parameters used in the analysis (after Adachi et al., 1989)**

Pile diameter (cm)	3
Unit weight ( $\text{kgf/cm}^3$ )	0.0021
Poisson's ratio	0.33
Cohesive strength ( $\text{kgf/cm}^2$ )	0
Internal friction angle (degree)	30

By varying the spacing,  $s$ , and incrementally increasing the prescribed displacement,  $\delta$ , on the boundary BC, the load acting on the drilled shafts are calculated. The calculated forces against the relative movement of soil are plotted in Fig. 5.6 for various shaft spacings. Some observations can be made from the results depicted in the figure as follows:

- (a) At the very beginning when there is no relative movement, i.e.,  $\delta = 0\text{mm}$ , the loads acting on the piles for each spacing layout case are almost the same as the downslope driving force;
- (b) As soil movement  $\delta$  increases, the loads acting on the piles grow rapidly as a

result of arching induced stress transfer;

- (c) When soil movement reaches a certain value,  $\delta = 3 \sim 5mm$  for cohesionless soils, the acting loads arrive at the maximum value and remain constant as the soil movement continues to increase. This indicates that the soil arching has been fully developed and the additional soil movement has no more influence on the arching induced stress re-distribution;
- (d) With an increase of the pile spacing  $s$ , the loads acting on the piles increase. However, when  $s$  becomes larger than  $8d$ , each pile behaves like a single pile without arching effect.

For the purpose of comparison, the numerical and experimental results of the spacings  $s = 2d$ ,  $s = 4d$  and  $s = 8d$  were plotted in Figs. 5.7, 5.8 and 5.9, respectively. In these figures, it can be clearly seen that the present numerical predictions match the experimental measurements quit well for each case. It should be noted that the numerical results conducted by Adachi, et al (1989) exceeded the experimental measurement by 25~60% when the pile spacing is greater than  $4d$ . Adachi, et al used the Miseses's yield criterion in the constitutive model and ignored the dilatation effect of cohesionless soils.

The second set of model tests for validating numerical solution techniques of soil arching were carried out by comparing with Bosscher and Gray (1986) experimental data. They performed a series of tests with the fixed gates representing pile and the swing gates representing the spacing between piles. The slope movement was triggered by the fallback of the swing gates. Different pile diameters and spacing were simulated by adjusting the widths of the gates. A typical test with parameters listed in Table 5.2 was

chosen for comparison purpose. Both dense and loose sands were considered in the analysis. The former has a tendency to experience dilation while the latter tends to contract in volume during the development of soil arching.

**Table 5.2. Parameters used in the analysis (after Bosscher and Gray, 1986)**

	Dense	Loose
Fixed gate width or pile diameter (cm)	10.16	10.16
Relative density (%)	92	12
Unit weight (kN/m <sup>3</sup> )	16.76	14.81
Poisson's ratio	0.33	0.33
Cohesive strength (kPa)	0	0
Internal friction angle (degree)	38.6	32.2

It was found that the load on the swing gate drops off and the load on the fixed gate at same time increases. This means that the load is being transferred to the fixed gate from the swing gate by the mechanism of soil arching. Similar to the finding obtained in the first set of tests, the load acting on the fixed gate, for a specific case of gate width, reaches a peak value and thereafter remains constant, indicating a fully developed arching. The peak value of the transferred load can be viewed as the ability of soil arching mechanism. By varying the width of the swing gate, an overall picture quantitatively depicting the arching effect against swing gate width can be drawn in Fig. 5.10, where the percent of total residual load on the swing gate is plotted. The agreement between the numerical predictions and the experimental measurements is reasonable, particularly with

regard to the trend of behavior.

## **5.4 INFLUENCE OF PARAMETER VARIATIONS ON SOIL ARCHING**

An extensive parametric study was carried out in the FEM simulations to investigate the effects of variation of parameters on the arching behavior. Specifically, the parameters selected for the study included pile diameter, pile spacing, pile shape, internal frictional angle of cohesionless soil, and cohesion value of cohesive soil. The pile diameter was varied as 30.48 cm, 60.96 cm and 91.44 cm. The internal friction angle ranging from 0 to 40° and cohesion ranging from 0 to 41.4 kPa were used.

### **5.4.1 EFFECT OF PILE SPACING**

A wide range of pile spacing ranging from  $s = 2d$  to  $s = 8d$  for the cases where pile diameter  $d = 30.48$  cm,  $d = 60.96$  cm and  $d = 91.44$  cm have been investigated to evaluate the influence of pile spacing. The corresponding numerical results are shown in Fig. 5.6, Fig. 5.10 and Fig. 5.11, respectively. In Fig. 5.6, the loads acting on the drilled shafts versus the soil movements at boundary BC are drawn. It can be seen that the load acting on the drilled shafts increases as the shaft spacing increases, but the rate of increase gradually decreases. This indicates that arching is not as effective at large spacing as in small spacing. This finding becomes apparent in Figs. 5.10 and 5.11, where the residual load acting on the soil mass was evaluated and then normalized with respect to the initial load to obtain a percentage of residual load. As the spacing increases, the percentage of the residual load acting on the soil mass between shafts increases. In other words, when shaft spacing increases, a smaller amount of load would

be transferred to the drilled shafts. Typically, for the cases of cohesionless soil, as shown in Figs. 5.10 and 5.11, around 70% of earth pressure would be transferred to the drilled shafts if the shafts are placed close, in a row with  $s/d=2$ . For a wide shaft spacing with  $s/d=5$ , however, less than 20% load have transferred to the shafts. Once the shaft spacing becomes larger than  $8d$ , there would be no arching effect such that each shaft behaves like a single shaft, as shown in Fig. 5.6.

#### **5.4.2 EFFECT OF PILE DIAMETER**

Fig. 5.11 summarizes the results of circular shafts with the diameters of 30.48 cm, 60.96 cm and 91.44 cm, respectively. Similar trend regarding the effect of shaft spacing can be observed for all three-shaft diameters investigated. However, if the ratio of spacing to diameter,  $s/d$ , remains constant, the variation in pile diameter has slight impact on the arching-induced load transfer. Nevertheless, the effects of diameter on percent of residual load are minimal, with a typical variation of 10% for lower value of  $s/d$ .

#### **5.4.3 EFFECT OF SHAPE**

To investigate the effect of shaft shape, both circular and square cross-sections were studied. The soil properties used for simulations in this study are the same as those listed in Table 5.1. It was generally believed that the square piles are more likely to provide solid support for the arching foothold and hence facilitating more arching-induced load transfer load. This expectation was verified by the results shown in Fig.5.12. The load acting on the square shaped drilled shafts is generally greater than that acting on the circular shafts, but only by about 5%.

#### 5.4.4 Effect OF INTERNAL FRICTION ANGLE OF COHESIONLESS SOIL

Soil arching in a row of drilled shafts occurs as the soil attempts to move through the opening between the drilled shafts. The drilled shafts firmly embedded in a non-yielding soil layer serve as a foothold for a potential arching to develop. As a result, the spatial parameters regarding the drilled shafts dimension and their spacing exert an important impact on the existence of soil arching, as clearly shown in the previous discussions. On the other hand, since it is within the soil where the arching action takes place, the soil's own properties such as internal friction angle and cohesion are expected to directly influence both the existence and the intensity of the soil arching. Tables 5.3a, 5.3b and 5.3c summarize the effects on arching-induced residual load due to variations of internal friction angle of cohesionless soils from 0 to 40°, and cohesion of cohesive soils ranging from 0 to 41.4 kPa. The shaft diameter  $d=30.48$  cm, 60.96 cm, and 91.44 cm and spacing ratio  $s/d=2, 3$  and 4, respectively, were used in tabulating these results.

**Table 5.3a. Percent of residual load acting on soil mass between piles ( $d=30.48$  cm)**

		c = 0 (kPa)	c = 6.9 (kPa)	c = 13.8 (kPa)	c = 27.6 (kPa)	c = 41.4 (kPa)
$\phi = 0^\circ$	s/d=2	100.00	39.10	10.64	10.47	10.46
	s/d=3	100.00	61.55	21.66	14.21	13.44
	s/d=4	100.0	71.73	39.21	21.02	15.35
$\phi = 10^\circ$	s/d=2	64.09	11.25	10.44	10.36	10.36
	s/d=3	76.72	37.71	14.27	14.11	13.41
	s/d=4	81.26	54.85	20.61	15.32	15.01
$\phi = 20^\circ$	s/d=2	34.92	10.83	10.68	10.31	10.31
	s/d=3	56.86	21.77	14.07	13.93	13.37

	s/d=4	64.72	40.72	14.88	14.21	13.35
$\phi = 30^\circ$	s/d=2	16.48	10.56	10.50	10.44	10.35
	s/d=3	47.71	15.03	14.06	13.91	13.34
	s/d=4	59.29	27.69	14.81	14.14	13.33
$\phi = 40^\circ$	s/d=2	16.32	10.47	10.41	10.34	10.31
	s/d=3	37.50	15.79	14.03	13.89	13.31
	s/d=4	54.51	29.32	14.74	14.02	13.27

**Table 5.3b. Percent of residual load acting on soil mass between piles (d=60.96 cm)**

		c = 0 (kPa)	c = 6.9 (kPa)	c = 13.8 (kPa)	c = 27.6 (kPa)	c = 41.4 (kPa)
$\phi = 0^\circ$	s/d=2	100.00	39.92	10.52	10.23	9.98
	s/d=3	100.00	65.41	25.91	15.05	14.52
	s/d=4	100.00	76.51	45.45	22.67	17.12
$\phi = 10^\circ$	s/d=2	69.03	16.54	10.26	10.14	9.89
	s/d=3	83.00	43.19	15.53	15.15	14.68
	s/d=4	86.68	60.05	26.52	16.51	16.37
$\phi = 20^\circ$	s/d=2	44.15	12.91	10.31	9.86	9.74
	s/d=3	67.36	24.37	15.23	15.03	14.66
	s/d=4	76.76	48.10	16.38	15.35	14.62
$\phi = 30^\circ$	s/d=2	28.95	10.29	10.11	9.73	9.63
	s/d=3	55.81	15.74	14.94	14.80	14.42
	s/d=4	68.42	36.01	15.81	14.96	14.36
$\phi = 40^\circ$	s/d=2	24.59	10.27	9.78	9.75	9.66
	s/d=3	46.60	18.08	14.80	14.68	14.30
	s/d=4	59.75	32.87	15.17	14.80	14.25

**Table 5.3c. Percent of residual load acting on soil mass between piles (d=91.44 cm)**

		c = 0 (kPa)	c = 6.9 (kPa)	c = 13.8 (kPa)	c = 27.6 (kPa)	c = 41.4 (kPa)
$\phi = 0^\circ$	s/d=2	100.00	40.13	10.44	10.07	9.65
	s/d=3	100.00	67.98	28.75	15.61	15.24
	s/d=4	100.00	78.18	48.50	23.30	17.91
$\phi = 10^\circ$	s/d=2	72.33	20.06	10.14	9.99	9.57
	s/d=3	85.33	45.68	16.01	15.52	15.18
	s/d=4	90.85	63.69	30.02	17.38	17.33
$\phi = 20^\circ$	s/d=2	49.80	14.18	10.09	9.57	9.39
	s/d=3	71.90	25.38	15.62	15.39	15.12
	s/d=4	81.48	50.98	16.86	15.68	15.02
$\phi = 30^\circ$	s/d=2	35.66	10.13	9.89	9.34	9.24
	s/d=3	60.58	16.16	15.46	15.32	15.06
	s/d=4	74.02	41.09	16.43	15.46	15.00
$\phi = 40^\circ$	s/d=2	31.26	10.02	9.34	9.32	9.21
	s/d=3	53.54	19.54	15.32	15.18	14.94
	s/d=4	64.82	35.14	15.46	15.31	14.87

As indicated in Tables 5.3a~5.33c, the variation in internal friction has a significant influence on the arching effect, particularly for soils with lower cohesion value. It can be seen that the soil with higher friction angle is more likely to produce greater granular interlocking and develop stronger arching. Consequently, more load will transfer to the shafts owing to the arching effect. Fig. 5.13 presents one set of results for a case where  $c=0$  kPa and  $d=91.44$  cm. As  $\phi$  increases from  $10^\circ$  to  $40^\circ$ , the percentage of residual load acting on the soil mass drops for all  $s/d$  investigated.

#### **5.4.5 EFFECT OF COHESION VARIATION**

The percentage of the residual load remaining on the soil mass between the shafts versus the variation in cohesion values is plotted in Figs. 5.14 and 5.15 for  $s/d=2$  and  $s/d=4$ , respectively. As can be seen, the percent of residual load drops dramatically with an increase of cohesion value. Once the cohesion reaches a certain value, e.g. 13.8 kPa for the case of narrow shaft spacing ( $s/d=2$ ) or 41.4 kPa for wide shaft spacing ( $s/d=4$ ), a fully developed soil arching is held. The behavior was characterized by the observation that the residual load remained unchanged with further increase of cohesion. This means that most of driving force would transfer to the drilled shafts if the soils are cohesive. The cohesion value of only 13.8 kPa is needed for fully developed arching. In this case, the load transfer mechanism is associated with the cohesion rather than the mobilization of internal friction. It is of interest to note that the cohesive soil with high cohesive strength may not need to experience yielding in order to develop an arching by which the driving force induced from the downslope soil movement can be transferred to the stabilizing drilled shafts. However, it should be noted that cohesive soils normally exhibit long-term

creep, which would eventually lessen the effect of arching to some extent. This is the main reason that most investigators discounted the possibility of arching occurring in the cohesive soil and treated it as an additional safety in dealing with the analysis and design of drilled shafts to stabilize a slope.

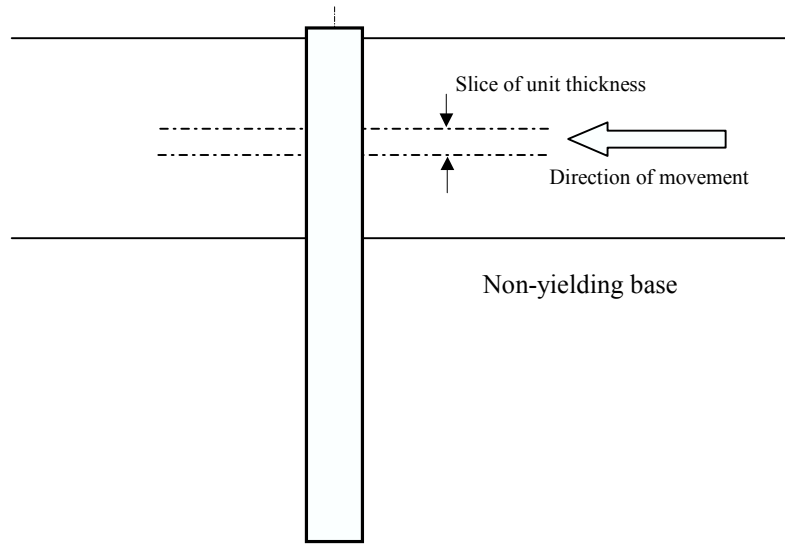
## **5.5 CONCLUSIONS**

In this chapter, a FEM simulation technique was developed for evaluating the soil arching mechanisms associated with the drilled shaft stabilized soil slopes. The essential features of the FEM models were described in details, including modeling techniques, soil constitutive models, and elements used. The FEM analysis results were compared favorably with experimental data reported in literature. A series of parametric study was carried out using the developed FEM modeling techniques. The information obtained from the parametric study provides not only qualitative understanding of arching in both cohesive and cohesionless soils, but also quantitative data about arching induced load transfer characteristics. Detailed conclusions based on the study can be summarized as below.

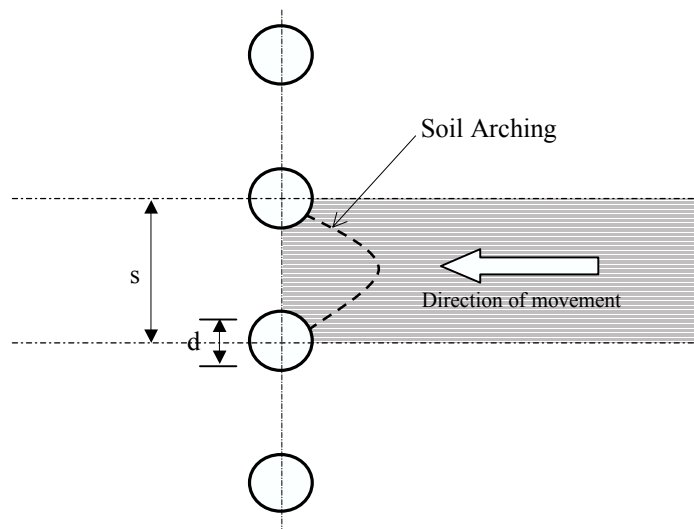
- 1) Drilled shafts embedded into a firm, non-yielding soil stratum in a slope can provide significant additional stability to a slope if soil arching is present.
- 2) Finite element simulations on soil arching have been carried out for a wide variation of soil strength and pile parameters. FEM simulation results have shown to match favorably with the experimental results. The good agreement between the numerical predictions and the experimental measurements provides evidence that the finite element modeling techniques described in

this paper can effectively depict the soil arching mechanism. The finite element method offers an effective approach for a parametric study as well.

- 3) Among the parameters that most affect the soil arching development were drilled shaft spacing, shaft diameter, internal friction angle and /or cohesion of the soil.
- 4) The ratio of shaft spacing to the shaft diameter was found to be the most important design factor impacting on both the possibility and intensity of soil arching.
- 5) As expected, the cohesionless soil with higher friction angle is more likely to develop stronger arching effect than the soil with smaller friction angle.
- 6) The load transfer ability of cohesive soil was found to be significant. In incorporating this arching ability into global stability analysis of drilled shafts stabilized slopes, however, the long-term creep effect of cohesive soils should be taken into account.



(a) Cross section



(b) Plan view

**Fig. 5.1 Drilled shafts in a row for stabilizing a deforming ground**

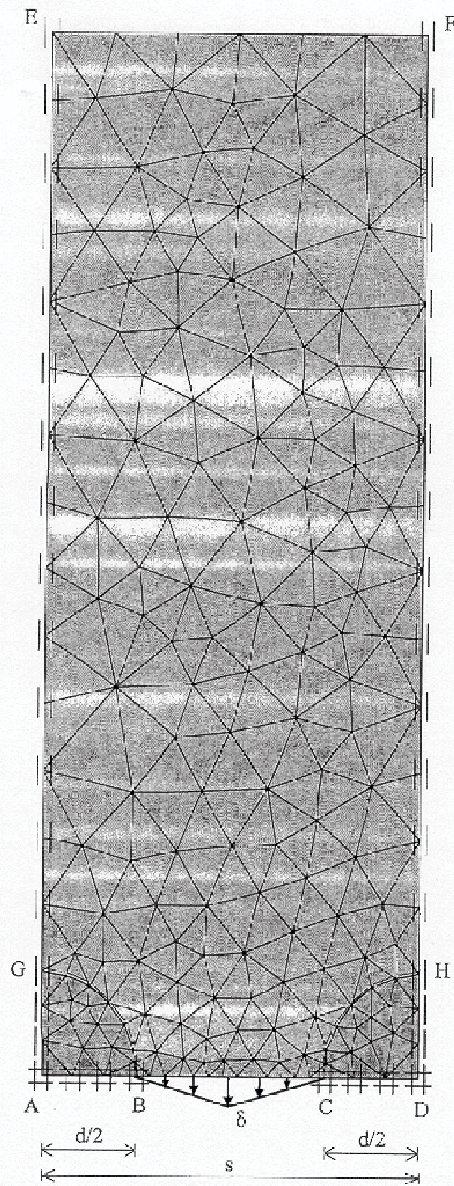
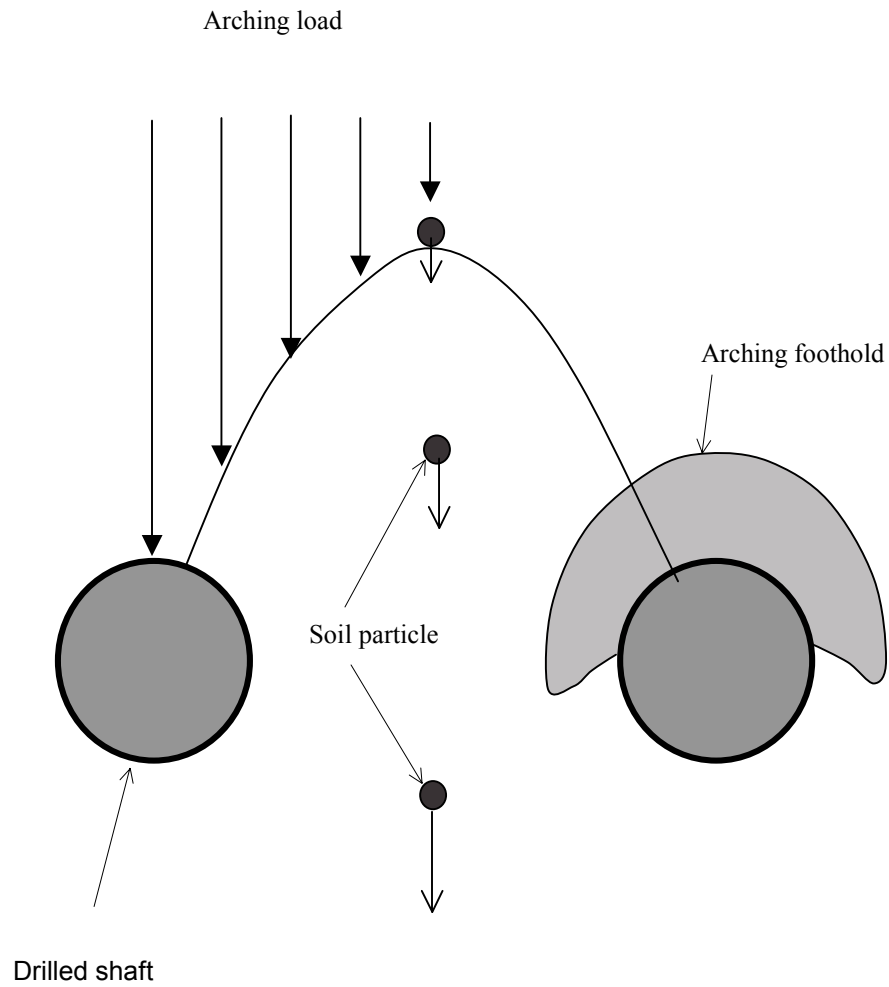


Fig. 5.2 FEM modeling



**Fig. 5.3 Schematic of arching effect (after Adachi et al., 1989)**

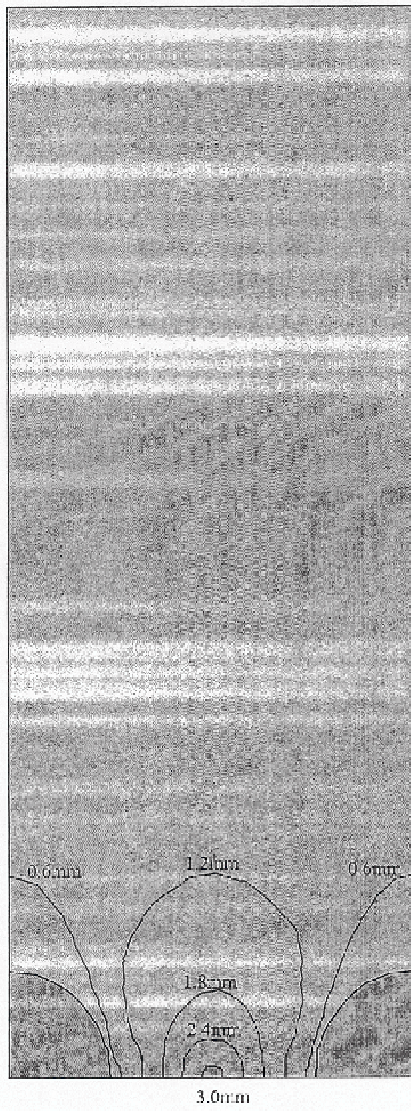


Fig. 5.4 Displacement contour ( $s = 2d$  with  $d = 5\text{cm}$ )

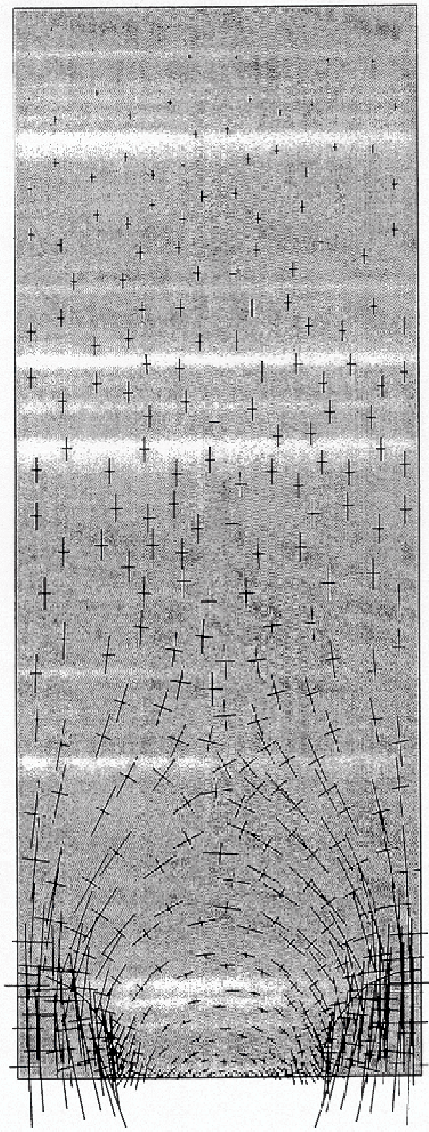


Fig. 5.5 Principal stress direction ( $s = 2d$  with  $d = 5\text{cm}$ )

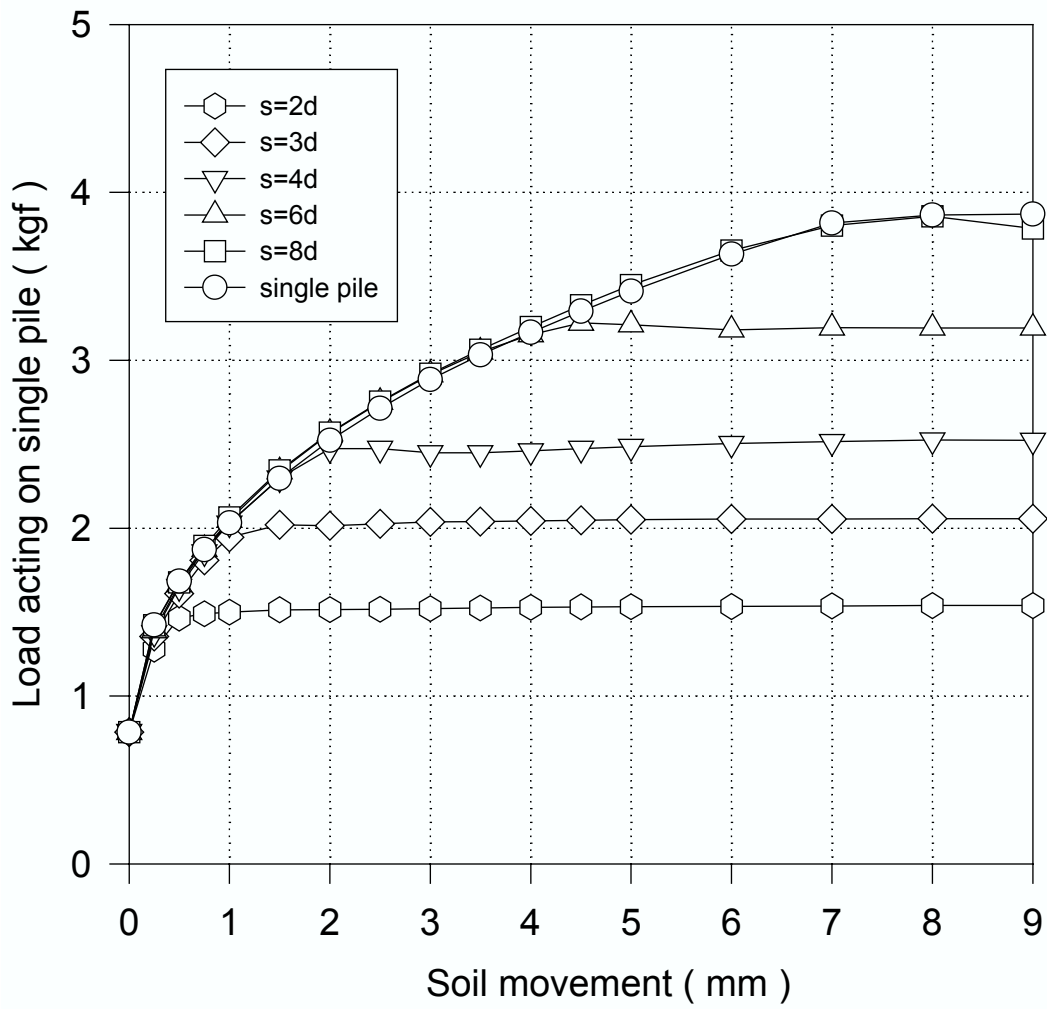


Fig. 5.6 Load acting on the pile versus soil movement (d=3cm)

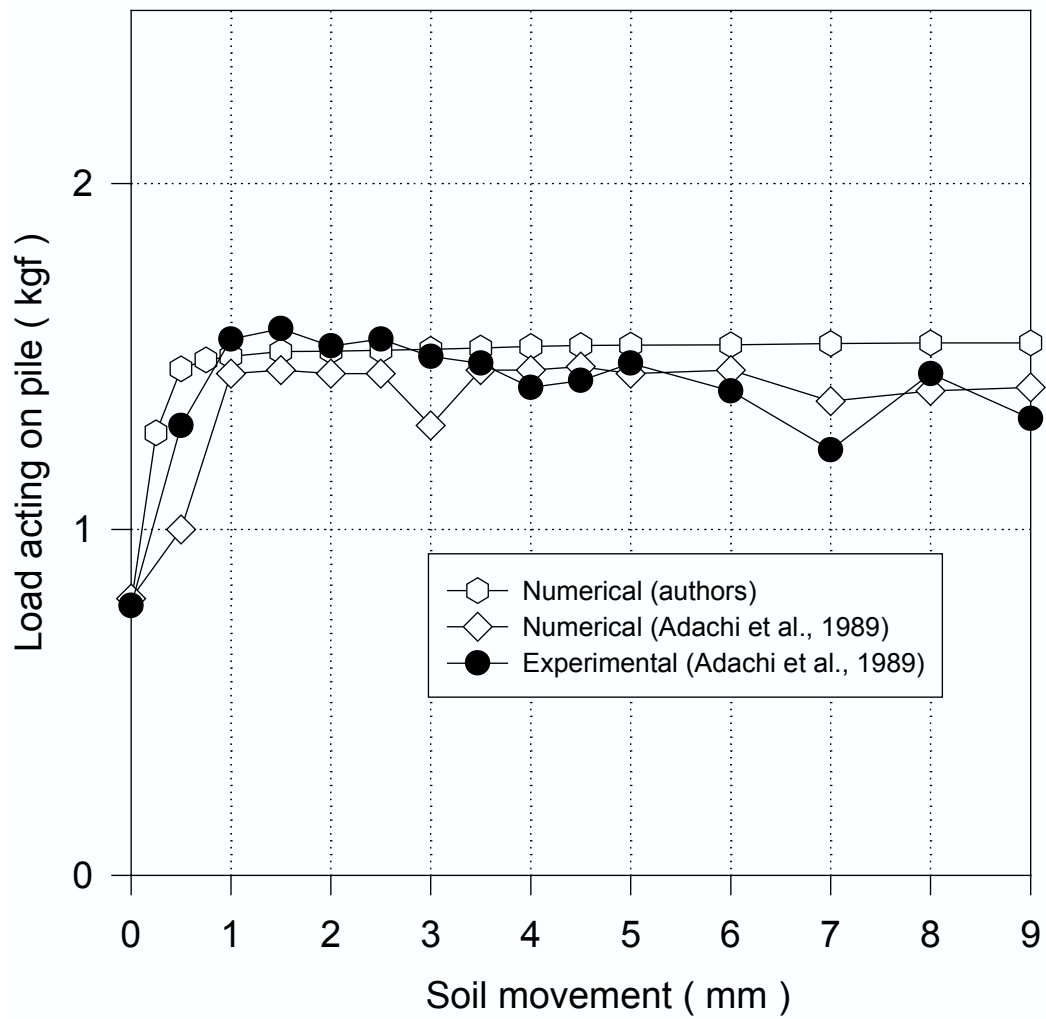


Fig. 5.7 Load acting on pile versus soil movement:  $s=2d$

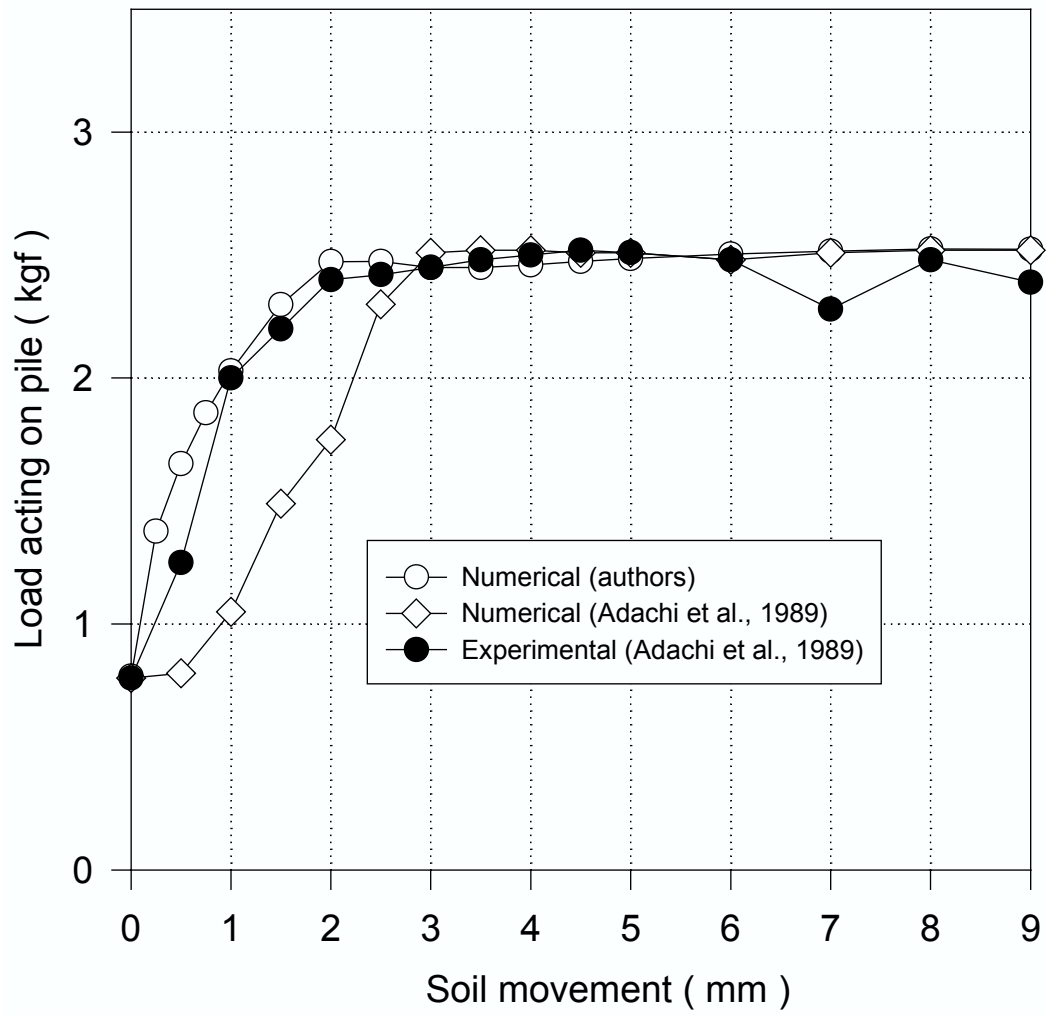


Fig. 5.8 Load acting on pile versus soil movement:  $s=4d$

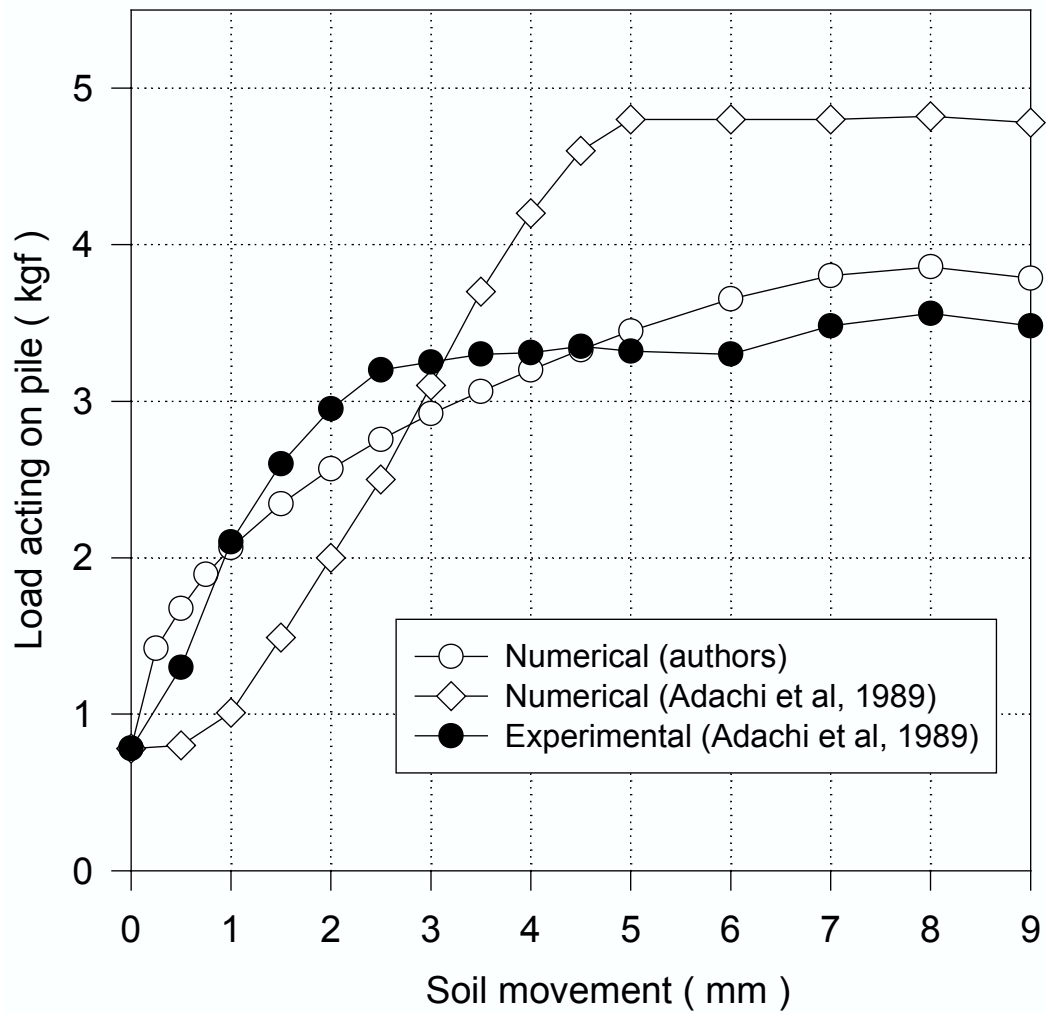


Fig. 5.9 Load acting on pile versus soil movement: s=8d

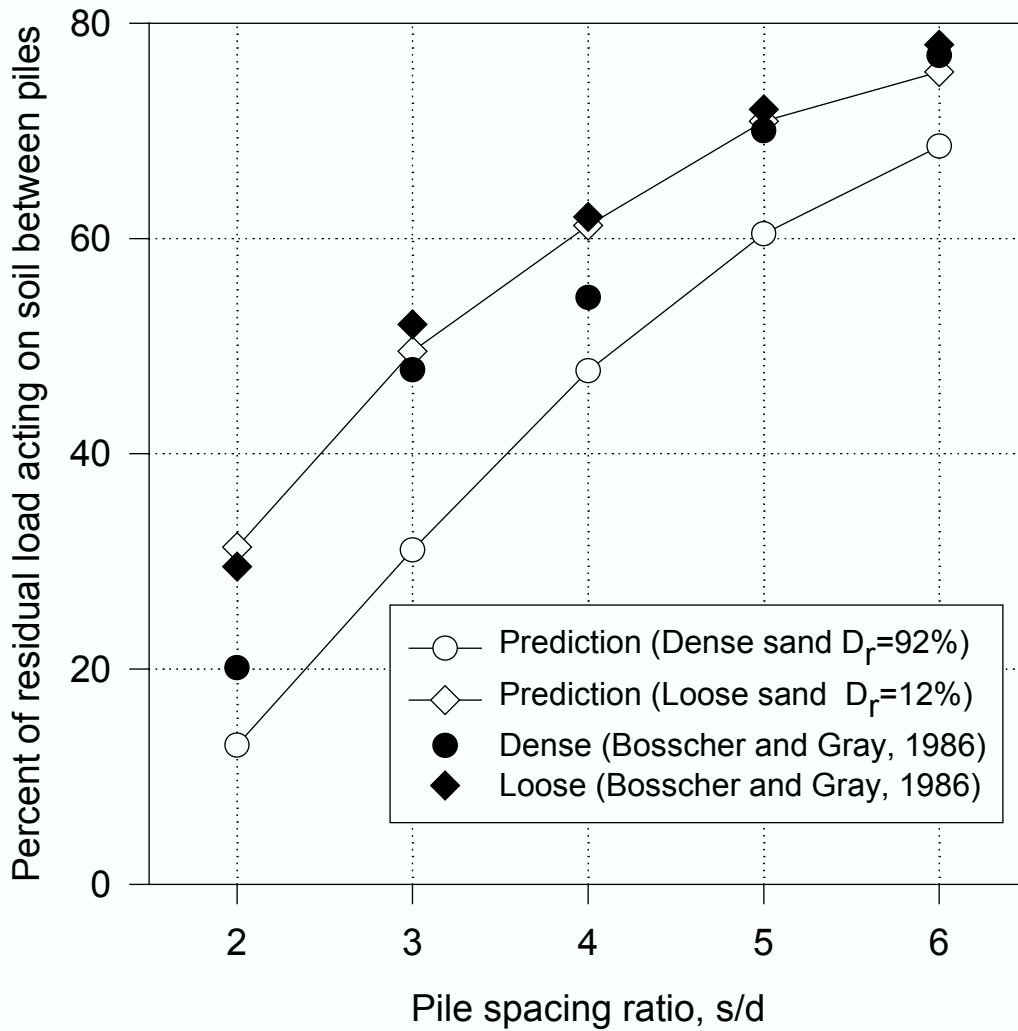


Fig. 5.10 Percent of residual load acting on soil between piles versus spacing ratio

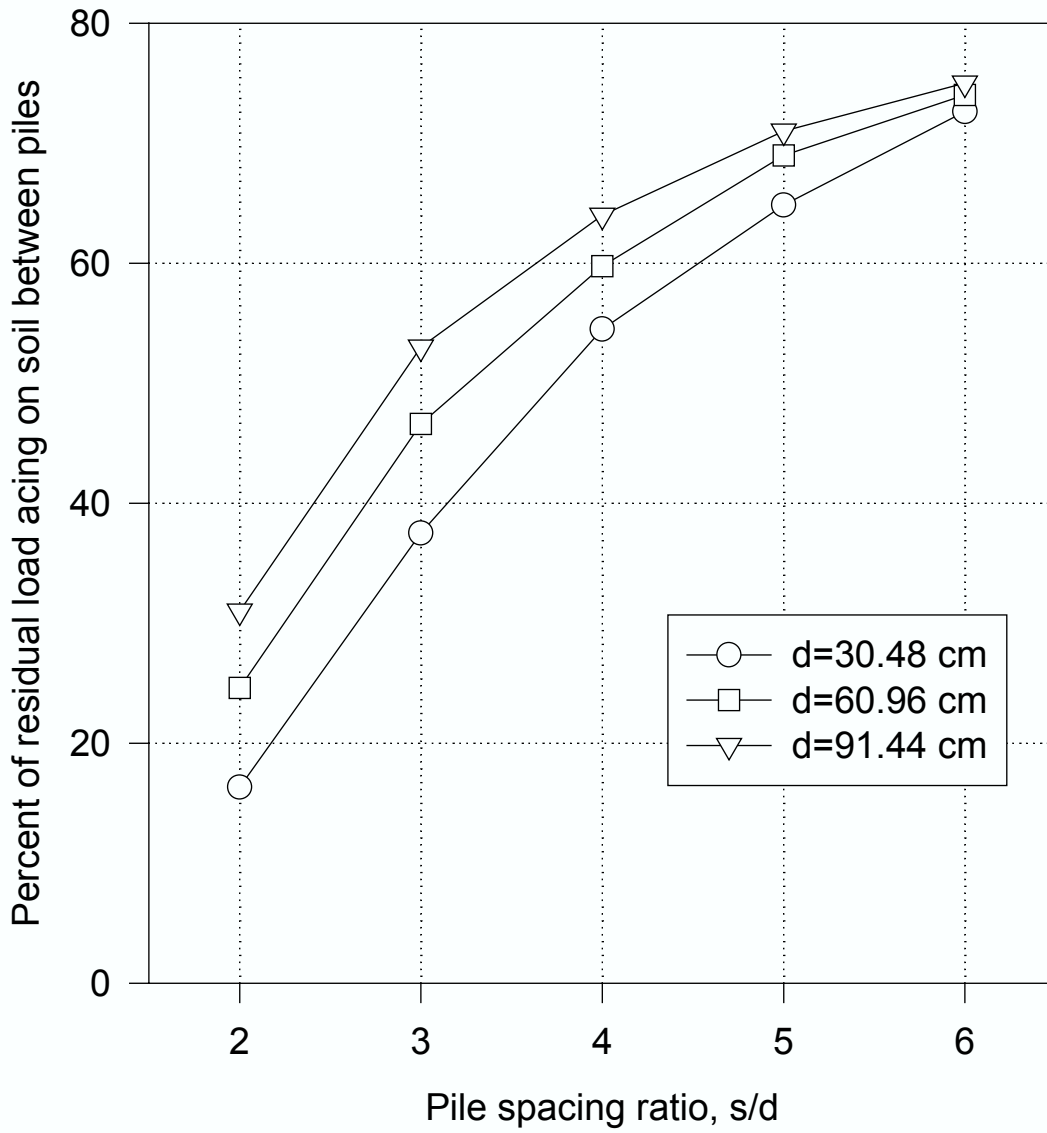


Fig. 5.11 Effect of variation in pile spacing: cohesionless soil with  $\phi=40^\circ$

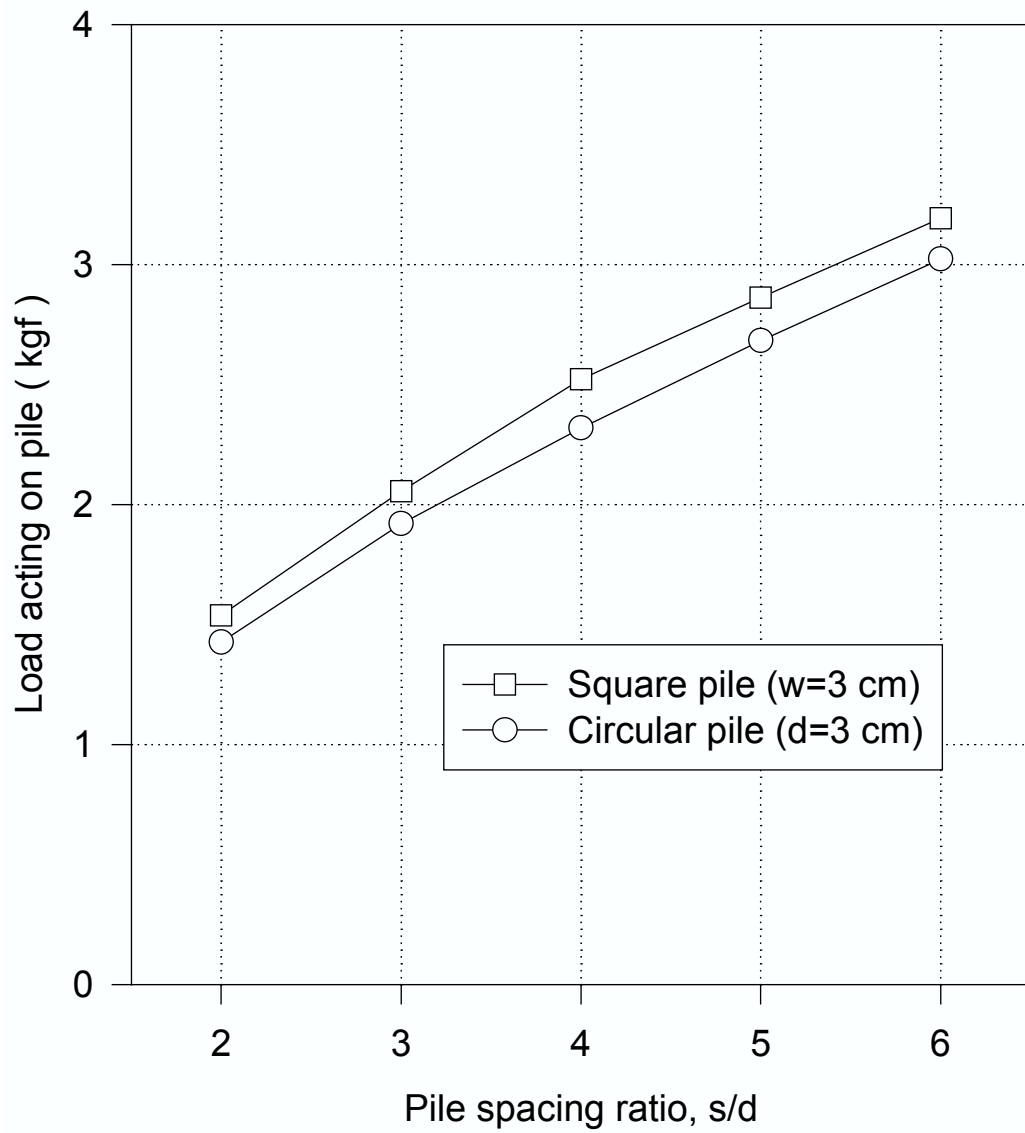


Fig. 5.12 Effect of variation in pile shape

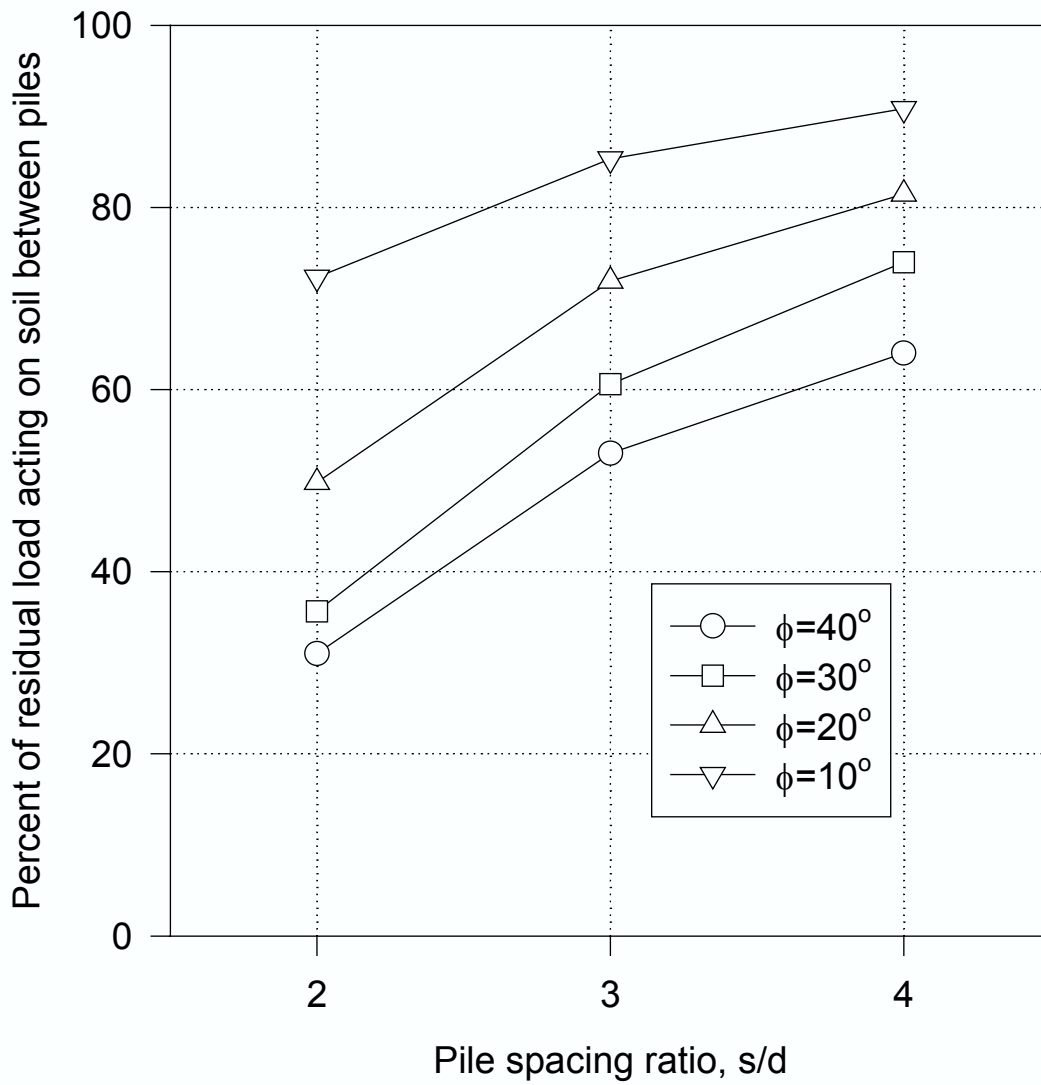


Fig. 5.13 Effect of variation in internal friction angle: cohesionless soil ( $d=91.44$  cm)

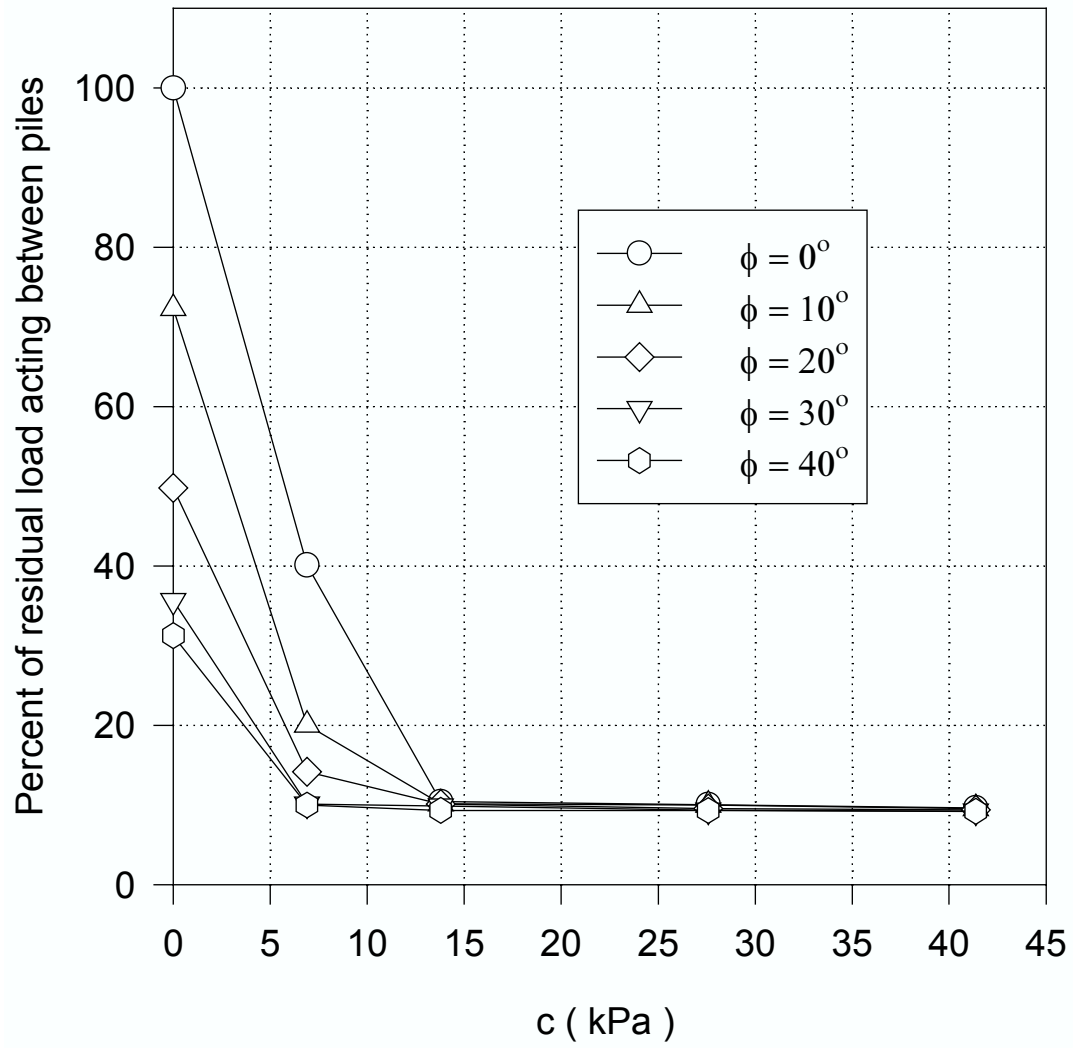


Fig. 5.14 Effect of variation in cohesion:  $s=2d$  with  $d=91.44$  cm

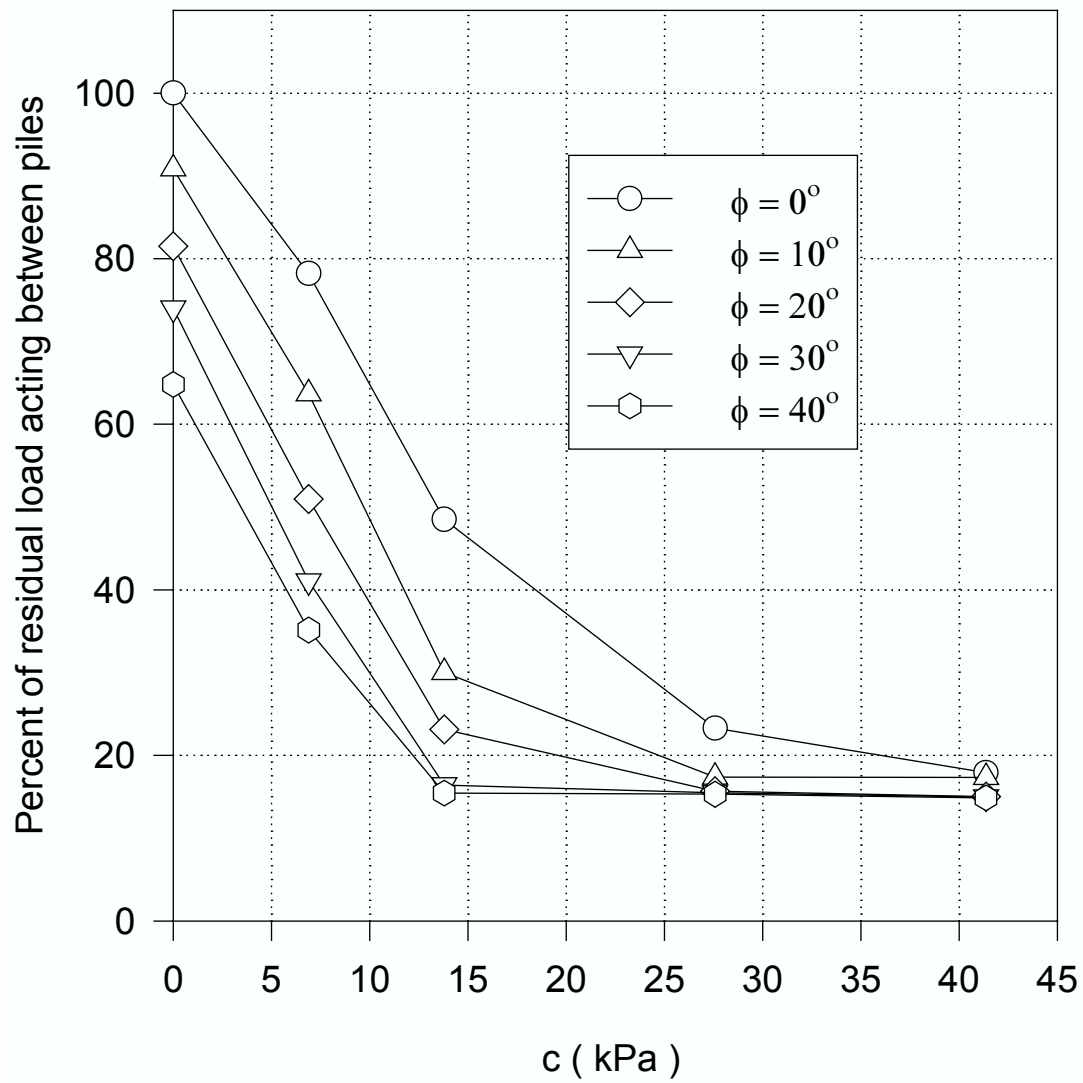


Fig. 5.15 Effect of variation in cohesion:  $s=4d$  with  $d=91.44$  cm

## CHAPTER VI

### STABILITY ANALYSIS OF DRILLED SHAFTS REINFORCED SLOPE

#### 6.1 INTRODUCTION

Drilled shafts have been used in cuts and bridge abutments for many decades. Recently, there has been an increasing interest in the use of drilled shafts for the purpose of slope stabilization. The increased popularity of such a slope stabilization technique may be attributed to the following factors: (1) various construction techniques are available for installing drilled shafts in almost any type of soil conditions; (2) numerous standard tests, such as lateral load test, can be readily performed to verify the load resistance capacity of the drilled shafts; (3) the use of drilled shafts seems to offer a reliable and economic solution with long-term resistance to environmental effects, such as corrosion.

The design of a drilled shaft supported wall calls for an adequate global stability to prevent excessive movement of the supported soil mass, and sufficient structural capability to resist bending moments developed in the shafts due to the earth pressure. The successful applications of drilled shafts in slope stabilization have been described by several investigators (e.g., Sommer (1977); Ito et al. (1981, 1982); Nethero (1982); Morgenstern (1982); Gudehus and Schwarz (1985); Reese et al. (1992); Rollins and Rollins (1992)); Yamagami et al. (2000); however, the methods used for the design and analysis of the stabilizing system varied widely. Furthermore, some of these methods appeared to be of doubtful validity as pointed out by Poulos (1995). Actually, the drilled

shafts used for stabilizing a slope are often referred to as passive shafts. In the passive shaft analysis, the lateral force acting on the shaft is related to the movement of the slope and the interaction between the shaft and the surrounding soils. Ideally, the stabilization mechanisms of drilled shafts should be investigated based on three-dimensional consideration, incorporating nonlinear and plastic nature of soil constitutive behavior as well as the soil-shaft interactions. At the present time, it is extremely difficult to explicitly take into account of these true three-dimensional phenomena. In most instances, some simplifying idealizations of the problem is made.

The most common approach is based on the classic earth pressure theories to estimate the load or pressure acting on the shafts. Chelapati and Finn (1963) are the two primary investigators using the elastic theory. The derived analytical results, by use of elasticity methods in soils, are only valid for small deformations and strains; whereas, the behavior of the soil mass in the vicinity of the shafts usually involves large and nonlinear deformations. Recent developments in the subject area are represented by the method proposed by Ito et al. (1975, 1979, 1981), where rigid-plastic soil behavior was taken into account. The mathematical deductions of analytical formulations for calculating the acting pressure were based on a certain number of simplifying assumptions, including (i) the soil becomes plastic only in the area just around the drilled shafts; (ii) two vertical sliding surfaces will occur along the lines making an angle  $(45 + \Phi/2)$  with the direction of soil movement; (iii) the friction force acting on the sliding surfaces is neglected; and (iv) the active earth pressure is assumed to act on the plane along the direction of a row of piles. Once the lateral force has been calculated, then the structural adequacy of the shafts and the stability of the slope can be analyzed separately. Several other similar works

using this analytical approach can be found in Wang and Yen (1974), Bransby and Smith (1975), and Reese et al. (1992). The various assumptions mentioned above, however, limit the validity of the solutions to certain specific cases.

In contrast to earth pressure methods, the displacement-based approaches emphasize on the assumptions of the magnitude and pattern of the lateral soil displacement of a free field, from which the resulting deflection and bending moment of the drilled shaft can be determined. Springman (1989) and Stewart et al. (1994) investigated the single pile behavior in an elastic soil layer subject to various types of assumed soil movements. Recent development was presented by Poulos (1994, 1995), in which the free field soil movement was used as input in a simplified boundary element method to compute the axial and lateral response of piles subjected to these prescribed soil movements. The influencing factors, such as positions of the drilled shafts, shear strength of the soil, soil layer thickness, the restraint at the pile head, and the installation sequence of piles, can be considered. Generally speaking, the displacement-based method is superior to the earth pressure method, because it reflects the true mechanism of soil-shaft interaction. However, it should be pointed out that accurate description of soil movements is a priori condition to the accuracy of the calculated loads applied to the drilled shaft. In most cases, such displacement description is very difficult to obtain in the field.

Limit equilibrium analysis in conjunction with the method of slices is the most widely used method for evaluating stability of slopes. The techniques can accommodate complex geometry and variable soil properties and water pressure conditions. The limit equilibrium analysis method can provide a global safety factor by which the safety of a

slope can be quantitatively assessed. Numerous limit equilibrium methods for slope stability analysis have been proposed by several investigators, including the celebrated pioneers Fellenius (1936), Bishop (1955), Janbu (1954), Morgenstern and Price (1965), Spencer (1967), and Sarma (1973). Recent developments on application or enhancement of those methods can be found in Sharma and Moudud (1992), Fredlund et al. (1992), Espinoza et al. (1994), and Zhang and Chowdhury (1995). These efforts, however, were related to a slope without drilled shafts. The analysis of a slope stabilized with the drilled shafts requires a development of an approach to account for the contribution of drilled shafts. The problem lies in the fact that the drilled shafts can only support a partial of resultant driving force, while the rest of earth pressure still transmitted to the downslope soil.

It has been recognized that discrete drilled shafts in a row embedded into a firm, non-yielding soil strata in a slope can provide significant additional stability to a slope if soil arching around the drilled shafts are developed. Soil arching, the transfer of stresses from a yielding mass of soil onto an adjacent non-yielding soil, is a phenomenon commonly encountered in the field. For a slope reinforced by the drilled shafts installed in a row, soil arching over the soil mass between drilled shafts may occur under certain circumstance as the soil attempts to move through the stiff drilled shafts which are firmly embedded in a non-yielding soil strata. There have been numerous literatures providing a wide range of information on the soil arching effects (e.g., Terzaghi 1943; Cox et al. 1983; Bosscher and Gray 1986; Adachi et al 1989; Reese et al. 1992; Low et al. 1994; and McVay et al. 1995). Unfortunately, a generally accepted guideline to incorporate the arching effects into the design of drilled shafts in stabilizing a slope is not universally

available due to the lack of adequate information on soil arching behavior. The key issues to be resolved in this context are: (a) What conditions should be met in order for soil arching to be fully developed, and (b) How much additional resistance force that can be provided by drilled shafts due to soil arching effect?

The main objective of the present study is to develop a practical methodology for stability analysis and design of drilled shafts reinforced slopes. The developed method utilizes the generalized procedure of slice for composite slip surfaces of any shape and incorporates the effect of the soil arching due to the installation of drilled shafts. Such integrated approach would allow for not only the determination of the safety factor of the reinforced slope, but also the forces acting on the drilled shafts. Parameters affecting the soil arching are investigated, and the load transfer curves characterizing the ability of soil arching mechanism are developed based on an extensive parametric study. The efficiency of stabilization of slope by drilled shafts is then discussed by examining the influence of shaft location, size and spacing on the computed factor of safety. Finally, a case study is presented.

## **6.2 GENERAL STATEMENTS**

As shown in Fig. 6.1, drilled shafts of diameter  $d$  with spacing  $s$  are installed in a row through a moving soil into a firm, non-moving soil stratum underneath. As the soil mass moves through the drilled shafts, soil arching will occur, by which the stress in the yielding soil is redistributed unto the unyielding portion of soil and eventually unto the supporting piles. As a result, the driving force transmitted to the soil mass behind the drilled shafts is reduced to some extent, say by a reduction factor  $R$ , leading to a higher

stability of the slope. The reduction factor,  $R$ , under certain circumstances, is related to both drilled shafts spatial parameters and soil conditions. Details about the determination of the reduction factor,  $R$ , will be given later in this paper.

For slope stability analysis, force and moment equilibrium equations together with the commonly adopted Mohr-Coulomb failure criterion are used in the method of slice technique. Some assumptions concerning the interslice forces, and their directions or locations are needed to render the problem determinate. Different assumptions will lead to different analytical procedures for calculation of safety factor. For the drilled shafts reinforced slope considered here, the main objective of an analysis procedure is to incorporate the contributions exerted by the drilled shafts. To accommodate complex slip surface usually encountered in the field, the analysis should allow for a composite-type of failure surfaces. Thus, a generalized method of slices for composite slip surfaces of any shape is employed herein, and the resultant interslice force is assumed to be parallel to the base of the previous up-slope slice (see Fig. 6.2), with point of application located at one-third from the bottom of the interface.

At failure, the available shear strength on the base of the slice is governed by Mohr-Coulomb's failure criterion expressed in terms of effective stresses

$$\tau_f = c' + (\sigma - u) \tan \phi' \quad (6.1)$$

where  $\tau_f$  is shear strength;  $c'$  is effective cohesion;  $\phi'$  is effective internal angle of friction;  $u$  is pore pressure at the base of the slice; and  $\sigma$  is total normal stress acting on the base of the slice.

The safety factor  $F$  is defined as the ratio of the available shear strength of the soil at failure to that mobilized for maintaining equilibrium. The mobilized shear stress  $\tau$  necessary for equilibrium is

$$\tau = \tau_f / F = c'_m + (\sigma - u) \tan \phi'_m \quad (6.2)$$

where

$$c'_m = c' / F \quad (6.3)$$

$$\tan \phi'_m = \tan \phi' / F \quad (6.4)$$

### 6.3 MATHEMATICAL FORMULATION

Consider the static equilibrium of a soil slice  $i$  overlying the slip surface segment of length  $l_i$ , as shown in Fig. 6.2. The forces acting on the slice are  $W_i$ , the weight of the slice;  $P_{i-1}$ ,  $P_i$ , the resultant interslice forces on the  $(i-1)$ th and  $i$ th interfaces, respectively;  $N_i$ , the normal force reaction on the base of the slice; and  $T_i$ , the shear force reaction on the base of the slice. Also,  $\alpha_{i-1}$  and  $\alpha_i$  are the average slopes of the bases of the slices  $i-1$  and  $i$ , respectively. As assumed,  $P_{i-1}$  has orientation of  $\alpha_{i-1}$  and  $P_i$  of  $\alpha_i$ .

The force equilibrium of slice  $i$  requires, in the direction parallel to  $N_i$ ,

$$N_i - W_i \cos \alpha_i - P_{i-1} \sin(\alpha_{i-1} - \alpha_i) = 0 \quad (6.5)$$

Similarly, in the direction perpendicular to  $N_i$

$$T_i + P_i - W_i \sin \alpha_i - P_{i-1} \cos(\alpha_{i-1} - \alpha_i) = 0 \quad (6.6)$$

Based on the expression (2), the corresponding mobilized shear force  $T_i$  is

$$T_i = \frac{c'_i l_i}{F} + (N_i - u_i l_i) \frac{\tan \phi'_i}{F} \quad (6.7)$$

Combining equations (6.5) and (6.7) yields

$$T_i = \frac{c'_i l_i}{F} + \left[ W_i \cos \alpha_i + P_{i-1} \sin(\alpha_{i-1} - \alpha_i) - u_i l_i \right] \frac{\tan \phi'_i}{F} \quad (6.8)$$

Substituting (8) into (6) gives

$$P_i = W_i \sin \alpha_i - \left[ \frac{c'_i l_i}{F} + (W_i \cos \alpha_i - u_i l_i) \frac{\tan \phi'_i}{F} \right] + k_i P_{i-1} \quad (6.9)$$

where

$$k_i = \cos(\alpha_{i-1} - \alpha_i) - \sin(\alpha_{i-1} - \alpha_i) \frac{\tan \phi'_i}{F} \quad (6.10)$$

Equation (6.9), together with equation (6.10), applies to each slice and relates the interslice force  $P_i$  to the previous one  $P_{i-1}$ . Thus, recursive formula for determining  $P_i$  with initial value  $P_0$  being zero or prescribed boundary force, can be established. It is also noted from Eqs. (6.9) and (6.10) that  $P_i$  depends on the safety factor  $F$ , thus an iterative computational scheme is required.

The iterative procedure is fairly straightforward. First, an initially postulated value of safety factor  $F$  is assumed. Next, the initial  $F$  is introduced in the recursive formulae (6.9) and (6.10), starting from the given  $P_0$  to obtain  $P_1$ , then  $P_2$ , and finally  $P_n$ . In most cases, the calculated  $P_n$  for the first try is not expected to satisfy the boundary conditions with respect to the force at the last slice. Thus, a different assumed value of safety factor is required and the iterative process continues until the calculated  $P_n$  matches the prescribed boundary forces within a specified accuracy.

It should be noted that if  $P_i < 0$  occurs at any computation step while using equation (6.9), the calculated  $P_i$  is reset to be zero in next step for calculation of  $P_{i+1}$ . This is to take into consideration that soils usually are weak in tension.

When drilled shafts are introduced in the slope, supposing installed in a line at the interface between slices  $i-1$  and  $i$ , the computational scheme discussed above is still valid and equation (6.9) is used for all slices except for the slice  $i$  which is right behind the drilled shafts wall. The interslice force acting on the  $i-1$ th interface, with respect to the boundary of slice  $i$ , is reduced to  $RP_{i-1}$ , where  $R$  is the reduction factor due to the soil arching arising from the presence of the drilled shafts. As a result, substituting  $RP_{i-1}$  for  $P_{i-1}$  in equation (6.9) leads to

$$P_i = W_i \sin \alpha_i - \left[ \frac{c'_i l_i}{F} + (W_i \cos \alpha_i - u_i l_i) \frac{\tan \phi'_i}{F} \right] + k_i R P_{i-1} \quad (6.11)$$

which can be used to calculate  $P_i$  for the slice  $i$ , locating just behind the drilled shafts.

It should be noted that during the above process there is no physical slice designated to simulate the drilled shafts wall due to the uncertainties regarding the equivalent thickness of such slice for the discrete drilled shafts. Instead, the contributions of the drilled shafts are mechanically incorporated with the introduction of the reduction factor  $R$ .

#### **6.4 SOIL ARCHING MECHANISM AND THE REDUCTION FACTOR $R$**

Soil arching, defined as the stress transfer from a yielding soil mass into an adjoining non-yielding soil, is a phenomenon commonly encountered in geotechnical engineering. For a slope reinforced by the drilled shafts in a row, soil arching in the soil mass may occur as the soil moves through the opening between the drilled shafts, as depicted in Fig. 6.3. Based on laboratory model tests conducted by Bosscher and Gray (1986) and Adachi, et al.(1989), the soil arching mechanism was found to be significant and the development of soil arching was affected by both the layout of the drilled shafts and the soil properties. In analysis and design of the drilled shafts stabilized slope, one requires an adequate information regarding the parameters most affecting soil arching. In particular, one needs to quantify the contribution of drilled shafts. For this purpose, a systematical parametric study has been carried out with the aid of a finite element computer program PLAXIS. Parameters varied included shaft diameter, shaft spacing, internal friction angle and cohesion of the soil. Details of FEM modeling techniques and

validation results are summarized in chapter V, together with the pertinent results of a numerical parametric study.

For the soil strength, the internal friction angle was varied from 0 to 40° and the cohesion was varied from 0 kPa to 91.44 kPa. For the drilled shafts, three shaft diameters were studied:  $d = 30.48$  cm,  $d = 60.96$  cm and  $d = 91.44$  cm, while the clearance (spacing) between the shafts was varied from 1 to 5 times of diameter. The development of soil arching was assessed by the degree to which the driving force was transferred to the drilled shafts, or by means of the residual stresses acting on the soil mass between the shafts. Here, the soil pressure acting on the soil mass between the piles due to soil arching effect was calculated and normalized with respect to the initial pressure to obtain a percentage factor  $R_p$ . Obviously, if the value of  $R_p$  is 100%, it means that no arching effect exists at all and all soil pressure would be fully transmitted to the soil mass downslope.

**Table 6.1. Percent of pressure acting on soil mass between piles (d=91.44 cm)**

		c = 0 (kPa)	c = 6.9 (kPa)	c = 13.8 (kPa)	c = 27.6 (kPa)	c = 41.4 (kPa)
$\phi = 0^\circ$	s/d=2	100.00	40.13	10.44	10.07	9.65
	s/d=3	100.00	67.98	28.75	15.61	15.24
	s/d=4	100.00	78.18	48.50	23.30	17.91
$\phi = 10^\circ$	s/d=2	72.33	20.06	10.14	9.99	9.57
	s/d=3	85.33	45.68	16.01	15.52	15.18
	s/d=4	90.85	63.69	30.02	17.38	17.33
$\phi = 20^\circ$	s/d=2	49.80	14.18	10.09	9.57	9.39
	s/d=3	71.90	25.38	15.62	15.39	15.12
	s/d=4	81.48	50.98	16.86	15.68	15.02
$\phi = 30^\circ$	s/d=2	35.66	10.13	9.89	9.34	9.24
	s/d=3	60.58	16.16	15.46	15.32	15.06
	s/d=4	74.02	41.09	16.43	15.46	15.00
$\phi = 40^\circ$	s/d=2	31.26	10.02	9.34	9.32	9.21
	s/d=3	53.54	19.54	15.32	15.18	14.94
	s/d=4	64.82	35.14	15.46	15.31	14.87

Fig. 6.4 summarizes the influences of variation of drilled shaft diameter  $d$  and spacing  $s$  on  $R_p$  for the case of cohesionless soil with an internal friction angle  $\phi = 40^\circ$ .

Figs. 6.5 and 6.6 show the influences of internal friction angle and cohesion, respectively, on the residual stresses acting on the soil mass. For general cases, with various combinations of parameters, the corresponding  $R_p$  is listed in Table 6.1. Based on the parametric study, some observations can be drawn as follows:

- a) The ratio of shaft spacing to shaft diameter,  $s/d$ , is found to be the key factor affecting the soil arching. As  $s/d$  increases, the effect of soil arching decreases.

- b) Soils with higher friction angle are more likely to produce greater granular interlocking and thus stronger soil arching effect.
- c) The arching-induced load transfer of cohesive soils is found to be significant, contrast to previous findings. The long-term creep effect of cohesive soil should be taken into account in incorporating this arching effect into the global stability analysis of the slope.

With the percent of residual soil pressure,  $R_p$ , developed from the FEM study, the force acting on the drilled shaft on the side facing upslope direction can be determined as

$$F_{shaft}^{up} = P_{i-1}d + (1 - R_p)P_{i-1}(s - d) \quad (6.12)$$

where  $d$  is shaft diameter,  $s$  is shaft spacing,  $P_{i-1}$  is the interslice force (unit width) acting on the slice right in front of the shafts, and the term  $(1 - R_p)P_{i-1}(s - d)$  is referred to as the transferred load due to the soil arching effect. On the other side of the drilled shafts (i.e., the side facing the downslope direction), the drilled shaft is subjected to the force induced from soil mass behind the shaft as

$$F_{shaft}^{down} = P_{i-1}d \quad (6.13)$$

Thus, the net force acting on one drilled shaft is

$$F_{shaft} = F_{shaft}^{up} - F_{shaft}^{down} = (1 - R_p)P_{i-1}(s - d) \quad (6.14)$$

Expression (6.14) relates the drilled shaft force  $F_{shaft}$  to the soil arching factor  $R_p$ . As it indicates, the stronger the soil arching effect (the smaller  $R_p$ ), the more net force would act on the drilled shaft. For any reason, if the soil can freely move through the shafts without any traction or the soil mass and the drilled shafts experience no relative movement between them, then there would be no arching effect and no net force acting on the drilled shafts. This scenario can be represented by letting  $R_p = 1$ , the case of no arching effect, in expression (6.14), which leads to  $F_{shaft} = 0$  as expected.

Assuming that the net drilled shaft force  $F_{shaft}$  is sustained by the drilled shaft itself, then the interslice force transmitted to the next slice right behind the drilled shafts is reduced to

$$P'_{i-1} = \frac{P_{i-1}s - F_{shaft}}{s} \quad (6.15)$$

Substituting expression (13) into (14) yields

$$P'_{i-1} = \left[ \frac{1}{s/d} + \left(1 - \frac{1}{s/d}\right)R_p \right] P_{i-1} \quad (6.16)$$

Recall the definition of reduction factor  $R$  introduced in equation (6.11), then the expression (6.16) implies

$$R = \frac{1}{s/d} + \left(1 - \frac{1}{s/d}\right)R_p \quad (6.17)$$

As it can be seen from the above expression, the interslice force reduction factor  $R$  is a function of the ratio of shaft spacing to shaft diameter and the arching effect factor  $R_p$ . For a given soil condition and drilled shafts layout (dimensions and spacing) with their parameters being within the range of the numerical values in Table 6.1, one could obtain the  $R_p$  directly from Figs. 6.4 to 6.6 or Table 6.1. The reduction factor  $R$  can then be calculated via. Equ. (617). However, if some of the parameters are outside the range in Table 6.1, either interpolation or extrapolation can be exercised to determine the corresponding numerical values. It is important to perform additional numerical simulations to confirm the extrapolated numerical values

## 6.5 EXAMPLE STUDIES

### (1) Example One: Comparison of Methods of Analysis

Fig. 6.7 shows an example problem considering a slope with a weak layer underneath. The presence of the phreatic ground water table was treated by either the constant water pressure ratio  $r_u$  or a direct input of phreatic surface location. This problem has been studied by quite a few investigators (Fredlund and Krahn, 1977; Baker, 1980; Donald and Giam, 1988; Zhang and Chowdhury, 1995). The validity of the present method was evaluated by comparing the calculated results with those obtained by other well-established methods.

Analyses were first performed for the case of circular slip surface. In this case, the slope was considered to be homogeneous with  $\gamma = 18.85 \text{ kN/m}^3$ ,  $c' = 28.73 \text{ kPa}$  and  $\phi' = 20^\circ$ . The height of the 2:1 slope is 12.2 m and the radius of the slip circle is 24.4 m.

The calculated safety factors for three different water conditions: no water, constant pressure ratio  $r_u = 0.25$  and specified phreatic line were 2.097, 1.720, and 1.844, respectively. The calculated results are listed in Table 6.2 along with those from various other methods.

**Table 6.2. Comparison of factors of safety for example problem (circular slip surface)**

Methods of analysis	Without water	$r_u = 0.25$	Phreatic line
Ordinary method	1.928	1.607	1.693
Simplified Bishop method	2.080	1.766	1.834
Spencer's method	2.073	1.761	1.830
Janbu's method	2.008	1.708	1.776
Morgenstern-Price method	2.076	1.765	1.833
Proposed method	2.097	1.720	1.844

For more complicated cases where the slope is underlain by a weak layer, a composite slip surface, consisting of parts of the above circle and a weak segment intersecting the circle, was used. The properties of the weak joint were  $\gamma = 18.85 \text{ kN/m}^3$ ,  $c' = 0 \text{ kPa}$  and  $\phi' = 10^\circ$ . Similarly, three possible water conditions were taken into account. The calculated factors of safety were 1.396, 1.165 and 1.255, as presented in Table 6.3.

**Table 6.3. Comparison of factors of safety for example problem (composite slip surface)**

Methods of analysis	Without water	$r_u = 0.25$	Phreatic line
Ordinary method	1.288	1.029	1.171
Simplified Bishop method	1.377	1.124	1.248
Spencer's method	1.373	1.118	1.245
Janbu's method	1.432	1.162	1.298
Morgenstern-Price method	1.378	1.124	1.250
Proposed method	1.396	1.165	1.255

The comparison results in Tables 6.2 and 6.3 show that the factors of safety obtained by the proposed method are generally similar to those computed by the simplified Bishop, Spencer and Morgenstern-Price methods for the case of circular failure surface. On the other hand, for the composite slip surface, the calculated results are much closer to those from Janbu's method. In all cases considered for possible combinations of water conditions, soil properties and various failure surfaces, the proposed method led to acceptable accuracy, with the average difference being within a narrow range of less than 3% when compared to the corresponding well-established methods.

## (2) Example Two: Drilled Shafts Reinforced Slope

To evaluate the validity of the proposed method for drilled shaft stabilized slopes, it was applied to a slope where the reinforcement measures were required to stabilize the slope. The example selected was a 2:1 slope of a height of 8m investigated by Hung and

Yamasaki (1993), as shown in Fig. 6.8. The ground water table was assumed to be far below the failure surface so that there was no pore water pressure involved. The failure surfaces determined by the local minimum factor-of-safety approach and Bishop's method were found to be very close and had factors of safety of 1.00 and 1.03, respectively, with the assumed soil properties of  $c = 10 \text{ kPa}$ ,  $\phi = 10^\circ$  and  $\gamma = 19.6 \text{ kN/m}^3$ .

Using a reduction factor  $R = 1$  in equation (6.11), meaning there are no drilled shafts in the slope, the calculated factor of safety is 1.005. This value compares favorably with 1.00 and 1.03 obtained by other methods, as listed in Table 6.4. The closeness of the safety factor to unity suggests the need of slope stabilization.

**Table 6.4. Comparison of results (plain slope)**

Methods of analysis	Factor of safety
Bishop's method	1.03
Local minimum FS method	1.00
Proposed method	1.005

The stabilization effect of the installation of drilled shafts was investigated by calculating the factor of safety of the reinforced slope using the proposed stability analysis procedure. To evaluate the influence of the layout of the drilled shaft on slope stability, the locations and spacings of the drilled shafts were varied in the analyses.

Table 6.5 lists the factors of safety of the drilled shafts reinforced slope and the corresponding net lateral force acting on one shaft with respect to the location of the drilled shafts, with shaft diameter  $d = 0.5 \text{ m}$  and shaft spacing  $s = 1.0 \text{ m}$ . The results are also shown in Figs. 6.9 and 6.10 in normalized forms. As expected, the contribution of

drilled shafts to the slope stabilization is comparatively less significant if the drilled shafts are located in the upper end of the slip surface, as characterized by a small increases on the factor of safety and drilled shaft force. The most effective location for the drilled shafts to improve slope stability is near the location of one-third of dimensionless distance from the toe.

**Table 6.5. Influence of shaft location on shaft force and global factor of safety**

x-coordinate (m)	Lateral force on shaft (kN)	Global factor of safety
6	0	1.005
8	7.109	1.019
10	69.118	1.159
12	133.594	1.364
14	217.129	1.812
16	273.263	2.322
18	321.331	3.026
20	314.335	3.032
22	297.490	2.803
24	185.479	1.719
26	0	1.005

For a specific position  $x = 20$  m, which is within the most effective location based on the sensitivity study discussed above, the effect of drilled shaft spacing was analyzed. The calculated results with the shaft spacing ratio varying from 1.5 to 5.0 for shaft diameters of  $d=0.5$ ,  $d=0.75$  and  $d=1.0$ m were listed in Table 6.6. The factors of safety against the ratio of shaft spacing to diameter are plotted in Fig. 6.11 for the case of  $d=0.5$ m. It can be seen that the stability of the slope considered can be significantly enhanced by the installation of drilled shafts in a row with appropriate spacing ratio. The

factor of safety increases rapidly from 1.4 to 5.0 as the ratio  $s/d$  decreases from 3.5 to 1.5. This is a concomitant result of soil arching mechanism where the closer drilled shafts are placed in a row, the stronger a soil arching effect would develop and consequently more transferred arching load to the drilled shafts would occur.

**Table 6.6. Influence of shaft layout on global factor of safety**

Spacing ratio (s/d)	d=0.5m	d=0.75m	d=1.0m
1.5	5.001	4.999	4.434
2.0	3.032	2.745	2.522
2.5	2.017	1.946	1.882
3.0	1.652	1.615	1.581
3.5	1.440	1.425	1.411
4.0	1.318	1.307	1.298
4.5	1.230	1.224	1.218
5.0	1.168	1.164	1.159

## 6.6 CASE STUDY

The case history selected was a slope stabilization analysis/design of the Pomeroy landslide at US RT 33 project. Shown in Fig. 6.12 is a typical cross-section of the slope together with the corresponding soil properties for each layer. The program STABL5M, a stability analysis program developed by the U.S. Federal Highway Administration, was applied to locate the failure surface as shown in Fig. 6.12. The analysis gave a factor of safety of 1.221 based on the given soil conditions. Since the inclinometer readings and surface investigation data indicated that the slope might have experienced significant slide along the slip surface, the higher value of factor of safety suggested that the soil

strength along the soil-rock interface or the failure surface should be reduced to some extent. For this reason, a parametric study was carried out to produce the back-calculated strength parameters along the soil-rock interface. The failure state determined by SATBL5M had a factor of safety of 1.007 with the assumed soil-rock interface properties of  $c=3.4$  kPa and  $\phi=16.5^\circ$ . The installation of drilled shafts was chosen as a remedy means for slope stabilization. Pertinent design recommendation for the drilled shafts is summarized as below.

- Diameter: 122 cm
- Length: goes through the slide surface with minimum rock socket length of 2 m.
- Spacing: 244 cm center-to-center
- Reinforcement: 14#11 main bars with #4@15 cm ties

The application of the proposed method to the original slope condition yielded the factor of safety of 1.231. For the case with reduced strength parameters, the proposed method gave a factor of safety of 1.012. The comparison between the results obtained by the proposed method and the other proven technique was presented in Table 6.7. As shown in the table, the results are very close to each other for both cases. This provides a solid base to review the recommended stabilization design by using the proposed method thereafter.

**Table 6.7. Comparison of factors of safety**

	In-situ ( $c=4.0$ kPa, $\phi=18^\circ$ )	Reduced ( $c=3.4$ kPa, $\phi=16.5^\circ$ )
STABM5L	1.221	1.007
Proposed method	1.231	1.012

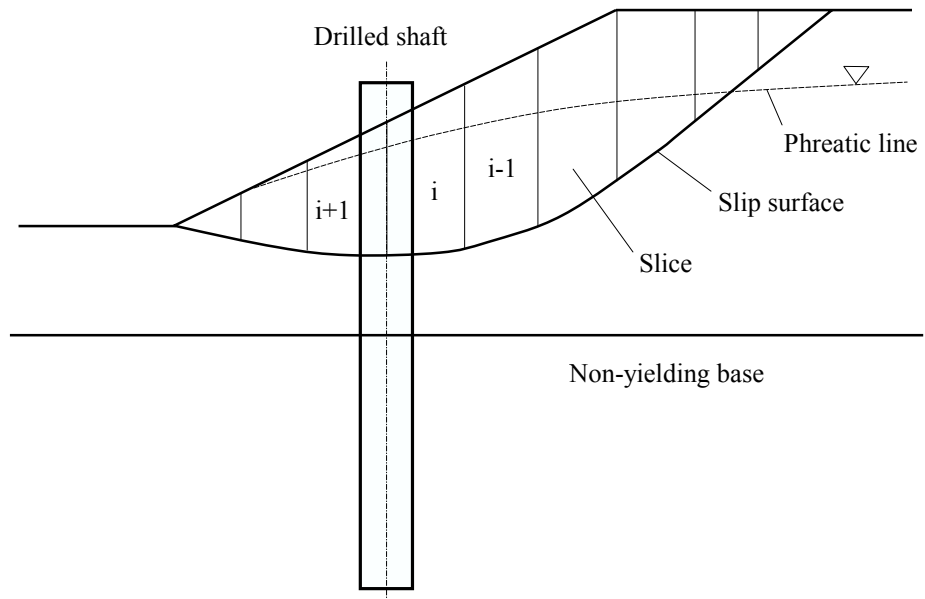
For the given layout of drilled shafts and the specified location as shown in Fig. 6.12, the global stability of the reinforced slope was found to be improved, with the calculated global factor of safety of the slope increasing from 1.012 to 1.297. The corresponding lateral force acting on the drilled shaft is 565 kN, which leads to a maximum bending moment  $M_{\max}=1684$  kN-m. Since the allowed bending moment of the drilled shaft is  $M_{\text{allow}}=2881$  kN-m, the factor of safety of the drilled shaft with respect to bending moment is:

$$FS_{\text{shaft}} = M_{\text{allow}} / M_{\max} = 1.71$$

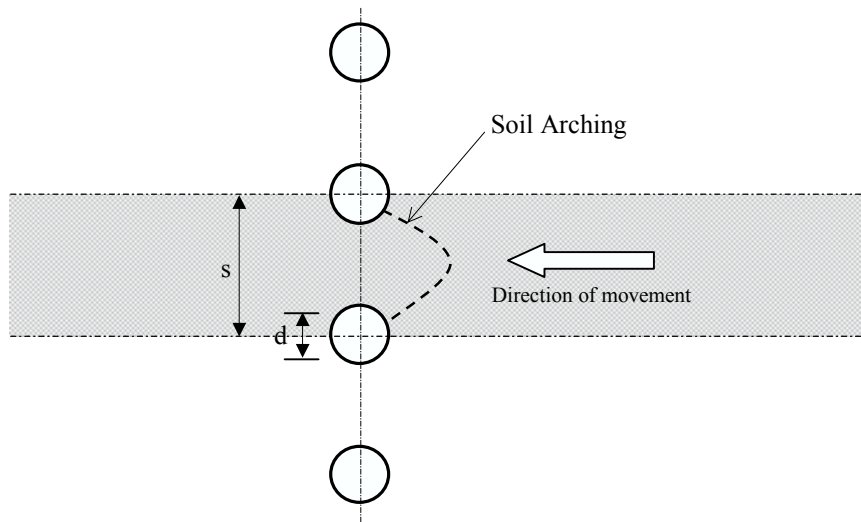
It can be concluded that both stability conditions of slope and drilled shaft are satisfied.

## 6.7 CONCLUSIONS

An approach has been described for the analysis and design of drilled shafts stabilized slope. The developed method utilizes the generalized procedure of slice for composite slip surface of any shape and incorporates the effect of soil arching due to the installation of drilled shafts. Such integrated approach can readily determine the global factor of safety for the slope reinforced with drilled shafts and the lateral force acting on the drilled shafts as well. Comparative studies have shown that the proposed method can lead to reasonable assessments on the stability of natural slope and reinforced slope using the drilled shafts. It has been found that the drilled shafts embedded into a firm, non-yielding soil stratum can provide significant additional stability to a slope if conditions for developing soil arching are present. Among the factors that most affect the reinforcement contribution exerted by the drilled shafts are the location, the ratio of spacing to diameter, and the properties of the soil.



(a) Cross section



(b) Plane view

Fig. 6.1 Drilled shafts in a row for stabilizing a slope

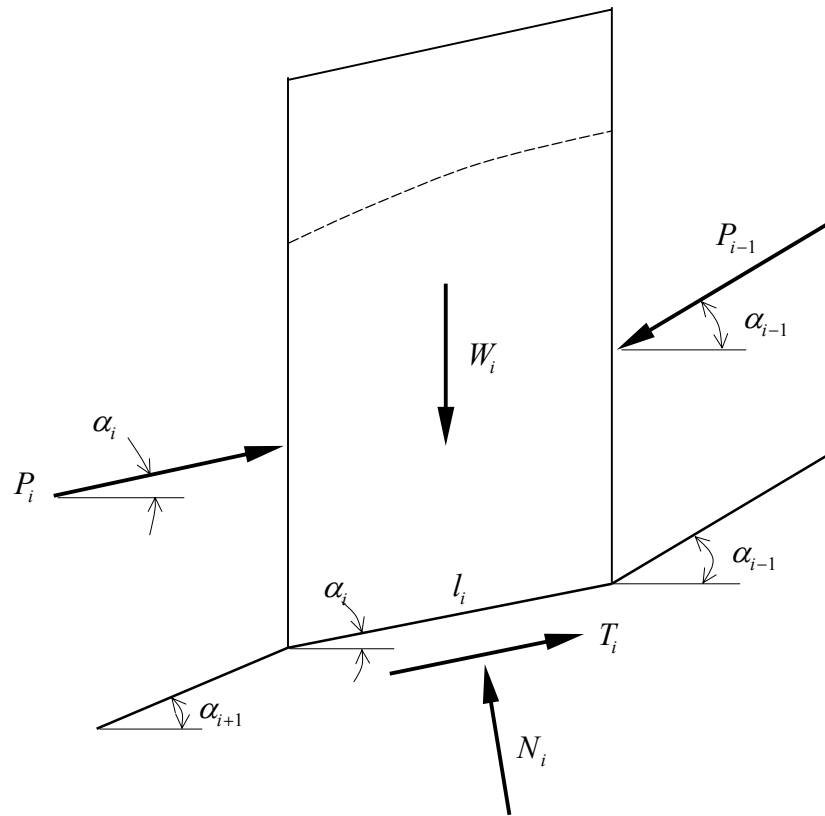


Fig. 6.2 Forces acting on a typical slice

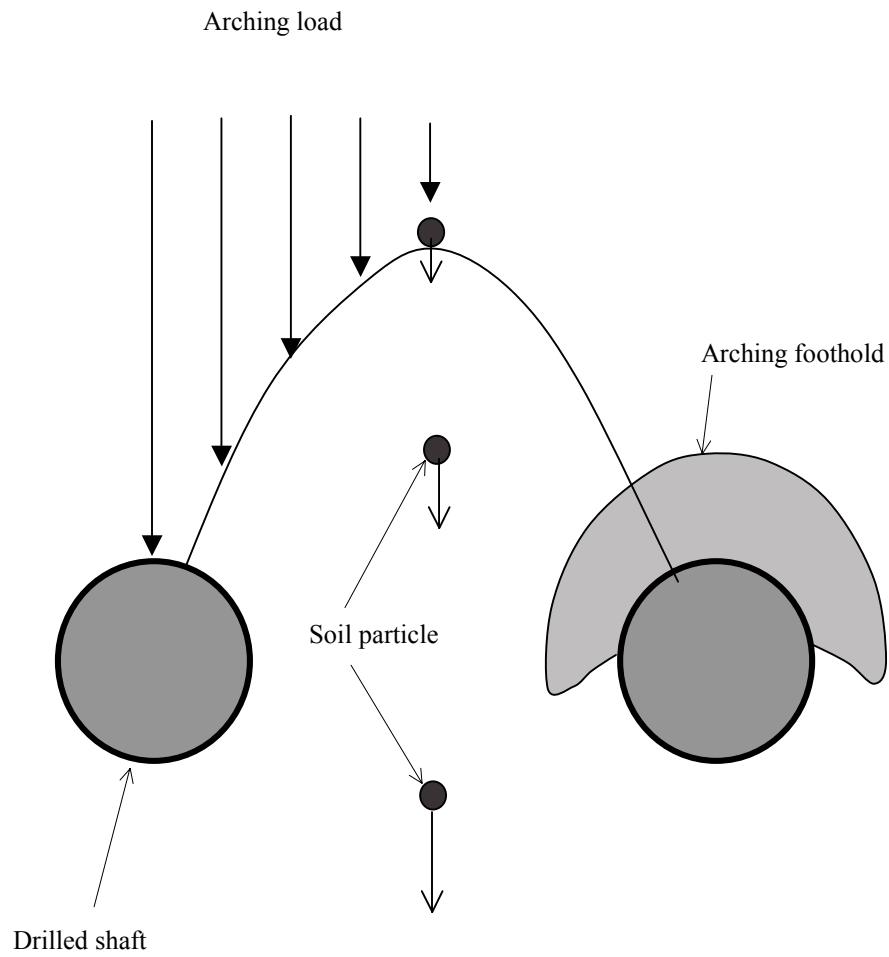


Fig. 6.3 Schematic of arching effect( after Adachi, 1989)

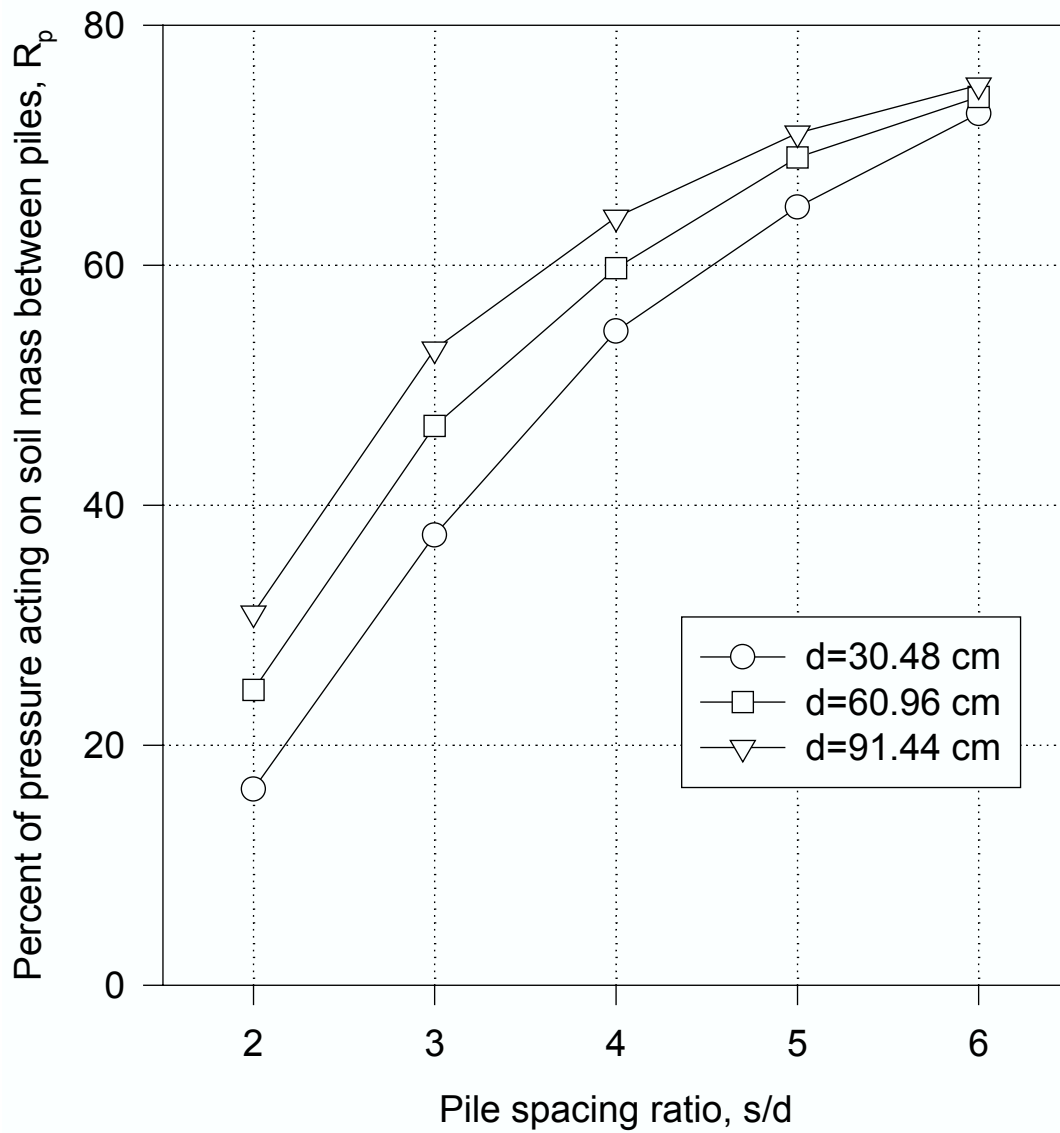


Fig. 6.4 Effect of variation in pile spacing ratio: cohesionless soil with  $\phi=40^\circ$

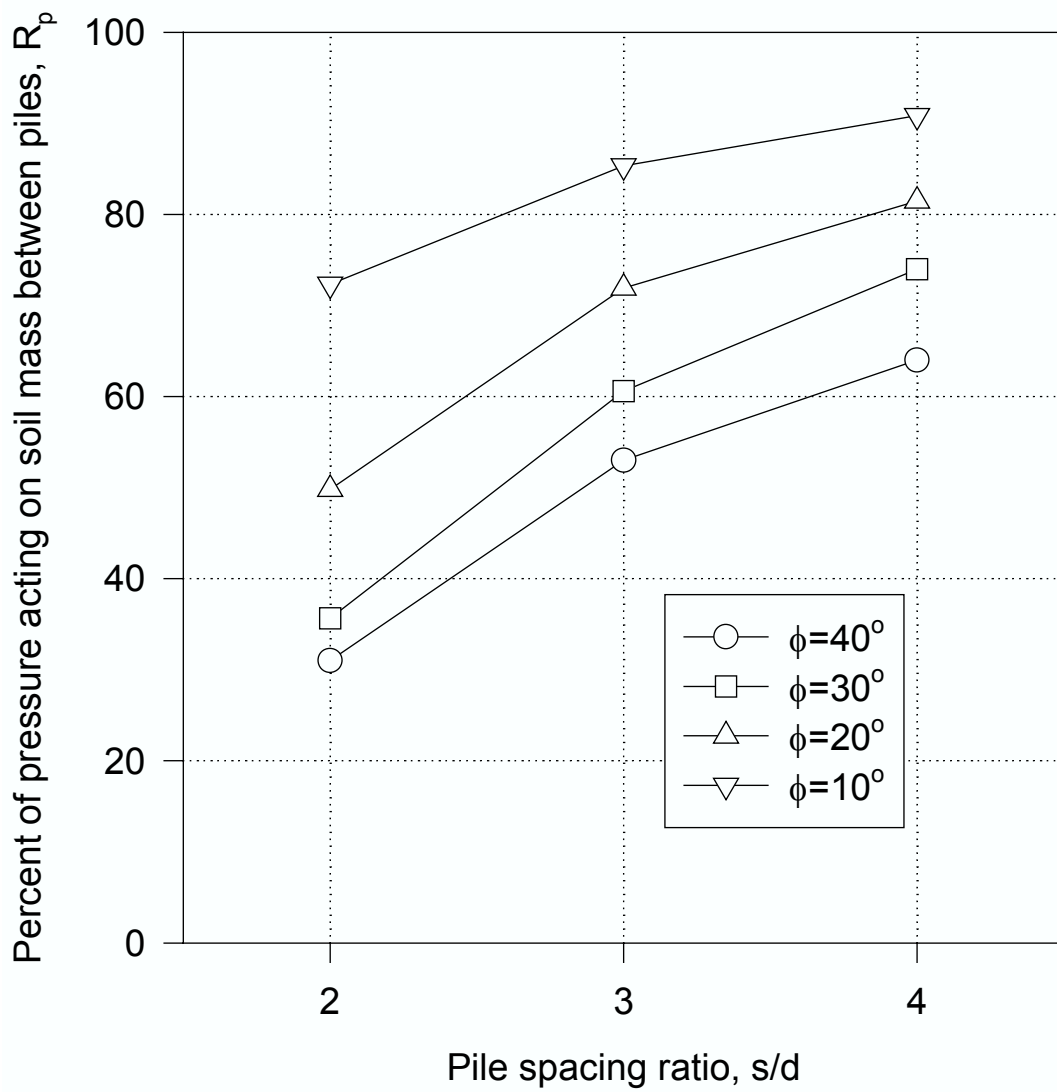


Fig. 6.5 Effect of variation in internal friction angle: cohesionless soil

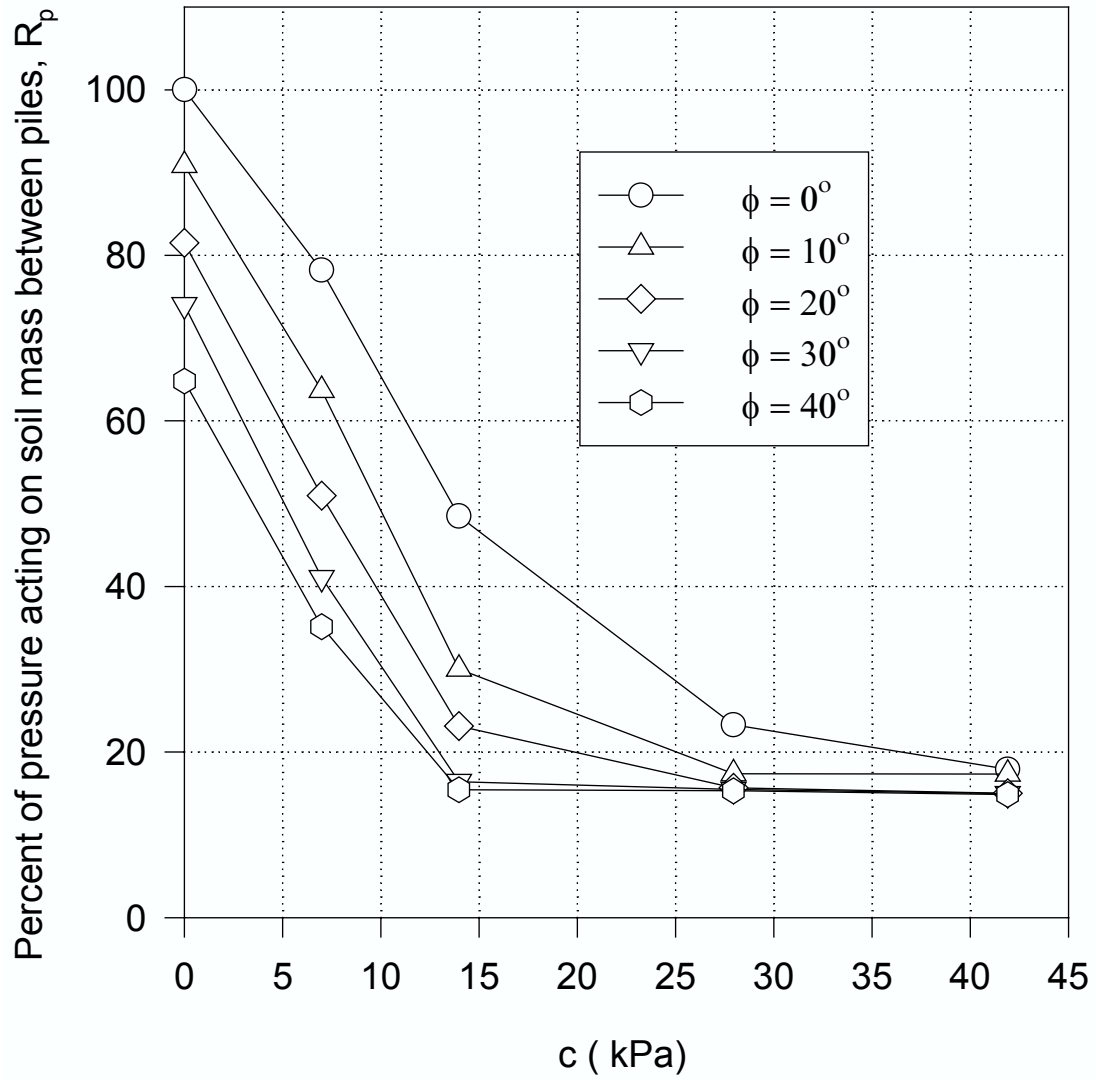


Fig. 6.6 Effect of variation in cohesion:  $s=4d$  with  $d=91.44$  cm

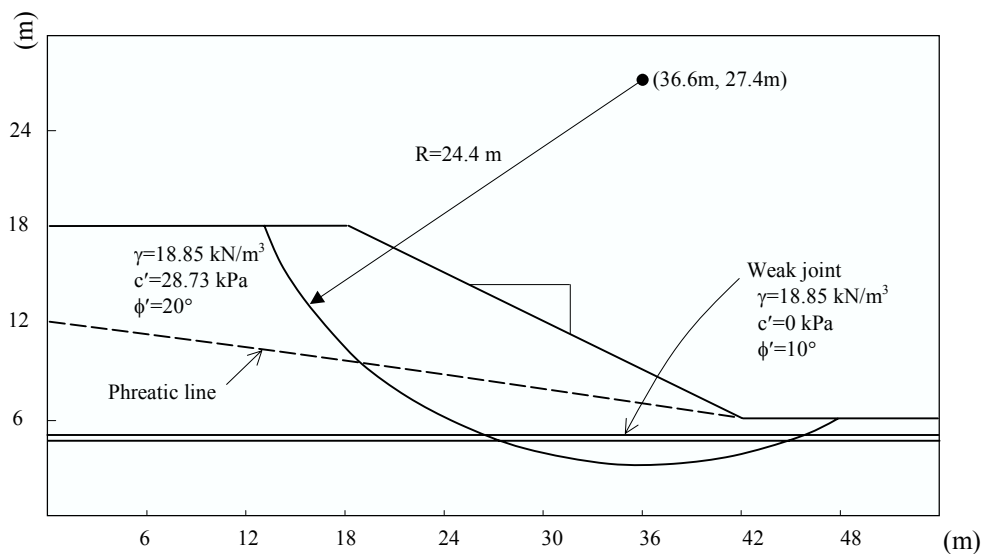


Fig. 6.7 Example problem (after Fredlund and Krahn, 1976)

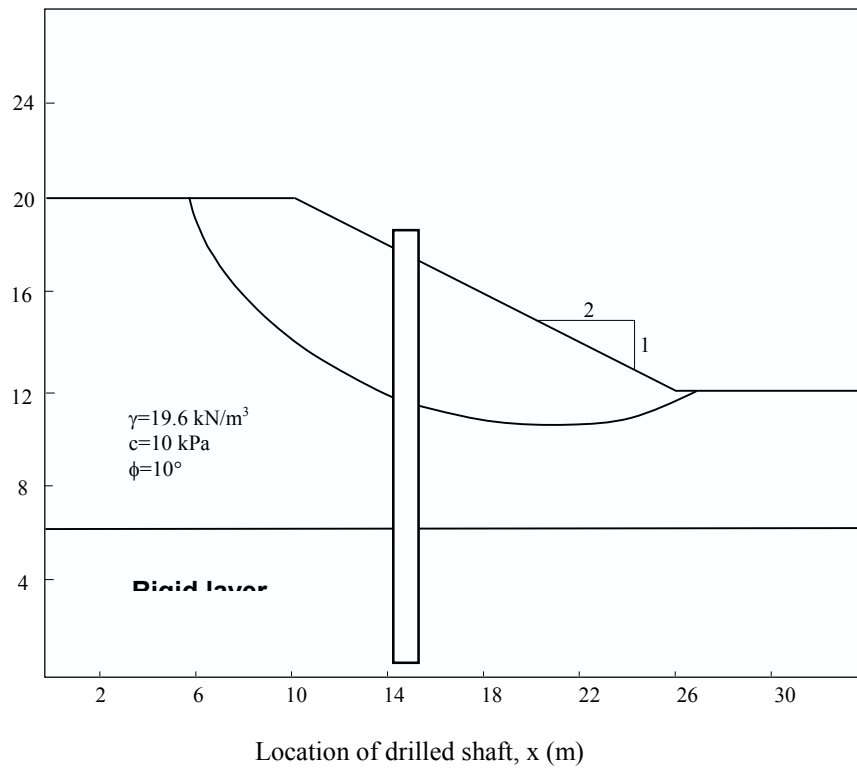


Fig. 6.8 Example problem two

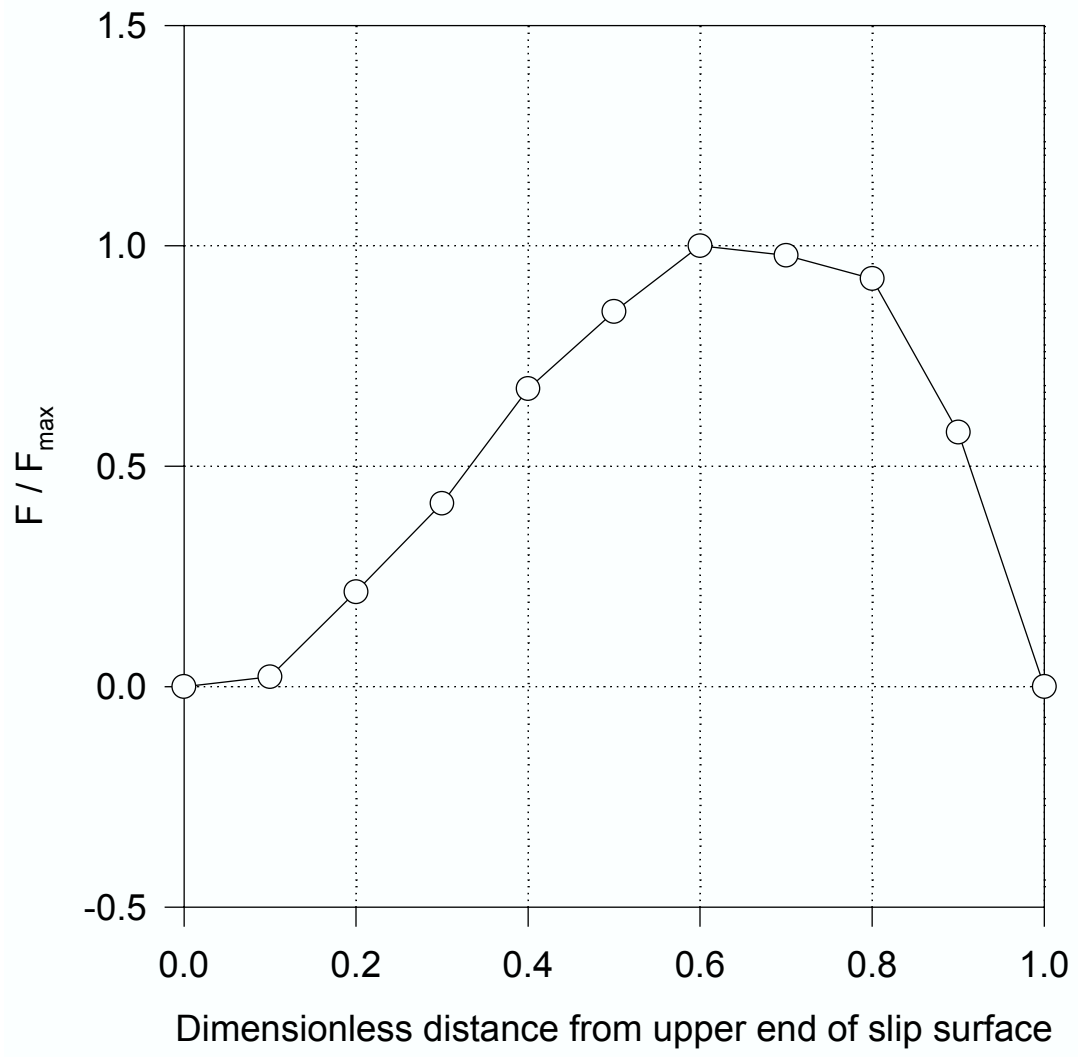


Fig. 6.9 Distribution of the ratio of drilled shaft lateral force  $F$  over the maximum  $F_{\max}$

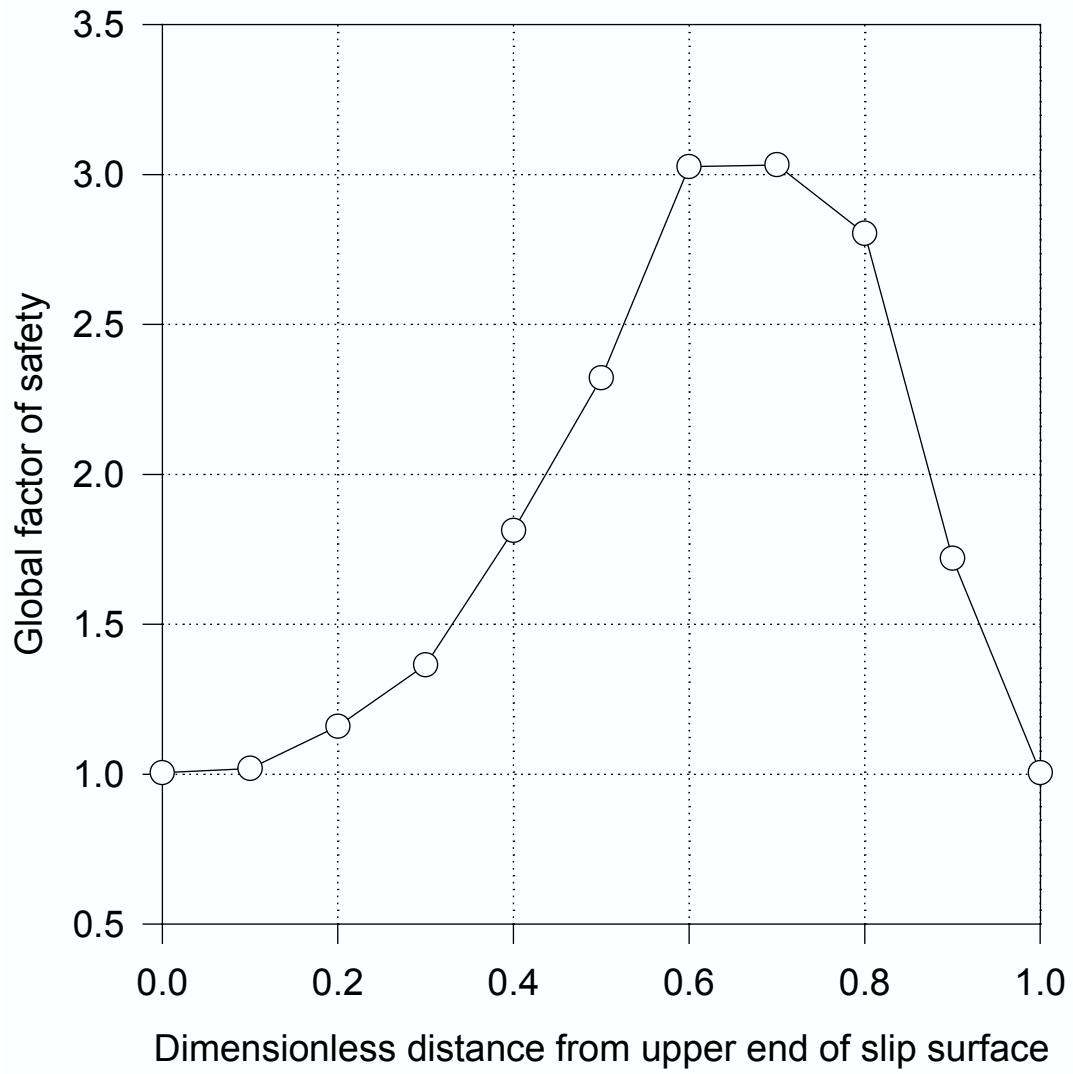


Fig. 6.10 Distribution of the global factor of safety

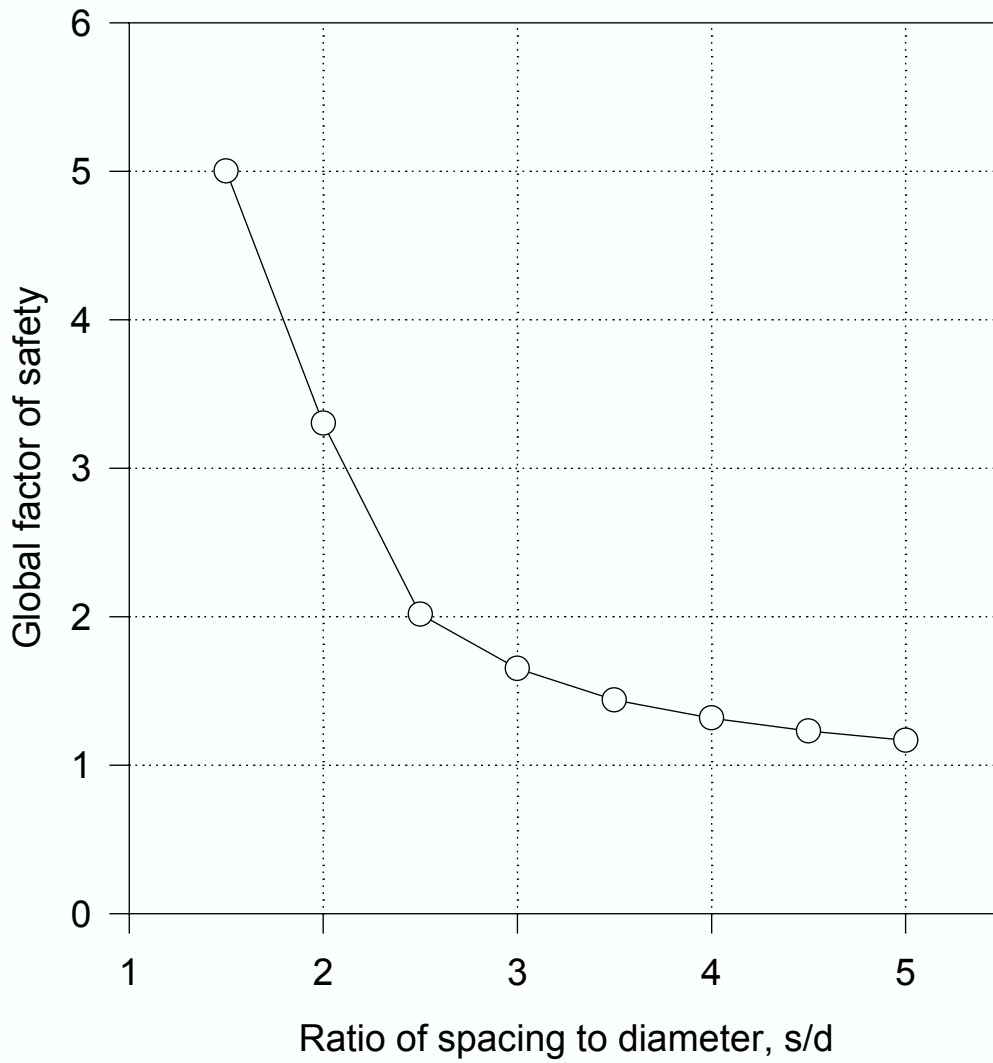


Fig. 6.11 Global factor of safety versus the ratio of spacing to diameter

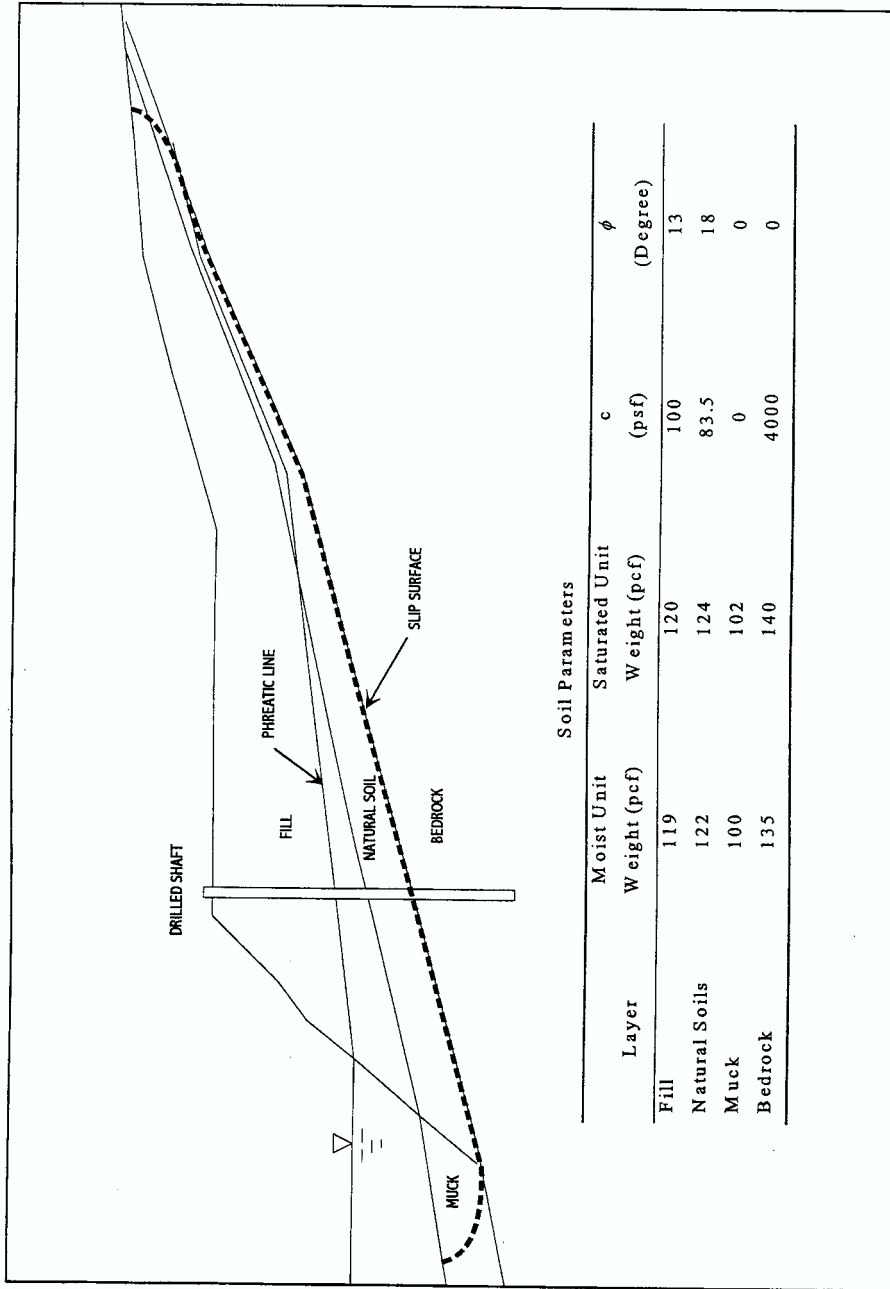


Fig. 6.12 Cross-section C-C of Pomeroy landslide

## **CHAPTER VII**

### **SUMMARY AND CONCLUSIONS**

#### **7.1 MAJOR RESEARCH RESULTS**

A database consisting of a total of 58 lateral load test results of the drilled shafts has been compiled. Also established in the database are the pertinent soil and rock profiles at each test site together with SPT profiles. The drilled shaft diameters range from 16 inch to 72 inch, while the length of the drilled shafts extends from about 10 ft to 95 ft. Some of them are socketed into rock, while some of them are in cohesive and/or cohesionless soils. Among these 58 cases, 32 of them are Ohio load test results. The most useful information of the data has been condensed and presented in Chapter III.

A correlation study has been successfully completed to establish the empirical relationship between the SPT N values and the important soil parameters for the p-y curves used in the computer program COM624. Specifically, the SPT N values are related to friction angle, subgrade reaction coefficient for cohesionless soils, and undrained shear strength, strain at 50% compression strength, and subgrade reaction coefficient for cohesive soils, respectively. These recommended correlations are summarized in Tables III. 3 and III.4 for cohesionless and cohesive soils, respectively. Based on these empirical correlations and the existing p-y curve criteria in the COM624 computer program, the computational results of laterally loaded drilled shafts deflections at the point of load application are shown to be in good agreement with the measured values for all the cases collected in the database. The quality of the goodness of the match

is calculated using a numerical index  $r$  to reflect the average of the ratio between the measured and predicted drilled shaft deflections at various applied load levels. Depending on the type of the soils and the load levels, the numerical values of the index  $r$  range from 0.78 to 1.1. Judging from the fact that other factors than soil properties, such as the construction method, drilled shaft dimensions, and load details, may also affect the behavior of the drilled shafts; the average  $r$  values seem to be very acceptable. As most highway agencies, including Ohio Department of Transportation, rely on SPT as the only practical means for routine geotechnical investigation for highway projects, the developed correlations for using the SPT  $N$  values to derive the  $p$ - $y$  curve parameters offer much needed advantages. Tables III.3 and III. 4 provide guidance for parameter selection that lead to very accurate predictions of drilled shaft deflections under applied lateral loads.

A centrifuge test technology for modeling the soil slopes with or without drilled shafts has been fully developed in this research study. The method for soil slope model preparation for both cohesive and cohesionless soils has been developed and validated. The methodology for using the increased centrifugal forces to model various dimensions of the soil slope and drilled shafts has been established as well. Issues such as data acquisition and modeling scales have been fully addressed and resolved in this study. The study has laid foundation for advanced centrifuge model testing technology and can be applied to other studies of geotechnical problems, such as embankment, foundations, and earth retaining structures.

A comprehensive series of centrifuge model tests have been performed in this study to gain quantitative information about the mechanisms of drilled shafts in stabilizing the soil slopes. The deflections of the model drilled shafts in the slopes are used to convert into net forces acting on the drilled shafts as well as the bending moments along the shaft length. Effects of drilled shaft diameter, shaft spacing, soil strength, and slope geometry on the model shaft behavior are quantified. In particular, the soil arching induced force re-distribution has been quantified. Specifically, in the sandy soil slope, when the S/D ratio ( $S$  = clear spacing of drilled shaft, and  $D$  = diameter of the drilled shaft) is equal to 2, then the arching effect is most pronounced. Similarly, when S/D is equal to 1.5 in the clay soil slope, then the arching effect is most pronounced. The increasing slope angle tends to reduce the magnitude of the force and moment in the drilled shafts.

To supplement the physical data obtained from the centrifugal model tests, an innovative finite element analysis technique using the program PLAXIS has been advanced. Both the finite element modeling techniques of the physical problem of shaft stabilized slopes and the use of appropriate constitutive soil models for sand and clay have been developed and validated with existing experiment results. Applying this proven numerical simulation technique, a comprehensive parametric study has been done to generate the soil arching induced force transfer curves for analyzing the drilled shafts in stabilizing the soil slopes. Among the parameters identified to influence the arching mechanisms are the drilled shaft spacing, shaft diameter, friction angle and cohesion of the soils. However, the S/D ratio is confirmed to be the most influential factor in impacting the development of full arching behavior. Arching is more likely to occur in

sand with high friction angle than in low friction angle. Arching could also develop in cohesive soils, even though over the time stress relaxation and creep may reduce the arching mechanism.

A new design and analysis method has been developed in this study to aid engineers in handling slope stabilization problems using the drilled shafts. The developed method utilizes the generalized procedure of method of slices for composite slip surface of any shape and incorporates the effect of soil arching due to the installation of drilled shafts. Such integrated approach can readily determine the global factor of safety for the slope with the drilled shafts and the lateral force acting on the shafts. Comparative studies of several cases have proven the reasonableness of the method. A computer program has been developed for stability analysis of the soil slopes stabilized by drilled shafts.

## **7.2 RECOMMENDATIONS FOR IMPLEMENTATION**

Two important research results are recommended for implementation.

First, it is recommended that the SPT correlation charts in Table III. 3 and III.4 be incorporated in the ODOT's Bridge Design Manual. Also, training courses materials should be developed to train engineers to use this correlation for designing drilled shafts subjected to lateral loads.

The other implementation suggestion is the development of a Technical Note for explaining and illustrating the design methodology for drilled shafts to stabilize the soil

slopes. The training courses should be offered to ODOT engineers and consultants alike to ensure that the most advanced engineering solutions developed in this research be applied to ODOT projects, resulting in safe and yet economic slope stabilization design.

### **7.3 RECOMMENDATION FOR FUTURE RESEARCH**

There are a few areas that are recommended for further research in the near future.

1. There is a need to continue the effort to conduct lateral load tests for construction projects with a large number of drilled shafts. The lateral load tests should be carried out in the beginning of the project so that the test results can be used to optimize the design of the drilled shafts for the remaining portion of the project. A standard plan note needs to be developed to enable ODOT engineers to implement this strategy of maximizing the benefits of field test results to produce safe and economic design. The test data should be continuously collected in a database for further calibration of the empirical correlations recommended in this report. In addition, the database could be eventually used for future calibration of the LRFD design method for laterally loaded drilled shafts.
2. There is a need to investigate the construction methods used to enhance the drilled shaft load carrying capacity in soils. Post grouting techniques have been advanced in several state highway agencies to improve the side friction and end bearing of the drilled shafts both in sand and clay soils. In situations where bedrock elevation is deep, perhaps this innovative construction method could be specified to reduce

the cost of long drilled shafts to reach the bedrock elevation. Research efforts are needed in the areas of understanding the load transfer mechanisms in the post grouted drilled shafts. Also, a better design and analysis method should be developed for such drilled shaft construction.

3. Construction methods and means for quality control for the auger cast piles have been advanced to a point where their uses in highways warrant a closer examination. There should be a systematic identification (best practice study) of the most promising applications of auger cast piles for highways, in terms of safety and economy. A standard needs to be developed and incorporated into ODOT's Construction and Materials Specifications as well as Highway Bridge Design Manual.
4. Drilled shafts used to support highway signs are also subjected to torsion loads, in conjunction with the lateral loads. Currently, there is no existing analysis and design method for torsion loads, other than using some approximate empirical formula. To allow engineers to design highway signs drilled shaft supports, more research is needed to understand the torsion behavior of the drilled shafts.
5. Deep foundations used in highway bridges are often in groups and connected to superstructures with pile caps. However, in current design approach, the group effect and the rigidity provided by the pile cap and superstructure have not been taken into consideration. To do this, a 3-D finite element analysis capability is

needed. A research effort should be devoted to the development of such an analysis capability. With comprehensive parametric study by the 3-D finite element method, design charts could be developed to incorporate the benefits of pile group effect as well as the added structural stiffness from the superstructure of the highway bridges.

6. The design method proposed in this report for the drilled shafts stabilized slopes should be applied to ODOT projects with detailed field instrumentation and monitoring so that the theory would be further verified for real, practical cases.
  
7. Maintenance and upgrade of unsafe slopes or man-made embankments has been a main mission of ODOT's Geotechnical Office. Remediation of unsafe slopes often involves the use of very conservative schemes including the rock anchors, tieback walls, drilled shafts, among others. However, as an alternative to these conventional slope remediation schemes, there are newer technologies emerged that could offer more expedient construction method as well as more economic solutions. Among these emerging technologies are the root piles, micro-piles, in-situ soil improvement such as vibro-concrete, vibroflotation, geopiers, lime columns, deep soil mixing, etc. ODOT could benefit tremendously by commission a best practice study to develop a suit of solutions for commonly occurred slope stabilization problems in Ohio.

8. Finally, geotechnical design of slope stabilization schemes could be benefited from a more intelligent database on geological hazards in Ohio, consisting of past practices in stabilization of the slopes, and current and future problem sites that require monitoring and maintenance. Certainly, a linkage of this database with soil boring and geological information in a GIS based platform would be highly desirable. Interconnectivity with Office of Structure's bridge database would also be needed so that critical structures could be protected from incipient slope or embankment failures due to the availability of a highly comprehensive and intelligent GIS based database. Work in this direction should be a high priority for ODOT.

## CHAPTER VIII

### REFERENCES

1. Adachi, T., Kimura, M. and Tada, S. (1989). "Analysis on the preventive mechanism of landslide stabilizing piles", 3rd International Symposium on Numerical Models in Geomechanics, 691-698.
2. Anderson, J.B. and Townsend, F.C. (2001). "SPT and CPT testing for evaluating lateral loading of deep foundations", Journal of Geotechnical and Geoenvironmental Engineering, Vol. 127, No. 11, 920-925.
3. Anagnostopoulous, A. G. and Papadopoulos, B. P. (1982), " SPT and the compressibility of cohesionless soils.", ISOPT I, 25-28.
4. ASTM (1992). " Standard Test Method for Penetration Test and Split-Barrel Sampling of Soil".
5. Atkinson, J. H. and Potts, D. M. (1977). "Stability of a shallow circular tunnel in cohesionless soil", Geotechnique, London, England, 27(2), 203-215.
6. Baker, R. (1980). "Determination of critical slip surface in slope stability computations", Int. J. Numerical and Analytical Methods in Geomechanics, Vol. 4, 333-359.
7. Beasley, D.H. (1973), "Centrifugal Modeling of Soft Clay Strata Subject to Embankment Loading", Ph.D. Thesis, Cambridge University.
8. Bishop, A.W. (1955). "The use of the slip circle in the stability analysis of slopes", Geotechnique 5, No. 1, 7-17.
9. Bolton, M. (1979). A guide to soil mechanics, Macmillan Press Ltd., London, England, 313-315.
10. Bolton, M. (1986). "The strength and dilatancy of sands", Geotechnique, Vol. 36, No. 1, 65-78.
11. Bosscher, P. J. and Gray, D. H. (1986). "Soil arching in sandy slopes", Journal of Geotechnical Engineering, Vol. 112, No. 6, 626-645.
12. Bouafia, A. and Garnier, J. (1991), "Experimental Study of p-y Curves for Piles in Sand", Centrifuge'91, pp.261-268, Balkema, Rotterdam.

13. Bransby, P. L. and Smith, I. A. A. (1975). "Side friction in model retaining wall experiments", *Journal of the Geotechnical Division, ASCE*, Vol. 101, No. GT7, 615-632.
- Carter, J. P. (1982). "A numerical method for pile deformations due to nearby surface loads.", *Proc. 4<sup>th</sup> ICONMIG, Edmonton*, 2, 811-817.
14. Chelapati, C. V. "Arching in soils due to the deflection of a rigid horizontal strip", *Proceedings, Symposium on Soil-Structural Interaction, Tucson, Ariz.*, 356-377.
15. Chen, L. T., Poulos, H. G. and Hull, T. S. (1997). "Model tests on pile groups subjected to lateral soil movement", *Soils and Foundations*, Vol. 37, No. 1, 1-12.
16. Clayton, C. R. I., Hababa, M. B. and Simons, N. E. (1985), "Dynamic penetration resistance and the prediction of the compressibility of a fine-grained sand- a laboratory study.", *Geotechnique* 35, no. 1, 19-31.
17. Cox, W. R., Dixon D. A., and Murphy, B. S. (1983). "Lateral-load tests on 25.4 mm (1 in.) diameter piles in very soft clay in side-by side and in-line groups", *Proc. of a symposium sponsored by ASTM Committee D- 18 on Soil and Rock, Kansas City*.
18. Craig, W.H. (1984) "Installation Studies for Model Piles", *Proc. Application of Centrifuge Modeling to Geotechnical Design*, pp. 440-455. Balkema, Rotterdam.
19. Craig, W.H., James, R.G. and Schofield, A.N.(eds)(1988) "Centrifuges in Soil Mechanics", Balkema, Rotterdam.
20. Donald, I. B. and Giam, S. K. (1988). "Application of the nodal displacement method to slope stability analysis", *5<sup>th</sup> Australia-New Zealand Conference on Geomechanics, Sydney*, 456-460.
21. Espinoza, R. D., Bourdeau, P. L. and Muhunthan, B. (1994). "Unified formulation for analysis of slopes with general slip surface", *Journal of Geotechnical Engineering*, Vol. 120, No. 7, 1185-1204.
22. Fellenius, W. (1936). "Calculation of the stability of earth dams", *Proceedings of the Second Congress on Large Dams*, Vol. 4, 445-463.
23. Figueroa, J.L., Saada, A.S., Dief, H. and Dietz, C.P. (1998), "Development of The Geotechnical Centrifuge at Case Western Reserve University", *Proceedings of The International Conference, Centrifuge 98*.
24. Finn, W. D. L. (1963). "Boundary value problems of soil mechanics", *Journal of the Soil Mechanics and Foundations Division, ASCE*, Vol. 89, No. SM5, 39-72.
25. Fredlund, D. G., Zhang, Z. M. and Lam, L. (1992). "Effect of the axis of moment equilibrium in slope stability analysis", *Can. Geotech. J.*, Vol. 29, 456-465.

26. Fredlund, D. G. and Krahn, J. (1977). "Comparison of slope stability methods of analysis", *Can. Geotech. J.*, Vol. 14, 429-439
27. Gibbs, H. J. and Holtz, W. G. (1957), "Research on determining the density of sands by spoon penetration testing", *Proc 4<sup>th</sup> International Conference on Soil Mechanics and Foundation Engineering*, Vol.1, London, 1957, 35-39.
28. Gibbs, H. J. and Holtz, W. G. (1960), "Correlation of field penetration and vane shear tests for saturated cohesive soils.", *Earth Laboratory Report No. EM-586*, US Department of The Interior, Bureau of Reclamation, Denver, Colorado, September.
29. Gudehus, G. and Schwarz, W. (1985). "Stabilization of creeping slopes by dowels", *Proc. 11<sup>th</sup> International Conference on Soil Mechanics and Foundation Engineering*, San Francisco, Vol. 3, 1679-1700.
30. Hegedus, E. and Peterson, J. H. (1988), "Penetration resistance and shear strength of cohesive soils", *ESOPT-1*, 347-352.
31. Huang, S. L. and Yamasaki, K. (1993). "Slope failure analysis using local minimum factor-of-safety approach", *Journal of Geotechnical Engineering*, Vol. 119, No. 12, 1974-1987.
32. Ito, T. and Matsui, T. (1975). "Methods to estimate lateral force acting on stabilizing piles", *Soils and Foundations*, Vol. 15, No. 4, 43-59.
33. Ito, T., Matsui, T. and Hong, P. W. (1979). "Design method for the stability analysis of the slope with landing pier", *Soils and Foundations*, Vol. 19, No. 4, 43-57.
34. Ito, T., Matsui T. and Hong P. W. (1981). "Design method for stabilizing piles against landslide -- one row of piles", *Soil and Foundations*, Vol. 21, No. 1, 21-37.
35. Ito, T., Matsui T. and Hong P. W. (1982). "Extended design method for multi-row stabilizing piles against landslide", *Soils and Foundations*, Vol. 22, No. 1, 1-13.
36. Jamiolkowski, M., Ghionna, V. N., Lancellotti, R. and Pasqualini E. (1988). "New correlations of penetration tests for design practice", *ISOPT- 1*, Balkema, Rotterdam, 263-296
37. Janbu, N. (1954). "Application of composite slip surface for stability analysis", *Proc., European Conference On Stability of Earth Slopes*, Sweden, Vol. 3, 43-49.
38. Kulhawy, F. H. and Mayne, P. W (1990), "Manual on estimating soil properties for foundation design.", *EPRI*, EL-6800, August.
39. Kusakabe, O. (1995), "Foundations", *Geotechnical Centrifuge Technology*, pp. 118-167, *Balckie Academic & Professional*.

40. Low, B. K., Tang, S. K. and Choa, V. (1994). "Arching in piled embankments", *Journal of Geotechnical Engineering*, Vol. 120, No. 11, 1917-1938.
41. Liang, R. and Zeng, S. (2001). "Numerical study of soil arching mechanism in drilled shafts for slope stabilization", tentatively accepted for publication in *Soils and Foundation*.
42. Lieng, J. T. (1988). "Behavior of laterally loaded piles in sand-large scale model tests", PhD Thesis, Dept. of Civil Engr., Norwegian Institute of Technology, 206 pages.
43. Marcuson, W. F., III and Bieganousky, W. A. (1977). "Laboratory standard penetration tests on fine sands.", *Journal of the Geotechnical Engineering Division, ASCE*, Vol. 103, No. GT6, Nov., 1295-1309.
44. Marcuson, W. F., III and Bieganousky, W. A. (1977). "Laboratory standard penetration tests on fine sands.", *Journal of the Geotechnical Engineering Division, ASCE*, Vol. 103, No. GT6, Nov., 1295-1309.
45. Marcuson, W. F., III and Bieganousky, W. A. (1977). "SPT and relative density in coarse sands.", *Journal of the Geotechnical Engineering Division, ASCE*, Vol. 103, No. GT11, Nov., 1295-1309.
46. McVay, M., Casper, R. and Shang, T. (1995). "Lateral response of three-row groups in loose to dense sands at 3D and 5D pile spacing", *Journal of Geotechnical Engineering*, Vol. 121, No. 5.
47. Mesri, G., Terzaghi, K. and Peck, R.B. (1996), "Soil Mechanics in Engineering Practice", 3<sup>rd</sup> edition, John Wiley & Sons, New York.
48. Morgenstern, N. R. and Price, V. E. (1965). "The analysis of the stability of general slip surfaces", *Geotechnique* 15, 70-93.
49. Morgenstern, N. R. (1982). "The analysis of wall supports to stabilize slopes", in *Application of Walls to Landslide Control Problems*, Edited by Reeves, R. B., ASCE, 19-29.
50. Nethero, M. F. (1982). "Slide control by drilled pier walls", in *Application of Walls to Landslide Control Problems*, Edited by Reeves, R. B., ASCE, 61-76.
51. Nixon, I. K. (1982). "Standard penetration test, state-of-the-art report", *Proc. of the 2<sup>nd</sup> ESOPT*, May, 3-24 .
52. Nunez, I.L., Hoadley, P.J., Randolph, M.F. and Hulett, J.M. (1988), "Driving and Tension Loading Piles in Sand on a Centrifuge", *Centrifuge'88*, pp.353-362. Balkema, Rotterdam.

53. Oakland, M. W. and Chameau, A. J. L. (1984), "Finite element analysis of drilled piers used for slope stabilization", Symposium on laterally loaded deep foundations: Analysis and performance.", Kansas City.
54. Ovesen, N.K. (1979) "The scaling Law Relationship", Proc. 7<sup>th</sup> European Conference in Soil Mechanics and Foundation Engineering, Brighton, No. 4, pp.319-323.
55. Parkash, S. (1962). "Behavior of pile groups subjected to lateral loads". Dissertation, University of Illinois.
56. Parkin, A. K. (1988), "The calibration of cone penetrometers." ISOPT I, Orlando, 221-243.
57. Peck, R. B., Hansen, W.E, and Thornburn, T.H. (1974), "Foundation Engineering", 2<sup>nd</sup> Ed., John Wiley and Sons, New York.
58. PLAXIS (1998)-Finite Element Code for Soil and Rock Analysis, Reference Manual, Version 7. A. A. Balkema/Rotterdam/Brookfield.
59. Poulos, H. G. (1994). "Analysis and design of piles through embankment", Proc. of Deep Foundation, 1403 -1421.
60. Poulos, H. G. (1995). "Design of reinforcing piles to increase slope stability", Can. Geotech. J., Vol. 32, 808-818.
61. Reese, L. C.,(1984). "Handbook on design of piles and drilled shafts under lateral load", FHWA-IP-84-11, 386pp.
62. Reese, L. C., Cox, W. R., and Koop, F. D. (1974). "Analysis of laterally loaded piles in sand.", Proc. Sixth Annual Offshore Tech. Conf., 2, Houston, Tex.
63. Reese, L. C., Cox, W. R., and Koop, F. D. (1974). "Analysis of laterally loaded piles in sand.", Proc. Fifth offshore technology conference, Vol. II, Paper 2080, Houston, Texas, 473-485.
64. Reese, L. C., Wang, S. T. and Fouse, J. L. (1992). "Use of drilled shafts in stabilizing a slope", Proc. Specialty Conference on Stability and Performance of Slopes and Embankments, Berkeley.
65. Rollins, K. M and Rollins, R. L. (1992). "Landslide stabilization using drilled shaft walls", in Ground movements and structures, Vol. 4, Edited by Geddes, J. D., Pentech Press, London, 755-770.
66. Sarma, S. K. (1973). "Stability analysis of embankments and slopes", Geotechnique 23, No. 3, 423-433.

67. Sharma, S. and Moudud, A. (1992). "Interactive slope analysis using Spencer's method", Proceeding of a Specialty Conference on Stability and Performance of Slopes and Embankments - II, ASCE Vol. 1, 506-520.
68. Shibata, T., Yashima, a. and Kimura, M. (1989). "Model tests and analysis of laterally loaded pile groups", Soils and Foundations, vol. 29, No. 1, JSSMFE.
69. Shmertmann, J. H. (1975), "Measurement of insitu shear strength", Proceedings of the Conference on Insitu Measurement of Soil Properties, ASCE, 57-111.
70. Shmertmann, J. H. (1979), "Statics of SPT", Journal of the Geotechnical Engineering Division, ASCE, Vol. 105, No. GT5, 655-669.
71. Shmertmann, J. H. and Palacios, A. (1979), "Energy dynamics of SPT", Journal of the Geotechnical Engineering Division, ASCE, Vol. 105, No. GT8, 909-926.
72. Sirawardane , H. J., Moulton, L. K. and Ched, T. J. (1984). "Prediction of lateral movement of bridge abutments on piles", Transportation Research Record, 998, TRB, Washington, 14-24.
73. Skempton, A. W. (1986). "Standard penetration test procedures and the effects in sands of overburden pressure, relative density, particles size, aging and overconsolidation", Geotechnique 36, No. 3, 425-447.
74. Smith, I. M. and Griffith, D. V. (1982). Programming the Finite Element Method, Second Edition, John Wiley & Sons, Chisester, U.K.
75. Sommer, H. (1977). "Creeping slope in a stiff clay", Proc. Special Session No. 10, 9<sup>th</sup> International Conference on Soil Mechanics and Foundation Engineering, Tokyo, 113-118.
76. Spencer, E. (1967). "A method of analysis of the stability of the stability of embankments assuming parallel interslice forces", Geotechnique, Vol. 17, No. 1, 11-26.
77. Springman, S. M. (1989). "Lateral loading of piles due to simulated embankment construction", Ph.D. Thesis, Engineering Department, Cambridge University.
78. Stewart, D. P., Randolph, M.F. and Jewell, R. J. (1994). "Recent developments in the design of piles loaded by lateral sod movements", Proc. of Deep Foundation, 922-1006.
79. Stewart, D. P., Jewell, R. J. and Randolph, M.F. (1993). "Numerical modeling of piled bridge abutments on soft ground", Computers and Geotechnics, 15(1), 21-46.
80. Terzaghi, K. (1936). "Stress distribution in dry and saturated sand above a yielding trap-door", Proceeding, 1st International Conference On Soil Mechanics, Harvard University, Cambridge, Mass., Vol.1, 307-311.

81. Terzaghi, K. (1943). Theoretical soil mechanics, John Wiley & Sons, New York, N.Y.
82. Terzaghi, K. and Peck, R. (1967). Soil mechanics in engineering practice, 2<sup>nd</sup> Edition, John Wiley & Sons, Inc.
83. Wang, W. L. and Liang, J. (1979). "Unsheathed excavation in soils", Journal of the Geotechnical Division, ASCE, Vol. 105, No. GT9, 1117-1121.
84. Wang, W. L. and Reese L. C. (1986). "Study of design method for vertical drilled shaft retaining walls.", Research Report 415-2F, Center for Transportation Research, Bureau of Engr. Research, the University of Texas at Austin.
85. Wang, W. L. and Yen, B. C. (1974). "Soil arching in slopes", Journal of the Geotechnical Division, ASCE, Vol. 104, No. GT4. 493-496.
86. Yamagami, T., Jiang, J., and Ueno, K. (2000). "A limit equilibrium stability analysis of slopes with stabilizing piles", Slope Stability 2000, Geotechnical Special Publication No. 101, 343-354
87. Yakovleva, T.G. (1988), "Use of Geotechnical Centrifuges in The USSR", Centrifuges In Soil Mechanics, pp. 29-34, Balkema, Rotterdam.
88. Zhang, S. and Chowdhury, R. N. (1995). "Interslice shear forces in slope stability analyses: A new approach", Soils and Foundations, Vol. 35, No. 1, 65-74.